Rare-Earth-Doped Gallium Lanthanum Sulphide Glasses for Mid-Infrared Fibre Lasers

Thorsten Schweizer

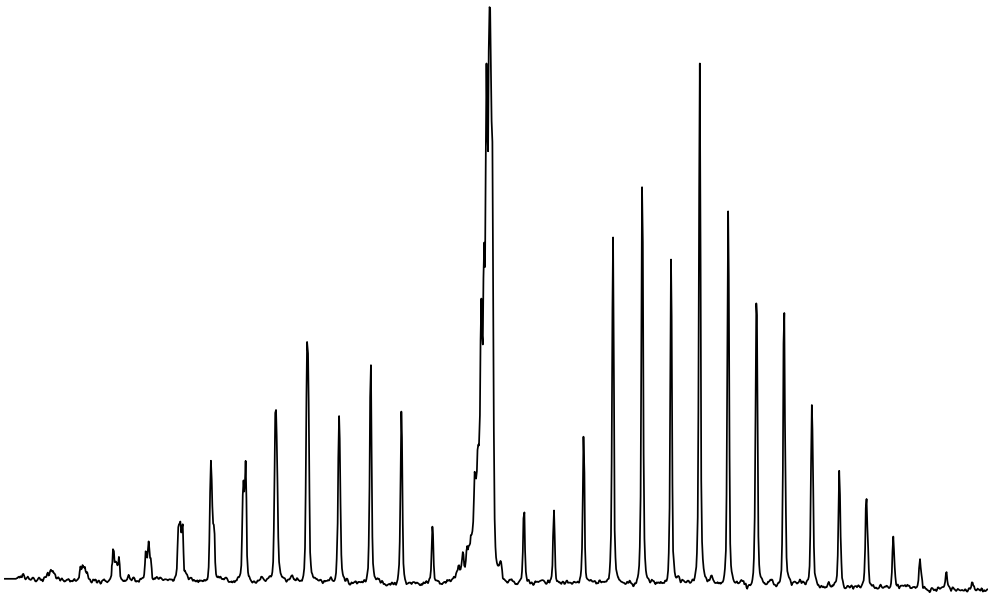

Optoelectronics Research Centre, University of Southampton
and
Institut für Laser-Physik, Universität Hamburg
1998

Rare-Earth-Doped
Gallium Lanthanum Sulphide Glasses
for Mid-Infrared Fibre Lasers

Dissertation

zur Erlangung des Doktorgrades
des Fachbereichs Physik
der Universität Hamburg

vorgelegt von

Thorsten Schweizer
aus
Nordhorn

Southampton
1998

Gutachter der Dissertation: Prof. Dr. G. Huber
Prof. Dr. W. Neuhauser

Gutachter der Disputation: Prof. Dr. G. Huber
Prof. Dr. G. Zimmerer

Datum der Disputation: 14. Juli 1998

Sprecher des Fachbereichs
Physik und Vorsitzender
des Promotionsausschusses: Prof. Dr. B. Kramer

Abstract

T. Schweizer, R*are-Earth doped gallium lanthanum sulphide glasses for mid-infrared fibre lasers*

Gallium lanthanum sulphide (GLS) glass was investigated as a potential host material for rare-earth (RE) doped mid-infrared fibre lasers.

Glasses were fabricated from gallium sulphide and lanthanum sulphide powders by melt quenching and drawn into fibres using the rod-in-tube technique. Typical values for the attenuation in the loss minimum around 4 μm are a few dB/m. The quality of the fibre is currently limited by impurities such as transitions metals, silicon, and aluminium, imperfections at the core/clad interface, and the tendency to crystallisation.

Absorption, fluorescence, and lifetime measurements were performed for eleven RE ions for wavelengths ranging from the visible to the mid-infrared with a focus on mid-infrared transitions. The results of the measurements were used to study the multiphonon decay in GLS glass and to obtain important laser parameters such as the absorption and emission cross sections, branching ratios, and quantum efficiencies from the Judd-Ofelt theory, the Füchtbauer-Ladenburg equation, and the McCumber theory. Twenty-one transitions with peak emission wavelengths longer than 2 μm were identified, seven of which have not been reported in a glass before. Some transitions overlap with the fundamental absorption bands of environmentally important gases such as the 3.4 μm (methane and other hydrocarbons) and 4.7 μm (carbon monoxide) praseodymium transitions and the 4.3 μm (carbon dioxide) dysprosium transitions, whereas the 3.8 μm thulium and the 3.9 μm holmium transitions coincide with an atmospheric transmission window.

Co-doping schemes such as thulium/terbium, praseodymium/ytterbium, praseodymium/erbium, and dysprosium/erbium which offer more favourable absorption bands for diode laser pumping were investigated with respect to ion-ion energy transfer.

Excited-state absorption (ESA) measurements in erbium and thulium doped GLS glasses revealed transitions from excited RE energy levels to levels at energies relative to the ground state which are larger than the energy bandgap of the glass (~ 2.6 eV). Transitions from the RE ions to the conduction band of the glass, as they have been reported in RE doped crystals, could not be found. The results support the model of isolated ions with shielded 4f levels and rule out ESA from RE ions to the conduction band of the glass as a potential loss mechanism for RE lasers in GLS glass.

Lasing was demonstrated in neodymium doped GLS glass and glass fibre at 1.08 μm, representing the first reported laser action in a RE doped chalcogenide bulk glass and glass fibre, respectively. The strong thermal lensing in the bulk glass rules out the use of GLS glass as a bulk laser material. The effect was eliminated by using a fibre geometry showing the advantages and necessity of GLS glass fibre.

Zusammenfassung

T. Schweizer, *Selten-Erd dotierte Gallium Lanthan Sulfid Gläser für Faserlaser im mittleren Infrarot*

Gallium Lanthan Sulfid (GLS) Glas wurde auf seine mögliche Verwendung als Selten-Erd (SE) dotiertes Wirtsmaterial für Faserlaser im mittleren Infrarot untersucht.

Gläser wurden aus Galliumsulfid- und Lanthansulfidpulvern mittels schnellen Abkühlens aus der flüssigen Phase hergestellt und mit der “Stab-in-Rohr”-Methode zu Fasern gezogen. Typische Dämpfungen im Verlustminimum um 4 μm sind einige dB/m. Die Qualität der Fasern ist zur Zeit durch Verunreinigungen wie Übergangsmetalle, Silizium und Aluminium, Fehlstellen an der Kern/Mantel-Grenzschicht und die Tendenz zur Kristallisation begrenzt.

Absorptions-, Fluoreszenz- und Lebensdauermessungen wurden für elf SE-Ionen im Wellenlängenbereich vom Sichbaren bis zum mittleren Infraroten durchgeführt, wobei der Schwerpunkt auf Übergänge im mittleren Infrarot gelegt wurde. Mit Hilfe der Meßergebnisse wurde der Multiphononenzerfall in GLS Glas untersucht und mittels der Judd-Ofelt-Theorie, der Füchtbauer-Ladenburg-Gleichung und der McCumber-Theorie wichtige Laserparameter wie die Absorptions- und Emissionswirkungs-querschnitte, die Verzweigungsverhältnisse und die Quanteneffizienzen ermittelt. Einundzwanzig Übergänge mit Emissionsmaxima länger als 2 μm, von denen sieben bisher nicht in der Literatur erwähnt wurden, konnten identifiziert werden. Einige der Übergänge, wie z.B. die 3.4 μm (Methan, Kohlenwasserstoffe) und 4.7 μm (Kohlenmonoxyd) Praseodym Übergänge und der 4.3 μm (Kohlendioxyd) Dysprosium Übergang überlappen mit den fundamentalen Absorptionsbanden wichtiger Umweltgase, während der 3.8 μm Thulium und der 3.9 μm Holmium Übergang mit einem atmosphärischen Transmissionfenster zusammenfallen.

Kodotierungskombinationen wie z.B. Thulium/Terbium, Praseodym/Ytterbium, Praseodym/Erbium und Dysprosium/Erbium wurden wegen ihrer für das Pumpen mit Diodenlasers günstigeren Absorptionsbanden auf Energietransfer hin untersucht.

Messungen der Absorption aus angeregten Zuständen in Erbium und Thulium dotierten GLS Gläsern zeigten Übergänge von angeregten SE-Energieniveaus zu Niveaus mit Energien relativ zum Grundzustand, die größer sind als die Bandlücke des Glases (~ 2.6 eV). Übergänge von SE-Ionen in das Leitungsband des Glases, wie sie von SE dotierten Kristallen bekannt sind, konnten nicht gefunden werden. Die Ergebnissse unterstützen das Model der isolierten Ionen mit abgeschirmten 4f Niveaus und schließen ESA von SE-Ionen zum Leitungsband des Glases als möglichen Verlustmechanismus für SE dotierte Laser in GLS Glas aus.

Laserbetrieb bei 1.08 μm konnte in Neodym dotierten GLS Glas und Glasfasern erzielt werden und stellt den ersten in der Literatur erwähnten Laserbetrieb in SE dotierten Chalkogenidgläsern bzw. -glasfasern dar. Aufgrund der starken thermischen Linsenbildung im Glaslaser kann GLS Glas als “bulk”-Lasermaterial ausgeschlossen werden. Durch die Verwendung der Faserlasergeometrie konnte dieser Effekt beseitigt werden, was die Vorteile und die Notwendigkeit der GLS Glasfaser zeigt.

Table of Contents

Chapter 1

Introduction

Why gallium lanthanum sulphide glass as a new rare-earth doped laser material? Since the first laser demonstration of a rare-earth doped laser material in 1961 by Sorokin and Stevenson [Sor61] and the first report of a rare-earth doped glass fibre laser by Snitzer in the same year [Sni61] a large number of materials have been investigated and laser action has been demonstrated over a wide wavelengths range from the ultraviolet to the mid-infrared. Rare-earth doped lasers and amplifiers have found application in a number of different areas including telecommunication, material processing, medical diagnosis and treatment, printing and marking, environmental sensing, LIDAR, counter measures, etc. The nature of the application determines the particular requirements for the laser source such as the laser wavelength, output power, beam quality, power consumption, size, fabrication and maintenance costs, etc. The fundamental parameter in this list is the laser wavelength which depends on the available radiative transitions between the energy levels of the rare-earth ions which in turn depend on the host material. The main factors which limit the number of available laser transitions are the competing multiphonon transitions and the transparency of the host material. This motivates the search for new laser materials with low phonon energies and extended transparency which could fill the gaps in the existing spectrum of laser wavelengths and extend the spectrum towards shorter and longer wavelengths. Gallium lanthanum sulphide (GLS) glass is such a potential new laser material having a low phonon energy, an extended infrared transparency and, being a glass, the potential to be pulled into fibre form. The fibre geometry offers a good overlap of pump and laser mode, a high pump intensity in the fibre core, the possibility to exploit weak rare-earth absorption bands, and an excellent heat dissipation, making fibre lasers efficient, high gain, and low threshold devices. The initial motivation to

study rare-earth doped GLS glasses was its possible application as a 1.3 µm praseodymium (Pr^{3+}) doped optical fibre amplifier for telecommunication, a device that cannot be realised in common silica glass and has a rather low efficiency in fluorozirconate (ZBLAN) glass fibre.

The purpose of his work was to investigate the potential for mid-infrared fibre lasers in GLS glass and is motivated by the lack of powerful, coherent, compact, robust, reliable, and cheap sources in this wavelength range. Sources for mid-infrared radiation range from simple heated tungsten wires and black-body sources to more sophisticated and bulky gas lasers, optical parametric oscillators, and difference frequency generation. The strongest competitors for mid-infrared fibre lasers are semiconductor lasers, in particular the new quantum cascade lasers [Fai94]. Although still in the research stage the quantum cascade laser can be designed to emit at any wavelength in the mid-infrared range up to 11.6 µm and has been shown to operate at room temperature and at high output powers of up to 1 W [Gma97]. Work is also ongoing on other rare-earth doped crystals and glasses for mid-infrared lasers. The "world record" for the longest emission wavelength of a rare-earth doped laser material is held by a group at the Naval Research Labs in Washington for the demonstration of lasing at 7.2 µm in a Pr^{3+} doped $LaCl_3$ crystal [Bow96], and the "world record" for the rare-earth doped fibre laser with the longest emission wavelength is held by a group at the Institut für Hochfrequenztechnik, Universität Braunschweig, for the demonstration of lasing at 3.9 µm in a holmium (Ho^{3+}) doped ZBLAN glass fibre [Sch95,Sch97]. Limitations of these two laser materials are the hygroscopic nature of both materials which is combined with the disadvantages of the bulk laser geometry for the $LaCl_3$ crystal; and the low quantum efficiency and the increasing transmission loss due to multiphonon absorption for wavelength longer than 3 µm in the ZBLAN glass fibre with a phonon energy more than twice as high as for the crystal (600 cm^{-1} compared to 250 cm^{-1}). GLS glass could potentially solve the problems of either material. Being environmentally stable it combines a lower phonon energy of 425 cm^{-1} and therefore a better infrared transparency with the potential to be pulled into fibre form, thereby offering a promising improvement to the existing ZBLAN fibre with the possible extension to longer wavelengths. Mid-infrared fibre lasers using relatively cheap commercially available near-infrared diode lasers as pump sources could offer an inexpensive, compact, and rugged alternative to currently available mid-infrared sources.

The potential applications of mid-infrared fibre lasers attracted financial funding of this work under the EPSRC / DTI LINK programme (LONGWAVE) which involves six industrial partners (British Aerospace, Crystalox, Crystran, Edinburgh Instruments, GEC Marconi, Merck). The final goals of this project are the fabrication of low loss infrared transmitting fibre for passive power transmission and the assembly of a prototype mid-infrared fibre laser for gas

sensing and remote sensing. The success of the project depends mainly on the fabrication of low loss fibre of sufficient length and with reasonably small core diameters; assuming the spectroscopic properties of the rare-earth ions are favourable for mid-infrared laser emission. The main contributions of the author to this project are the identification and characterisation of mid-infrared rare-earth transitions and to a lesser extend the characterisation of the fibre.

The main body of this thesis is formed by a number of journal papers either written by the author himself or with significant contributions from the author. These papers have been embedded in the chapters in the original form they were published in. The thesis contains four major chapters (2-5). Chapter 2 gives an introduction to the GLS glass system, outlines the techniques and problems in the fabrication of glasses and fibres, and summarises the current status of fibre quality. Chapter 3 introduces the basic theory necessary for the understanding of the spectroscopic properties of the rare-earth ions and the influence of the host material (3.1, 3.2) and gives a spectroscopic study of ten rare-earth ions and combinations of these. Chapter 4 deals with a more fundamental problem; the excited-state absorption of rare-earth ions in a host material with a small energy band gap (~ 2.6 eV). A separate chapter 5 is dedicated to the spectroscopy and laser operation of neodymium (Nd^{3+}) doped glasses and glass fibres. Chapter 6 summarises the current status of the project and gives some ideas for future work. The essential experimental set-ups are given in the appendix.

Parts of this thesis have previously been published in:

Journals

1. D.W. Hewak, R.C. Moore, T. Schweizer, J. Wang, B. Samson, W.S. Brocklesby, D.N. Payne, and E.J. Tarbox, “Gallium lanthanum sulphide optical fibre for active and passive applications”, Electron. Lett. **32** (1996) 384

2. T. Schweizer, D.W. Hewak, D.N. Payne, T. Jensen, and G. Huber, “Rare-earth doped chalcogenide glass laser”, Electron. Lett. **32** (1996) 666

3. T. Schweizer, D.W. Hewak, B.N. Samson, and D.N. Payne, “Spectroscopic data of the 1.8, 2.9 and 4.3 μm transitions in dysprosium-doped Ga:La:S glass”, Opt. Lett. **21** (1996) 1594

4. T. Schweizer, D.W. Hewak, B.N. Samson, and D.N. Payne, “Spectroscopy of potential mid-infrared laser transitions in gallium lanthanum sulphide glass”, J. Lumin. **72-74** (1997) 419

5. B.N. Samson, T. Schweizer, D.W. Hewak, and R.I. Laming, "Spectroscopy of dysprosium doped and dysprosium/terbium co-doped GaLaS glass", accepted for publication in J. Lumin.

6. T. Schweizer, B.N. Samson, R.C. Moore, D.W.Hewak, and D.N. Payne, "Rare-earth doped chalcogenide glass fibre laser", Electron. Lett. **33** (1997) 414

7. B.N. Samson, T. Schweizer, D.W. Hewak, and R.I. Laming, "Properties of dysprosium doped GaLaS fibre amplifiers operating at 1.3μm", Opt. Lett. **22** (1997) 703

8. T. Schweizer, D.J. Brady, and D.W.Hewak, "Fabrication and spectroscopy of erbium doped lanthanum sulphide glass fibres for mid-infrared laser applications", Optics Express **1** (1997) 102

9. T. Schweizer, P.E.-A. Möbert, J.R. Hector, D.W. Hewak, W.S. Brocklesby, D.N. Payne, and G. Huber, "Optical measurement of narrow band rare-earth 4f levels with energies greater than the bandgap of the host", Phys.Rev.Lett. **80** (1998) 1537

10. T. Schweizer, B.N. Samson, J.R. Hector, W.S. Brocklesby, D.W. Hewak, and D.N. Payne, "Infrared emission and ion-ion interactions in thulium and terbium doped gallium lanthanum sulphide glasses," submitted to J. Opt. Soc. Am. B

11. D.J. Brady, T. Schweizer, J. Wang, and D.W. Hewak, "Minimum loss predictions and measurements in gallium lanthanum sulphide based glasses and fibre," submitted to J. Non-Cryst. Solids

12. B.N. Samson, T. Schweizer, J.R. Hector, W.S. Brocklesby, and D.W. Hewak, "Multiphonon decay rates in rare earth doped chalcogenide glasses," submitted to J. Non-Cryst. Solids

13. T. Schweizer, B.N. Samson, J.R. Hector, W.S. Brocklesby, D.W. Hewak, and D.N. Payne, "Infrared emission from holmium doped gallium lanthanum sulphide glass," submitted to Infrared Phys. Technol.

14. E. Martins, T. Schweizer, W.S. Brocklesby, and D.W. Hewak, "The effect of oxide on the spectroscopy of the dysprosium 1.3, 1.7, and 2.9 μm transitions in gallium-lanthanum-sulphide glass," to be submitted to J. Non-Cryst. Solids

International Conferences

1. D.W. Hewak, R.C. Moore, T. Schweizer, J. Wang, B. Samson, W.S. Brochlesby, D.N. Payne, and E.J. Tarbox, "Gallium lanthanum sulphide optical fibre for active and passive applications", 10th International Symposium on Non-oxide Glasses, June 19-22, 1996, Corning, NY USA, paper 30, 157-162
2. T. Schweizer, D.W. Hewak, D.N. Payne, T. Jensen, and G. Huber, "Neodymium-doped gallium lanthanum sulphide glass laser", CLEO/Europe '96 Digest, 8-13 September, 1996, Hamburg, Germany, paper CFD3

3. T. Schweizer, D.W. Hewak, B.N. Samson, and D.N. Payne, "Spectroscopy of potential mid-infrared laser transitions in gallium lanthanum sulphide glass", International Conference on Luminescence and Optical Spectroscopy of Condensed Matter ICL'96, 18-23 August, Prague, Czech Republic, paper O4-5

4. D.W. Hewak, T. Schweizer, J. Hector, J. Wang, B.N. Samson, and W.S. Brocklesby, "Properties of rare-earth doped gallium lanthanum sulphide glass", International Conference on Luminescence and Optical Spectroscopy of Condensed Matter ICL'96, 18-23 August, Prague, Czech Republic, poster P4-140

5. T. Schweizer, B.N. Samson, D.W.Hewak, and D.N. Payne, "Neodymium doped gallium lanthanum sulphide glass fibre laser", CLEO'97 Digest, 18-23 May 1997, Baltimore, Maryland, USA, paper CWQ4

6. B.N. Samson, T. Schweizer, R.C. Moore, D.W.Hewak, and D.N. Payne, "Neodymium doped chalcogenide glass fibre laser", CLEO Pacific Rim'97, 14-18 July 1997, Chiba, Japan, paper TuP4

7. D.W. Hewak, R.C. Moore, T. Schweizer, J. Wang, B. Samson, W.S. Brocklesby, D.N. Payne, and E.J. Tarbox, "Gallium lanthanum sulphide optical fibre for active and passive applications", 1997 Annual Meeting of the American Ceramic Society, 4-7 May 1997, Cincinnati, Ohio, USA,

8. T. Schweizer, J.R. Hector, D.J. Brady, J. Wang, D.W. Hewak, W.S. Brocklesby, and D.N. Payne, "Visible upconversion in rare-earth doped gallium lanthanum sulphide based glasses", CIMTEC'98, 14-19 June 1998, Florence, Italy, paper SX-2:L02

9. E. Martins, T. Schweizer, W.S. Brocklesby, and D.W. Hewak, "The effect of oxide on the spectroscopic properties of the 1.3, 1.7, and 2.9 μm transitions in dysprosium-doped gallium-lanthanum-sulphide glass," CLEO/Europe '98, 13-18 September 1998, Glasgow, Scotland, poster CWF37

10. B.N. Samson, T. Schweizer, J.R. Hector, W.S. Brocklesby, and D.W. Hewak, "Multiphonon decay rates in chalcogenide glasses," submitted to Advances in Photonic Glasses, September 1998, Korea

11. D.W. Hewak, D.J. Brady, and T. Schweizer, "Gallium lanthanum sulphide fiber for active and passive applications," SPIE's International Symposium on Lasers and Materials in Industry, 13-16 July 1998, Québec, Canada, invited paper number 3416-17

12. D.W. Hewak, D.J. Brady, T. Schweizer, J. Wang, J.R. Hector, C.R. Haythornthwaite, W.S. Brocklesby, and D.N. Payne, "Application of novel chalcogenide glasses based on gallium lanthanum sulphides in optical fibre devices," 18. International Congress on Glass (ICG XVIII), San Francisco, California, July 1998

National Conferences

1. T. Schweizer, D.J. Brady, B.N. Samson, D.W. Hewak, and D.N. Payne, "Progress towards mid-infrared fibre lasers in rare-earth doped gallium lanthanum sulphide glass

for gas sensing and remote sensing", Digest of the 13th National Quantum Electronics Conference QE-13, 8-11 September, Cardiff, Wales, United Kingdom

2. D.J. Brady, T. Schweizer, J. Wang, and D.W. Hewak, "Gallium lanthanum sulphide based glass fibre for passive mir delivery applications", Digest of the 13th National Quantum Electronics Conference QE-13, 8-11 September, Cardiff, Wales, United Kingdom

Meetings/Seminars/Summer Schools/Books

1. T. Schweizer, "Rare-earth doped low phonon glasses for mid-infrared wavelength applications", Meeting on: (i) Semiconductor doped "Quantum dot" materials and (ii) halide and sulphide glasses for optoelectronics, Society of Glass Technology, UK GO, UK special interest group: Glasses for optoelectronics, 20 January 1995, at British Telecom Research Laboratories, Martlesham Heath, Ipswich, United Kingdom

2. T. Schweizer, D.W. Hewak, R.C. Moore, J. Amin, B.N. Samson, D.N. Payne, "Ga:La:S, a low phonon glass for long wavelength applications?", NATO ASI, 42th SUSSP Summer School, New Perspectives in Laser Sources and Applications, 25 June-8 July 1995, St. Andrews, Scotland, poster p1z

3. T. Schweizer, "Gallium Lanthanum Sulphide fibre for active and passive applications", presentation given at the Seminar über Festkörperlaser, 12 December 1995, University of Hamburg, Germany

4. T. Schweizer, "Why GLS is Better than Silica - Sometimes!", presentation given at the OSA Student Chapter Seminar Series at the Optoelectronics Research Centre, 5 December 1996, University of Southampton, Southampton, United Kingdom

5. T. Schweizer, D.J. Brady, D.W. Hewak, R.C. Moore, M. Kluth, B.N. Samson, and D.N. Payne, "LONGWAVE: Mid-infrared fibres and fibre lasers", presentation at the Optoelectronics Research Centre Colloquium, 17 April 1997, University of Southampton, Southampton, United Kingdom

6. T. Schweizer, "Spectroscopy of neodymium doped chalcogenide glass" and "Fibre lasers based on rare-earth doped chalcogenide glass", accepted for publication in "Properties of Glass and Rare-Earth Doped Glasses for Optical Fibres", Volume 20, EMIS Datareview Series

Chapter 2

Glass and fibre fabrication and characterisation

2.1 Introduction

The history of chalcogenide glasses, non-oxide glasses began in 1870 when the German scientist Carl Schultz-Sellack reported experiments on radiative heat transport through a series of materials [Sch70]. He showed that the As_2S_3 glass slides which he fabricated himself were highly transparent for heat, an indication of the good infrared transparency of the chalcogenide glasses. It was not until the 1950's that the scientific community became interested in chalcogenide glasses motivated by the increasing demand for optical materials which can be used beyond the infrared limit of transparency of oxide glasses and can, in contrast to crystals, be produced in almost any form and size [Fre53]. A good overview about the synthesis and the physical, chemical, and optical properties of chalcogenide glasses can be found in V.F. Kokorina's book [Kok96].

Infrared transmitting chalcogenide glass fibres based on As_2S_3 were introduced in the 1960's by Kapany and co-workers [Kap65] with possible applications for infrared non-destructive testing of electronic components and integral circuits, monitoring temperatures or fire hazards in remote environments, image conveying, and image dissectors.

Gallium lanthanum sulphide (GLS), the first chalcogenide glass in which a rare-earth was a main constituent, was first reported in 1973 by Flahaut's group and has been studied for its chemical, physical, and optical properties since [Bar92,Fla83,Kum94,Loz73].

Chalcogenides are compound glasses whose anions belong to group VI of the Periodic Table, i.e. sulphur, selenium, and tellurium but not oxygen and whose cations are metals such as arsenic, germanium, and antimonide. A number of glass forming systems has been reported in the literature [Kok96,Kum94]. The

glass-forming tendency decreases in the order S > Se > Te. The covalent metal-metal and metal-chalcogen bonds form long chain networks (A structural study of GLS glass was performed recently by Asal et al. [Asa97]). Chalcogenide glasses are characterised by a high refractive index and a large non-linear refractive index which was found to be particularly high in GLS glasses [Kan95]. The low bond strength leads to low softening points and high coefficients of thermal expansion compared to silica glass. These properties along with the low thermal conductivity and the large changes of refractive index with temperature render chalcogenide glasses unsuitable for rare-earth doped bulk laser applications as will be shown in chapter 5. On the other hand, the large weight of the glass ions and their weak bond strengths give rise to low vibrational frequencies, i.e. low phonon energies.

A material with low phonon energies has two desirable properties. Firstly, the infrared multiphonon absorption edge is shifted further into the infrared. The good infrared transparency of chalcogenides was the initial motivation to study the fabrication and optical properties of these glass systems for passive applications. Secondly, the non-radiative multiphonon decay rate of rare-earth energy levels is greatly reduced as it will be shown in chapter 3.

The work on rare-earth doped chalcogenides for active applications such as lasers and optical amplifiers began in 1977 with a paper about the absorption and emission spectroscopy of neodymium (Nd^{3+}) doped GLS glass by Reisfeld and Bornstein [Rei77]. GLS glass still remains one of the most extensively studied systems because it combines several advantages over other chalcogenide glasses.

GLS glass is nontoxic (no As, Se, Te, etc.), chemically stable (non-hygroscopic) and has a high glass transition temperature (561ºC compared to 153ºC for As_2S_3 and 47ºC for As_5Se_{95}) making the glass more resistant to environmental effects and thermal damage by high power pump laser sources. GLS can be melted in large glass ingots and pulled into fibre form. In general chalcogenide glasses are prone to crystallisation during fibre pulling due to the proximity of the crystallisation and fibre pulling temperature. The glass is transparent down to 500 nm which allows pumping of rare-earths in the visible and near-infrared with convenient diode laser sources, whereas a substantial number of other chalcogenide glasses are opaque in the visible and near-infrared, in particular Se and Te based glasses. Another important advantage is the high rare-earth solubility due to the presence of the rare-earth La in the glass matrix. In general chalcogenide glasses are notorious for their low rare-earth solubility. For these reasons we have chosen GLS as the best candidate for rare-earth doped devices.

Section 2.2 describes the fabrication of GLS glasses and fibres and gives an overview over the problems which currently limit the quality of the fibre.

2.2 Fabrication and characterisation of gallium lanthanum sulphide glass fibres

A typical chalcogenide glass is fabricated either from the elements or from the chalcogen compounds in powder form. The mixture of the starting materials is melted in an evacuated silica ampoule at temperatures from a few hundred to above a thousand degrees centigrade for several hours and than quenched to room temperature. The melting is followed by annealing the glass at the glass transition temperature for several hours or days before the samples are ready for cutting and polishing.

GLS glasses are fabricated from gallium and lanthanum sulphide powders with the typical molar ratio $70Ga_2S_3$:$30La_2S_3$. Glasses are formed over a wide range of ratios from 58:42 to 72:28 [Fla83]. Glasses with a higher La content have a higher refractive index which can be used to raise the index of the core glass for a guiding fibre structure. Although the work presented here is almost entirely based on pure GLS glass, modified GLS glasses are mentioned at some points in this thesis (section 3.11). GLS glasses can be modified by replacing part or all of the La_2S_3 with La_2O_2 (oxide modified glass, GLSO) or caesium halides (CsCl, CsBr, CsI) [Hec97,Wan97]. The advantages of the modifications are increased visible transparency and easier fibre pulling. The disadvantages of the oxide modified glasses are an increased phonon energy which is not acceptable for mid-infrared rare-earth transitions (chapter 3). The halide modified glasses have a tendency to shatter during or after quenching and hence are more difficult to be fabricated into bulk sizes sufficient for fibre drawing.

GLS glass reacts with the silica ampoules during melting and is therefore melted in vitreous carbon crucibles which are placed inside the silica ampoules. A new melting technique for GLS glass has been developed at the ORC. The gallium and lanthanum sulphide powders are filled into a vitreous carbon boat which is pushed into a horizontal silica tube which sits in a resistance furnace. During the melting a constant argon gas flow is passed over the glass melt. After melting at 1150ºC for about 8 hours the boat is pushed outside the furnace region into a part of the silica tube which is surrounded by a flowing water jacket and the melt is quenched to form a glass. From there the boat can be pushed into a smaller furnace for annealing at 530ºC for typically 24 hours. The set-up also allows reactive atmosphere melting with H_2S and SF_6 which could compensate for sulphur loss and to remove oxygen and OH^- impurities. The flowing atmosphere melting was an important step towards higher glass quality and quantity.

Chalcogenide glass fibres are usually fabricated using the rod-in-tube and the double-crucible methods [Kap65]. The double-crucible method with the inner of the two concentric crucibles containing the core glass and the outer crucible

containing the cladding glass is not suitable for GLS due to its high melting temperature of 830ºC and its low viscosity at that point. We have successfully used the rod-in-tube technique to fabricate core/clad structures in GLS glass fibre. For this technique the glass ingots are cut and polished into rods and tubes of typically 120 mm length and 8 mm diameter (a photograph of the glass ingots and rods is shown on page 67). The rods are stretched in the fibre pulling tower to an outer diameter of about 3 mm and inserted into a tube. This process can be repeated two or three times depending on the required core size. The stretching and the final fibre pulling of the assembly of rod and tubes fuse the different glass components and produce fibre with typical outer diameters of 100 to 400 μm and typical core diameters of 5 to 50 μm.

Typical losses of unclad and uncoated GLS fibre in the attenuation minimum around 4 μm are about 5 dB/m. The shape of the fibre attenuation spectrum, the position of the attenuation minimum, and the absolute loss values are determined by the three main loss components: the electronic absorption, the multiphonon absorption, and the scattering loss. The electronic absorption, i.e. the formation of electron-hole pairs by photon absorption, causes the UV absorption edge around 500 nm and decreases exponentially to longer wavelengths into the transmission window. The long-wavelength edge of the transmission window is defined by the multiphonon absorption, i.e. the absorption of photons by optic phonon modes in the glass, which becomes effective at about 5 μm and increases exponentially to longer wavelengths. Scattering loss can be caused by small scale fluctuations of the refractive index that are frozen into the glass lattice and by scattering centres such as crystals, impurities or bubbles. Fluctuations in the refractive index are created by density fluctuations and compositional fluctuations. If the scattering centres are much smaller than the wavelength of light the scattering loss follows a λ^{-4} dependence (Rayleigh scattering) whereas larger particles either show a lower or no wavelengths dependence at all but scatter much stronger than the smaller particles (Mie scattering). Taking the above processes into account a theoretical loss minimum of 0.5 dB/km at 3.5 μm, four orders of magnitude lower than the current experimental loss values, has been predicted for GLS glass clearly showing the potential of GLS glass fibre for passive mid-infrared power transmission and active mid-infrared laser devices [Bra98].

The following paper (paper 1) reports the first demonstration of optical fibres based on GLS glass.

Gallium lanthanum sulphide optical fibre for active and passive applications

*D.W. Hewak, R.C. Moore, **T. Schweizer**, J. Wang, B.N. Samson, W.S. Brocklesby, D.N. Payne and E.J. Tarbox.*

Abstract

The authors report on the first demonstration of optical fibres based on the Ga:La:S system. Core-clad structures have been fabricated by rod and tube method and pulled into lengths > 200 m. Transmission over the wavelength range 1.0 to 6.5 μm, with fibre losses approaching the absorption and scattering level of the bulk glass, is obtained, opening the possibility of new fibre device applications of this promising glass host.

Chalcogenide glasses based on the sulphides has recently attracted considerable interest for their possible role as new optical fibre materials [1-5]. When doped with the rare-earths these glasses, by virtue of their low-phonon-energy and high refractive index, open up the possibility of new transitions and significantly increased pump efficiencies. Undoped sulphide glasses provide a waveguide with a transmission range which extends from the visible to wavelengths approaching 10 μm.

A variety of sulphide glass systems are under study, including those based on gallium and germanium sulphides [1-3], arsenic trisulphide [4] and chalcohalides which combine a sulphide and halide glass-forming structure [5]. However, apart from arsenic trisulphide which suffers from poor rare-earth solubility, no optical fibre structures have been achieved in these materials. For the most part, the sulphide glasses tend to suffer from a propensity to devitrification, with the onset of crystallisation coinciding with the temperature for fibre-drawing.

Here we report, for the first time, on an optical fibre fabricated in the gallium-lanthanum glass system [6,7]. This material provides an ideal host for the rare-earths, which substitute directly for the lanthanum ions, while at the same time providing a wide transmission range and a relatively stable and nontoxic glass matrix.

Gallium lanthanum sulphide glass was prepared by melt quenching. Compositions were based on a molar ratio of 70% gallium and 30% lanthanum, with the ratio adjusted to modify the refractive index. Substitutions of a few percent gallium sulphide for lanthanum sulphide were sufficient to raise the core

Paper 1: published in Electron. Lett. **32** (1996) 384

glass index and allow guided modes to be supported by the structure. Analysis revealed residual oxide levels of < 0.5% in the starting materials. Transition metal impurities were of the order of a few parts per million and dominated by copper and iron. Both undoped glasses and glasses doped with praseodymium, erbium and dysprosium have been used in fibre drawing trials.

Both rods and preforms of the gallium lanthanum sulphide glass have been drawn into fibres. Bulk glass melts of core and cladding glasses in batches of 175 g were melted simultaneously. After quenching and annealing the ingots were cut and mechanically polished to form rods and tubes of diameter ~ 8 mm and 120 mm in length. Both solid rods and core-cladding structures formed by the rod-in-tube technique were used. These were then drawn using a conventional low temperature fibre drawing furnace at speeds up to 15 m/min. In some cases a UV cured acrylate coating was applied to the fibre during drawing. Uncoated fibre with a diameter of typically 125 μm and > 200 m in length was obtained from a single preform. Coated fibre in lengths of several 10s of metres was also obtained. The fibre was mechanically strong and stable, showing no signs of devitrification or attack by moisture even after one year in our laboratories. The cross-section of a typical fibre is shown in Fig. 1.

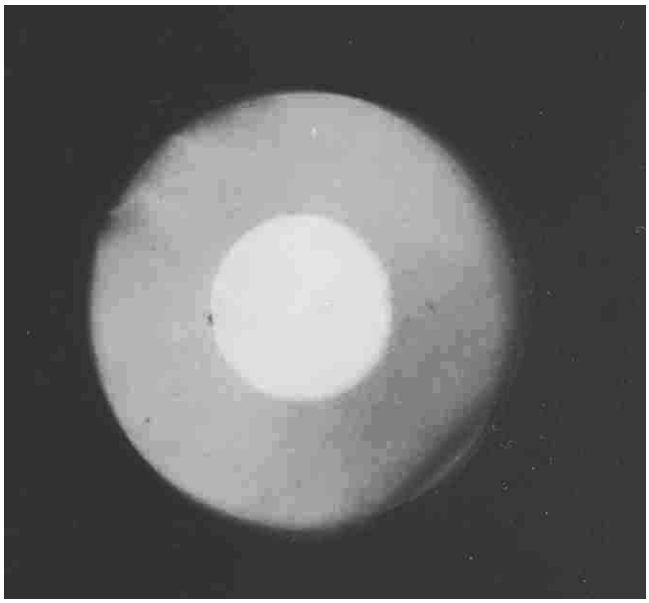

Fig. 1 Photograph of multimode fibre fabricated in Ga:La:S glass

Loss measurements were performed first on bulk glass samples polished on two parallel faces. Three samples of length 5.9, 19 and 49 mm were measured on a Fourier transform infrared spectrometer, using in each case a shorter sample as a reference for correction to end reflection. The absorption, normalised to a 1

cm thick sample, is shown in Fig. 2. Clearly visible in the spectrum are absorption bands which correspond to OH^-, oxide impurities, SH^- and the transition metals. A background absorption of 1.8 dB/m is indicated at ~1 μm and a loss of < 1.0 dB/m at the intrinsic loss minimum at ~ 4.5 μm.

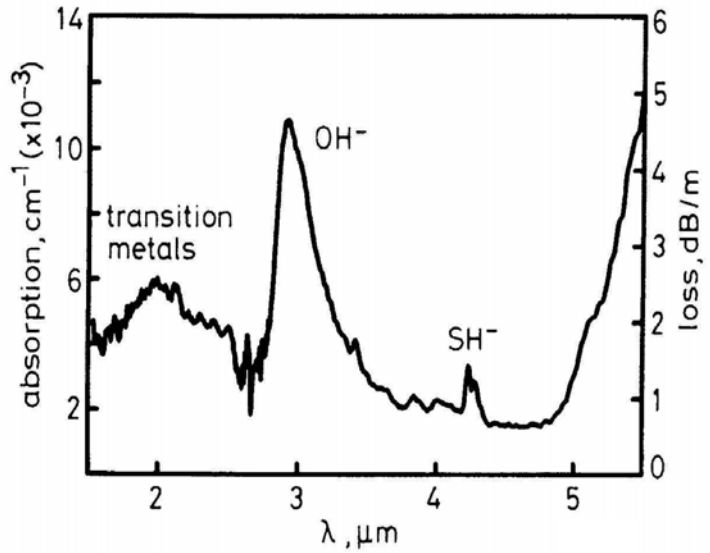

Fig. 2 Loss estimated from absorption measurements on 4.6 cm thick glass sample

Fibre loss measurements were made on the same apparatus, modified with gold mirrors and a reflecting microscope object lens to allow measurements directly on an optical fibre. Transmission loss was estimated by the cutback method over a 63 cm section of praseodymium doped multimode fibre clad. As shown in Fig. 3, between the absorption bands a loss of < 5.0 dB/m is measured at 1.34 μm and 4.9 dB/m at the intrinsic loss minimum at ~ 4.7 μm. Across this wavelength range loss appears to be dominated by wavelength independent scattering. Around wavelengths of 1-2 μm, loss is also affected by the intrinsic absorptions of the transition metal ions. We expect that this source of loss can be eliminated through careful preparations of the starting materials, as was shown for fluoride glasses a decade ago [8]. A loss of ~ 10 dB/m is associated with the fundamental OH^- absorption at ~ 3.0 μm. Measurements on undoped fibres have revealed SH^- absorptions of < 0.2 dB/m at 4.05 μm. Efforts are under way to improve the glass melting procedure and thereby reduce the level of these impurities. Overall, these measurements indicate that with further improvements in the glass purity, the gallium lanthanum sulphide fibre will provide an optical waveguide covering the wavelength range from 1.0 to over 5.0 μm.

Power handling of these fibres was assessed by coupling to a Nd:YAG laser operating at 1064 nm. A total of 5 W of power was guided through a core of

Paper 1: published in Electron. Lett. **32** (1996) 384

~150 μm with no decrease in transmission and no apparent laser damage. With their high glass transition temperature (560°C compared to 200 - 300°C in other sulphide glasses) these glasses offer the potential for greater power handling capacity and also reduced toxicity due to elimination of arsenic-containing compounds. This opens the range of applications to infra-red power delivery of medical, imaging or sensing applications.

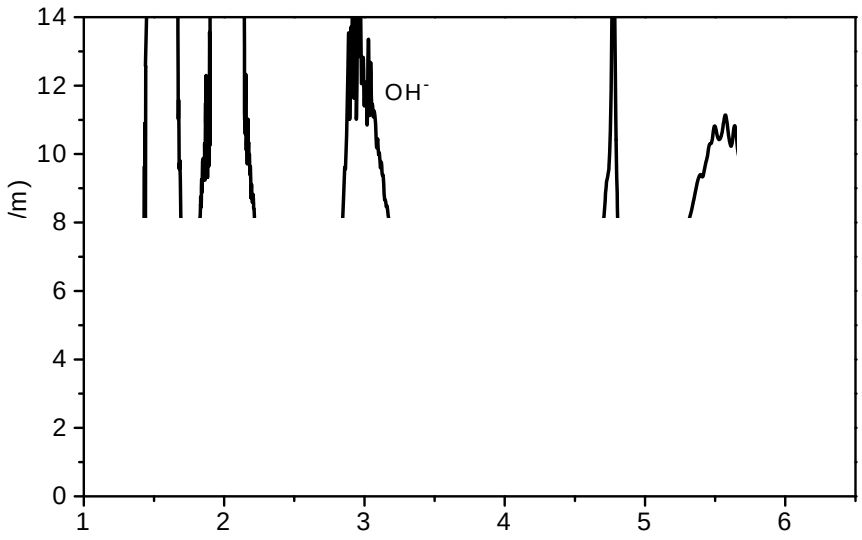

Fig. 3 Pr^{3+}-doped Ga:La:S fibre loss as measured over 63 cm cutback

Fluorescence has been measured in doped gallium lanthanum sulphide fibres and will be reported in a future publication.

To summarise, doped and undoped multimode fibres have been achieved in the gallium lanthanum sulphide glass system. Fibre losses are approaching that of the bulk glass, and thus, with further materials purification, practical fibre device applications of this important new glass system are imminent.

Acknowledgements

Chalcogenide starting materials were supplied by Merck Ltd. of Poole, England. This work was funded in part by Pirelli Cables Ltd., a UK DTI EPSRC Link programme, and by British Gas plc. We are grateful to S. Rutt of the Infrared Science and Technology Group for constructing the infrared measurement apparatus.

References

1. Quimby, R.S., Gahagan, K.T., Aiken, B.G., and Newhouse, M.A.: 'Self-calibrating quantum efficiency measurement technique and application to Pr^{3+}-doped sulphide glass', Opt. Lett., 1995, **20**, p. 2021-2023.
2. Wei, K., Machewirth, D.P., Wenzel, J., Snitzer, E., and Sigel, G.H.: 'Pr^{3+}-doped Ge-Ga-S glasses for 1.3 micron optical fibre amplifiers', Opt. Lett., 1994, **19**, pp. 904-907.
3. Simons, D.R. Faber, A.J., and De Waal, H.,: 'GeS glass for Pr^{3+}-doped fibre amplifiers at 1.3 microns', J. Non-Cryst. Solids, 1995, **185**, pp. 283-288.
4. Ohisihi, Y., Mori. A., Kanaomori, T., Fujura, K., and Sudo, S.: 'Fabrication of praseodymium-doped arsencic sulfide chalcogenide fibre for 1.3 micron fibre amplifiers', Appl. Phys. Lett., 1994, **65**, pp. 13-15.
5. Marchese, D., Kakaranatzas G., and Jha, A.: '$^1G_4$ lifetimes, optical and thermal characteristics of Pr-doped GeS_2-chalcohalide glasses, to be published in J. Non. Cryst. Solids.
6. Becker, P.C., Broer, M.M., Lambrecht, V.G., Bruce, A.J., and Nykolak, G.: 'Pr^{3+}:La-Ga-S Glass: A Promising Material for 1.3 μm Fibre Amplification', in Technical Digest of Topical Meeting Optical Amplifiers and their Applications, 1993 (Optical Society of America, Washington, DC, 1993), postdeadline paper PDP5
7. Hewak, D.W., Medeiros, J.A., Samson, B., Brown, R.S., Jedrzejewshi, P., Wang, J., Taylor, E., Laming R.I., Wylangowski, G., and Payne, D.N.: 'Quantum Efficiency of praseodymium doped Ga:La:S glass for 1.3 micron optical fibre amplifiers', IEEE Photonics Tech. Lett., 1994, **6**, pp. 609-612.
8. Mitachi, S., Terunuma, Y., Ohishi, Y., and Takahai, S.: 'Reduction of impurities in fluoride glass fibres', J. Lightwave Technol. 1984, **2**, pp. 587-592.

2.3 Conclusion

The advances in GLS glass and fibre fabrication laid the foundation for the work presented in chapters 3-5. However, fibre losses are still too high for efficient fibre devices. A reasonable goal for the reduction of the fibre loss for active applications would be a loss of 1 dB/m in a fibre with a core diameter of 5-10 μm or larger with similar loss for passive applications. The fibre loss is limited by the materials loss which is caused by absorption and scattering loss due to impurities and crystals, and - in particular for single mode fibres - by the quality of the core/clad interface.

New initiatives at the ORC to overcome these problems are to set up our own sulphide powder fabrication and purification facilities and to use extrusion as a new method to fabricate core/clad structures. Initial extrusion trials which were performed by forcing two viscous glass disks through a metal die showed encouraging results. A single extrusion process may produce a rod with a core/clad ratio large enough to directly pull a single mode fibre without further rod-in-tube cycles.

The successful application of GLS glass fibres for mid-infrared light transmission and rare-earth doped lasers depends critically on the improvement of the fibre quality. Better quality fibre could also find application in acousto-optic devices and all-optical switching devices for telecommunications [Abd93, Aso96].

It should be mentioned here for completeness that GLS glass can also be fabricated in the form of thin film waveguides by pulsed laser deposition starting from bulk glass samples [Asa97,Gil95,You93]. The quality of the films is poor with high losses of ~600 dB/m at 633 nm and is not suitable for devices yet. Grating structures which have been written into GLS glass films with 442 nm light or electron beams show the potential to write gratings into GLS glass fibres to form laser cavities, etc.

Chapter 3

Spectroscopy of rare-earth doped glasses and fibres

3.1 Introduction

This chapter deals with the spectroscopic properties of a number of rare-earth (RE) ions in gallium lanthanum sulphide glass (GLS). More general overviews about the spectra and energy levels of RE ions can be found in [Die68, Pea75, Rei75, Wyb65]. The brief introduction given here follows Miniscalco [Min93].

The RE's are divided into the lanthanides and actinides. In this thesis RE's means lanthanides which are characterised by the filling of the 4f shell and begin with cerium (Z=58) and end with lutetium (Z=71). The most stable level of ionisation of RE's in condensed matter is trivalent (3+) although ions with a nearly half-full (samarium, europium) and a nearly full (ytterbium) 4f shell have a tendency to form divalent ions. The electronic configuration of the RE ions is that of xenon plus a certain number of 4f electrons (1-14). The wave functions of the 4f electrons lie within the closed $5s^2 5p^6$ xenon shell (lanthanide contraction). The 5s and 5p electrons shield the 4f electrons from the environment which has several effects. The RE ions have very similar chemical properties to each other and to lanthanum which is a major constituent of GLS glass (high RE solubility). The 4f energy levels are relatively insensitive to the host, have small host-induced splittings, are only weakly mixed with higher energy states, have little or no vibronic structure, and weak non-radiative relaxation of excited states. The Hamiltonian to describe the 4f electrons of a RE ion in a host material can be written as:

$$H = H_{\text{free ion}} + V_{\text{ion-static lattice}} + V_{\text{EM}} + V_{\text{ion-ion}} + V_{\text{ion-dynamic lattice}} \qquad (3.1.1)$$

The terms in equation 3.1.1 can be divided into static, which produce the electronic structure (term 1 and 2), and dynamic, which induce transitions

between the electronic states (term 3-5). The interaction terms 2-5 are weak compared to term 1 and are treated as perturbations. The terms 1 to 4 are discussed in this section in order of their occurrence in equation 3.1.1 while a separate section (3.2) is dedicated to the discussion of term 5.

$H_{\text{free ion}}$ has three contributions which are the central field, the electron-electron interactions, and the spin-orbit interactions. The central field approximation assumes each electron to move independently in a spherically symmetric potential formed by the nucleus and the average potential of all other electrons. The solutions are a product of a radial and angular function and are constructed from hydrogen states. The total orbital angular momentum *L* and the total spin *S* are "good" quantum numbers and are added vectorially to form the total angular momentum *J* (Russel-Saunders or *LS* coupling). The states are labelled $^{2S+1}L_J$ and are degenerate in the central field approximation. The electrostatic interaction of the 4f electrons lifts the angular degeneracy and produces a spectrum of states whose energies now depend on *L* and *S* but not on *J*. The magnetic spin-orbit interaction lifts the degeneracy of the total angular momentum and splits each *LS* term into *J* levels. Electric dipole transitions between these levels are forbidden for the free ion because the initial and final states have the same parity. Transitions can occur only for the much weaker magnetic-dipole and electric-quadrupole processes.

$V_{\text{ion-static lattice}}$ takes the small influence of the host on the electronic structure into account. The host is replaced by an effective crystal field potential which splits the free ion *J* multiplets into Stark components which are separated by 10-100 cm^{-1} and are degenerate for ions with an odd number of electrons (Kramers degeneracy). The Stark levels determine the spectral shape of the absorption and emission bands. If the RE site lacks inversion symmetry, as it usually does in glasses, the odd terms of the crystal field potential admix higher lying states of opposite parity (e.g. $(4f)^{n-1}5d^1$) into the $(4f)^n$ configuration. This does not affect the position of the energy levels but it introduces a degree of electric-dipole strength into the 4f transitions and makes electric-dipole transitions the dominant transitions between RE 4f levels.

The host also effects $H_{\text{free ion}}$ through covalent bonding which partially screens the 4f electrons and reduces the effective nuclear charge. This results in a rescaling of the entire energy level diagram which is usually referred to as the nephelauxetic effect [Jør62]. More covalent glasses, like GLS, absorb and emit at longer wavelengths, while more ionic ones, like fluorides, absorb and emit at shorter wavelengths.

The dynamic interaction terms in equation 3.1.1 are usually treated using time dependent perturbation theory. V_{EM} describes the interaction of RE ions with an electromagnetic field which gives rise to the absorption and emission of photons. The four principal processes are absorption from the ground state (GSA), absorption from an excited state (ESA), spontaneous emission from an

excited state, and stimulated emission from an excited state by an incoming photon with resonant energy to the 4f transition. If $V_{\text{ion-static lattice}}$ was known one could in principle calculate the intensities and shapes of the absorption and emission bands. In practice a semiempirical technique which was developed independently by Judd [Jud62] and Ofelt [Ofe62] is used to calculate the strength of RE transitions. The following brief overview about the Judd-Ofelt analysis is presented in SI units and uses the equations presented in [Ami96]. A detailed discussion of the mathematics and the simplifying assumptions made is given in [Pea75].

Judd-Ofelt theory

The aim of the Judd-Ofelt analysis is the calculation of the radiative transition probabilities between the RE energy levels. The rate of spontaneous emission, $A = A_{ed} + A_{md}$, for electronic and magnetic-dipole transitions between two levels a and b is given by:

$$A(a \to b) = \frac{16\pi^3 n^2}{3h\varepsilon_o (2J_a + 1)\bar{\lambda}^3} (X_{ed} S_{ed} + X_{md} S_{md}) \qquad (3.1.2)$$

n is the refractive index of the host at the average emission wavelength $\bar{\lambda}$ and J_a is the total angular momentum of the upper level.

$$X_{ed} = \frac{(n(\lambda)^2 + 2)^2}{9n(\lambda)} \qquad \text{and} \qquad X_{md} = n(\lambda) \qquad (3.1.3)$$

are the local field corrections and represent the enhancement of the electric field in the vicinity of the RE ion due to the polarizability of the medium. S_{ed} and S_{md} are the line strengths of the electric and magnetic-dipole transitions and can be expressed by:

$$S_{ed}(a,b) = e^2 \sum_{t=2,4,6} \Omega_t |\langle a||U^{(t)}||b\rangle|^2 \qquad (3.1.4)$$

$$\text{and} \qquad S_{md}(a,b) = \left(\frac{eh}{4\pi mc}\right)^2 |\langle a||L + 2S||b\rangle|^2 \qquad (3.1.5)$$

The host dependence in the above equations is contained in the three intensity parameters Ω_t. The host-independent matrix elements of $L + 2S$ and $U^{(t)}$ have been tabulated for RE doped LaF_3 crystals [Car78]. The transition strength is also commonly expressed as the dimensionless oscillator strength $f = f_{ed} + f_{md}$:

$$f(a,b) = \frac{8\pi^2 mc}{3h(2J_a+1)\bar{\lambda}}\left(X_{ed}\frac{S_{ed}}{e^2} + X_{md}\frac{S_{md}}{e^2}\right) \quad (3.1.6)$$

which can be obtained experimentally from the measured ground state absorption spectrum (absorption coefficient $\alpha(\lambda)$) of a sample with RE ion concentration, *N*, using:

$$f_{meas}(a,b) = \frac{4m\varepsilon_o c^2}{Ne^2\bar{\lambda}^2}\int \alpha(\lambda)d\lambda \quad (3.1.7)$$

The magnetic-dipole strength is either zero (selection rules: $\Delta J=\pm 1$, $\Delta S=0$, $\Delta L=0$, $\Delta l=0$) or, if non-zero, can be calculated and subtracted from the measured oscillator strength so that equations 3.1.4, 3.1.6, and 3.1.7 can be combined to:

$$S_{ed}(a,b) = e^2 \sum_{t=2,4,6} \Omega_t |\langle a||U^{(t)}||b\rangle|^2 = \frac{3h\varepsilon_o c(2J_a+1)}{2\pi^2 XN\bar{\lambda}}\int \alpha(\lambda)d\lambda - S_{md} \quad (3.1.8)$$

Least-squares fitting of the theoretical and experimental line strengths gives one set of the three Judd-Ofelt parameters Ω_t for a given combination of dopant and host. The intensity parameters do not have a clear physical meaning, however, Ω_2 is found to be higher in materials with covalent bonding, like GLS, and lower in materials with ionic bonding. A large value for Ω_2 increases in particular the oscillator strengths of the so called "hypersensitive" transitions which have large $U^{(2)}$ matrix elements [Jør64,Jør83,Pea75]. We therefore expect to find an increased absorption coefficients for hypersensitive transitions in GLS glass, which was confirmed by the results of the absorption measurements presented in later sections.

Once the Judd-Ofelt parameters have been determined the spontaneous emission rate for any transition can be obtained from equations 3.1.2 to 3.1.5. The reciprocal of the total sum of the transitions from a level *a* to all final levels *b* is equal to the radiative lifetime of level *a*:

$$\tau_r(a) = \left(\sum_b A(a,b)\right)^{-1} \quad (3.1.9)$$

The branching ratio for the transition $a \rightarrow b$ is the fraction of all spontaneous emission processes from level *a* that occur through this transition:

$$\beta(a,b) = \tau_r(a)A(a,b) \quad (3.1.10)$$

The measured lifetime of the fluorescence decay, τ_m, can be shorter than the calculated radiative lifetime due to non-radiative processes as will be discussed further down. The ratio of measured to calculated lifetime gives the radiative quantum efficiency which can be defined for a level *a* or for a particular transition $a \rightarrow b$ from this level:

$$\eta(a) = \frac{\tau_m}{\tau_r} \qquad \text{or} \qquad \eta(a,b) = \beta(a,b)\frac{\tau_m}{\tau_r} \tag{3.1.11}$$

What results and problems do we expect when we apply the Judd-Ofelt analysis to RE doped GLS glass? From equations 3.1.2, 3.1.3, and 3.1.9 we can expect large spontaneous emission probabilities and short radiative lifetimes due to the covalent nature of the glass bonds and the high refractive index which is around 2.4 compared to about 1.5 in silica and about 1.45 in fluorides. The branching ratios (3.1.10) are only weakly host dependent. An example for varying branching ratios in Nd^{3+} doped glasses is given in section 5.2. In general we can say that mid-infrared transitions will have low radiative rates (3.1.2) and low branching ratios if they are competing with visible or near-infrared transitions from the same excited level which could cause amplified spontaneous emission (ASE) losses. From this point of view the mid-infrared emitting level should ideally be at a low energy relative to the ground state. The radiative quantum efficiencies (3.1.11) are expected to be high in GLS compared to oxide and fluoride glasses due to the high radiative rates and the low non-radiative decay rates which will be discussed in section 3.2.

A problem encountered in GLS glass is the limited number of absorption bands which can be used for the fitting procedure due to the electronic glass absorption edge at 500 nm. This can lead to large uncertainties for the Judd-Ofelt parameters such as the 77% error of Ω_2 for Er^{3+} doped GLS glass [Ye96]. The error for the radiative rates is typically smaller than 20% and the Judd-Ofelt analysis is still a valuable tool for gaining knowledge about the radiative properties of the RE ions.

The radiative emission rates, A, obtained from the Judd-Ofelt calculations can be used along with the measured emission spectra, I(λ), to calculate the emission cross sections from the Füchtbauer-Ladenburg equation [Aul82]:

$$\sigma_{em,FL}(\lambda) = \frac{A\lambda^5 I(\lambda)}{8\pi n^2 c \int \lambda I(\lambda) d\lambda} \tag{3.1.12}$$

This equation can be applied to all transitions with known radiative emission rates and emission spectra.

A second method to calculate the emission cross sections for transitions to the ground state from the measured absorption cross section, $\sigma_{abs}(\lambda)=\alpha(\lambda)/N_{RE}$, *without* knowledge of the emission rates was proposed by McCumber [McC64]:

$$\sigma_{em,MC}(\lambda) = \sigma_{abs}(\lambda)\frac{Z_l}{Z_u}\exp\left(\frac{E_{ZL} - 10^4 / \lambda}{kT}\right) \qquad (3.1.13)$$

The McCumber transform also generates the shape of the emission cross section spectrum from a measurement of the absorption spectrum. It requires the knowledge of E_{ZL}, the energy separation between the lowest Stark level of the upper manifold to the lowest Stark level of the ground state, and the knowledge of the position of the Stark levels within these multiplets in order to calculate the partition functions Z_l and Z_u. If this information is not available, as it is the case for the RE ions in GLS glass, a modified McCumber method can be used [Min91]. This method is described in more detail in section 3.7 where it is first used in this thesis for Dy^{3+} and is applied to Ho^{3+}, Tm^{3+}, and Yb^{3+} in later sections.

Back to the discussion of equation 3.1.1 (page 17). Term 4, $V_{\text{ion-ion}}$, describes the interaction between two or more RE ions, i.e. ion-ion energy transfer. The energy transfer can be radiative or non-radiative. The theory of non-radiative energy transfer by dipole-dipole interactions was first presented by Förster [För48] and Dexter [Dex53]; a good overview over possible transfer processes was given by Auzel [Auz73].

Radiative energy transfer occurs if one ion emits a photon which is then reabsorbed by another ion. This process can distort the emission spectrum and lengthen the emission lifetime by radiation trapping, particularly in highly concentrated samples.

Non-radiative energy transfer can have the form of migration, cross-relaxation, and upconversion. The probability of such processes depends on the spectral overlap of the donor and acceptor transitions and is proportional to the reciprocal of the donor-acceptor distance to the power of six [Dex53]. The better the spectral overlap and the closer the RE ions, the higher the transfer probability will be. The transfer processes can either be beneficial, as for the energy transfer from a donor with strong absorption bands to an only weakly absorbing acceptor, the shortening of lower laser level lifetimes, or the conversion of infrared photons to visible photons in upconversion pumped lasers, or they can be deleterious when they lead to loss of excitation energy and shortened lifetimes of upper laser levels. The energy transfer can be resonant or non-resonant. The energy mismatch in the non-resonant case is provided by the absorption and emission of phonons. The transfer probability depends exponentially on the energy mismatch and is temperature dependent [Auz73].

Migration transfers energy between one type of RE ions (donor-donor transfer) until the energy is lost by emission of a photon or transfer to an acceptor ion or a trap.

A cross-relaxation process is energy transfer between two RE ions of which at least one needs to be excited and both ions end up in energy states which are *lower* than the highest initial energy level. The probability for cross-relaxation depends on the ion concentration if one involved ion is in the ground state and it depends on the excitation density if both ions need to be in an excited state. Cross-relaxations lead to shortened and non-exponential fluorescence decay times but can be useful to populate lower energy levels as in the case of Tm^{3+} (section 3.10).

Upconversion can take place between two or more excited RE ions and therefore depends directly on the excitation density and indirectly on the ion concentration. One ion ends up in an energy level which is *higher* than the highest initial excited state of the ions involved. Upconversion is the reverse of cross-relaxation. Which of the two processes is more efficient is determined by the energy mismatch. The process which emits phonons will be more important than the process which absorbs phonons since processes involving the emission of phonons are much faster than those requiring the absorption of phonons.

Energy transfer processes have been identified for a number of RE ions and co-doping schemes in GLS glass.

Section 3.2 describes the most important property of GLS glass, the low multiphonon decay rates (term 5 in equation 3.1.1). Sections 3.3 to 3.11 present more or less detailed studies of the different RE ions depending on their importance for mid-infrared devices. The sections follow the order of the Periodic Table with the exemption of Tb^{3+} which is discussed together with Tm^{3+} (3.10). Section 3.11 (Yb^{3+}) also includes co-doping experiments with Er^{3+} as an alternative co-dopant to Yb^{3+}. The spectroscopy of Nd^{3+} was included in chapter 5 because Nd^{3+} was the first and still is the only lasing ion in GLS glass. Absorption from excited states was measured in Er^{3+} and Tm^{3+} doped GLS glass and is presented in a separate chapter 4.

3.2 Non-radiative properties of gallium lanthanum sulphide glass

In addition to radiative transitions and transitions due to ion-ion interactions RE ions can also undergo transitions between electronic energy levels as a result of their interactions with vibrations of the host material. The ions make a non-radiative transition to a lower electronic state through the emission of multiple phonons. The probability of these processes depends exponentially on the number of phonons needed to bridge the energy gap, i.e. it increases exponentially with decreasing energy gap and increasing phonon energy (decreasing phonon number). The highest energy phonons, which are determined by the ionic weight and the bond strength in the host material, were found to be responsible for the multiphonon relaxation process [Rei75]. Although high non-radiative decay rates can be desirable for some situations, as for the fast non-radiative decay from a pump level to an upper laser level, they are undesirable for applications which involve transitions from energy levels with a small energy gap to the next lower lying level, e.g. mid-infrared transitions. The host dependence of the non-radiative rates is much stronger than that of the radiative rates discussed in the previous section. The search for new glass compositions with heavier glass ions and weaker bond strengths than oxide glasses first lead to the development of fluoride and later of chalcogenide glasses as hosts for RE doped devices. Fig. 3.2.1 shows the Raman spectra of silica, ZBLAN, and GLS glasses.

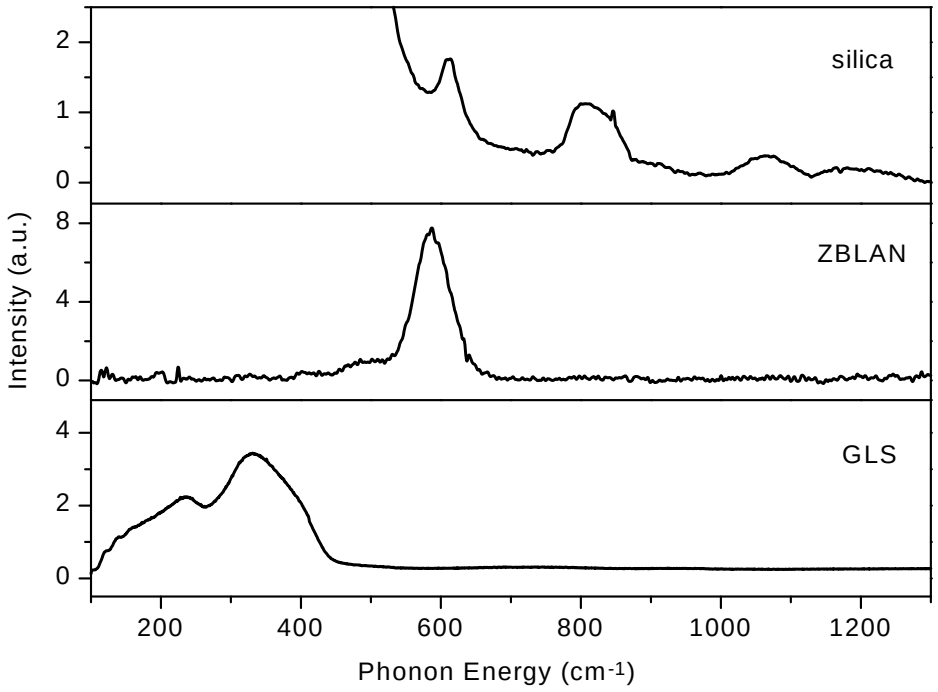

Fig. 3.2.1 Raman spectra of silica, ZBLAN, and GLS glass (courtesy of J.R. Hector)

The maximum phonon energy decreases from 1150 cm^{-1} for silica and 600 cm^{-1} for ZBLAN to 425 cm^{-1} for GLS. Although the non-radiative decay is strongly dependent on the host material it is relatively independent on the nature of the electronic states involved and on the RE ion [Rei75]. The mathematical description is complex and requires higher order perturbation theory [Lay77, Rei75, Ris68]. A simplified expression for the multiphonon decay rate, W_{mp}, can be derived for energy gaps, ΔE, larger than the maximum phonon energy, $\hbar\omega$ [Min93,Rei85]:

$$W_{mp} = B(n(T)+1)^p \exp(-\alpha\Delta E) \tag{3.2.1}$$

$n(T)$ is the Bose-Einstein occupation number and p is the number of phonons required to bridge the gap, ΔE:

$$n(T) = \frac{1}{\exp(\hbar\omega / kT) - 1} \qquad \text{and} \qquad p = \frac{\Delta E}{\hbar\omega} \tag{3.2.2}$$

W_{mp} decreases with decreasing temperature and converges towards a value W_0 for low temperatures.

One set of the empirical parameters B, α, and $\hbar\omega$ describe the multiphonon decay in a given host material for any RE ion. The parameter $\alpha = -\ln(\gamma)/\hbar\omega$ is related to the electron-phonon coupling constant γ. Whereas $\hbar\omega$ can be obtained from the Raman spectrum the parameters B and α result from a fit to the curve of the experimentally determined non-radiative decay rates versus the size of the energy gap.

The total decay rate from the RE energy level can be written as the sum of the radiative and non-radiative decay processes. The radiative rate A includes all radiative transitions from that level. The non-radiative decay rate, W_{nr}, can be split into decay (or population) by ion-ion interactions and multiphonon decay:

$$W_{total} = A + W_{nr} = A + W_{ion-ion} + W_{mp} \tag{3.2.3}$$

It should be noted that each of the parameters in equation 3.2.3 is a statistical value averaged over a large number of ions.

If the concentration of the RE ions is kept low, ion-ion interactions are negligible and the multiphonon rate is equal to the difference between the total decay rate, which is the reciprocal of the measured fluorescence decay time, and the radiative rate obtained from Judd-Ofelt calculations:

$$W_{mp} = W_{total} - A_{calc} = \frac{1}{\tau_m} - A_{calc} \tag{3.2.4}$$

A good fit requires lifetime measurements for as many energy levels and RE ions as possible. The number of data points is restricted by the number of suitable energy gaps which should be small enough to have a high ratio of non-radiative to radiative rate to minimise the error introduced by the Judd-Ofelt analysis, and which should be large enough to avoid complete fluorescence quenching. Values of the parameters B, α, and $\hbar\omega$ have been published for GLS glass and various other glasses by Reisfeld [Rei80,84,85]. This is the only set of parameters describing the multiphonon relaxations in RE doped chalcogenide glasses reported in the literature. Fig. 3.2.2 shows the dependence of the multiphonon relaxation rate on the size of the energy gap for various glasses using the published parameters and equation 3.2.1.

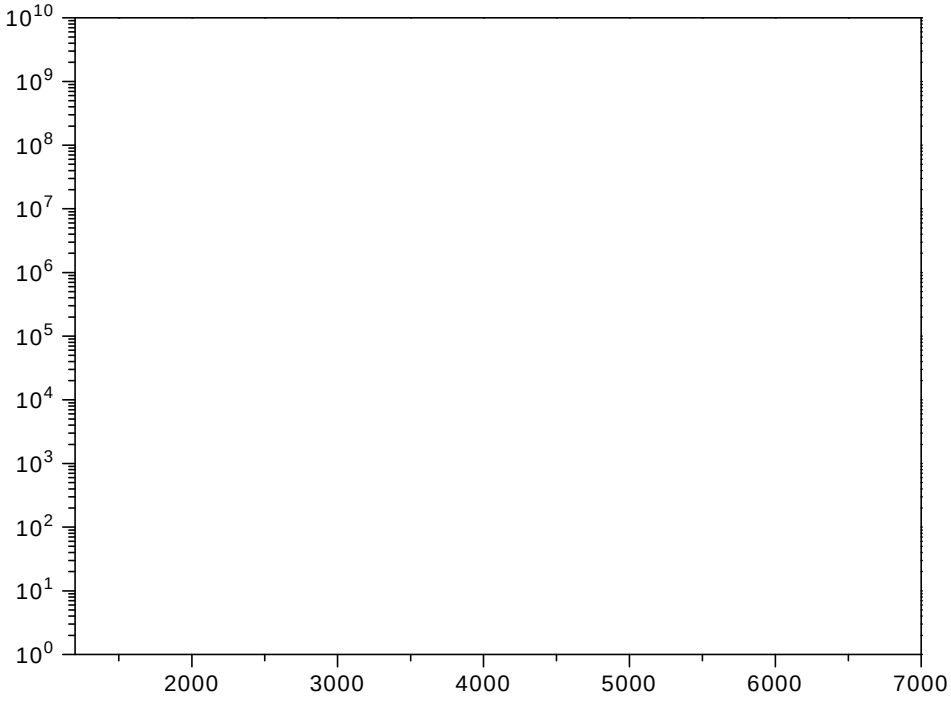

Fig. 3.2.2 Dependence of the multiphonon relaxation rate on the energy gap, and phonon energy (in brackets) for GLS and various other glasses according to Reisfeld [Rei80,84,85]

As expected the multiphonon decay rates are highest for high phonon energy glasses and decrease with decreasing phonon energy. The curve for GLS glass stands out because of the smaller slope which leads to higher non-radiative rates in these glasses compared to glasses with higher phonon energies for energy gaps larger than about 3800 cm^{-1}. Nevertheless, GLS is the glass with the lowest non-radiative rates in the 3 to 5 μm region (2000 - 3300 cm^{-1}) and therefore the best candidate for mid-infrared devices.

The three parameters *B*, α, and $\hbar\omega$ are 1×10^{6} s^{-1}, 2.9×10^{-3} cm, and 350 cm^{-1}, respectively, and lead to a value of 0.36 for the electron-phonon coupling constant [Rei80,84,85]. The electron-phonon coupling strength is one to two orders of magnitude larger than for common glasses which was attributed to the covalency of the glass bonds by Reisfeld. The parameters were obtained from a very limited set of data (Er^{3+} and Ho^{3+} only) and included emission decay times from level pairs in thermal contact and levels close to the UV absorption edge which are likely to introduce large errors in the calculated and measured lifetimes. In addition the early GLS glasses had high levels of oxide and hydroxyl impurities compared to the current low oxide GLS glasses. Since this is the only set of parameters published in the literature for a chalcogenide glass it has been used by other authors to describe the non-radiative properties of GLS and other chalcogenide glasses [Heo96,Heo97,Hew94,Shi96,Ye96].

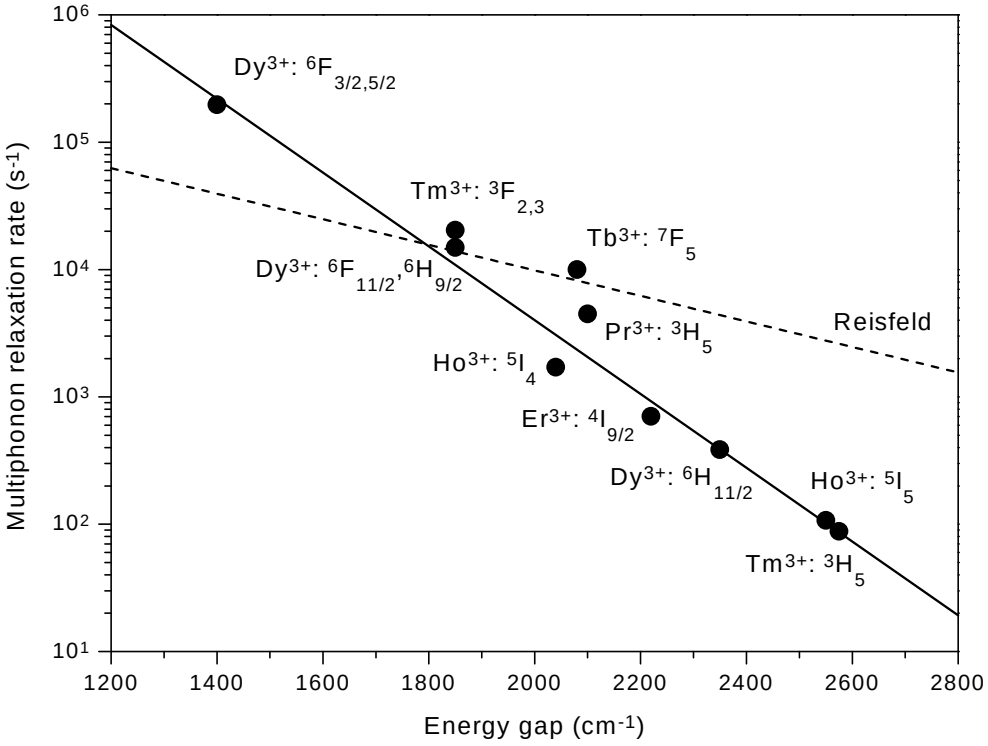

Fig. 3.2.3 Multiphonon relaxation rates obtained from Judd-Ofelt calculations and lifetime measurements for six RE ions in GLS glass with fit to the data (solid line) and fit as previously reported by Reisfeld (dashed line) [Rei80,84,85]

We have performed Judd-Ofelt calculations and lifetime measurements for a number of RE ions in GLS glass (see subsequent sections of this chapter) and calculated the multiphonon decay rates for several energy levels with small energy gaps to the next lower lying level. The energy gaps have either been

determined from the mid-infrared emission spectra, if available, or from the energy difference of the absorption peaks of the levels involved. The peak-peak definition of the energy gap corresponds nicely with the peak of the measured mid-infrared fluorescence bands. Fig. 3.2.3 shows the experimental data for ten different energy levels of six RE ions. The linear fit to the data (solid line) deviates considerably from the fit reported by Reisfeld (dashed line). With a phonon energy of 425 cm^{-1} from the Raman spectrum we obtained values of 2.5×10^{9} s^{-1} and 7.0×10^{-3} cm for the parameters B and α which are significantly different from the values of 1×10^{6} s^{-1} and 2.9×10^{-3} cm published by Reisfeld. The electron-phonon coupling constant is reduced to 0.051 compared to 0.36 before. Our slope is steeper avoiding the intersection with the curves of the other glasses for larger energy gaps (Fig. 3.2.2). Our result predicts higher multiphonon rates for gaps smaller than 1900 cm^{-1} and lower multiphonon rates for gaps larger than 1900 cm^{-1} which covers the 3-5 μm region of interest for mid-infrared devices.

A typical error in the determination of the multiphonon relaxation rate would be a measured lifetime which is shortened by ion-ion interactions giving a higher rate than the actual multiphonon rate (equation 3.2.3). This could apply to the Tm^{3+}: $^{3}F_{2,3}$, the Tb^{3+}: $^{7}F_{5}$, and the Pr^{3+}: $^{3}H_{5}$ levels in Fig. 3.2.3 which show strong lifetime quenching for higher concentrations and could not be measured in samples with sufficiently low RE doping due to the weakness of the fluorescence bands. The nature of the double-level structure of the $^{3}F_{2,3}$ Tm^{3+} levels may also cause a discrepancy between calculation and measurement. These three data point have therefore been excluded from the fitting procedure. The opposite effect, the measurement of a increased lifetime which would result in a smaller multiphonon rate than expected is much more unlikely giving us confidence in those of our experimental data which show up to two orders of magnitude smaller rates than predicted by Reisfeld. This has important consequences for calculations of the radiative quantum efficiencies for many mid-infrared transitions and improves the prospects for chalcogenide glass fibre lasers operating in this wavelength range.

The favourable non-radiative properties of GLS glass discussed in this section form the basic motivation to investigate GLS glass for its suitability as a RE doped mid-infrared laser material. The mid-infrared emission described in the following sections of this chapter “prove” the expected low non-radiative decay rates in GLS glass.

3.3 Cerium

The trivalent cerium ion (Ce^{3+}) is the first optically active ion in the lanthanide series. It has one electron in the 4f orbital and has only two 4f levels, the $^2F_{5/2}$ ground state and the $^2F_{7/2}$ excited state which is about 2200 cm^{-1} above the ground state. Emission from the $^2F_{7/2}$ level has not been reported in the literature.

Ce^{3+} is usually known for its $4f^15d^0 \leftrightarrow 4f^05d^1$ transitions which are parity allowed dipole transitions and thus have large oscillator strength. The strong interaction of the 5d orbitals with the conduction band of the host material shifts the energetic position of the 5d levels with the UV absorption edge [Sch82] causing a range of different emission wavelength from the ultraviolet in wide bandgap materials to the near-infrared in small bandgap materials [Com97,Ju96,Lei81,Mat93,Sch82a]. Laser action in the ultraviolet has been achieved in fluoride crystals [Pin94].

Red emission from the $4f^05d^1 \rightarrow 4f^15d^0$ transition with a decay time of 50 ns has been reported in Ce^{3+} doped and Ce^{3+}/Nd^{3+} co-doped β-La_2S_3 crystals [Lei81,Sch82,Sch82a]. Excitation spectra showed efficient transfer from the conduction band of the crystal to the 5d bands of the Ce^{3+} ions and from Ce^{3+} to the 4f levels of Nd^{3+} which could potentially be useful for electrically pumped rare-earth laser action in these semiconducting crystals. Similar emission and energy transfer have been reported by Mattos and Clare in Ce^{3+}/Nd^{3+} co-doped GLS glass but are not supported by our initial experiments [Mat93].

Fig. 3.3.1 shows the absorption spectrum of 1.5 mol% Ce_2S_3 doped GLS glass along with an energy level diagram. The electronic absorption edge of the glass appears at 0.5 μm and the multiphonon absorption edge at 10 μm. The UV absorption edge is similar to undoped GLS glass. Not even a long wavelength tail of the lowest 5d absorption band, which is expected to be about two orders of magnitude stronger than the $^2F_{5/2} \rightarrow {}^2F_{7/2}$ absorption band, can be seen in Fig. 3.3.1. This implies that the 5d bands lie at energies relative to the 4f ground state which are larger than the bandgap of the glass and luminescence and energy transfer to other rare-earth ions are not expected [Sch82]. In good agreement with this is the band structure model proposed by Mauricot *et al.* for γ-Ce_2S_3 which assumes that the two 4f levels lie within the bandgap of the crystal whereas the 5d orbitals are delocalised in the conduction band, so that no well defined $4f \leftrightarrow 5d$ absorption and luminescence bands can be identified [Mau96].

The GLS glasses reported in Mattos and Clare's paper had a UV transparency to shorter wavelength and a very high OH^- absorption band around 3 μm which implies that their starting materials and glasses contained most likely a high percentage of gallium and lanthanum oxide. Hence, direct comparison to our low oxide GLS glasses is not appropriate. To what extent the reported energy transfer to Nd^{3+} ions will work in our purer GLS glasses needs further investigation.

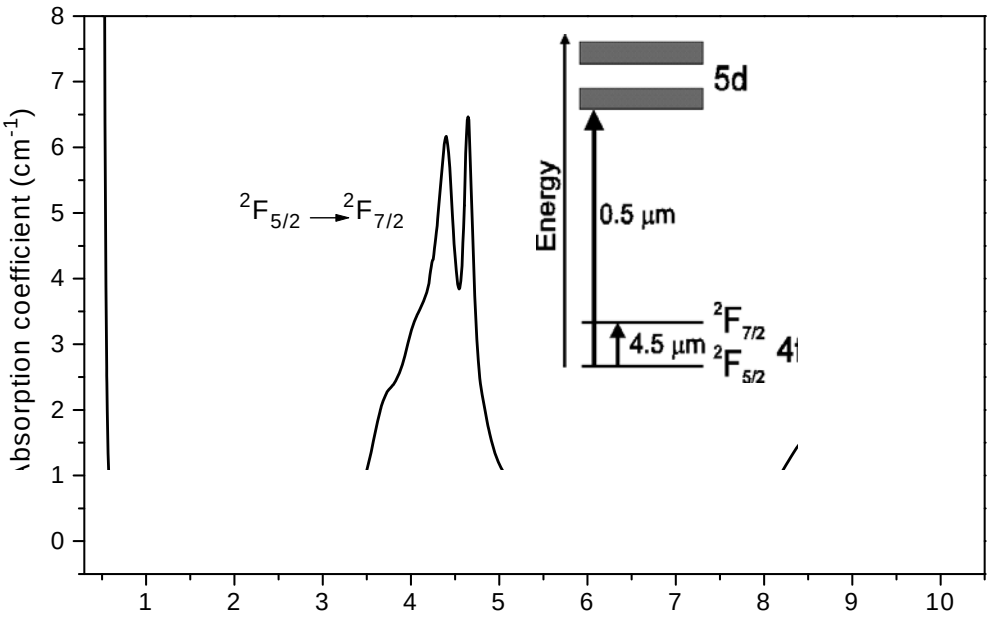

Fig. 3.3.1 Absorption spectrum of 1.5 mol% Ce_2S_3 doped GLS glass and energy level diagram

A possible use of Ce^{3+} doping in GLS glass is as a co-dopant for other rare-earth ions in order to shorten the lifetime of unsuitably long lived energy levels as it has been demonstrated in $Er^{3+}/Yb^{3+}/Ce^{3+}$ doped crystals to shorten the $^4I_{11/2}$ Er^{3+} level lifetime and increase the efficiency of the $Yb^{3+} \rightarrow Er^{3+}$ energy transfer [Sim96].

Another interesting question is how the excitation of Ce^{3+} ions into the 5d bands could change the electrical properties of the glass. Scharmer observed an increasing photocurrent in Ce^{3+} doped La_2S_3 crystals when pumping into the 5d bands [Sch82]. An amorphous semiconductor such as GLS glass, however, may behave in a different way. The electronic bandgap will be closed by a continuum of localised states most of which will be created by dangling sulphur bonds [Mot87]. Any free electrons in the conduction band will therefore immediately be captured by traps in the bandgap (See section 4.1 for more details.).

Ce^{3+} doping in GLS glass may also prove useful for increasing the efficiency of photoinduced refractive index changes as it has been reported in fluorozirconate glass fibre [Poi94].

3.4 Praseodymium

Praseodymium (Pr^{3+}) doped GLS glass was first proposed in 1992 as a promising alternative material to the existing fluorozirconate glass based 1.3 μm fibre amplifier [Bec92]. The radiative quantum efficiency of the upper level of the 1.3 μm transition ($^1G_4$) is about fifteen times larger in GLS glass (~ 60%) compared to ZBLAN (~ 4%) [Hec97,Hew94]. The potential for more efficient and cheaper 1.3 μm fibre amplifiers for telecommunications built the initial motivation to study the fabrication and spectroscopy of Pr^{3+} doped GLS glasses and glass fibres at the Optoelectronics Research Centre. The spectroscopy of the 1.3 μm transition and of the higher lying visible energy levels has been studied in detail and has been reported in a number of publications and two PhD theses [Hec98,Pea94]. Gain on the 1.3 μm transition has not been demonstrated in GLS fibre to date due to high losses and large core sizes but has been reported recently in a gallium sodium sulphide (GNS) glass fibre for the first time [Taw97]. The GNS fibre, for which the preform was prepared by an extrusion method, was doped with 750 ppm Pr^{3+}, had a core diameter of 2.5 μm, a numerical aperture of 0.31, a length of 6.1 m, a loss of 1.2 dB/m at 1.31 μm, and showed a net gain of 30 dB at 1.34 μm for 100 mW of Ti:sapphire pump power at 1.017 μm. This encouraging result shows the potential for near-infrared and mid-infrared devices in GLS fibres after successful purification of the starting materials and improved core/clad interfaces obtained from extrusion techniques.

This section will concentrate on the discussion of the emission bands at wavelengths longer than 1.3 μm which have not been measured and reported for Pr^{3+} doped GLS glasses so far.

Fig. 3.4.1 shows the absorption spectrum of 1.5 mol% Pr_2S_3 doped GLS glass and the energy level diagram with the observed fluorescent transitions. The $^1G_4$ absorption band at 1.02 μm, which is the pump level for the 1.3 μm amplifier as well as for the other transitions starting from this level, is extremely weak and shows the need for the fibre geometry with its long interaction length. In addition the $^1G_4$ level suffers from concentration quenching due to efficient cross relaxation which starts to become effective at very low Pr^{3+} concentrations of only 100 ppm (316 μs) and limits the maximum concentration to about 2000 ppm (224 μs) [Hec98]. Much stronger absorption bands are located at 1.58 and 2.0 μm for Er^{3+} laser, Tm^{3+} laser, and diode laser pumping of the lower energy levels. The absorption spectrum has been used to perform Judd-Ofelt calculations the results of which are summarised in Table 3.4.1 for the relevant energy levels [Hew94]. The calculated emission probabilities predict the strengths of the transitions in the measured fluorescence spectra and help to identify the emission bands taking the expected non-radiative rates into account.

The discussion of the fluorescence spectra is divided into two parts, emission from the $^1G_4$ level and emission from the lower Pr^{3+} levels, as it is also reflected by the division of Table 3.4.1.

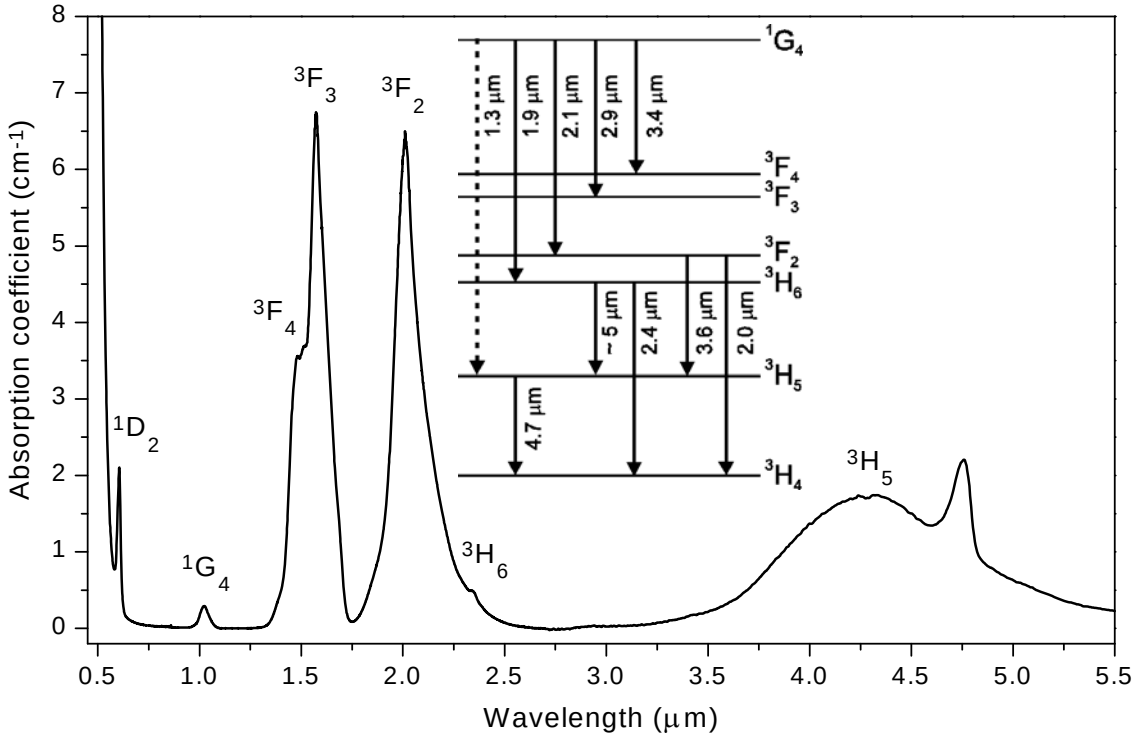

Fig. 3.4.1 Absorption spectrum of 1.5 mol% Pr_2S_3 doped GLS glass and energy level diagram with relevant Pr^{3+} levels and fluorescent transitions

Table 3.4.1 Emission wavelengths, electric-dipole transition rates, and branching ratios for transitions from the $^1G_4$ level (a) and the three lower levels (b) in Pr^{3+} doped GLS glass ($\Omega_2 = 7.3\times10^{-24}$ m^2, $\Omega_4 = 6.2\times10^{-24}$ m^2, $\Omega_6 = 3.9\times10^{-24}$ m^2) [Hew94]

a)

Transition	λ (μm)	A_{ed} (s^{-1})	β (%)
$^1G_4 \rightarrow {}^3F_4$	3.4	71	3.6
$\rightarrow {}^3F_3$	2.9	13	0.7
$\rightarrow {}^3F_2$	2.1	14	0.7
$\rightarrow {}^3H_6$	1.9	740	38
$\rightarrow {}^3H_5$	1.3	1020	52
$\rightarrow {}^3H_4$	1.0	103	5.3

b)

Transition	λ (μm)	A_{ed} (s^{-1})	β (%)
$^3F_2 \rightarrow {}^3H_6$	14	1.4	<0.1
$\rightarrow {}^3H_5$	3.6	178	9
$\rightarrow {}^3H_4$	2.0	1865	91
$^3H_6 \rightarrow {}^3H_5$	4.5	25	34
$\rightarrow {}^3H_4$	2.4	48	66
$^3H_5 \rightarrow {}^3H_4$	4.7	61	100

Emission from the $^1G_4$ level

As mentioned before the 1.3 μm transition to the first excited state will not be discussed here, and the same applies to the 1.0 μm ground state transition. Of the remaining four transitions from the $^1G_4$ level at about 1.9, 2.1, 2.9, and 3.4 μm, the latter is the most interesting for a mid-infrared laser due its spectral overlap with the fundamental absorption band of hydrocarbon gases such as methane, propane, and butane.

The first three emission bands are shown in Fig. 3.4.2.

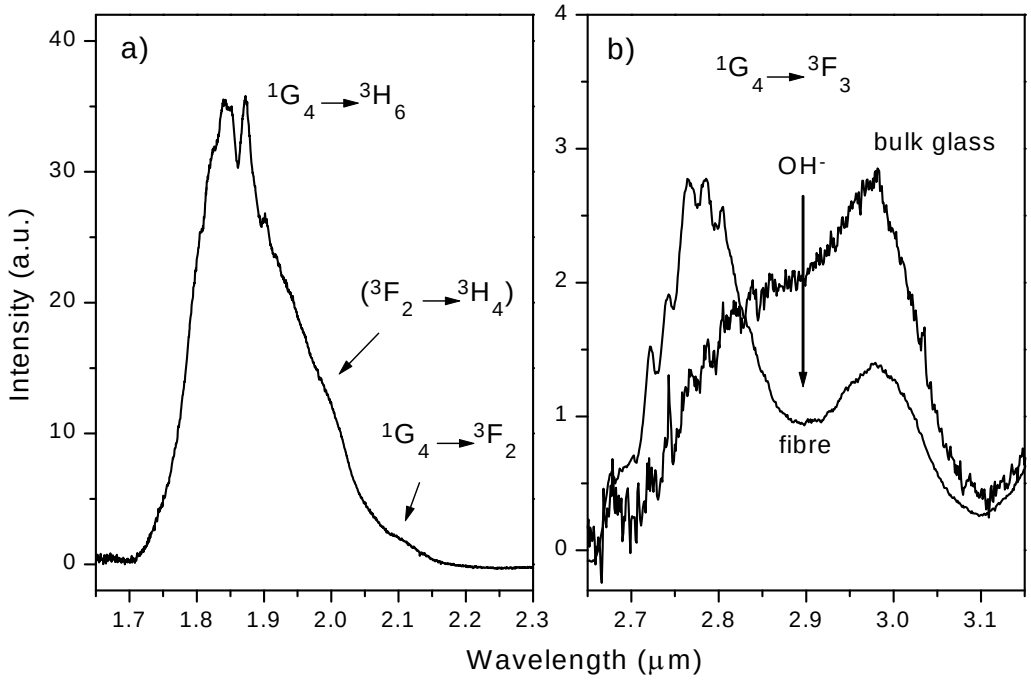

Fig. 3.4.2 Fluorescence spectra of a 2000 ppm Pr^{3+} doped GLS bulk glass (a and b) and a 70 cm long, 500 ppm Pr^{3+} doped GLS glass fibre (b only) pumped with a 1.064 μm Nd:YAG laser (a and b not to scale, see text)

The fluorescence was collected from the side of a 2000 ppm Pr^{3+} doped GLS bulk glass sample in order to avoid distortion of the spectra due to reabsorption by Pr^{3+} ions in the ground state and due to absorption features of the glass host. Measured from the end of a fibre sample the long wavelength edge of the 1.9 μm emission band is reabsorbed by the strong 2.0 μm $^3F_2$ absorption band (Fig. 3.4.1) and the 2.9 μm emission band is distorted by the absorption of hydroxyl (OH^-) impurities in the glass (Fig. 3.4.2.b). OH^- groups can not only absorb emission from the $^1G_4$ level but they can also quench the lifetime of this level by non-radiative energy transfer from Pr^{3+} ions to the OH^- impurities as it has been reported for other chalcogenide glasses [Fab94]. The concentration of OH^- impurities should therefore be kept as low as possible.

The 1.9 μm emission band is mainly due to the $^1G_4 \rightarrow {}^3H_6$ transition which is expected to be about fifty times stronger than the $^1G_4 \rightarrow {}^3F_2$ transition from the

data in Table 3.4.1 which is also reflected by the spectrum in Fig. 3.4.2.a. The 1.9 μm band will also have a small contribution from the $^3F_2 \rightarrow {}^3H_4$ transition which is thermally coupled to the $^3H_6$ level and has a large radiative rate (Table 3.4.1). The 2.9 μm emission is about one hundred times weaker (sixty times according to Table 3.4.1) than the 1.9 μm band which in turn is weaker than the 1.3 μm emission. The 3.4 μm emission is several times stronger than the 2.9 μm emission but nevertheless it is obvious that strong amplified spontaneous emission (ASE) at 1.3 and/or 1.9 μm may become problematic and clamp the gain of the 3.4 μm transition.

The 3.4 μm fluorescence overlaps with the absorption bands of hydrocarbon gases. The overlap and strength of the hydrocarbon absorption was determined by measuring the transmission of the 3.4 μm emission through a gas sample cell filled with either butane or town gas (mixture of methane, butane, and others) in order to determine the suitability of a Pr^{3+} doped GLS glass fibre fluorescence or laser source for gas sensing applications. The set-up is presented in section 7.1.

The GLS glass sample used for the measurements was doped with 0.1 mol% Pr_2S_3 and co-doped with 2 mol% Er_2S_3 which allows pumping at 0.8 μm using the $Er^{3+} \rightarrow Pr^{3+}$ energy transfer. The co-doping with Er^{3+} will be explained in more detail in section 3.11.

Fig. 3.4.3.a and b show the 3.4 μm $^1G_4 \rightarrow {}^3F_4$ Pr^{3+} transition as measured through the gas cell filled with air and different concentrations of either butane (a) or town gas (b). The graph shows the excellent overlap of the Pr^{3+} emission with the fundamental hydrocarbon absorption bands. The butane absorption band (a) can also be identified in (b) by the two absorption peaks at 3.35 and 3.46 μm. The additional absorption peak at 3.3 μm in (b) is due to the presence of methane in town gas. The butane concentration was estimated from the strength of the 3.35 μm absorption peak in the measured Pr^{3+} fluorescence spectra using a value of 4.21×10^{-4} ppm^{-1} m^{-1} for the absorbance of butane at this wavelength [Mit98]. The lowest concentration measured was about 3000 ppm (0.3%). A lower concentration of 500 ppm would correspond to a decrease in fluorescence intensity at a wavelength of 3.3 μm of about 10%, and 50 ppm would correspond to a decrease of 1%. The detection limit would therefore be several hundred ppm but can be increased by increasing the length of the gas cell and by lasing on the 3.4 μm transition.

Emission cross sections for potential laser transitions starting from the $^1G_4$ level were determined for the important 3.4 μm transition only. A peak emission cross section of 0.86×10^{-20} cm^{-1} at 3.4 μm was obtained from the results of the Judd-Ofelt calculation (Table 3.4.1) and a corrected emission spectrum.

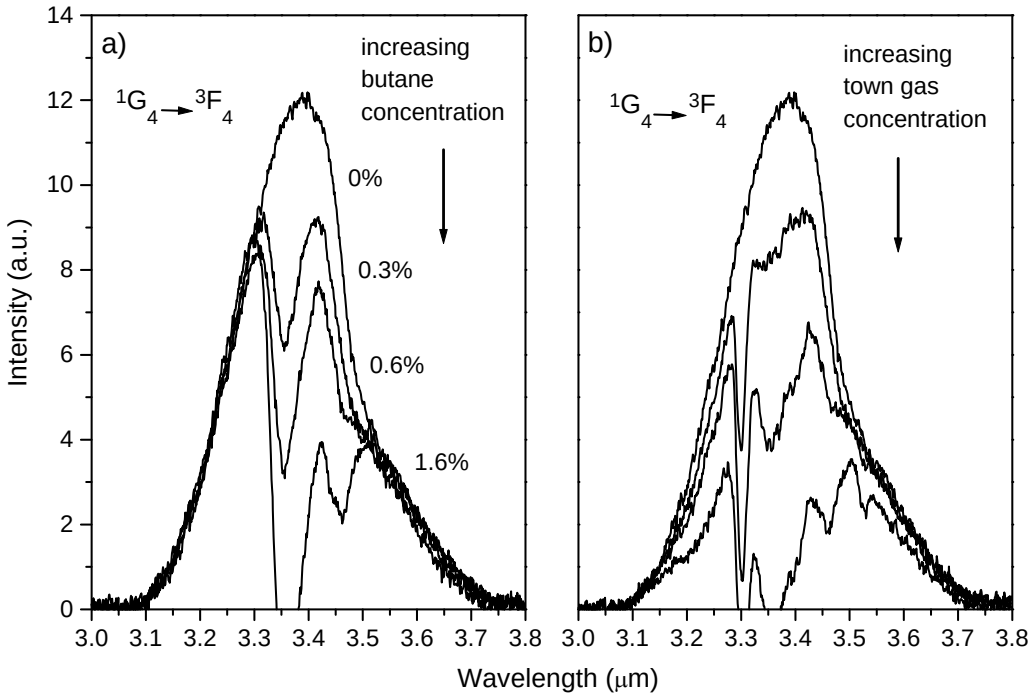

Fig. 3.4.3 Pr^{3+} emission measured through gas cell filled with air and different concentrations of either butane (a) or town gas (b)

Emission from the $^3F_2$, $^3H_6$, and $^3H_5$ levels

While emission from the $^1G_4$ level can also be obtained in fluorozirconate glass hosts, emission from the three lower Pr^{3+} levels has not been observed due to multiphonon quenching. The situation changes in chalcogenide glasses with lower multiphonon decay rates.

For $^1G_4$ pumping a weak 2.4 μm emission band was detected between the strong 1.9 and 2.9 μm bands (Fig. 3.4.4.a). From comparison of the features on the absorption and fluorescence spectra and from the transition assignments of other workers with Pr^{3+} doped host materials this fluorescence can be assigned as the $^3H_6 \rightarrow {}^3H_4$ ground state transition [Gan94,Sha97].

A diode pumped Tm:YAG laser was used to excite the lower energy levels directly into the $^3F_2$ level at 2 μm. The resulting broad emission spectrum extends from 3.4 μm beyond the detection limit of the fluorescence set-up (Fig. 3.4.4.b). The fluorescence peak at 3.6 μm can be identified as the $^3F_2 \rightarrow {}^3H_5$ transition [Gan94]. The $^3F_2$ level which is coupled to the underlying $^3H_6$ level is thermally populated with a few percent of the combined ($^3F_2$,$^3H_6$) population and has a relatively high radiative rate. The fluorescence peak at 4.7 μm mirrors the characteristic shape from the $^3H_4 \rightarrow {}^3H_5$ absorption band (Fig. 3.4.1) and can therefore be attributed to the transition from the $^3H_5$ level to the ground state. The measured fluorescence band will also have a contribution from the $^3H_6 \rightarrow {}^3H_5$ transition which cannot be identified clearly in the spectrum but is typically

found at wavelength slightly shorter than the 4.7 μm band at around 4.5 μm [Gan94,Sha97]. The fluorescence spectrum also shows some residual CO_2 absorption at 4.23 μm despite correction of the spectrum with a blackbody radiation source due to changing CO_2 content in the laboratory atmosphere. The 4.7 μm fluorescence overlaps with a strong carbon monoxide (CO) absorption band and a fluorescence or laser source at this wavelength could find application as a CO gas sensor.

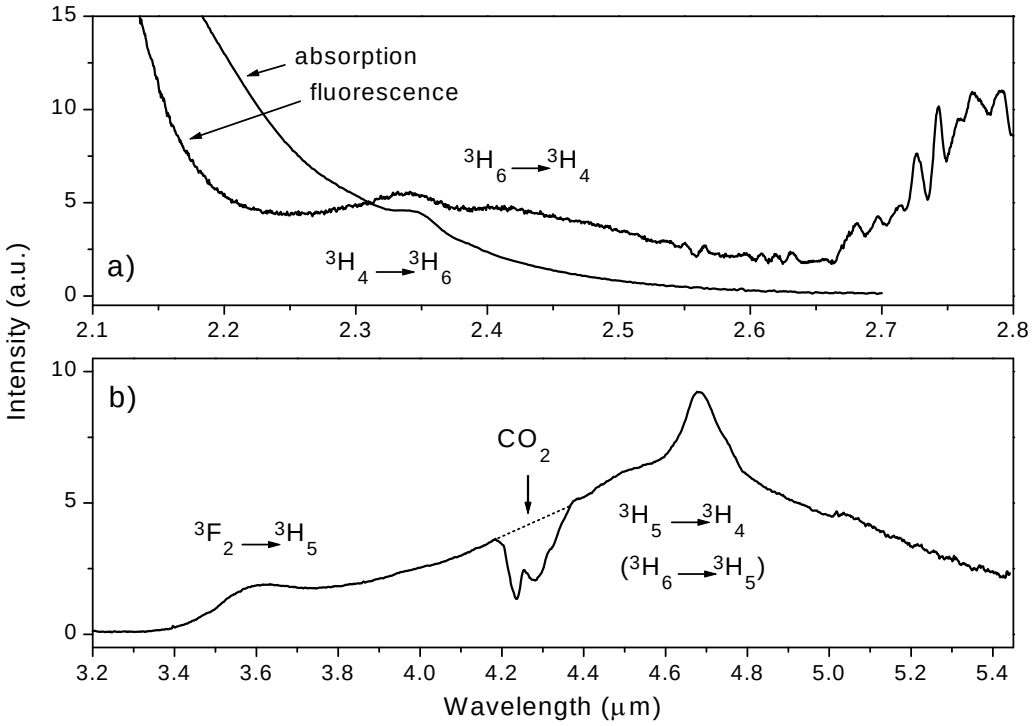

Fig. 3.4.4 Emission from three lower Pr^{3+} levels:
a) Fluorescence from 2 m long, 500 ppm Pr^{3+} doped GLS fibre pumped with 1.064 μm Nd:YAG laser and absorption spectrum
b) Fluorescence from 2000 ppm Pr^{3+} doped GLS bulk glass pumped with 2 μm Tm:YAG laser

For lifetime measurements the 2 μm Tm:YAG pump laser was modulated using a mechanical chopper with an on-to-off ratio of 1:40 in the focus of a 10 cm focal length lens. The fluorescence decay time of the 4.5 and 4.7 μm emission bands was measured with an InSb detector through a 4 μm long wavelength pass filter. The measured lifetimes reflect a combined lifetime of the ($^3F_2$,$^3H_6$) and $^3H_5$ levels which are expected to have similar lifetimes because they have similar energy gaps to the next lower lying level and their decay will be dominated by multiphonon processes. The decay time of the > 4 μm emission is about 220 μs for 200 ppm Pr^{3+} and decreases due to concentration quenching to about 30 μs

for 20500 ppm (1.5 mol%). The radiative lifetimes calculated from the data in Table 3.4.1 would be 13700 and 16400 μs for the ($^3F_2$,$^3H_6$) and $^3H_5$ levels, respectively, showing the detrimental effect of the multiphonon decay.

As for the $^1G_4$ level (page 31) concentration quenching limits the maximum useful Pr^{3+} concentration to about 2000 ppm. The lifetime decreases from 220 μs for 200 ppm to 160 μs for 2000 ppm and 30 μs for 20500 ppm. However, low concentrations do not require long fibre lengths for laser transitions from the lower Pr^{3+} levels since these levels can be excited by pumping the 1.58 μm and 2.01 μm absorption bands which are much stronger than the 1.02 μm $^1G_4$ absorption. One absorption length is about 1.5 cm at 1.58 and 2.01 μm compared to 35 cm at 1.02 μm for a concentration of 2000 ppm (Fig. 3.4.1, page 32).

Laser operation on the above mid-infrared Pr^{3+} transitions has not been achieved in glasses to date but was reported in crystals ($^1G_4 \rightarrow {}^3F_4$ in $BaYb_2F_8$ at 3.6 μm [Kam87] and $^3H_5 \rightarrow {}^3H_4$ in $LaCl_3$ at 4.9 μm [Kue89,Koc86]).

Even longer wavelength laser emission was obtained for transitions from the $^3F_3$ level at 5.2 μm (to $^3H_6$) and 7.2 μm (to $^3F_2$) in $LaCl_3$ crystals and represent the two longest laser wavelengths in RE doped materials to date [Bow94, Bow96]. Fluorescence from this level was also reported in selenide glasses (AsGeSe and BIGGSe) [Gu96,Sha97] but was not observed in GLS glass suggesting that multiphonon quenching limits the useful wavelengths range for mid-infrared fluorescence for our host material to 2-5 μm.

In conclusion, Pr^{3+} doped GLS glasses and fibres showed a number of infrared emission bands of which the 3.4 and 4.7 μm bands in particular are useful for mid-infrared gas sensing of hydrocarbons and carbon monoxide. Similar mid-infrared emission from Pr^{3+} doped chalcogenide glasses was not reported before in sulphide glasses but only in even lower phonon energy selenide glasses.

It should be mentioned for completeness that Pr^{3+} doped GLS glass fibre has been considered for its potential use as a saturable absorber at the 1.5 μm telecommunications wavelength due to its strong absorption band in this wavelength region (Fig. 3.4.1).

3.5 Samarium

Samarium ions have two stable valence states, the divalent and the trivalent, depending on the host material and the fabrication process. The first laser operation in a RE doped material was demonstrated in Sm^{2+} doped CaF_2 crystals [Sor61]. The divalent state has been reported in silicate glasses [Nog94, Oh97] and the trivalent state in silica and phosphate glasses [Far92,Pat97]. Both states can be present simultaneously [Oh97] and the trivalent state can be reduced to the divalent by hydrogenation [Nog94]. In the sulphide crystal $SmNbS_3$ samarium exists mainly in the trivalent state and the number of Sm^{2+} ions is less than a few percent of the number of Sm^{3+} ions suggesting a similar situation in a sulphide glass [Ohn92].

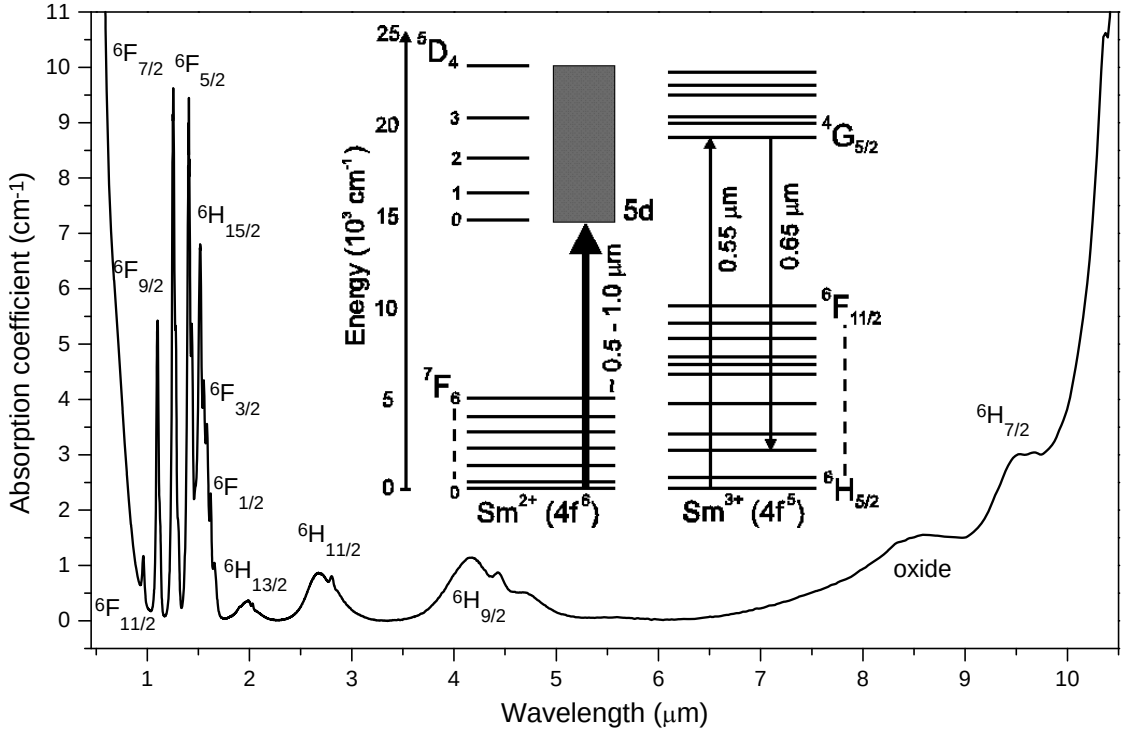

Fig. 3.5.1 Absorption spectrum of 1.5 mol% Sm_2S_3 doped GLS glass and energy level diagrams of Sm^{2+} and Sm^{3+} [Far90,Law91,Oh97]

Fig. 3.5.1 shows the absorption spectrum of 1.5 mol% Sm_2S_3 doped GLS glass and the schematic energy level diagrams of Sm^{2+} and Sm^{3+}. The energy levels of Sm^{3+} are split into two main groups separated by an energy gap of about 9500 cm^{-1} making the $^4G_{5/2}$ level the only metastable level in the system. Laser operation on the $^4G_{5/2} \rightarrow {}^6H_{9/2}$ transition at 0.65 μm was obtained in silica glass fibre [Far90]. The absorption spectrum in Fig. 3.5.1 shows the absorption bands of the eleven levels of the lower group from 0.96-9.5 μm while the absorption bands of the higher group overlap with the UV absorption of the

glass. The 9.5 μm $^6H_{5/2} \rightarrow {}^6H_{7/2}$ absorption is the longest measured in this work and cannot be detected in conventional glass hosts due to overlapping multiphonon absorption bands.

Mid-infrared fluorescence from the lower set of the Sm^{3+} levels was not observed under 0.96 μm Ti:sapphire pumping. The transitions between the closely spaced levels are dominated by non-radiative multiphonon decay.

While active applications of Sm^{3+} doped GLS glass can be ruled out it may still be interesting for passive applications using the strong near-infrared absorption bands. Sm^{3+} doped silica fibres have for example been used for fast optical switching and self-frequency locking of erbium doped fibre lasers [Lia96,Wu96]. Similar devices in GLS glass fibres, potentially in the mid-infrared, may also make use of the Sm^{3+} absorption bands.

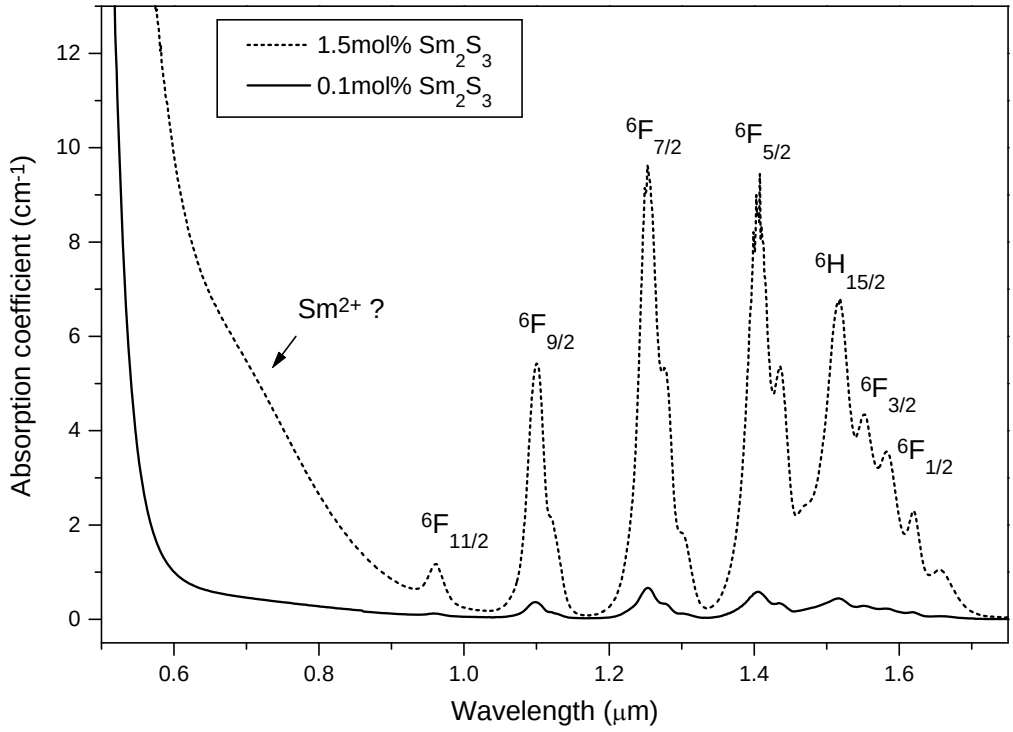

Fig. 3.5.2 Absorption spectra of 0.1 and 1.5 mol% Sm_2S_3 doped GLS glass

In addition to the Sm^{3+} absorption bands a strong and unstructured absorption in the 0.5-1.0 μm region closes the visible transmission window of GLS glass leading to completely black glasses for the 1.5 mol% concentration. This absorption is shown in more detail in Fig. 3.5.2 for concentrations of 0.1 and 1.5 mol% Sm_2S_3. The absorption can most likely be attributed to the tail of the strong dipole-allowed $4f^6 \rightarrow 4f^5 5d^1$ transition of Sm^{2+} in the UV and visible region with cross sections about two orders of magnitude larger than for the 4f absorption bands (see inset in Fig. 3.5.1) [Law91,Oh97]. The 0.1 mol% sample is transparent in the visible but its absorption spectrum is identical to that of the

1.5 mol% sample if multiplied by a factor of fifteen which indicates that the Sm^{2+}/Sm^{3+} ratio is constant. Red to infrared fluorescence from Sm^{2+} has not been investigated to date but may be observed in future experiments.

The presence of Sm^{2+} in GLS glass may increase its photosensitivity. Photoinduced refractive index changes have been reported in Sm^{2+}/Sm^{3+} doped silicate fibre and are attributed to the photoionisation of Sm^{2+} which is supported by the simultaneous bleaching of the Sm^{2+} absorption band [Oh97]. Whether this process can be observed in GLS glass and to what extend the transfer of an electron could change the electronic properties of the glass, as discussed earlier for Ce^{3+}, needs further investigation.

3.6 Europium

Europium is known to have the most stable divalent state among the RE's. Eu^{2+} doped materials are characterised by a strong absorption and emission band around 400 nm due to the dipole allowed $4f^7 \leftrightarrow 4f^6 5d^1$ transition and are usually used as blue phosphors [Tsu97]. The trivalent state of europium can for example be achieved in silicate glasses and shows a number of 4f absorption bands in the mid-infrared and visible wavelengths regions [Gat97]. Eu^{3+} is known for the possibility of vibronic sideband measurements and for the strong red emission from the hypersensitive $^5D_0 \rightarrow {}^7F_2$ transition [Gat97] and could potentially show mid-infrared emission from the lower energy levels.

Europium sulphide powder is available only in the form of EuS already indicating that the most likely state in GLS will be divalent. Ga:Eu:S glasses have a tendency to crystallise and show a restricted glass forming range compared to other RE's [Bar92,Fla83,Kum94,Mat93]. We doped GLS and oxide modified GLS ($70Ga_2S_3$:$30La_2O_3$) with 1000 ppm wt. EuS and measured the absorption spectra. Both samples did not have any absorption features within the optical transmission window of the glasses showing that europium is incorporated in the divalent state. The blue 5d absorption band is degenerate with the UV absorption of the glass which may, depending on the energetic position of the 5d band relative to the conduction band, change the electronic properties of the glass under optical pumping of Eu^{2+} or increase its photosensitivity as discussed earlier for Ce^{3+} and Sm^{2+}. Fluorescence experiments with espect to visible Eu^{2+} emission from the 5d levels have not been performed yet. Eu^{2+} is of no further interest for active mid-infrared applications, while Eu^{3+} could have been.

3.7 Dysprosium

The dysprosium ion (Dy^{3+}) has been studied to a much smaller extend than the more common rare-earth ions such as neodymium, erbium, and thulium. In particular Dy^{3+} doped glasses have hardly been investigated at all. This apparent lack of interest is caused by the nature of the energy level structure which is shown in Fig. 3.7.1 (See page 45, Fig. 1 for a Dy^{3+} absorption spectrum).

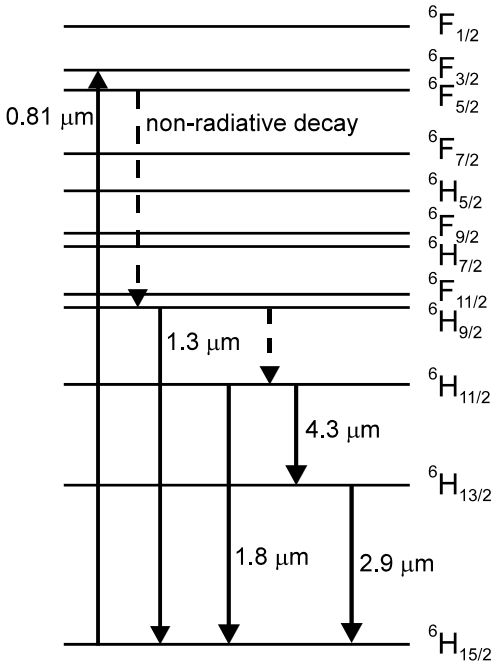

Fig. 3.7.1 Energy level diagram of Dy^{3+} along with pump and fluorescent transitions

The energy levels up to an energy of about 13300 cm^{-1} (0.75 μm, $^6F_{1/2}$) are separated by energy gaps smaller than 3300 cm^{-1}, i.e. fluorescence from these energy levels is quenched in conventional oxide glasses and oxide crystals. Emission is usually observed in the visible wavelength range from the $^4F_{9/2}$ level which is the lower level of a second set of closely spaced energy levels at energies of 20800 cm^{-1} (0.48 μm) and higher (not shown in Fig. 3.7.1) [Tan95]. These energy levels are not measurable in GLS glass due to the UV absorption edge at 0.5 μm. However, emission from the lower set of energy levels is observed in low phonon energy host materials. In fact the 3.022 μm laser demonstrated in a Dy^{3+} doped BaY_2F_8 crystal in 1973 was the rare-earth laser with the longest emission wavelength at that time [Joh73]. It was followed by a 4.34 μm laser in a Dy^{3+} doped YLF crystal in 1984 showing the potential of Dy^{3+} as an active ion for mid-infrared fibre lasers [Bar84].

Recently Dy^{3+} doped chalcogenide glasses attracted much interest for their potential application as a 1.3 μm optical amplifier for telecommunications (Fig. 3.7.1) [Hew94a,Sam94,Tan95,Wei94]. The 1.3 μm level, which is completely quenched in fluoride and oxide glasses due to strong multiphonon decay across the small energy gap of 1850 cm^{-1} to the next lower level, has a radiative quantum efficiency of 13% in GLS glass. Based on this value even higher quantum efficiencies are expected for the $^6H_{11/2}$ and $^6H_{13/2}$ levels which have larger energy gaps to the next lower level (Fig. 3.7.1). Indeed 2.9 μm and 4.3 μm emission have been reported from Dy^{3+} doped chalcogenide glasses [Bra97,Heo95,Heo97,Heo97a]. The following paper (paper 2) describes the spectroscopic properties of Dy^{3+} doped GLS glass with respect to the 1.8, 2.9, and 4.3 μm transitions of which the 4.3 μm transition is of particular interest for carbon dioxide sensing (Fig. 3.7.1). Spectroscopic information about the 1.3 μm transition in GLS including a Judd-Ofelt analysis can be found in [Hew94a,Sam94,97,98]. Paper 2 is followed by a discussion of the concentration and temperature dependence of the lifetime of the $^6H_{11/2}$ level which is the upper level of the 4.3 μm transition. Section 3.7 closes with a brief introduction to the phenomenon of site-selectivity of Dy^{3+} ions in GLS glass. The possibility of co-doping Dy^{3+} with Er^{3+} is discussed in section 3.11.

Spectroscopic data of the 1.8, 2.9 and 4.3 μm transitions in dysprosium-doped gallium lanthanum sulfide glass

***T. Schweizer**, D.W. Hewak, B.N. Samson, and D.N. Payne*

Abstract

Infrared emission at 1.8, 2.9, and 4.3 μm is measured in dysprosium-doped Ga:La:S glass when excited at 815 nm. Emission cross sections were calculated using Judd-Ofelt analysis, the Füchtbauer-Ladenburg equation, and the theory of McCumber. The στ-value for the 4.3 μm transition is about 4000 times larger in the Ga:La:S glass than it is in a dysprosium-doped YLF crystal which has lased on this transition. The large στ-value and the recently reported fiberisability of Ga:La:S glass show the potential of an efficient, low threshold, mid-infrared fibre laser. The fluorescence peak at 4.3 μm coincides with the fundamental absorption of atmospheric carbon dioxide, making the glass a potential laser source for gas sensing applications.

A number of important properties including the low phonon energy, the high refractive index, and the high rare-earth solubility make the chalcogenide glass Ga:La:S an interesting host material for rare-earth ions. The low phonon energy of about 425 cm^{-1} results in low non-radiative decay rates of rare-earth energy levels and the high refractive index of 2.4 results in high radiative emission rates. These two effects lead to much higher radiative quantum efficiencies for all transitions originating from energy levels with a small energy gap to the next lower lying level. This gives rise to new rare-earth transitions that cannot be observed in conventional silica glasses or low phonon fluoride glasses like ZBLAN. Examples in other Dy^{3+}-doped chalcogenide glasses are the 1.34 μm, 1.76 μm, and 2.86 μm fluorescence in Ge:Ga:S glass and the 2.98 μm and 4.4 μm fluorescence in As_2S_3 glass [1,2]. Another effect of the low phonon energy is a shift of the multiphonon absorption edge to longer wavelengths causing infrared transparency with a loss minimum around 5 μm. All these properties make Ga:La:S glass an ideal candidate for a mid-infrared rare-earth laser host material.

In this paper we present spectroscopic measurements of Dy^{3+}-doped Ga:La:S glass. The emission cross sections of the 1.76, the 2.83, and the 4.27 μm transitions were calculated from the fluorescence spectra using the Füchtbauer-Ladenburg equation and the results of a Judd-Ofelt analysis. These values are compared with those obtained from the absorption spectrum using the modified theory of McCumber after Miniscalco and Quimby [3]. Room temperature laser operation on the 4.3 μm transition was achieved by Barnes et al. in a Dy^{3+}-doped $LiYF_4$ (YLF) crystal [4]. Comparison of the emission cross sections and

Paper 2: published in Opt. Lett. **21** (1996) 1594

lifetimes of YLF and Ga:La:S show the potential of a 4.3 μm laser in the glass with a much lower threshold than in YLF. We estimate a threshold 4000 times smaller indicating the possibility of efficient diode pumping. A further decrease of the threshold could be achieved by using Dy^{3+}-doped Ga:La:S glass fibre [5]. A laser source at this important wavelength would find application in CO_2 gas sensing.

A series of gallium lanthanum sulphide (Ga:La:S) glasses were melted with the molar ratio $70Ga_2S_3$:$30La_2S_3$ and doped with Dy^{3+} by substituting between 0.033 mol% and 0.652 mol% of the La_2S_3 by Dy_2S_3. A sample of 7.8 mm thickness and doped with 9900 ppm by weight (0.652 mol%) of Dy_2S_3 was used for absorption measurements. The absorption spectrum from 500 nm to 3000 nm was measured with a Perkin Elmer Lambda 9 spectrophotometer. A second spectrum from 1540 nm to 3400 nm was measured with a Fourier transform spectrometer (Perkin Elmer System 2000 FT-IR) and added to the first spectrum.

Fluorescence measurements were performed with the above mentioned highly doped sample which was excited by a Ti:sapphire laser operating at 815 nm. Two CaF_2-lenses imaged the fluorescence onto the entrance slit of a 300 mm focal length monochromator containing a grating blazed at 3 μm. A third CaF_2-lens imaged the exit slit onto an InSb detector cooled with liquid nitrogen. The measured signal was processed by a lock-in amplifier and a computer.

For correction measurements the sample was replaced by a black-body source (Optronic Laboratories, Model OL 480) operating at temperatures of 400°C, 760°C, and 900°C for the 4.27 μm, the 2.83 μm, and the 1.76 μm transitions, respectively.

Lifetime measurements of the $^6H_{11/2}$ and the $^6H_{13/2}$ level were performed using the chopped output of the Ti:sapphire laser at 815 nm and a suitable set of filters for wavelengths selection of the levels. The 1.76 μm emission of the $^6H_{11/2}$ level was detected with an InGaAs detector and the 2.83 μm emission of the $^6H_{13/2}$ level with an InSb detector. The fluorescence decay curves were averaged with a TEK2232 digital storage oscilloscope and transferred to a PC for the fitting procedure.

The absorption spectrum is shown in Fig. 1. The relatively weak absorption of the closely spaced $^6F_{3/2}$,$^6F_{5/2}$ levels with a peak at 815 nm was used to excite the Dy^{3+}-ions for fluorescence and lifetime measurements. The excited ions decay mainly via fast non-radiative processes down to the metastable $^6H_{11/2}$ and $^6H_{13/2}$ levels. We measured three different infrared transitions originating from these two levels.

Paper 2: published in Opt. Lett. **21** (1996) 1594

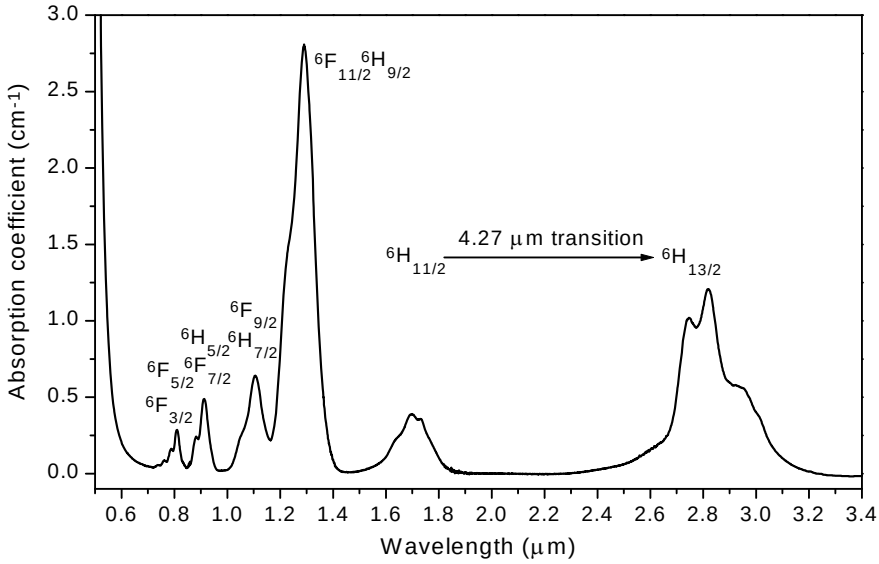

Fig. 1 Room temperature absorption spectrum of 9900 ppm Dy^{3+} doped Ga:La:S glass

The 1.76 μm transition ($^6H_{11/2} \rightarrow {}^6H_{15/2}$) and the 2.83 μm transition ($^6H_{13/2} \rightarrow {}^6H_{15/2}$) were used to obtain the lifetimes of the $^6H_{11/2}$ and the $^6H_{13/2}$ levels, respectively. The measured lifetimes of the 9900 ppm Dy^{3+}-doped glass are 540 μs for the $^6H_{11/2}$ level and 510 μs for the $^6H_{13/2}$ level, compared to the lifetimes of 1300 μs and 3600 μs, respectively, for a Dy^{3+}-doped glass with the much lower ion concentration of 500 ppm. This shows that the sample used in the fluorescence experiments suffers from concentration quenching. It should be mentioned here that the measured $^6H_{13/2}$ lifetime is influenced by the decay of the $^6H_{11/2}$ level. For more accurate measurements the $^6H_{13/2}$ level should be excited resonantly around 2.7 μm.

The fluorescence spectra of the 1.76 μm, the 2.83 μm, and the 4.27 μm transitions are shown in Fig. 2 and 3. The peak of the 4.27 μm emission spectrum overlaps exactly with the fundamental absorption of the atmospheric CO_2 as shown in Fig. 2.a. Fig. 2.b shows the absorption of CO_2 in the background spectrum of a Fourier transform spectrometer using a mid-infrared light source. The two emission peaks of the corrected fluorescence spectrum in Fig. 2.c can also be seen in the 2.83 μm fluorescence spectrum but not in the 1.76 μm fluorescence spectrum and might be caused by a Stark splitting of the $^6H_{13/2}$ level into two groups.

Paper 2: published in Opt. Lett. **21** (1996) 1594

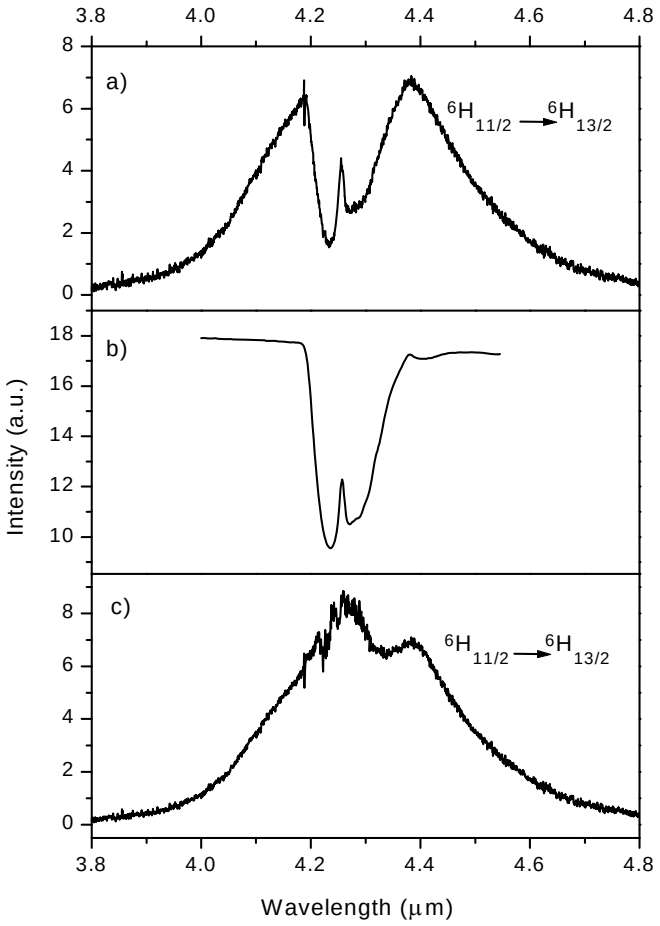

Fig. 2 a) Uncorrected Dy^{3+}-fluorescence spectrum ($^6H_{11/2} \rightarrow {}^6H_{13/2}$)
b) CO_2 absorption of a "white light" source measured with the FT-IR
c) Corrected Dy^{3+}-fluorescence spectrum ($^6H_{11/2} \rightarrow {}^6H_{13/2}$)

The Judd-Ofelt parameters ($\Omega_2=11.3\times10^{-20}$ cm^2, $\Omega_4=1.0\times10^{-20}$ cm^2, $\Omega_6=1.3\times10^{-20}$ cm^2) from [6] were obtained from the measured absorption spectrum excluding the absorption from the $^6H_{15/2}$ ground state to the $^6H_{13/2}$ level which has a magnetic dipole contribution (selection rules: $\Delta J=0,\pm1$, $\Delta S=0$, $\Delta L=0$, $\Delta l=0$). The electric and magnetic dipole contributions, A_{ed} and A_{md}, of the radiative transition rate $A=A_{ed}+A_{md}$ were calculated from the equations given in [7] and are listed in Table 1. The branching ratios β and the radiative lifetimes τ_r were derived from the radiative rates $A=\beta/\tau_r$. Comparison of τ_r with the measured lifetimes τ_m gives the quantum efficiencies $\eta=\beta\times\tau_m/\tau_r$. The overall quantum efficiency of the $^6H_{11/2}$ level (51%) and the quantum efficiency of the 4.27 μm transition (7.4%) in particular are remarkably high considering the small energy gap of about 2350 cm^{-1} to the next lower lying level. A second

Judd-Ofelt calculation omitting the hypersensitive $(^6H_{9/2}, ^6F_{11/2}) \rightarrow ^6H_{15/2}$ transition at 1.3 μm yielded values for the radiative rates that lie in the range of accuracy (≈20%) of the previous calculation.

Table 1 Radiative properties of Dy^{3+} doped Ga:La:S glass

Transition	λ (μm)	A_{ed} (s^{-1})	A_{md} (s^{-1})	β (%)	τ_r (μs)	τ_m (μs)	η (%)	$\sigma_{em,FL}$ ($10^{-20}cm^2$)	$\sigma_{em,MC}$ ($10^{-20}cm^2$)
$^6H_{11/2} \rightarrow ^6H_{13/2}$	4.27	42	15	14	2532	1300	7.4	1.17	—
$\rightarrow ^6H_{15/2}$	1.76	338	—	86	2532	1300	44	0.57	0.64
$^6H_{13/1} \rightarrow ^6H_{15/2}$	2.83	129	30	100	6289	3600	57	0.92	1.16

The emission cross sections were calculated following two different approaches. First we used the Füchtbauer-Ladenburg equation as given in [8]:

$$\sigma_{em,FL}(\lambda) = \frac{A\lambda^5 I(\lambda)}{8\pi n^2 c \int \lambda I(\lambda) d\lambda} \quad (1)$$

Comment [ORC1]:

I(λ) is the measured intensity spectrum of the fluorescence. The refractive index n is 2.36 for all three transitions. The emission cross sections for the 1.76 μm and the 2.83 μm transitions (Table 1) are slightly smaller than those reported for Dy^{3+} doped Ge:Ga:S glass although the magnetic dipole contribution of the latter transition was not included in [1].

In order to check the above results we used the theory of McCumber after Miniscalco and Quimby [3] to calculate the emission cross sections $\sigma_{em,MC}$ of the two ground state transitions at 1.76 μm and 2.83 μm from the absorption cross sections σ_{abs}:

$$\sigma_{em,MC}(\lambda) = \sigma_{abs}(\lambda) \frac{Z_l}{Z_u} \exp\left(\frac{E_{ZL} - 10^4 / \lambda}{kT} \right) \quad (2)$$

Z_l and Z_u are the partition functions of the lower and the upper manifold, respectively. E_{ZL} is the energy gap between the lowest Stark level of the ground state manifold and the lowest Stark level of the upper manifold measured in cm^{-1}, λ is the wavelength in microns and $k = 0.695\ cm^{-1}K^{-1}$ is the Boltzmann constant. Z_l, Z_u, and E_{ZL} are usually obtained from the energy levels of the manifolds and the Stark levels within these manifolds. As this information is not

available for the case of Ga:La:S glass, the parameters Z_l, Z_u, and E_{ZL} can be obtained from a simplified model [3]. The Stark levels of a given manifold are assumed to be equally spaced. The width of the ground state is given by the long wavelength half-width of the emission spectrum measured from the peak of the spectrum to the point where the spectrum falls to 5% of the peak value. The width of the excited manifold is obtained in a similar way from the short wavelength half-width of the absorption spectrum. The width of a manifold divided by the number of Stark levels gives the energy spacing of the Stark levels that is necessary for the calculation of the partition functions Z_l and Z_u. The values for Z_l/Z_u are 1.84 and 1.07 for the 1.76 μm and the 2.83 μm transitions, respectively. E_{ZL} can be taken as the average of the absorption and emission peak.

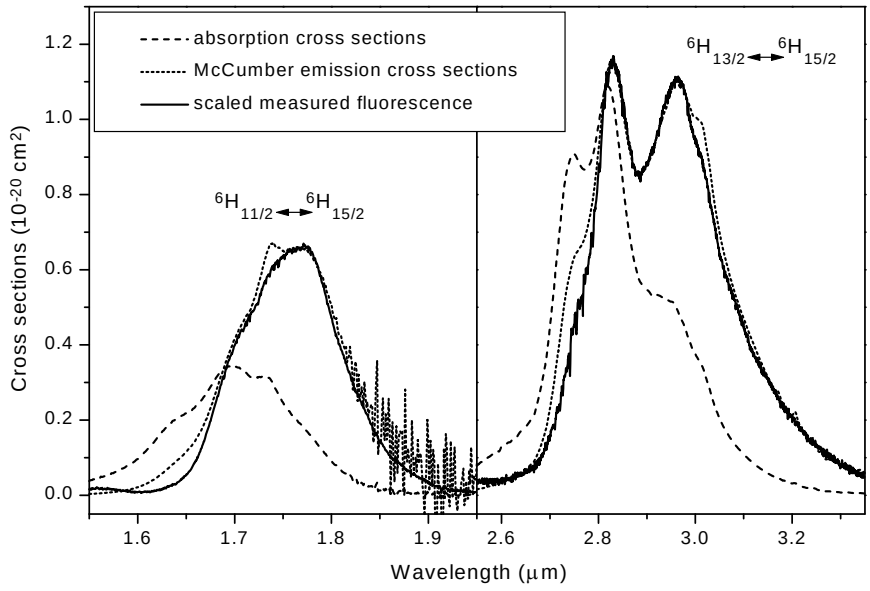

Fig. 3 Absorption cross sections (dashed lines) and McCumber emission cross sections (dotted lines) together with the scaled measured fluorescence spectra (solid lines) of the 1.76 μm and the 2.83 μm transitions of Dy^{3+}-doped Ga:La:S glass

The calculated emission cross section spectra of the 1.76 μm and the 2.83 μm transitions are shown in Fig. 3 together with the absorption spectra and the measured fluorescence spectra which were multiplied by λ^5 and a constant C. The good spectral correspondence of the calculated emission cross sections and the scaled measured fluorescence show that the modified McCumber theory is

Paper 2: published in Opt. Lett. **21** (1996) 1594

capable of producing absolute emission cross sections and the right emission shape without a detailed knowledge of the electronic structure of the Dy^{3+} ions.

The emission cross sections obtained from the theory of McCumber (Table 1) confirm the values calculated from the Judd-Ofelt calculations and the Füchtbauer-Ladenburg equation. They are slightly larger, especially for the $^6H_{13/2} \rightarrow {}^6H_{15/2}$ transition, but lie in the range of accuracy [3].

To date laser action on the 4.27 μm transition could only be achieved in a low phonon YLF crystal [4]. The reported emission cross section for this transition and the $^6H_{11/2}$ lifetime in Dy^{3+} doped YLF are 0.44×10^{-20} cm^2 and 0.83 μs, respectively. Thus the στ-product of Dy^{3+} doped Ga:La:S glass, which is a measure of the laser threshold, should be about 4000 times larger than the στ-product of YLF. The laser threshold in turn should be about 4000 times smaller. Together with the recent progress in Ga:La:S glass fibre fabrication these calculations show the potential of a diode-pumped Dy^{3+} doped fibre laser operating at 4.27 μm which would be useful for CO_2 gas sensing [5].

In conclusion we present infrared absorption, lifetime, and fluorescence measurements of Dy^{3+} doped Ga:La:S glass. Emission cross sections for three infrared transitions were calculated using Judd-Ofelt calculations, the Füchtbauer-Ladenburg equation and the modified theory of McCumber yielding promising στ-values for the 4.27 μm transition when compared to the existing 4.34 μm laser in a bulk YLF crystal. A Dy^{3+} doped Ga:La:S glass fibre would make use of the advantages of the fibre geometry and could provide a more efficient and compact laser source using 0.8 μm or 1.3 μm laser diodes for pumping.

Acknowledgements

Thanks to Roger Moore for his help with sample preparation. Chalcogenide materials were supplied by Merck Ltd. The authors thank Prof. H. Rutt for providing equipment and for helpful discussions.

References

1. K. Wei, D.P. Machewirth, J. Wenzel, E. Snitzer, and G.H. Sigel, Jr., Opt. Lett., **19**, 904 (1994)
2. J. Heo, J. Mater. Sci. Lett., **14**, 1014 (1995)
3. W.J. Miniscalco and R.S. Quimby, Opt. Lett., **16**, 258 (1991)
4. N.B. Barnes, R.E. Allen, IEEE J. Quantum Elect., **27**, 277 (1991)
5. D.W. Hewak, R.C. Moore, T. Schweizer, J. Wang, B. Samson, W.S. Brocklesby, D.N. Payne, and E.J. Tarbox, Electron. Lett., **32**, 384 (1996)
6. D.W. Hewak, B.N. Samson, J.A. Medeiros Neto, R.I. Laming, D.N. Payne, Electron. Lett., **30**, 968 (1994)
7. M.J. Weber, Phys. Rev., **157**, 262 (1966)
8. T.Y. Fan, M.R. Kokta, IEEE J. Quantum Elect., **25**, 1845 (1989)

Paper 2: published in Opt. Lett. **21** (1996) 1594

Concentration and temperature dependence of the $^6H_{11/2}$ level lifetime

The fluorescence decay times of the 1.8 μm level ($^6H_{11/2}$), which is the upper level of the 4.3 μm transition, were determined for different concentrations and at low temperatures. The lifetimes were measured by chopping the Ti:sapphire pump laser beam with an acousto-optic modulator and detecting the fluorescence decay with an InGaAs detector. The pump wavelengths were 0.81 μm for the concentration dependence and 0.915 μm for the low temperature measurements. The low temperature measurements were made with the sample inside a continuous flow liquid helium cryostat over the temperature range 4K to 360K.

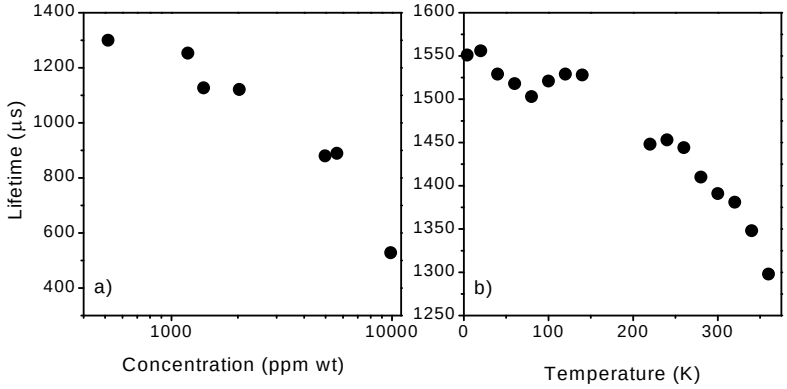

Fig. 3.7.2 Dependence of the $^6H_{11/2}$ lifetime
a) on the Dy^{3+} concentration at room temperature and
b) on the temperature for 500 ppm wt Dy_2S_3

The room temperature $^6H_{11/2}$ lifetime is shown in Fig. 3.7.2.a for different Dy^{3+} concentrations. The lifetime decrease from 1300 μs for 500 ppm Dy_2S_3 to 530 μs for 10000 ppm Dy_2S_3 is caused by the increasing probability for ion-ion interactions. The onset of the lifetime quenching is about 1000 ppm, concentrations higher than 2000 ppm should be avoided for active devices to prevent high threshold powers and low efficiencies. The lifetime quenching of the 1.3 and 2.9 μm levels shows a similar dependence on concentration. The lifetime of the 1.3 μm level is shortened from 55 μs to 22 μs, and the lifetime of the 2.9 μm level from 3600 μs to 500 μs over the same range of concentrations. It should be noted that under the present pumping scheme the measured 2.9 μm lifetime cannot be less than the lifetime of the 1.8 μm energy level since population of the $^6H_{13/2}$ occurs mostly via the $^6H_{11/2}$ level. A more accurate

measurement of the 2.9 μm level would be obtained by pumping this energy level directly for which no sources were available.

The lifetime of the $^6H_{11/2}$ level as a function of temperature is shown in Fig. 3.7.2.b and is seen to decrease from 1550 μs at approximately 4K to 1300 μs at 360K (The increase from 80 to 120K is less than 2% of the lifetime and lies within the error of the lifetime measurement and the fitting procedure.). The lifetime decrease corresponds to only a small decrease in radiative quantum efficiency of the 4.3 μm transition from 8.6% to 7.2% and shows that a potential 4.3 μm laser would not require cryogenic cooling despite the small energy gap of 2230 cm^{-1}. Since the multiphonon decay rates are independent of the rare-earth ions this result also applies to other mid-infrared transitions.

Site selectivity in Dy^{3+} doped GLS glass

The Dy^{3+} absorption bands show an unusual double structure (Fig. 1, page 45). The absorption bands at 0.76, 0.81, and 0.91 μm are all accompanied by a smaller absorption peak at 0.74, 0.79, and 0.88 μm. The 1.1 and 1.3 μm bands have a shoulder at their short-wavelength side while this particular structure is not obvious for the 1.7 and 2.8 μm bands. The fact that the absorption bands at 0.81, 0.91, 1.1, and 1.3 μm are all comprised of two energy levels (Fig. 3.7.1) offers a possible explanation for the double structure. However, the double structure is not apparent in the absorption spectra of other chalcogenide glasses [Heo96,Tan95,Wei94].

The measurement of excitation spectra revealed an interesting answer to this question. Excitation spectra of the 1.3, 1.8, and 2.9 μm emission bands were measured by tuning the Ti:sapphire pump wavelength from 0.72-0.85 μm while monitoring the intensity of the fluorescence signals at each of the three emission wavelengths for constant pump power. Fig. 3.7.3 shows the excitation spectra of the 1.8 μm and 2.9 μm emission bands along with a Dy^{3+} absorption spectrum in the 0.72-0.85 pump wavelength region. (The excitation spectrum for the 1.3 μm emission is not shown and is identical to that of the 1.8 μm emission.) Clearly the excitation spectra do not follow the absorption spectrum. Pumping into the short-wavelength absorption peaks does not generate fluorescence signals at 1.8 and 2.9 μm.

A similar result was obtained for an excitation spectrum of the 4.3 μm emission for the 0.93-1.08 μm pump wavelength range ($^6F_{9/2}$,$^6H_{7/2}$ levels, Fig. 3.7.1, page 41). The upper level of the 4.3 μm transition is the same level as for the 1.8 μm transition. Again pumping into the short-wavelength shoulder of the 1.1 μm absorption band did not give measurable 4.3 μm fluorescence.

This result suggests the existence of two different types of Dy^{3+} sites, each of which has a statistical distribution of different sites leading to the

inhomogeneous line broadening observed in glasses. Dy^{3+} ions in one of the two types of sites absorbs at slightly shorter wavelength and either shows very weak fluorescence or no fluorescence at all. A very similar effect, though less pronounced, has been reported by our group in Pr^{3+} doped GLS glass [Bro96]. The authors concluded that oxide impurities in the glass lead to a second, more favourable Pr^{3+} site which absorbs at shorter wavelength than the sulphide site and also shows a reduced fluorescence decay time due to locally increased multiphonon decay rates for ions in the oxide site.

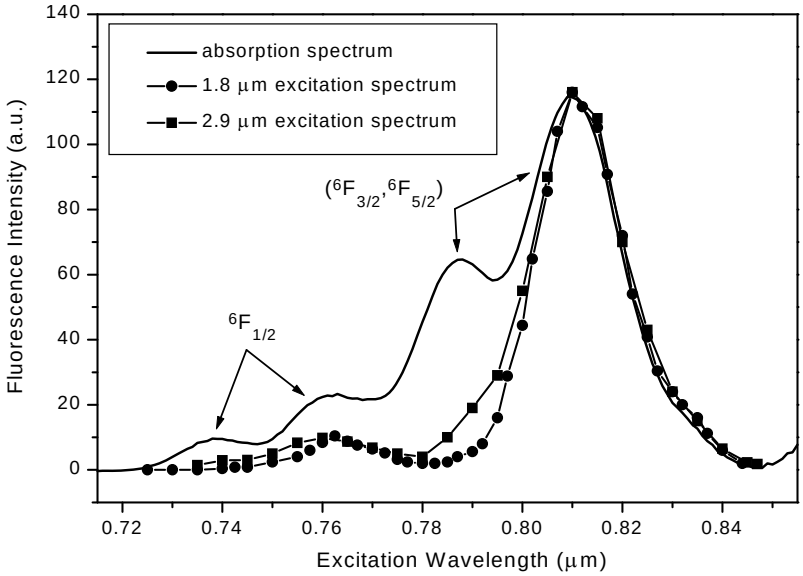

Fig. 3.7.3 Excitation spectra of the 1.8 μm and 2.9 μm Dy^{3+} transitions along with the Dy^{3+} absorption spectrum

The reasoning of two sites with different phonon energies can be applied to Dy^{3+} doped GLS and is supported by the small difference of the 1.8 and 2.9 μm excitation spectra. The 2.9 μm level has a larger energy gap to the ground state than the 1.8 μm level has to the 2.9 μm level (Fig. 3.7.1, page 41) and should therefore have lower multiphonon decay rates. Indeed some 2.9 μm emission was measured for 0.74 and 0.79 μm pumping (Fig. 3.7.3) indicating that emission can be obtained from the oxide site from levels with larger energy gaps to the next lower level. The excitation spectrum of an energy level with an even larger energy gap than the 2.9 μm level may even be identical to the absorption spectrum since the multiphonon decay rates for ions in either site are negligible. Unfortunately no such level is available in Dy^{3+} doped GLS. The important implication of these findings is that the pump wavelength of Dy^{3+} doped active devices needs to be selected carefully to avoid pumping the oxide sites.

3.8 Holmium

Holmium (Ho^{3+}) is commonly known for its 2 μm transition in crystal lasers for coherent laser radar and medical applications [Fan88]. Laser operation at longer wavelengths can be achieved in low phonon energy hosts. The 3.9 μm Ho^{3+} ZBLAN fibre laser represents the fibre laser with the longest emission wavelength to date [Sch95,Sch97]. However, this laser requires cryogenic cooling to reduce the multiphonon decay rates. The lower phonon energy GLS glass offers the possibility for a room temperature fibre laser at 3.9 μm. This wavelength is of particular interest for the LONGWAVE project because it coincides with the attenuation minimum of the 3.4-4.1 μm atmospheric transmission window. Fig. 3.8.1 shows the atmospheric transmission from 0.1 μm to 100 μm. The window is determined by the H_2O and CH_4 absorption bands on the short-wavelength side and the CO_2 absorption on the long-wavelength side (sections 3.4 and 3.7).

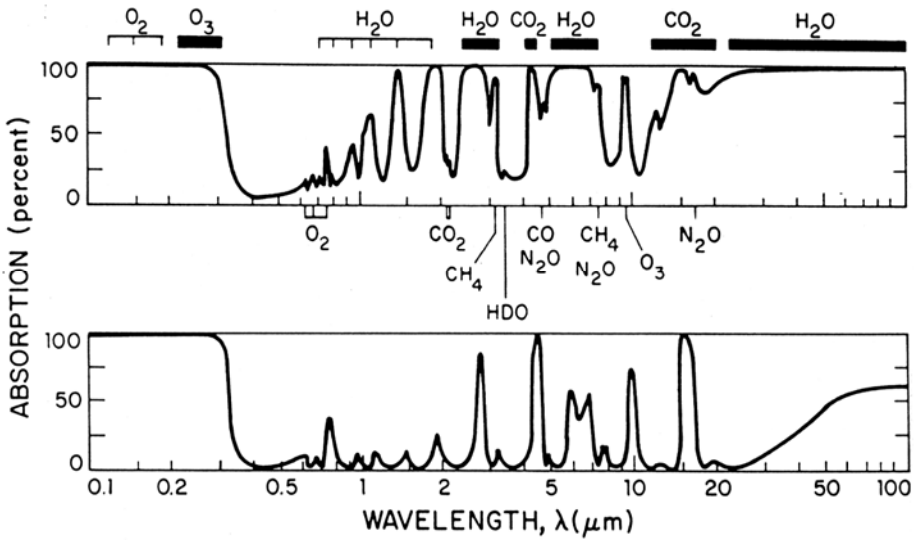

Fig. 3.8.1 Absorption spectra of solar radiation reaching the earth's surface (top) and reaching an altitude of 11 km (bottom) [Zue76]

The following paper (paper 3) describes the spectroscopy of potential infrared laser transitions in Ho^{3+} doped GLS glasses and compares this to the transitions reported for silica and fluorozirconate glasses. Eight infrared transitions ranging from 1.2-4.9 μm have been observed. The emission bands from the $^5I_4$ level (1.25, 2.2, and 4.9 μm) have, to our knowledge, not been reported for any host material before.

Infrared emission from holmium doped gallium lanthanum sulphide glass

***T. Schweizer**, B.N. Samson, J.R. Hector, W.S. Brocklesby, D.W. Hewak, and D.N. Payne*

Abstract

Infrared emission at 1.2, 1.25, 1.67, 2.0, 2.2, 2.9, 3.9, and 4.9 μm is measured in holmium (Ho^{3+}) doped gallium lanthanum sulphide (GLS) glass. Branching ratios, radiative quantum efficiencies, and emission cross sections are calculated from lifetime, absorption, and emission measurements using Judd-Ofelt analysis and the Füchtbauer-Ladenburg equation. The fluorescence band at 3.9 μm coincides with an atmospheric transmission window and the fluorescence band at 4.9 μm overlaps with the fundamental absorption of carbon monoxide, making the glass a potential fibre laser source for remote sensing and gas sensing applications. This is the first time this latter transition has been reported in any holmium doped host.

1 Introduction

Most gas molecules have strong fundamental absorption bands in the mid-infrared wavelength region (3-5 μm). These specific "fingerprints" can be used to identify gas species, and the strength of the absorption over a certain path length includes information about the concentration of a particular species in a gas mixture. Mid-infrared light sources would therefore find application in atmospheric sensing of environmentally important gases such as methane, nitrogen dioxide, carbon dioxide, and carbon monoxide, and in on-line monitoring of exhaust gas pollution by industrial plants, vehicles, and jet engines. Other possible applications include optical radar, e.g. collision avoiding radar, ammonia and water vapour sensing in agriculture, medical diagnostics, molecular spectroscopy, point-to-point atmospheric communi-cation, remote control, etc. The most promising example of the group of mid-infrared emitting light sources, which includes thermal emitters, optical parametric oscillators, and difference frequency generation, are the semiconductor light emitting diodes (LED) and laser diodes. A good overview about the application of laser diodes for monitoring gaseous pollutants can be found in Ref. [1].

It is less well known that rare-earth doped materials are also capable of emitting mid-infrared radiation. Transitions between closely spaced electronic energy levels (2000-3300 cm^{-1}) of trivalent rare-earth ions emit radiation in the 3-5 μm wavelength range if the transition probability of competing non-radiative transitions is kept as low as possible by choosing a host material with a low

Paper 3: submitted to Infrared Phys. Technol.

phonon energy. The rare-earth laser with the longest emission wavelength reported to date operates in a pulsed mode at room temperature at a wavelength of 7.2 μm in a praseodymium (Pr^{3+}) doped $LaCl_3$ crystal [2]. The only rare-earth doped laser operating *continuous wave at room temperature* at a wavelength longer than 3 μm is the 3.5 μm erbium (Er^{3+}) doped fluorozirconate (ZBLAN) fibre laser which benefits from the advantages of the fibre geometry [3]. The fibre geometry offers high gain due to the long interaction length of pump and laser modes, small pump powers due to the high intensities in the fibre core, favourable thermal conditions due to the good heat dissipation, and the possibility to exploit weak rare-earth absorption bands due to the long optical path in the fibre. The longest emission wavelength of a fibre laser was obtained in a holmium (Ho^{3+}) doped ZBLAN fibre [4]. This laser operates continuous wave at a wavelength of 3.9 μm but needs cryogenic cooling to reduce the competing non-radiative decay processes which depopulate the upper laser level. As an alternative to cooling the multiphonon decay rate can be reduced by choosing a host material with an even lower phonon energy than fluorozirconate glass (~ 580 cm^{-1}). Chalcogenide glasses, non-oxide glasses based on sulphur, selenium, or tellurium, have lower phonon energies (~ 300 - 400 cm^{-1}), a good infrared transparency, and can be fabricated into fibre form [5,6]. Mid-infrared fluorescence has previously been reported from Pr^{3+}, Dy^{3+} (dysprosium), and Er^{3+} doped chalcogenide glasses [7-9].

In this paper we present spectroscopic data of infrared emission bands from Ho^{3+} doped gallium lanthanum sulphide (GLS) glass. We chose GLS from the group of chalcogenide glasses because it combines several desirable properties. The glass is nontoxic (no As, Se, Te, etc.), chemically stable (non-hygroscopic) and has a high glass transition temperature (561ºC compared to 153ºC for As_2S_3 and 47ºC for As_5Se_{95}) making the glass more resistant to environmental effects and thermal damage by high power pump laser sources. Other advantages include the good transparency in the visible and near-infrared pump wavelength range and the mid-infrared laser wavelength range, along with a high rare-earth solubility due to the presence of lanthanum in the glass matrix. Furthermore, GLS can be melted in large glass ingots and, most importantly, can be pulled into fibre form using the rod-in-tube technique [10].

Ho^{3+} doped GLS glasses have first been reported 20 years ago by Reisfeld and co-workers with emphasis on visible and near-infrared emission [11-13]. Since then the qualities of the glasses has improved considerably, in particular due to the reduction of lanthanum oxide and hydroxyl impurities.

In the present work Ho^{3+} doped glasses have been characterised by absorption, fluorescence, and lifetime spectroscopy. The radiative properties of the infrared transitions such as radiative rates, branching ratios, radiative lifetimes, and emission cross sections have been obtained from Judd-Ofelt calculations and the Füchtbauer-Ladenburg equation. Infrared emission bands

have been observed at 1.2, 1.25, 1.67, 2.0, 2.2, 2.9, 3.9, and 4.9 μm, some of which have not been reported in glass or other rare-earth host materials before.

2 Experiments

We melted a series of GLS glasses with the molar ratio $70Ga_2S_3$:$30La_2S_3$ and doped them with Ho^{3+} by replacing La_2S_3 with the required amount of Ho_2S_3. Glasses were doped with 0.05 mol% Ho_2S_3 (n_{Ho} = 8.9 × 10^{18} ions/cm^3), 0.2 mol% Ho_2S_3, and 1.5 mol% Ho_2S_3. These samples will be referred to simply by Ho(0.05%):GLS, etc. The glasses were cut and polished on three sides for absorption, fluorescence, and lifetime measurements. Absorption spectra were measured from 0.45 μm to 2.25 μm with a Perkin-Elmer Lambda 9 spectrophotometer. Samples were excited with a tuneable Ti:sapphire laser at 0.76 μm and 0.9 μm, and a 2 μm diode pumped Tm:YAG laser for fluorescence and lifetime measurements. Fluorescence spectra were recorded with a computer driven monochromator and an InGaAs detector (1.1 - 1.4 μm) or liquid nitrogen cooled InSb detector (1.5 - 5.45 μm). Fluorescence decay curves were measured with a photomultiplier (0.76 μm), with an InGaAs detector (0.9 μm), and a liquid nitrogen cooled InSb detector (2.0 μm) using an acousto-optic modulator or a chopper to modulate the pump beam and a monochromator or a suitable set of filters for wavelengths discrimination. The decay curves were averaged using a photon counting device (Stanford Model SR430 Multi-Channel Scaler) for the photomultiplier and a TEK2232 digital storage oscilloscope for the InGaAs and InSb detectors and transferred to a PC for the fitting procedure. All measurements were performed at room temperature.

3 Results and Discussion

Fig. 1 shows the ground state absorption bands from the $^5I_8$ to the seven lowest energy levels for a Ho(1.5%):GLS glass and Fig. 2 a schematic energy level diagram. The electronic absorption edge of the host glass starts at about 0.5 μm and obscures the higher energy levels of the rare-earth ($^5F_3$, $^5F_2$, etc.). The closely spaced $^5S_2$,$^5F_4$ levels have been treated as one level for the Judd-Ofelt calculations. The infrared multiphonon absorption edge of the glass starts at about 8 μm (not shown). The location and spectral shape of the Ho^{3+} absorption bands are similar to other glasses. The strength of the absorption bands, however, is larger due to the high covalency and high refractive index of the glass bonds [14].

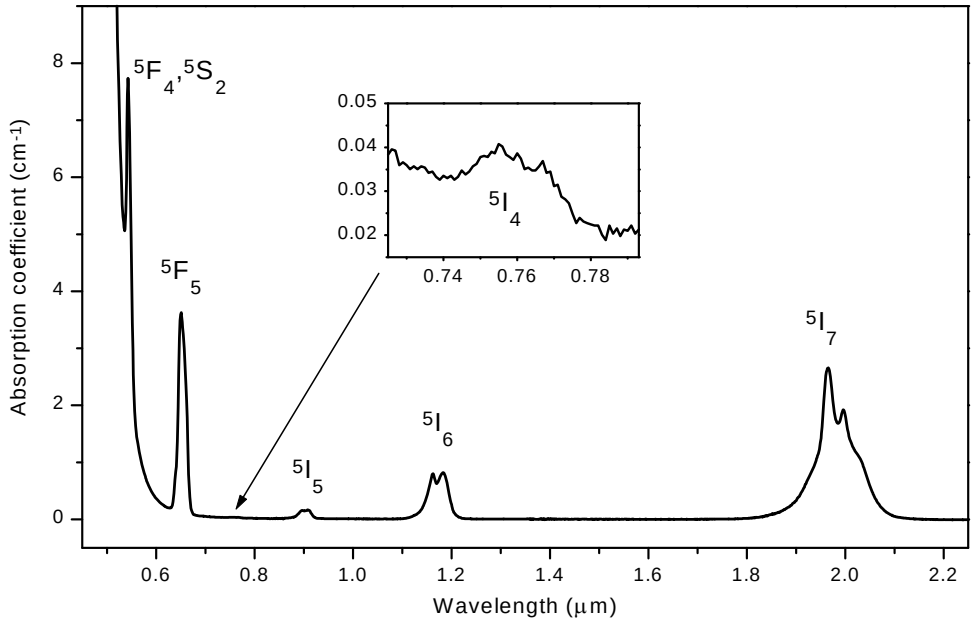

Fig. 1 Absorption spectrum of 1.5 mol% Ho_2S_3 doped GLS glass. The inset shows the pump absorption band at 0.76 μm.

We excited the Ho^{3+} ions for fluorescence measurements into the 0.76 μm band populating the $^5I_4$ level and subsequently the $^5I_5$, $^5I_6$, and $^5I_7$ levels via radiative and non-radiative transitions (Fig. 2). Although the strength of this absorption band is particularly weak (inset in Fig. 1) it was chosen for its convenient pump wavelength. Pumping at 0.76 μm not only populates the lower but also some higher energy levels leading to green and red upconversion emission from the $^5F_4$,$^5S_2$ levels and the $^5F_5$ level. For lifetime measurements the $^5I_4$, $^5I_5$, and $^5I_7$ levels were excited resonantly at 0.76 μm and 0.9 μm and at 2.0 μm, respectively, in order to avoid distortion of the fluorescence decay times of these levels caused by population from higher energy levels.

The identification and characterisation of potential laser transitions in Ho^{3+} doped GLS glass requires an understanding of the spectroscopic properties of this material. The radiative properties of the fluorescent Ho^{3+} transitions can be obtained from Judd-Ofelt calculations [15,16]. The absorption spectra of Ho^{3+} doped GLS glasses were used to calculate the Judd-Ofelt parameters which in turn allow the calculation of the radiative rates, lifetimes, and branching ratios of the fluorescent transitions. All six absorption bands shown in Fig. 1 were used in the fitting after subtracting the magnetic dipole contribution of the $^5I_8 \rightarrow {}^5I_7$ transition. The electric and magnetic dipole contributions, A_{ed} and A_{md}, of the radiative transition rate $A = A_{ed} + A_{md}$ were calculated from the equations

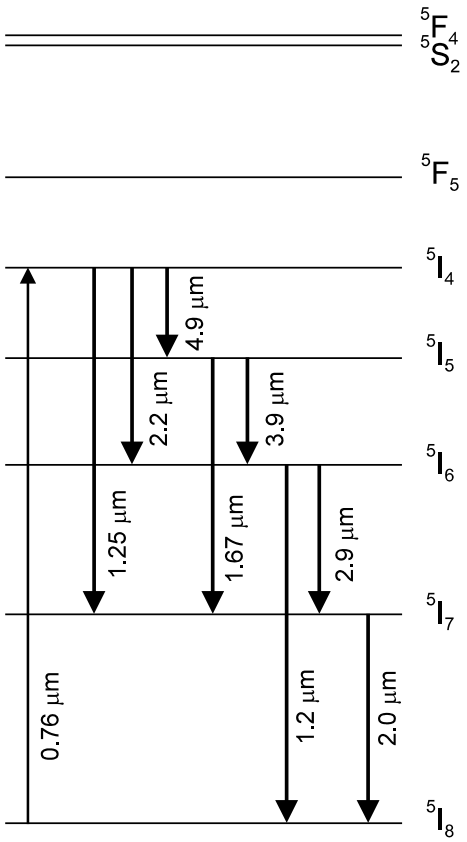

Fig. 2 Energy level diagram and fluorescent transitions of Ho^{3+}

Table 1 Radiative properties and emission cross sections of infrared transitions in Ho^{3+} doped GLS glass

Transition	λ (μm)	A_{ed} (s^{-1})	A_{md} (s^{-1})	β (%)	τ_r (ms)	τ_m (ms)	η (%)	$\sigma_{em,FL}$ ($10^{-20}cm^2$)
$^5I_7 \rightarrow {}^5I_8$	2.00	228	95	100	3.10	3.0	97	1.08
$^5I_6 \rightarrow {}^5I_8$	1.19	489		81	1.65			
$\rightarrow {}^5I_7$	2.86	73	44	19				2.22
$^5I_5 \rightarrow {}^5I_8$	0.90	212		42	2.00	1.7	36	
$\rightarrow {}^5I_7$	1.67	239		48			41	0.71
$\rightarrow {}^5I_6$	3.90	28	20	10			9	2.29
$^5I_4 \rightarrow {}^5I_8$	0.76	24		8	3.58	0.5	1	
$\rightarrow {}^5I_7$	1.25	114		41			6	
$\rightarrow {}^5I_6$	2.19	114		41			6	
$\rightarrow {}^5I_5$	4.92	19	8	10			1	1.27

given in [17] and are listed in Table 1. The branching ratios $\beta = A / A_{total}$ and the radiative lifetimes $\tau_r = 1 / A_{total}$ were derived from the radiative rates. Comparison of τ_r with the measured lifetimes τ_m gives the quantum efficiencies $\eta = \beta \times (\tau_m / \tau_r)$. The measured lifetimes in Table 1 were obtained from the sample with the low Ho^{3+} concentration of 0.05 mol% but are very similar to the lifetimes measured in glasses with higher concentrations of 0.2 and 1.5 mol% indicating a very low probability of lifetime quenching by ion-ion interactions. The lifetime of the $^5I_6$ level could not be measured due to the lack of a 1.2 μm pump source but is expected to be very close to the calculated radiative lifetime of 1.65 ms because the rate of multiphonon decay should be negligible. Unlike β, which is only weakly dependent on the host material, A (and therefore τ_r) and τ_m (and therefore η) show a much stronger dependence.

The above parameters have been compared among various chalcogenide glasses, a fluorozirconate glass (ZBLAN) and a silicate glass for one specific transition. The Judd-Ofelt parameters for Ho^{3+} along with the radiative rates, the measured lifetimes, the quantum efficiencies, and the emission cross sections of the $^5I_7 \rightarrow {}^5I_8$ transition (2.0 μm) are listed in Table 2. Our Ω_2 and Ω_4 values do not agree with the values reported in the early 80's for a GLS glass with a slightly different composition (75:25 compared to 70:30) but the Ω_2 value is in line with the values published for the other two chalcogenide glasses [13,18]. The Judd-Ofelt parameter Ω_2, the radiative rates A, and the emission cross sections σ_{em} are higher in chalcogenide glasses compared to fluoride (ZBLAN) and silicate glasses, which is an indication of the higher covalency of the glass bonds [14].

Table 2 Judd-Ofelt parameters, radiative emission probabilities and emission cross sections for the $^5I_7 \rightarrow {}^5I_8$ transition (2.0 μm), and measured lifetimes of the $^5I_7$ level for different Ho^{3+} doped glasses

Glass (Ho^{3+} conc.)	Ω_2 ($10^{20}cm^2$)	Ω_4 ($10^{20}cm^2$)	Ω_6 ($10^{20}cm^2$)	A (s^{-1})	τ_m (ms)	η (%)	σ_{em} ($10^{-20}cm^2$)
GLS (1.5%)	6.9	5.5	1.07	323	3.1	97	1.08
GLS (75:25) [13]	2.31	2.81	1.08				
$3Al_2S_3$:$1La_2S_3$ [13]	8.09	3.85	1.40				
$Ge_{30}As_{10}S_{60}$ [18]	6.98	2.53	0.78	177			
ZBLAN [19]	2.30	2.30	1.71	79	12.01	95	0.56
Silicate (2%) [20]	3.60	3.01	0.61	61.65	0.32	2	0.70

The measured lifetimes reflect the variations in both the radiative rates (mostly via changes in the refractive index of the glass) and the multiphonon decay rates (via changes in the phonon energy) in these hosts. The lifetime is longest in the

fluoride glass due to the low radiative rate (ionic, low refractive index of 1.5) and the low non-radiative rate (small phonon energy of ~ 580 cm^{-1}). It is shorter in the GLS glass due to the higher radiative rates (strongly covalent, high refractive index of 2.4) and the low non-radiative rate (small phonon energy of ~ 425 cm^{-1}), but shortest in the silicate glass due to the high non-radiative rate (large phonon energy of ~ 1160 cm^{-1}) along with the small radiative rate (intermediate bonding, low refractive index of 1.5). Hence the low quantum efficiency of the $^5I_7$ level in the silicate glass. For the chalcogenide and the fluoride glass the 2 μm transition is almost purely radiative, so the quantum efficiencies are nearly 100%. However, this does not apply to energy levels with an even smaller energy gap to the next lower lying level, such as the $^5I_4$, $^5I_5$, and the $^5I_6$ levels. For these levels non-radiative decay becomes important in fluoride glasses decreasing the lifetimes and the fluorescence intensities. Emission from the $^5I_4$ level has not been reported in fluoride glasses but could be measured in GLS glass in this work.

The emission cross sections (Table 1.) were calculated using the Füchtbauer-Ladenburg equation as given in [21]:

$$\sigma_{em}(\lambda) = \frac{A\lambda^5 I(\lambda)}{8\pi n^2 c \int \lambda I(\lambda) d\lambda} \qquad (1)$$

Comment [ORC1]:

I(λ) is the measured intensity spectrum of the fluorescence, n is the refractive index.

We also applied the theory of McCumber after Miniscalco and Quimby [22] to calculate the emission cross sections of the 2 μm ground state transitions from the measured absorption spectrum. The value of 0.95×10^{-20} cm^2 from the McCumber method confirms the value of 1.08×10^{-20} cm^2 from the Füchtbauer-Ladenburg equation and gives us some confidence in the accuracy of the cross sections in Table 1.

We can compare the prospective emission wavelengths of Ho:GLS fibre lasers with reported work on Ho:silica and Ho:fluoride fibre lasers. In a silica fibre, laser operation on the 2 μm ground state transition has been reported despite the low radiative quantum efficiency, estimated to be about 1.5% [23]. The low quantum efficiency increased the threshold pump power. The higher energy levels $^5I_6$, $^5I_5$, and $^5I_4$ have even smaller energy gaps to the next lower lying levels, increasing the multiphonon decay rates and quenching fluorescence from these levels in silica glass (see Fig. 2).

In a fluoride glass fibre, reduced multiphonon rates increase the radiative quantum efficiency for the $^5I_6$ level to about 60%, making room temperature continuous wave laser operation at 1.2 and 2.9 μm possible [19,24]. However,

multiphonon processes from the $^5I_5$ level are so strong that superfluorescence and laser operation at 3.9 μm require cryogenic cooling to reduce the non-radiative decay rate [4,25]. Emission from the $^5I_4$ level with an even smaller energy gap is completely quenched.

In GLS glass, the lower phonon energy leads to emission from all four ^5I levels. Fig. 3.a shows the 2 μm emission from the first excited state $^5I_7$ under continuous wave pumping at 0.76 μm. The 2 μm band overlaps with the 2.2 μm emission from the $^5I_4$ pump level which is not obvious under continuous wave pumping. The strength of the 2 μm transition is much larger than the strength of the 2.2 μm transition due to the higher branching ratio and the higher quantum efficiency (Table 1).

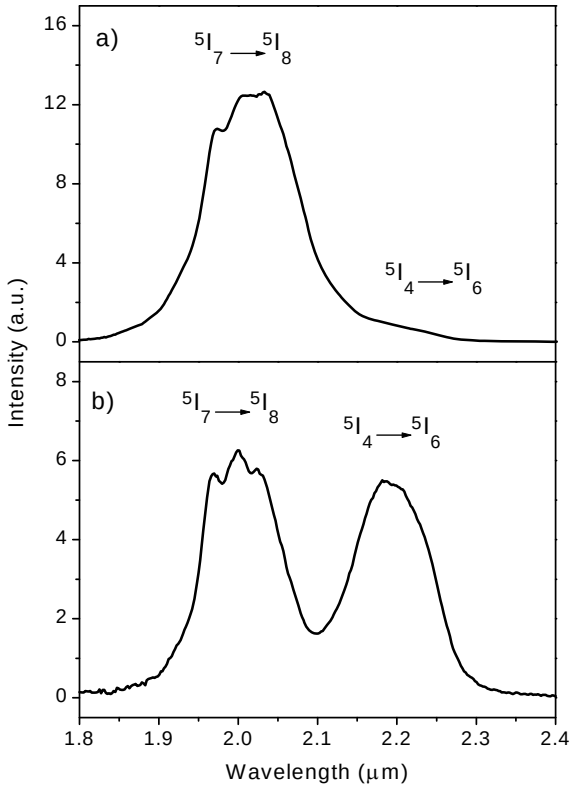

Fig. 3 Overlapping emission at 2.0 and 2.2 μm from the $^5I_7$ and the $^5I_4$ levels in Ho(1.5%):GLS pumped at 0.76 μm
a) continuous wave pump laser
b) pump laser chopped at 400 Hz

Modulating the pump laser at a frequency of 400 Hz decreases the intensity of the 2 μm emission relative to the intensity of the 2.2 μm emission (Fig. 3.b). The $^5I_4$ level is excited directly and instantaneously whereas the $^5I_7$ level is mainly populated by slow radiative decay from the higher levels which cannot follow

the fast pump modulation (Fig. 2). The 2.2 μm emission is unique to a host material with a low phonon energy and is not observed in silica and fluoride glasses. The 2.0 μm fluorescence, however, has been measured in other chalcogenide glasses before [18,26].

Near-infrared emission from the $^5I_6$, $^5I_5$, and $^5I_4$ levels is shown in Fig. 4.a and b. While the 1.2 μm and 1.67 μm transitions can also be observed in fluoride glasses, though with lower efficiencies, the 1.25 μm emission is unique to chalcogenide glasses. The 1.67 μm emission coincides exactly with the overtone of the 3.35 μm CH_4 absorption band and is of interest for gas sensing [27].

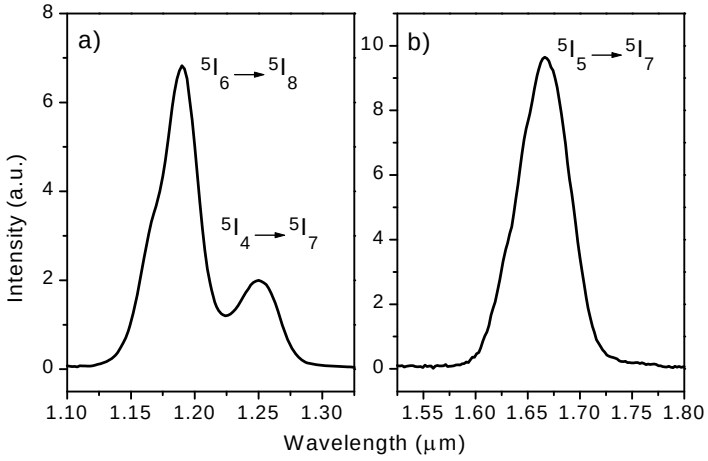

Fig. 4 Near-infrared emission a) from the $^5I_4$ and $^5I_6$ levels, and b) from the $^5I_5$ level in Ho(1.5%)GLS pumped at 0.76 μm

Fig. 5 shows the emission spectra of three mid-infrared transitions at 2.9, 3.9, and 4.9 μm. The fluorescence intensities are high considering the low pump absorption at 0.76 μm and reflect the relatively high branching ratios and quantum efficiencies of the 2.9, 3.9, and 4.9 μm transitions (Table 1). Even the 4.9 μm transition still has a quantum efficiency of 1% at room temperature which can be seen as a lower limit for a viable laser transition. However, we note that a lower phonon energy chalcogenide glass could have up to 8% quantum efficiency, limited by the branching ratio. While the 2.9 μm emission has been measured before in chalcogenide glasses [18] the 3.9 μm and the 4.9 μm bands have been identified in a chalcogenide glass for the first time in this work. To our knowledge, the 4.9 μm emission has not been reported in any host before.

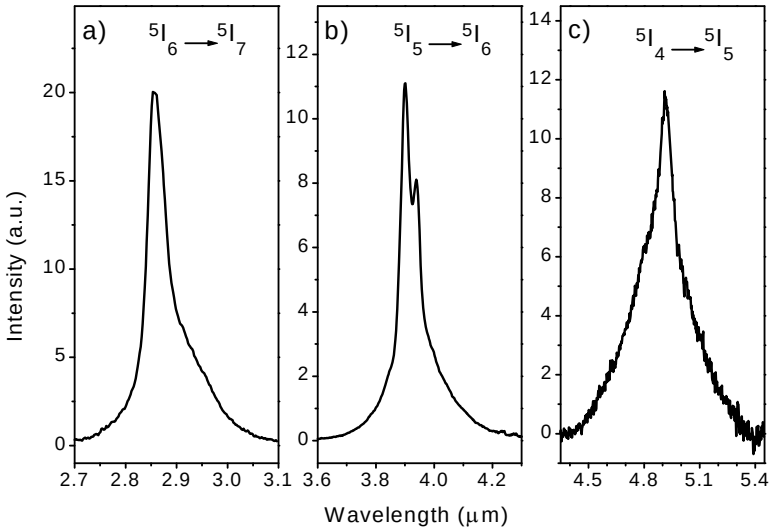

Fig. 5 Mid-infrared emission a) from the $^5I_6$ level, b) from the $^5I_5$ level, and c) from the $^5I_4$ level in Ho(1.5%):GLS pumped at 0.76 μm

The 2.9 μm emission band overlaps with the absorption of water and may prove useful for medical applications. The 3.9 μm emission coincides with the attenuation minimum of an atmospheric window making a fibre laser at this wavelength interesting for applications that require a low atmospheric attenuation. The 4.9 μm emission bands overlaps with the absorption bands of CO and OCS gas and could find application as a gas sensor [27].

4 Conclusion

In conclusion, we have presented spectroscopic data of Ho^{3+} doped GLS glasses with respect to their suitability for mid-infrared laser devices. A quantitative analysis using Judd-Ofelt calculations, the Füchtbauer-Ladenburg equation, and the modified McCumber theory along with absorption, fluorescence, and lifetime measurements has delivered important laser parameters such as absorption coefficients, emission cross sections, laser level lifetimes, and quantum efficiencies. The quantum efficiencies for mid-infrared transitions are higher than in common low phonon energy fluoride glasses opening the potential for mid-infrared fibre lasers with higher efficiencies and longer emission wavelengths. GLS glass is a promising host material for mid-infrared fibre lasers because it is one of the few chalcogenide glasses that has been pulled into fibre form successfully [10] and is the only rare-earth doped chalcogenide fibre with demonstrated laser action to date [28].

Acknowledgements

This work was supported by the UK EPSRC/DTI LINK programme (LONGWAVE). Chalcogenide powders were supplied by Merck Ltd., Poole, UK, and samples were polished by Crystran Ltd, Poole, UK. Thanks to R.A. Hayward for providing the 2 μm Tm:YAG laser source.

References

[1] Infrared Phys. Technol. **37** (1996) whole issue, Proceedings of the 4th International symposium on monitoring of gaseous pollutants by tuneable diode lasers, 19-20 October 1994, Freiburg, Germany, ed. R. Grisar, M. Tacke, H. Böttner
[2] S.R. Bowman, L.B. Shaw, B.J. Feldman, and J. Ganem, IEEE J. Quantum Electron. **32** (1996) 646
[3] H. Többen, Electron. Lett. **28** (1992) 1361
[4] J. Schneider, C. Carbonnier, and U.B. Unrau, Appl. Optics **36** (1997) 8595
[5] P.N. Kumta and S.H. Risbud, J. Mater. Sci. **29** (1994) 1135
[6] H. Suto, Infrared Phys. Technol. **38** (1997) 93
[7] L.B. Shaw, B.B. Harbison, B. Cole, J.S. Sanghera, and I.D. Aggarwal, Optics Express **1** (1997) 87
[8] J. Heo and Y.B. Shin, J. Non-Cryst. Solids **196** (1996) 162
[9] T. Schweizer, D.W. Hewak, B.N. Samson, and D.N. Payne, J. Lumin. **72-74** (1997) 419
[10] D.W. Hewak, R.C. Moore, T. Schweizer, J. Wang, B. Samson, W.S. Brocklesby, D.N. Payne, and E.J. Tarbox, Electron. Lett. **32**, (1996) 384
[11] R. Reisfeld, A. Bornstein, J. Flahaut, M. Guittard, and A.M. Loireau-Lozac'h, Chem. Phys. Lett. **47** (1977) 408
[12] R. Reisfeld, A. Bornstein, J. Bodenheimer, and J. Flahaut, J. Lumin. **18/19** (1979) 253
[13] R. Reisfeld, Ann. Chim. Fr. **7** (1982) 147
[14] C. K. Jørgensen and R. Reisfeld, J. Less-Common Metals **93** (1983) 107
[15] B.R. Judd, Phys. Rev. **127** (1962) 750
[16] G.S. Ofelt, J. Chem. Phys. **37** (1962) 511
[17] M.J. Weber, Phys. Rev. **157** (1966) 262
[18] Y.B. Shin, J.N. Jang, and J. Heo, Opt. Quant. Electron. **27** (1995) 379
[19] L. Wetenkamp, G.F. West, and H. Többen, J. Non-Cryst. Solids **140** (1992) 35
[20] B. Peng and T. Izumitani, Opt. Mater. **4** (1995) 797
[21] B.F. Aull and H.P. Jensen, IEEE J. Quantum Elect. **QE-18** (1982) 925
[22] W.J. Miniscalco and R.S. Quimby, Opt. Lett. **16** (1991) 258
[23] D.C. Hanna, P.M. Percival, R.G. Smart, J.E. Townsend, and A.C. Tropper, Electron. Lett. **25** (1989) 593
[24] L. Wetenkamp, Electron. Lett. **26** (1990) 883
[25] J. Schneider, Int. J. Infrared Millimeter Waves **16** (1995) 75
[26] Y.S. Kim, W.Y. Cho, Y.B. Shin, and J. Heo, J. Non-Cryst. Solids **203** (1996) 176
[27] P. Werle, Infrared Phys. Technol. **37** (1996) 59
[28] T Schweizer, B.N. Samson, R.C. Moore, D.W. Hewak, and D.N. Payne, Electron. Lett. **33**, (1997) 414

3.9 Erbium

Erbium (Er^{3+}) doped GLS glass was first reported in the late 70's by Reisfeld and co-workers who concentrated mainly on visible fluorescence bands and near-infrared fluorescence up to 1 μm [Rei78,Rei82]. More recent papers discuss the infrared-to-visible upconversion emission in GLS glasses along with Judd-Ofelt calculations, absorption and lifetime measurements [Hig98, Kad95].

A detailed paper about the spectroscopy of Er^{3+} doped GLS glass with focus on the near-infrared transitions, in particular the 1.55 μm transition for optical fibre amplifiers for telecommunication, has been published by our group prior to the start of this work [Ye96].

The following paper (paper 4) presents several new mid-infrared transitions and also reviews the fabrication of GLS glasses and fibres. The 3.6 μm emission is of interest to the LONGWAVE project because it falls into the atmospheric transmission window (see page 53, Fig 3.8.1) and also overlaps with the absorption bands of H_2S, NO, and SO_2. The 4.5 μm emission could find application as a CO and O_3 gas sensor.

Fabrication and spectroscopy of erbium doped gallium lanthanum sulphide glass fibres for mid-infrared laser applications

T. Schweizer, D.J. Brady and D.W. Hewak

Abstract

Gallium lanthanum sulphide based glasses are proposed as high quality hosts for rare-earth doped, mid-infrared fibre lasers, that would offer compact and rugged sources for gas sensing, atmospheric transmission, and medical applications. The infrared emission spectroscopy of erbium doped glasses and fibres shows the potential of this glass host for the above applications. Mid-infrared transitions at 2.0, 2.75, 3.6, and 4.5 μm have been detected and characterised.

1 Introduction

There is considerable international interest in developing mid-infrared (MIR) laser sources for gas sensing, atmospheric transmission, and medical applications. Many characteristic absorption 'fingerprints' of gases and vapours lie in the 2-5 μm wavelength range, as do the atmospheric transmission windows. Our work targets specific wavelengths for these applications such as 4.3 μm emission from Dy^{3+} for CO_2 detection, 4.7 μm from Pr^{3+} and 4.8 μm from Tb^{3+} for CO and O_3 detection, 3.4 μm from Pr^{3+} for CH_4 detection, and 3.9 μm emission from Ho^{3+} for atmospheric transmission. Diode pumped rare-earth doped fibre lasers would offer compact and efficient alternatives to the either relatively weak, or very complex MIR sources currently available, such as thermal emitters, gas lasers, OPO's or semiconductor lasers.

A fibre laser geometry is advantageous as the waveguiding gives good overlap of pump and laser modes, and the pump intensity is high, reducing the threshold, and increasing efficiency. A prerequisite for the rare-earth host material is a low phonon energy leading to MIR transparency and low non-radiative decay rates and therefore high quantum efficiency of radiative transitions. Conventional silica fibres do not fulfil these requirements leading to a need for new host materials with lower phonon energies that must also be suitable for fibre drawing. Mid-infrared transmitting fibres are currently either fluorozirconate based, with the disadvantages of being hygroscopic, and having a relatively small transmission window (~ 1-3 μm), or As_2X_3 (X = S, Se etc.) based with the disadvantage of toxicity should the fibre burn or degrade, and low rare-earth solubility. Our approach to MIR lasers is based on stable, non-toxic, and non-hygroscopic chalcogenide glasses based on gallium and lanthanum sulphides with the molar composition $70Ga_2S_3$:$30La_2S_3$ (GLS), and $70Ga_2S_3$:$30La_2O_3$ (GLSO), both of which have been drawn into fibre

Paper 4: published in Optics Express **1** (1997) 102

successfully [1]. They have a low phonon energy (425 cm^{-1} for GLS) and a wide transmission window that extends to beyond 8 μm with an absolute loss minimum around 4 μm.

2 Glass properties

Starting materials of Ga_2S_3, La_2S_3, or La_2O_3 powders are batched and mixed, before transferring to a vitreous carbon crucible in a silica tube. Melting is done at 1150^oC for several hours to give a homogeneous glass ingot upon quenching.

Fig. 1 A photograph of GLS glass; a 220 g ingot, some polished rods (110 mm x 8 mm), and a drawn ‘cane’.

For thermal analysis 30 g test melts are produced, which also give enough glass for small bulk glass samples to be cut and polished from. These are used for spectroscopic measurements. Fibre drawing is done by a rod-in-tube method, for which 220 g ingots of glass are produced, cut, and optically polished into rods and tubes. Fig. 1 shows a glass ingot, some polished tubes, and a tube that has been stretched into a cane for insertion into a tube.

Thermal analysis is performed using a Perkin-Elmer DTA7 for transition temperatures, and for viscosity measurements a Perkin Elmer TMA7 is used, which has been adapted for parallel plate rheometry. It is best to perform fibre drawing at temperatures well below the crystallisation temperature of the glass. To this end a simple test of the thermal quality of a glass with respect to fibre drawing may be measured by the separation of the drawing temperature (T_η; the temperature at which the viscosity ~ 10^6 poise) and the peak crystallisation temperature (T_p). A large value for T_p - T_η would give a glass that is more suitable for fibre drawing. For GLS T_p - T_η = 46^{o}C, and for GLSO T_p - T_η = 130^{o}C. This makes GLSO an easier glass to draw into fibre without crystallisation. A typical cross section of a double clad uncoated GLSO fibre is shown in Fig. 2.

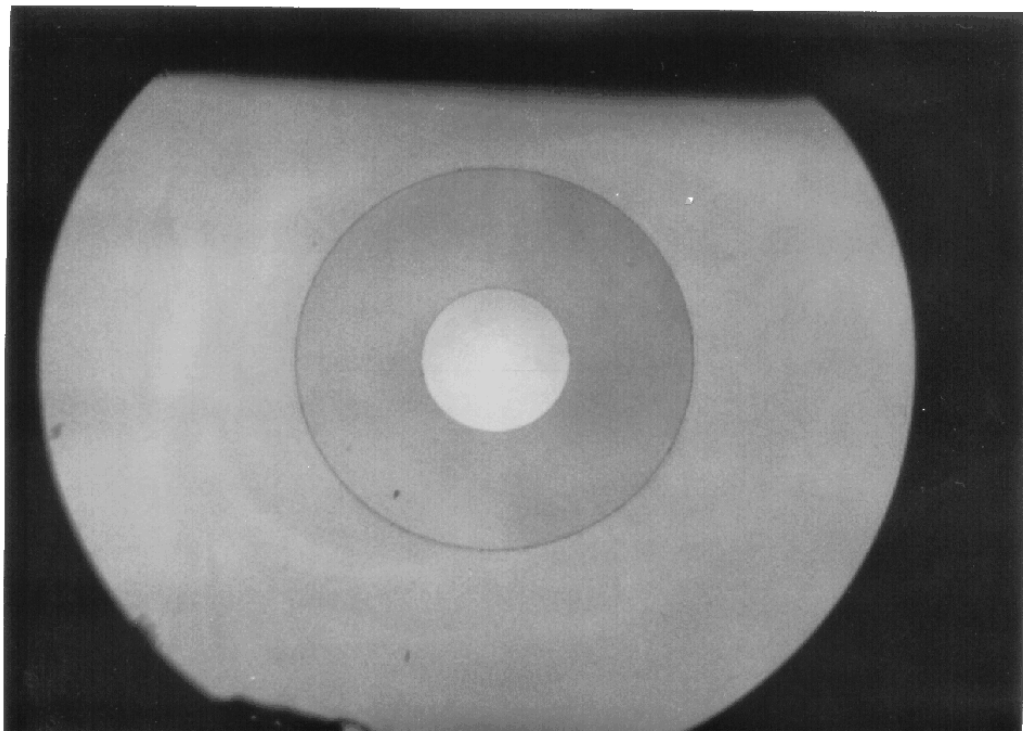

Fig. 2 Cross section of a double clad uncoated GLSO fibre.

Minimum losses of about 4 dBm^{-1} at 4 µm have been achieved in unclad GLSO fibres. The attenuation spectrum is largely flat over a wide wavelengths

range. The loss in the 1-3 μm region of the spectrum has a complex dependence on wavelength that is a combination of absorptions from transition metal impurities and scattering effects. Transition metal absorptions in GLS based glasses have been measured by intentionally doping the glass with transition metals, to identify individual contributions of transition metal ions to the materials loss. In the 3-5 μm region the absorption comes primarily from scattering from inclusions, crystallites and bubbles, and from OH^- impurity introduced by the La_2O_3. It is anticipated that purification of the starting materials will improve the loss considerably by removing the absorptions from transition metals, and also reducing the number of nucleation sites for crystallisation, and hence the scattering loss [2].

These glasses have several advantages over other glass materials as rare-earth hosts. The solubility of rare-earth ions is extremely high due to the presence of lanthanum as a glass former, and the emission cross sections of rare-earth levels are enhanced by the high refractive index (n = 2.4 for GLS and 2.2 for GLSO). Combined with the low phonon energy, this potentially gives access to MIR transitions for lasers. We have chosen the erbium ion as an example to show the effect of the glass host on the spectroscopy of the incorporated rare-earth ions.

3 Mid-infrared spectroscopy of erbium doped GLS glasses and fibres

The trivalent erbium ion (Er^{3+}) is probably the most widely studied rare-earth dopant in glass fibres due to the success of the EDFA (Erbium Doped Fibre Amplifier) in silica based glasses [3]. EDFA's make use of the 1.55 μm transition from the $^4I_{13/2}$ level to the ground state (Fig. 3). In silica glasses the $^4I_{13/2}$ level is the only metastable level with a typical lifetime of 10 ms whereas all the higher lying levels show lifetimes shorter than 10 μs. The high phonon energy of the glass host causes large non-radiative decay rates for levels with small energy gaps to the next lower level and quenches emission from these levels. Changing the host material from silica to a material with lower phonon energies considerably changes the spectroscopic properties of the embedded Er^{3+} ions.

Absorption and emission cross sections of Er^{3+} doped GLS glasses are about 2.5 times higher than in silica glasses whereas the multiphonon decay rates can be orders of magnitude lower for levels with small energy gaps reflecting the high refractive index and the low phonon energy of the glass [4]. The absorption spectrum of a 9.7 mol% Er^{3+} doped GLS glass in Fig. 3 shows the excellent rare-earth solubility and the potential of high doping concentrations and hence short devices which represents a major advantage of GLS glass compared to conventional chalcogenide glasses such as As_2S_3 which suffer from very low rare-earth solubility. For example, a 1.57 mol% Er^{3+} doped glass, as was used for the fluorescence measurements, gives absorption lengths (1/e) of about

3 mm, 12 mm, and 7 mm for the $^4F_{9/2}$, $^4I_{9/2}$, and $^4I_{11/2}$ levels, respectively, without showing any lifetime quenching compared to the low doped sample (Table 1).

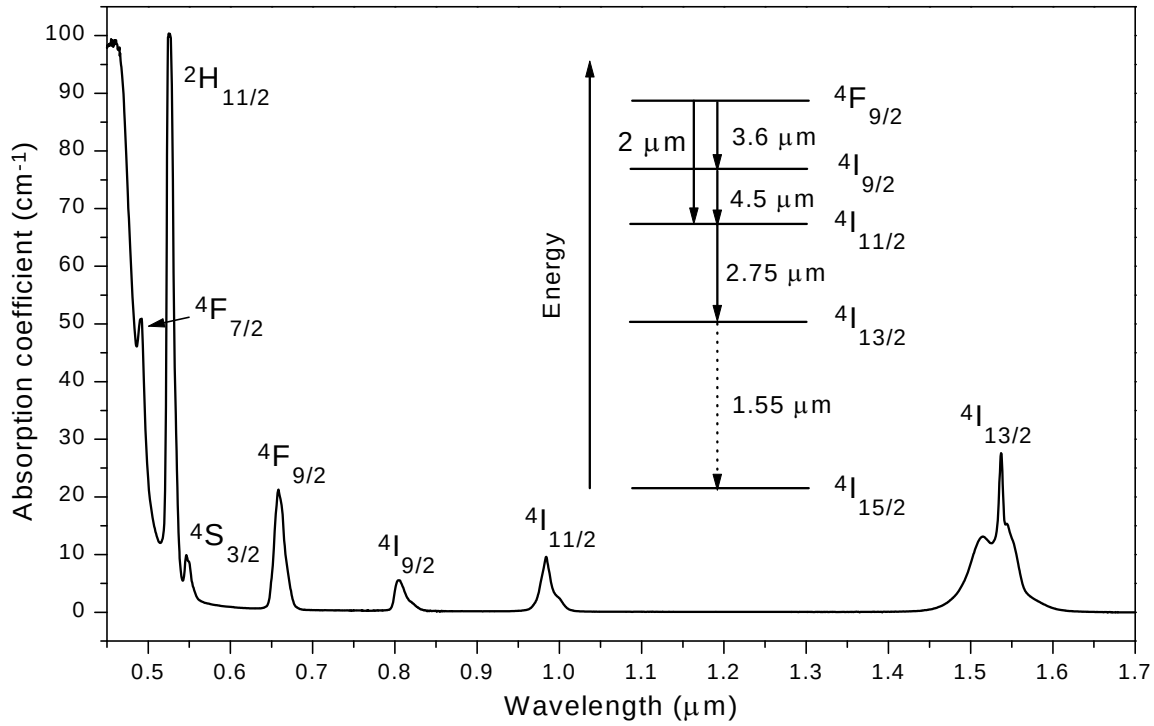

Fig. 3 Absorption spectrum of 9.7 mol% Er^{3+} doped GLS glass and Er^{3+} energy levels indicating the infrared transitions

For spectroscopic measurements the Er^{3+} ions were excited at 660 nm ($^4F_{9/2}$) with a DCM dye laser and at 810 nm ($^4I_{9/2}$) with a Ti:sapphire laser. Fluorescence spectra were measured with a 300-mm monochromator and a liquid nitrogen cooled InSb detector. The fluorescence was collected from the end of the fibres and from the side of the bulk sample, both doped with 1.57 mol% Er^{3+}. Spectra were corrected for system response and atmospheric gas absorptions using a black body source. Fig. 4 shows four infrared Er^{3+} emission bands at 2.0, 2.75, 3.6, and 4.5 μm. The inhomogeneously broadened emission line shapes, typical for glass hosts, offer the possibility of wide wavelengths tuneability. None of these would be observed in silica glasses or other high phonon energy host materials.

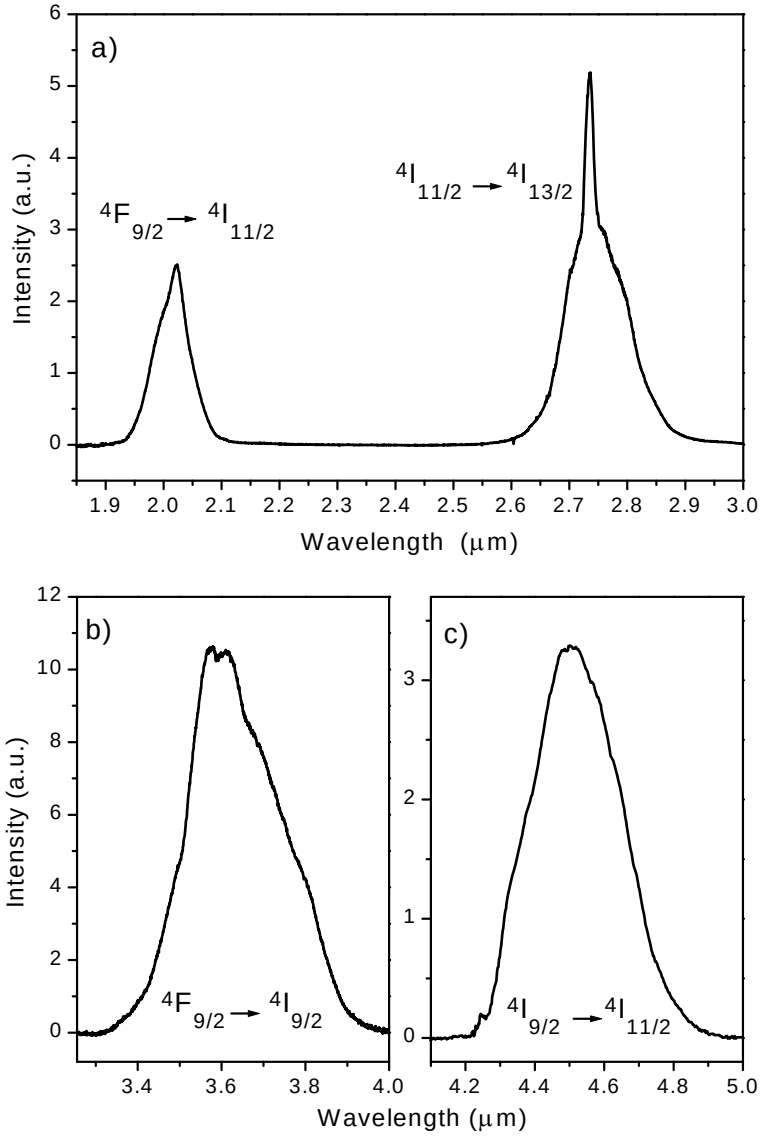

Fig. 4 Fluorescence spectra of 1.57 mol% Er^{3+} doped GLS glasses and fibres
a) 2.0 μm and 2.75 μm emission from 3.9 cm of 270 μm diameter fibre pumped with 60 mW at 660 nm
b) 3.6 μm emission from 8.6 cm of 270 μm diameter fibre pumped with 70 mW at 660 nm
c) 4.5 μm emission from a bulk glass sample pumped with 570 mW at 810 nm

Judd-Ofelt calculations and lifetime measurements for Er^{3+} doped GLS glass are given in Ref. 4. We used the given electric and magnetic dipole contributions, A_{ed} and A_{md}, of the radiative transition rate $A = A_{ed} + A_{md}$ and the radiative and measured lifetimes τ_r and τ_m to calculate the branching ratios $\beta = A \times \tau_r$ and the quantum efficiencies $\eta = \beta \times \tau_m/\tau_r$ for the above transitions (Table 1). The emission cross sections σ_{em} were calculated from the radiative rates A and the measured intensity spectra $I(\lambda)$ using the Füchtbauer-Ladenburg equation as given in Ref. 5:

$$\sigma_{em}(\lambda) = \frac{A\lambda^5 I(\lambda)}{8\pi n^2 c \int \lambda I(\lambda) d\lambda}$$

The refractive index n is 2.36 for all four transitions. Table 1 summarises the radiative properties of the four infrared transitions.

Table 1 Radiative properties of mid-infrared transitions in Er^{3+} doped GLS glass (A_{ed}, A_{md}, τ_r, and τ_m from Ref. 4)

Transition	λ (μm)	A_{ed} (s^{-1})	A_{md} (s^{-1})	β (%)	τ_r (μs)	τ_m (μs)	η (%)	σ_{em} (10^{-20} cm^2)
$^4F_{9/2} \rightarrow {}^4I_{11/2}$	2.02	249	18	3.7	140	100	2.6	1.52
$^4F_{9/2} \rightarrow {}^4I_{9/2}$	3.62	21	8	0.4	140	100	0.3	0.43
$^4I_{9/2} \rightarrow {}^4I_{11/2}$	4.53	4	4	1.0	1200	590	0.5	0.25
$^4I_{11/2} \rightarrow {}^4I_{13/2}$	2.74	70	26	14.7	1530	1230	11.8	1.10

The values in the second and third rows are in good agreement with the results reported recently by L.B. Shaw et. al who obtained branching ratios of 1% both for the 3.6 μm and 4.5 μm transitions with measured lifetimes of 100 μs and 500 μs and cross sections of 0.45×10^{-20} cm^2 and 0.25×10^{-20} cm^2, respectively, in an Er^{3+} doped barium indium gallium germanium sulphide glass [6].

The measured lifetimes for the 0.0158 mol% Er^{3+} doped samples from Ref. 4 do not correspond to the size of the energy gaps to the next lower lying level, i.e. the lifetime of the $^4I_{9/2}$ level is longer than the lifetime of the $^4F_{9/2}$ level although the energy gap is smaller. This clearly indicates that the decay rates are dominated by the radiative decay and that non-radiative rates are very low in GLS glasses.

Nevertheless, quantum efficiencies are relatively low due to the low branching ratios, i.e. strong competing visible and near-infrared transitions from the same levels. However, the demonstration of lasing on the 3.6 μm transition in an Er^{3+} doped fibre based on a fluorozirconate glass with less favourable spectroscopic properties (lower radiative rates and higher non-radiative rates) shows the potential for mid-infrared fibre lasers based on GLS glass [7]. A first step towards the realisation of these devices was the recent demonstration of the first rare-earth doped chalcogenide glass fibre laser in a Nd^{3+} doped GLS glass fibre at 1.08 μm [8].

Radiation at 2 μm finds application in LIDAR systems, radiation at 2.75 μm coincides with a strong water absorption in tissue and is used for medical

applications, the 3.6 μm transition could be useful for H_2S, NO, and SO_2 sensing or remote sensing depending on the wavelengths it is tuned to, and the 4.5 μm transition could find use as CO and O_3 gas sensors when tuned to 4.7 μm.

In conclusion we present the fabrication and spectroscopy of Er^{3+} doped gallium lanthanum sulphide based glasses and fibres showing the suitability of this glass host for rare-earth doped mid-infrared fibre lasers.

Acknowledgements

Starting materials were supplied by Merck Ltd, Poole, UK. This work was in part carried out under the LINK Photonics project LONGWAVE with support from the DTI and the EPSRC.

References

1. D. W. Hewak, R. C. Moore, T. Schweizer, J. Wang, B. Samson, W. S. Brocklesby, D. N. Payne, E. J. Tarbox, "Gallium lanthanum sulphide optical fibre for active and passive applications," *Electron. Lett.* **32,** 384-385 (1996)
2. J. S. Sanghera, V. Q. Nguyen, P. C. Pureza, R. E. Miklos, F. H. Kung, I. D. Aggarwal, "Fabrication of long lengths of low-loss IR transmitting $As_{40}S_{(60-x)}Se_x$ glass fibre," *J. Lightwave Technol.* **14**, 743-748 (1996)
3. P. Urquhart, "Review of rare earth doped fibre lasers and amplifiers," *IEE Proc.-J: Optoelectron.* **135**, Pt. J, No. 6, 385-407 (1988)
4. C.C. Ye, D.W. Hewak, M. Hempstead, B.N. Samson, and D.N. Payne, "Spectral properties of Er3+-doped gallium lanthanum sulphide glass," *J. Non-Cryst. Solids* **208**, 56-63 (1996)
5. B. F. Aull, and H. P. Jenssen, "Vibronic interactions in Nd:YAG resulting in nonreciprocity of absorption and stimulated emission cross sections," *IEEE J. Quantum Elect.* **QE-18**, 925-930 (1982)
6. L.B. Shaw, D. Schaafsma, J. Moon, B. Harbison, J. Sanghera, I. Aggarwal, "Evaluation of the IR transitions in rare-earth-doped chalcogenide glasses," in *Conference on Lasers and Electrooptics*, Volume 11 of 1997 OSA Technical Digest Series (Optical Society of America, Washington, DC, 1997), p. 255.
7. H. Többen, "Room temperature cw fibre laser at 3.5μm in Er^{3+}-doped ZBLAN glass," *Electron. Lett.* **28**, 1361-1362 (1992)
8. T. Schweizer, B.N. Samson, R. C. Moore, D.W. Hewak, and D.N. Payne, "Rare-earth doped chalcogenide glass laser," *Electron. Lett.* **33**, 414-416 (1997)

3.10 Thulium and Terbium

Thulium (Tm^{3+}) and terbium (Tb^{3+}) are discussed together in one section because they form an interesting co-doping combination. Tb^{3+} is considered as a co-dopant for Tm^{3+} to reduce the lower level lifetime of the 1.47 and 3.8 μm Tm^{3+} transitions, whereas Tm^{3+} is considered as a co-dopant for Tb^{3+} to compensate for the lack of convenient near-infrared absorption bands by pump energy transfer from Tm^{3+} to Tb^{3+} (energy level diagram on page 79). The energy transfer is followed by 4.8 μm emission from the Tb^{3+} ions. Little study has been done on either of the two RE ions in chalcogenide glasses. The 3.8 μm emission from Tm^{3+} and the 4.8 μm emission from Tb^{3+} have not been reported in a sulphide glass host before. The following paper describes the spectroscopic properties of Tm^{3+} and Tb^{3+} in singly and co-doped GLS glasses. In addition to the mid-infrared emission bands several cross-relaxation and upconversion processes which are unique to low phonon energy hosts have been observed. The two mid-infrared transitions are of interest to the LONGWAVE project due to their high atmospheric transmission (3.8 μm) (see page 53, Fig. 3.8.1) and overlap with the carbon monoxide absorption band (4.8 μm).

Infrared emission and ion-ion interactions in thulium and terbium doped gallium lanthanum sulphide glass

***T. Schweizer**, B.N. Samson, J.R. Hector, W.S. Brocklesby, D.W. Hewak, and D.N. Payne*

Abstract

Infrared emission at 0.7, 0.8, 1.2, 1.5, 1.8, 2.3, 3.8, and 4.8 μm is measured in thulium (Tm^{3+}) and terbium (Tb^{3+}) doped gallium lanthanum sulphide (GLS) glass. Emission cross sections are calculated from the absorption and emission spectra using Judd-Ofelt analysis, the Füchtbauer-Ladenburg equation, and the theory of McCumber. Fluorescence and lifetime measurements confirm energy transfer from Tm^{3+} to Tb^{3+} ions and reveal a number of new cross-relaxation/upconversion processes between Tm^{3+} ions involving the $^3F_{2,3}$ and $^3H_5$ levels that can only be observed in low phonon energy materials. These processes indicate that the most efficient pump wavelength for the 1.2 μm and 3.8 μm transitions is 0.7 μm. The Tm^{3+} fluorescence at 3.8 μm coincides with an atmospheric transmission window and the Tb^{3+} fluorescence at 4.8 μm overlaps with the fundamental absorption of carbon monoxide, making the glass a potential fibre laser source for remote sensing and gas sensing applications.

1 Introduction

The trivalent thulium ion (Tm^{3+}) is best known as a rare-earth dopant for 2 μm solid-state lasers for LIDAR applications [1]. Although most of the work for this high power application is centred around Tm^{3+} doped laser crystals, continuous wave output powers of more than 1 W at 2 μm have been reported in Tm^{3+} doped silica fibre lasers [2]. The fibre geometry offers high gain due to the long interaction length of pump and laser modes, small pump powers due to the high intensities in the fibre core, favourable thermal conditions due to the good heat dissipation, and the possibility to exploit weak rare-earth absorption bands due to the long optical path in the fibre. In silica fibre Tm^{3+} lasers are limited mainly to the 2 μm transition because strong non-radiative multiphonon decay is competing with the radiative decay and shortens the lifetimes of the energy levels [2,3]. Changing the host for the Tm^{3+} ions from an oxide glass with a high phonon energy (~ 1160 cm^{-1}) to a fluoride glass with a much lower phonon energy (~ 580 cm^{-1}) opens up the possibility of new laser transitions. Lasing has been reported on the 0.8, 1.47, 1.8, and 2.3 μm bands in Tm^{3+} doped fluorozirconate fibre with output powers of up to 1 W on the 1.47 μm transition [4-6]. Amplification at 0.8, 1.47, and 1.65 μm close to the first and third

Paper 5: submitted to J. Am. Soc. B

telecommunication windows has also been demonstrated [7-9]. Lasing on the 2.3 μm transition has proved to be useful for methane gas sensing [10].

Changing the host from fluoride glass to chalcogenide glass (non-oxide glasses based on S, Se, or Te) with an even lower phonon energy (~400 cm^{-1}) offers new radiative transitions in addition to the transitions available in fluoride and oxide glasses. Spectroscopic investigations of Tm^{3+} doped chalcogenide glasses have been reported only recently for GeGaS and GeAsS glasses [11-13]. Emission bands at 0.7 μm and 1.2 μm from transitions which are completely quenched in oxide glasses could be detected in the chalcogenide samples.

We have performed a spectroscopic study of Tm^{3+} doped gallium lanthanum sulphide (GLS) glass which has revealed a new mid-infrared transition at 3.8 μm that has, to our knowledge, not been reported in a glass or any other host before. We also co-doped the glasses with trivalent terbium (Tb^{3+}) and observed energy transfer from Tm^{3+} to Tb^{3+} and 4.8 μm emission from Tb^{3+}. The 4.8 μm emission from Tb^{3+} has, to our knowledge, only been reported once in a chalcogenide glass to date [15]. The emission bands at 3.8 μm and 4.8 μm are unique to chalcogenide glasses and have not been observed in fluoride and oxide glasses. The potential for mid-infrared fibre lasers has been demonstrated before for different chalcogenide glasses and rare-earth dopants other than Tm^{3+} and shows, depending on the emission wavelength, possible applications in gas sensing and remote sensing through the atmospheric transmission window [15-22].

This paper describes the spectroscopic properties of Tm^{3+}, Tb^{3+}, and Tm^{3+}/Tb^{3+} doped gallium lanthanum sulphide (GLS) glasses using absorption, fluorescence, and lifetime measurements. Judd-Ofelt calculations and calculations of the emission cross sections deliver important laser parameters. Variations of the fluorescence intensities with pump wavelength and upconversion emission reveal new cross-relaxation/upconversion processes and indicate the most efficient pump wavelength.

2 Experiments

We melted a series of GLS glasses with the molar ratio $70Ga_2S_3$:$30La_2S_3$ and doped them with Tm^{3+} and Tb^{3+} by replacing La_2S_3 with the required amount of Tm_2S_3 and Tb_2S_3, respectively. Glasses were doped with 0.2 mol% Tm_2S_3 (n_{Tm} = 0.35×10^{20} ions/cm^3), 1.5 mol. % Tm_2S_3, 1.5 mol% Tm_2S_3 and 0.2 mol% Tb_2S_3, and 1.5 mol% Tb_2S_3. These glasses will be referred to simply by Tm(0.2%):GLS, etc. The glasses were cut and polished on three sides for absorption, fluorescence, and lifetime measurements. Absorption spectra were measured from 0.4 μm to 3 μm with a Perkin-Elmer Lambda 9 spectrophotometer and from 1.5 μm to 10 μm with a Fourier-transform spectrometer (Perkin-Elmer System 2000 FT-IR). Samples were excited with a tuneable Ti:sapphire laser at 0.7 μm and 0.8 μm and a 2 μm diode pumped Tm:YAG laser for

fluorescence and lifetime measurements. Fluorescence spectra were recorded with a liquid nitrogen cooled CCD spectrometer (0.7 μm, 0.8 μm), and with a computer driven monochromator and an InGaAs detector (1.1 - 1.6 μm) or liquid nitrogen cooled InSb detector (1.1 - 5.45 μm). Fluorescence decay curves were measured with a photomultiplier (0.7 μm, 0.8 μm), with an InGaAs detector (1.2 μm, 1.7 μm), and a liquid nitrogen cooled InSb detector (4.8 μm) using an acousto-optic modulator or a chopper to modulate the pump beam and a monochromator or a suitable set of filters for wavelengths discrimination. The decay curves were averaged using a photon counting device (Stanford Model SR430 Multi-Channel Scaler) for the photomultiplier and a TEK2232 digital storage oscilloscope for the InGaAs and InSb detectors and transferred to a PC for the fitting procedure. All measurements were performed at room temperature.

3 Results and discussion

Figure 1.a shows the ground state absorption bands from the $^3H_6$ to the five lowest energy levels for a Tm(1.5%):GLS glass. The electronic absorption edge starts at about 0.5 μm and obscures the higher energy levels ($^1G_4$, $^1D_2$, etc.) which have been reported to emit visible and ultraviolet fluorescence in fluoride glasses [23,24]. The closely spaced $^3F_{2,3}$ levels have been treated as one level for the Judd-Ofelt calculations, calculation of radiative lifetime, etc. The infrared multiphonon absorption edge starts at about 8 μm (not shown).

The assignment of the $^3F_4$ and the $^3H_4$ levels is ambiguous in the literature. We designated these levels by their dominant LS contribution [3] which means that the $^3F_4$ level is the lower energy level (see Fig. 1.a and 2). This notation is used in the Ref. [3,9-13] whereas other authors assign the lower level as $^3H_4$ [2,4-8,23,24,26,32,33].

The location and spectral shape of the absorption bands is similar to other glasses. The strength, however, is larger due to the high covalency of the glass bonds [3,11,16,25]. An indication for high covalency is a large value for the Judd-Ofelt parameter Ω_2 which is higher in chalcogenide glasses compared to fluoride and silicate glasses (see Table 2). A large value for Ω_2 is reported to increase the strength of the so called hypersensitive pseudoquadrupolar transitions [25,26] and indeed we find that the absorption strength of the hypersensitive $^3H_6 \rightarrow {}^3H_4$ transition [26] at 0.8 μm is increased by a factor of two relative to the $^3H_6 \rightarrow {}^3F_{2,3}$ transition when compared to the strength in more ionic fluoride glasses with smaller Ω_2 [3,8,23,24]. The peak absorption cross section of the 0.8 μm transition is more than six times higher in GLS than in a high fluorine content fluorophosphate glass [3].

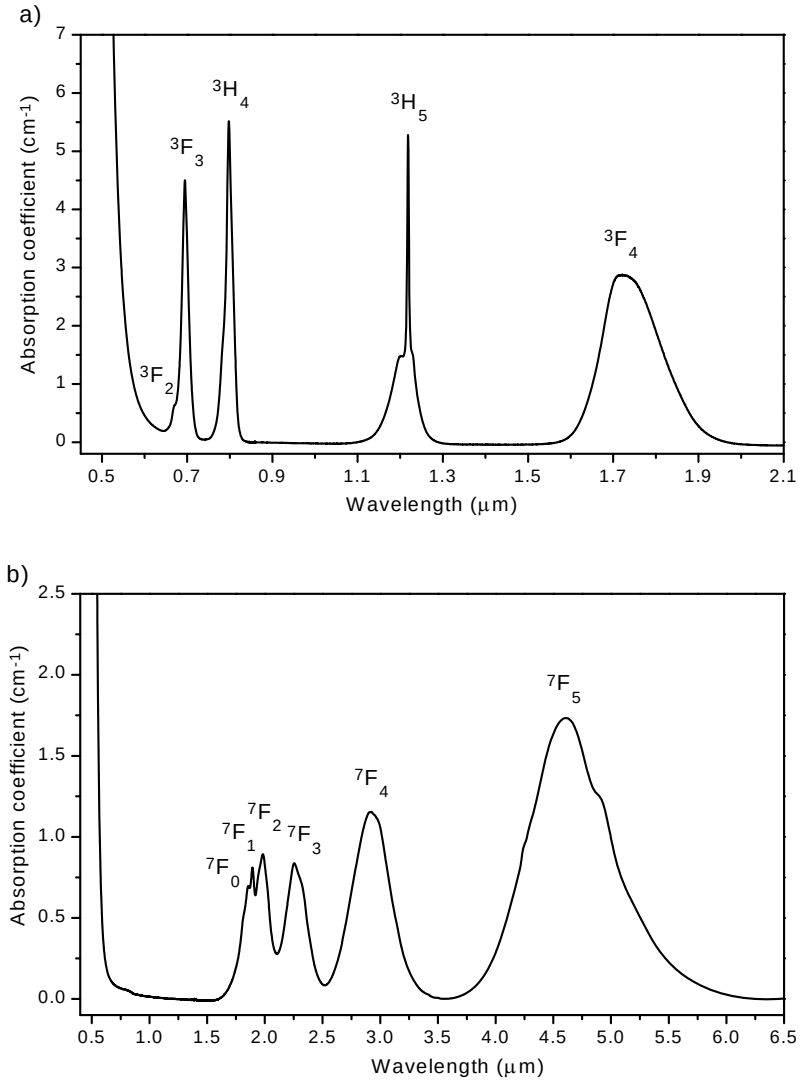

Fig. 1 Room temperature absorption spectra of a) Tm(1.5%):GLS glass and b) Tb(1.5%):GLS glass

We excited the Tm^{3+} ions for fluorescence and lifetime measurements into the 0.7 μm and 0.8 μm bands with a Ti:sapphire laser. In a Tm^{3+} only doped GLS glass excitation at 0.8 μm populates the $^3H_4$ level and subsequently the $^3H_5$ and $^3F_4$ levels via radiative and non-radiative transitions ($^3H_5 \rightarrow {}^3F_4$ in particular). We therefore expect fluorescence at 0.8, 1.47, and 2.3 μm from the $^3H_4$ level, at 1.22 and 3.8 μm from the $^3H_5$ level and at 1.83 μm from the $^3F_4$ level (Fig. 2, 3, 4). Emission from the $^3H_5$ level would not be expected in fluoride and oxide glasses due to much stronger non-radiative multiphonon decay to the $^3F_4$ level. Excitation at 0.7 μm produces additional fluorescence bands at 0.7, 1.1, 1.6, and

5.4 μm, of which only the first two could be detected whereas the third could not be distinguished from the strong 1.8 μm fluorescence and the fourth was beyond the detection limit.

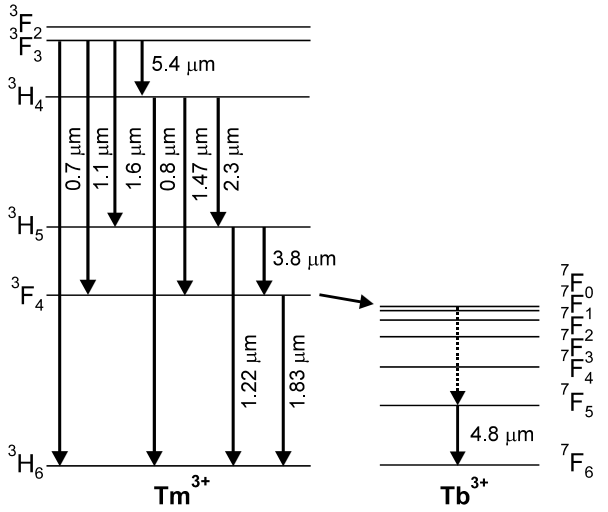

Fig. 2 Energy level diagrams of Tm^{3+} and Tb^{3+} showing the fluorescent transitions and the $Tm^{3+} \rightarrow Tb^{3+}$ energy transfer

The ground state ($^7F_6$) absorption spectrum of Tb(1.5%):GLS glass shows the absorption bands of the $^7F_{0,1,2,3,4,5}$ levels in the mid-infrared wavelengths region (Fig. 1.b). The higher energy levels ($^5D_4$, $^5D_3$, $^5G_6$, etc.) which are usually studied for their visible emission [14] are covered by the fundamental absorption in GLS glass. The Tb^{3+} ions lack convenient absorption bands in the near-infrared wavelengths region but can be pumped directly with a 2 μm Tm:YAG laser. The lack of suitable absorption wavelengths suggests the use of co-doping with other rare-earth ions. The energetic position of the overlapping $^7F_{0,1,2}$ levels is nearly resonant to the lowest Tm^{3+} level, $^3F_4$, providing the possibility of efficient energy transfer from Tm^{3+} ions with absorption bands in the near-infrared to Tb^{3+} ions. Tb^{3+} has been used before as a co-dopant for Tm^{3+} in fluoride glass to reduce the lifetime of the $^3F_4$ Tm^{3+} and thereby increase the inversion on the 1.47 μm transition (Fig. 2) [5].

Emission from the closely spaced ^7F levels of Tb^{3+} is usually quenched by non-radiative multiphonon decay in fluoride and oxide glasses, making comparison to other materials difficult. Only one report of fluorescence from the lowest excited state, $^7F_5$, to the ground state, $^7F_6$, has been reported for chalcogenide glasses to date [15]. We measured Tb^{3+} fluorescence on this transition at 4.8 μm in a Tm^{3+}/Tb^{3+} co-doped GLS glass under direct 2 μm

pumping and under 0.7 μm and 0.8 μm pumping as a result of the $Tm^{3+} \rightarrow Tb^{3+}$ energy transfer (Fig. 2 and 7). This pumping scheme for the Tb^{3+} 4.8 μm transition has, to our knowledge, not been reported before.

Table 1 Judd-Ofelt parameters and radiative properties of Tm^{3+} and Tb^{3+} doped GLS glass

Thulium (Tm^{3+}): $\Omega_2 = 5.7 \times 10^{20}$ cm^2, $\Omega_4 = 1.7 \times 10^{20}$ cm^2, $\Omega_6 = 1.4 \times 10^{20}$ cm^2									
Transition	λ (μm)	A_{ed} (s^{-1})	A_{md} (s^{-1})	β (%)	τ_r (μs)	τ_m (μs)	η (%)	$\sigma_{em,FL}$ (10^{-20}cm^2)	$\sigma_{em,MC}$ (10^{-20}cm^2)
$^3F_4 \rightarrow {}^3H_6$	1.83	1034		100	970	1160	100	1.25	1.22
$^3H_5 \rightarrow {}^3H_6$	1.22	1085	195	97	760	730	93	2.68	2.51
$\rightarrow {}^3F_4$	3.88	36		3			3	0.27	
$^3H_4 \rightarrow {}^3H_6$	0.80	5708		90	158	220	90	2.16	2.82
$\rightarrow {}^3F_4$	1.47	490		8			8	0.52	
$\rightarrow {}^3H_5$	2.32	86	35	2			2	0.51	
$^3F_{2,3} \rightarrow {}^3H_6$	0.70	10799		65	60	27	29	1.79	1.68
$\rightarrow {}^3F_4$	1.16	3331	231	21			9		
$\rightarrow {}^3H_5$	1.62	2188	102	14			6		
$\rightarrow {}^3H_4$	5.38	87	2	0.5			0.2		
Terbium (Tb^{3+}): $\Omega_2 = 6.4 \times 10^{20}$ cm^2, $\Omega_4 = 3.9 \times 10^{20}$ cm^2, $\Omega_6 = 2.2 \times 10^{20}$ cm^2									
$^7F_5 \rightarrow {}^7F_6$	4.8	55	5	100	16700	~100	0.6	0.89	0.81
$^7F_4 \rightarrow {}^7F_6$	3.0	142		92	6450				
$\rightarrow {}^3F_5$	8.1	11	2	8					

The radiative properties of the fluorescent Tm^{3+} and Tb^{3+} transitions can be obtained from Judd-Ofelt calculations [27,28]. The absorption spectra of Tm^{3+} and Tb^{3+} doped GLS glasses were used to calculate the Judd-Ofelt parameters which in turn allow the calculation of the radiative rates, lifetimes, and branching ratios of the fluorescent transitions. The electric and magnetic dipole contributions, A_{ed} and A_{md}, of the radiative transition rate $A = A_{ed} + A_{md}$ were calculated from the equations given in [29] and are listed in Table 1. The branching ratios $\beta = A / A_{total}$ and the radiative lifetimes $\tau_r = 1 / A_{total}$ were

derived from the radiative rates. Comparison of τ_r with the measured lifetimes τ_m gives the quantum efficiencies $\eta = \beta \times (\tau_m / \tau_r)$. Whereas β is only weakly dependent on the host material, A (and therefore τ_r) and τ_m (and therefore η) show a much stronger dependence. The Judd-Ofelt parameters for Tm^{3+}, and the radiative rates, the measured lifetimes, the quantum efficiencies, and the emission cross sections of the $^3H_4 \rightarrow {}^3H_6$ transition (0.8 μm) are listed for different glasses in Table 2. The radiative rates, A, are highest in the chalcogenide glasses, the materials with the largest Ω_2 parameters and hence the highest covalency, and smallest in the ionic fluoride glasses. The same applies

Table 2 Judd-Ofelt parameters, radiative emission probabilities and emission cross sections for the $^3H_4 \rightarrow {}^3H_6$ transition (0.8 μm), and measured lifetimes of the $^3H_4$ level for different Tm^{3+} doped glasses

Glass (Tm^{3+} conc.)	Ω_2 ($10^{20}cm^2$)	Ω_4 ($10^{20}cm^2$)	Ω_6 ($10^{20}cm^2$)	A (s^{-1})	τ_m (μs)	η (%)	σ_{em} ($10^{-20}cm^2$)
GLS (0.2%)	5.7	1.7	1.4	5708	220	90	2.16-2.82
$Ge_{30}As_{10}S_{60}$ [11]	5.67	1.74	1.82	6463			
$Ge_{25}Ga_5S_{70}$ [11]	6.91	3.41	2.72	5473			
Fluoride (0.5%) [32]	1.90	1.65	1.11	594	1380	82	0.315
ZBLALi (0.5%) [23]	2.80	1.91	1.01	703	970	68	
Silicate (0.5%) [32]	3.26	1.20	0.46	702	35	2.5	0.49

to the emission cross sections. The measured lifetimes show the influence of the non-radiative decay via multiphonon emission. The lifetime is longest in the fluoride glass due to the low radiative rate (ionic, low refractive index) and the low non-radiative rate (small phonon energy of ~ 580 cm^{-1}), shorter in GLS glass due to the higher radiative rates (strongly covalent, high refractive index) and the low non-radiative rate (small phonon energy of ~ 425 cm^{-1}), and shortest in the silicate glass due to the high non-radiative rate (large phonon energy of ~ 1160 cm^{-1}) along with the small radiative rate (intermediate bonding, low refractive index). This is also reflected by the low quantum efficiency of the $^3H_4$ level in the silicate glass, making this glass unsuitable as a laser material for transitions originating from that level. For the chalcogenide and the fluoride glass the transition is almost purely radiative, so the quantum efficiencies are equal to the branching ratios. This does not apply to energy levels with an even smaller energy gap to the next lower lying level, such as the $^3F_{2,3}$ and the $^3H_5$ levels. For these levels non-radiative decay becomes dominant in fluoride

glasses quenching the lifetime and the fluorescence. Emission from these levels, however, has been measured in GLS glass and other chalcogenide glasses [11,12] and will be described later.

The emission cross sections (Table 1) were calculated following two different approaches. First we used the Füchtbauer-Ladenburg equation as given in [30]:

$$\sigma_{em,FL}(\lambda) = \frac{A\lambda^5 I(\lambda)}{8\pi n^2 c \int \lambda I(\lambda) d\lambda} \qquad (1)$$

Comment [ORC1]:

I(λ) is the measured intensity spectrum of the fluorescence, n is the refractive index.

In order to check the above results we used the theory of McCumber after Miniscalco and Quimby [31] to calculate the emission cross sections $\sigma_{em,MC}$ of the four Tm^{3+} ground state transitions at 0.7, 0.8, 1.2, and 1.8 μm and the Tb^{3+} transition at 4.8 μm from the absorption cross sections σ_{abs}:

$$\sigma_{em,MC}(\lambda) = \sigma_{abs}(\lambda)\frac{Z_l}{Z_u}\exp\left(\frac{E_{ZL} - 10^4/\lambda}{kT}\right) \qquad (2)$$

Z_l and Z_u are the partition functions of the lower and the upper manifold, respectively. E_{ZL} is the energy gap between the lowest Stark level of the ground state manifold and the lowest Stark level of the upper manifold measured in cm^{-1}, λ is the wavelength in microns and k = 0.695 $cm^{-1}K^{-1}$ is the Boltzmann constant. Z_l, Z_u, and E_{ZL} are usually obtained from the energy levels of the manifolds and the Stark levels within these manifolds. As this information is not available for the case of GLS glass, the parameters Z_l, Z_u, and E_{ZL} can be obtained from a simplified model which has been explained in detail in Ref. [31] and has recently been applied to dysprosium (Dy^{3+}) doped GLS glass [19]. The calculated emission cross section spectra of the four Tm^{3+} transitions are shown in Fig. 3 together with the absorption spectra and the measured fluorescence spectra which were multiplied by λ^5 and a constant C. A high resolution spectrum of the 1.22 μm fluorescence was not available, and the Tb^{3+} spectra are not shown. The modified McCumber theory is capable of producing absolute emission cross sections as well as the right emission line shape (Fig. 3) from the absorption spectra without a detailed knowledge of the electronic structure of the rare-earth energy levels.

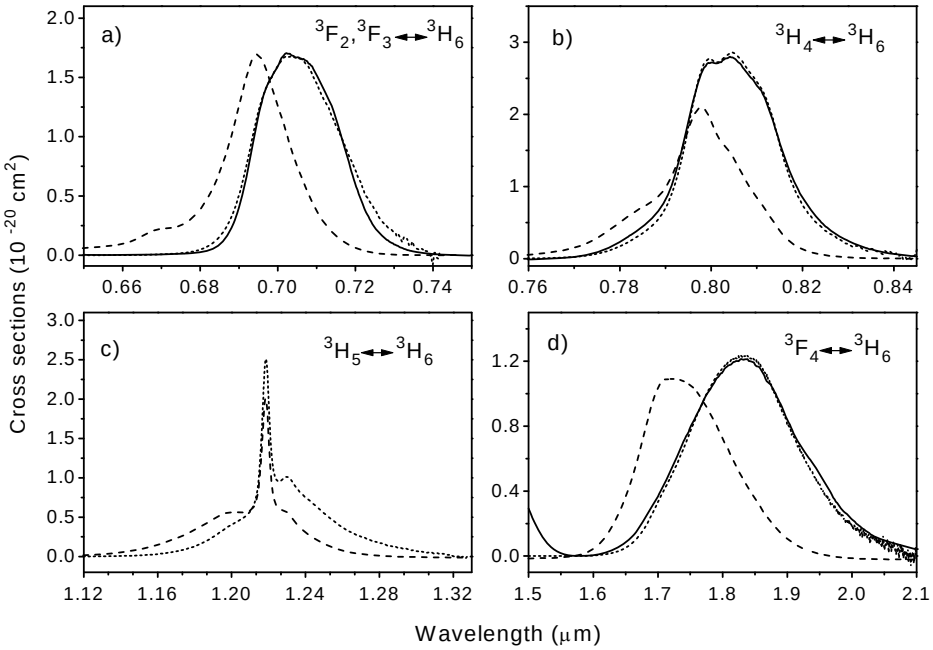

Fig. 3 Absorption cross sections (dashed lines) and McCumber emission cross sections (dotted lines) together with the scaled measured fluorescence spectra (solid lines) of a) the 0.7 μm, b) the 0.8 μm, c) the 1.22 μm, and d) the 1.83 μm ground state transitions of Tm^{3+} doped GLS glass

The emission cross sections obtained from the theory of McCumber (Table 1) confirm the values calculated from the Judd-Ofelt calculations and the Füchtbauer-Ladenburg equation. They are slightly smaller, except for the $^3H_4 \rightarrow {}^3H_6$ Tm^{3+} transition which may be larger due to the hypersensitivity of this transition, but lie in the range of accuracy [31].

Fig. 4 shows Tm^{3+} fluorescence bands starting from the $^3H_4$ (1.47 and 2.3 μm), $^3H_5$ (1.22 μm), and $^3F_4$ (1.83 μm) levels under 0.8 μm pumping directly into the $^3H_4$ level (see also Fig. 2). Increasing the Tm^{3+} concentration from 0.2 % (Fig. 4.a) to 1.5 % (Fig. 4.b) significantly increases the fluorescence intensity of the 1.83 μm band compared to the emission bands from the $^3H_4$ and $^3H_5$ levels. This effect can be explained by the well known cross-relaxation ($^3H_4$,$^3H_6$) $\rightarrow$ ($^3F_4$,$^3F_4$) [11-13,32] and is shown schematically in Fig. 5.a. One excited ion interacts with an ion in the ground state and both end up in the $^3F_4$ state. The process is also reflected by the results of lifetime measurements which are summarised in Table 3. A higher Tm^{3+} concentration increases the probability of the cross-relaxation process providing an additional decay channel for ions in the $^3H_4$ state and thereby shortening the lifetime of this level from 220 μs in Tm(0.2%):GLS to 94 μs in Tm(1.5%):GLS.

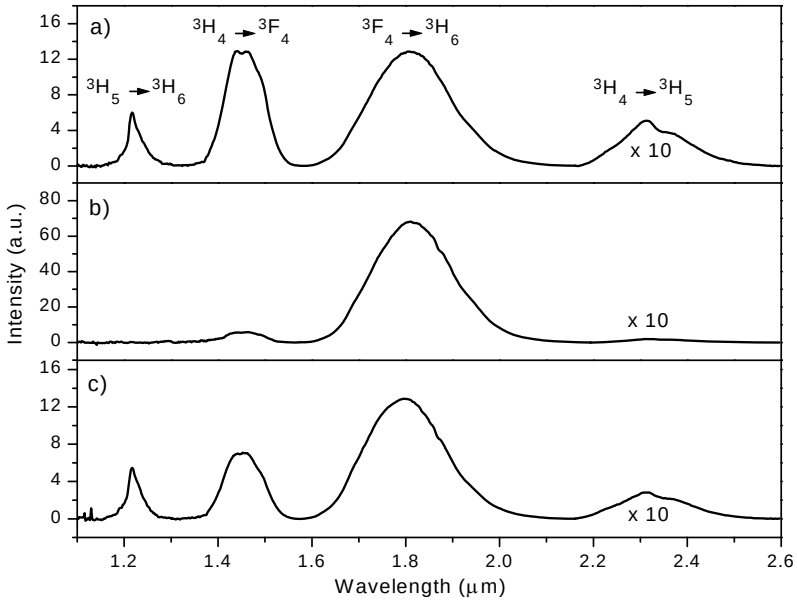

Fig. 4 Fluorescence spectra of a) Tm(0.2%):GLS, b) Tm(1.5%):GLS, and c) Tm(1.5%),Tb(0.2%):GLS for 0.8 μm pumping (The 2.3 μm band has been multiplied by 10.)

Table 3 Lifetimes of the $^3F_{2,3}$, $^3H_4$, $^3H_5$, and $^3F_4$ levels in Tm^{3+} and Tm^{3+}/Tb^{3+} co-doped GLS glasses

Level	0.2mol% Tm_2S_3	1.5mol% Tm_2S_3	1.5mol% Tm_2S_3 + 0.2mol% Tb_2S_3
$^3F_2, ^3F_3$	27μs	11μs	11μs
$^3H_4$	220μs	94μs	86μs
$^3H_5$	730μs	178μs	123μs
$^3F_4$	1160μs	1020μs	128μs

Addition of 0.2 % Tb^{3+} to Tm(1.5%):GLS decreases the intensity of the 1.83 μm fluorescence (Fig. 4.c) due to the efficient energy transfer from Tm^{3+} to Tb^{3+} as it is indicated in Fig. 2. The transfer almost reverses the effect of the higher Tm^{3+} concentration completely (Fig. 4.a and c). Again this process is supported by lifetime measurements (Table 3). The $^3F_4$ lifetime is quenched most strongly from 1020 μs to 128 μs by the addition of Tb^{3+} while the lifetimes of the other levels which are already shortened by Tm^{3+}-Tm^{3+} interactions are

affected much less. The additional Tm^{3+} decay rates due to the Tb^{3+} co-doping can be calculated from the lifetimes in Table 3. They are about 1000 s^{-1}, 2500 s^{-1}, and 6800 s^{-1} for the $^3H_4$, $^3H_5$, and $^3F_4$ levels, respectively, and reflect the different efficiencies of the cross-relaxation processes involved. The lifetime of the $^3F_4$ level is similar to the lifetime of the Tb^{3+} $^7F_5$ level (~ 100 μs)

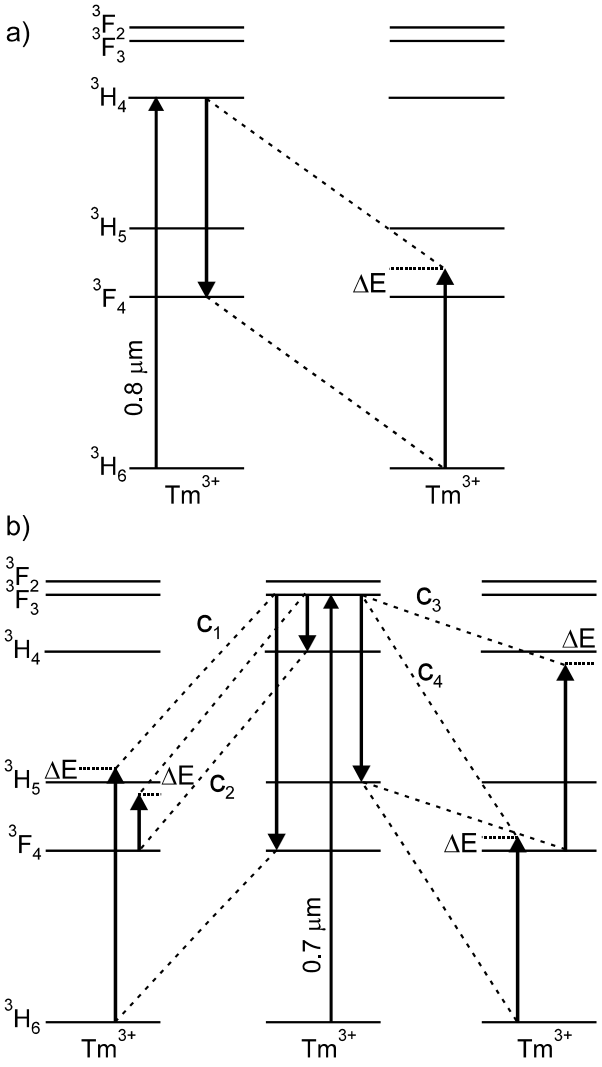

Fig. 5 Energy transfer via cross-relaxation from excited Tm^{3+} ions a) in the $^3H_4$ level and b) in the $^3F_{2,3}$ levels

showing the efficiency of the energy transfer. The Tb^{3+} co-doping decreases the population of the Tm^{3+} $^3F_4$ level and thereby decreases the threshold for inversion on the Tm^{3+} 1.47 μm and 3.8 μm transitions (Fig. 2) [5]. This can also be achieved by lasing on the 1.83 μm $^3F_4 \rightarrow {}^3H_6$ transition as reported in [4].

Changing the pump wavelength from 0.8 μm to 0.7 μm caused some unusual

changes to the relative Tm^{3+} fluorescence intensities. Initially one would expect the excited $^3F_{2,3}$ levels to decay mainly non-radiatively by multiphonon processes to the $^3H_4$ level (energy gap of about 1850 cm^{-1}), resulting in a similar emission spectrum for 0.7 μm and 0.8 μm pumping (Fig. 2). This would be the case in fluoride and oxide glasses. In GLS glass, however, significant differences in the relative intensities of the emission bands were observed. Fig. 6 shows the intensities of the 1.22 μm and the 1.47 μm bands in a) Tm(0.2%):GLS and b) Tm(1.5%):GLS for the two different pump wavelengths.

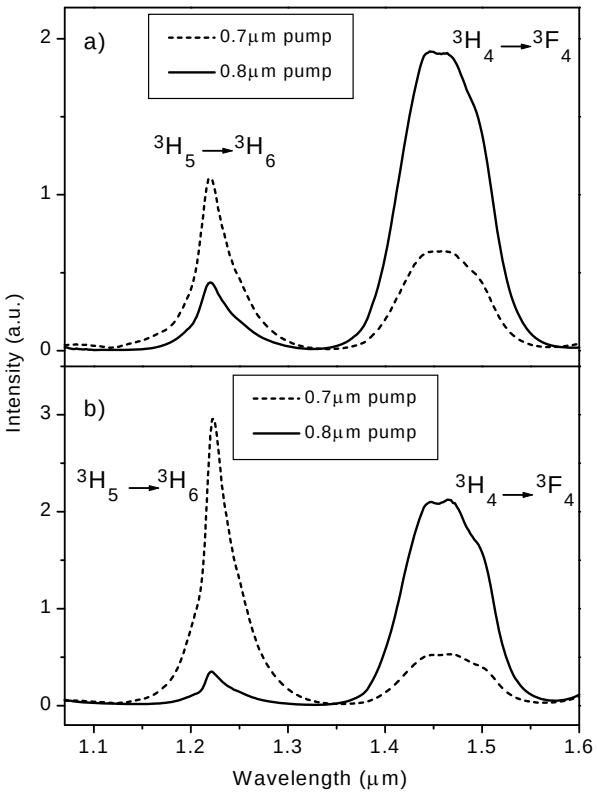

Fig. 6 Variation of the fluorescence intensities from the $^3H_5$ and the $^3H_4$ levels for 0.7 μm (dotted line) and 0.8 μm (solid line) excitation for a) Tm(0.2%):GLS and b) Tm(1.5%):GLS glass

The emission from the $^3H_5$ level (1.22 μm) increases and the emission from the $^3H_4$ level (1.47 μm) decreases when the pump wavelength is changed from 0.8 μm to 0.7 μm (The emission from the $^3F_4$ level (1.83 μm) is not effected significantly.). For this to happen a part of the excitation energy that has been deposited in the $^3F_{2,3}$ levels must bypass the $^3H_4$ level and fill the $^3H_5$ level (see

Fig. 2). A radiative transition from the $^3F_{2,3}$ levels to the $^3H_5$ level would occur at about 1.6 μm and but was not observed in the fluorescence spectra. It is possibly too weak to be distinguished from the strong 1.83 μm fluorescence. Another transition originating from the $^3F_{2,3}$ levels, the $^3F_{2,3} \rightarrow {}^3F_4$ transition at 1.1 μm (Fig. 2), can be seen as a very weak band in Fig. 6 for 0.7 μm pumping (dotted curve). The 1.6 μm transition ($^3F_{2,3} \rightarrow {}^3H_5$) will be of the same order of magnitude and can therefore not be responsible for the large increase of population in the $^3H_5$ level.

After we ruled out radiative processes we now consider non-radiative processes. Since the effect of the different pump wavelengths is more pronounced for the higher concentration (Fig. 6) it may be caused by ion-ion interactions. Fig. 5.b shows four possible cross-relaxations (c_1 to c_4) for a Tm^{3+} ion which has been excited into the $^3F_{2,3}$ levels by 0.7 μm radiation (central ion). The cross-relaxations are c_1: ($^3F_{2,3}$,$^3H_6$) → ($^3F_4$,$^3H_5$), c_2: ($^3F_{2,3}$,$^3F_4$) → ($^3H_4$,$^3H_5$), c_3: ($^3F_{2,3}$,$^3F_4$) → ($^3H_5$,$^3H_4$), and c_4: ($^3F_{2,3}$,$^3H_6$) → ($^3H_5$,$^3F_4$). Note that all four cross-relaxations have the $^3H_5$ level as one of their final states and can therefore explain the increase in population in that level for 0.7 μm pumping. It
should also be pointed out that the energy mismatch, ΔE, for all four cross-relaxations is smaller than the mismatch of the cross-relaxation from the $^3H_4$ level (Fig. 5). Since the probability for the process to occur is exponentially dependent on the energy mismatch [33] the cross-relaxations from the $^3F_{2,3}$ levels should be several times more efficient. Of these four cross-relaxations c_1 and c_4 will be of greater importance than c_2 and c_3 because the first two processes involve the emission of phonons whereas the last two involve the absorption of phonons which requires the availability of exited phonon modes and hence has a lower probability. Two of the cross-relaxations (c_1 and c_4) involve a neighbouring ion in the ground state and therefore depend on ion concentration only, neglecting ground state bleaching at high pump intensities. The other two processes (c_2 and c_3) require a neighbouring ion in the first excited state, $^3F_4$, and will therefore be negligible at low pump intensities. For these two reasons the processes c_1 and c_4 will have the greatest impact on the shortening of the $^3F_{2,3}$ levels lifetime from 27 μs to 11 μs with increasing Tm^{3+} concentration (Table 3). The fluorescence decay curves of the $^3H_4$ and $^3H_5$ levels which are exponential for 0.8 μm pumping become non-exponential for 0.7 μm pumping, again showing the additional cross-relaxations for the shorter pump wavelength. The effect could be observed for all three samples listed in Table 3 implying that even the decay times for the Tm^{3+} doped sample with the low concentration may be shortened by ion-ion interactions. We conclude that the unexpected dependence of the 1.22 μm and 1.47 μm fluorescence intensities on the pump wavelength can be accounted for by ion-ion interactions which transfer energy directly from the $^3F_{2,3}$ levels to the $^3H_5$ level bypassing the $^3H_4$ level. The implication of this effect is that 0.7 μm will be the more efficient

pump wavelength for laser transitions originating from the $^3H_5$ level. A way to increase the pump efficiency for 0.8 μm pumping could be lasing on the 2.3 μm $^3H_4 \rightarrow {}^3H_5$ transition (Fig. 2) [4].

The reverse process to the cross-relaxation is the upconversion process. The reverse processes of the cross-relaxations c_1 to c_4 will be denoted u_1 to u_4 and describe interactions between one excited Tm^{3+} ion in the $^3H_5$ state and one ion in either the $^3H_4$ (u_3) or $^3F_4$ (u_1, u_2, and u_4) states which would lead to population in the higher $^3F_{2,3}$ levels. In the same way as c_1 and c_4 will be the most likely cross-relaxations, u_2 and u_3 will be the most likely upconversion processes following the reasoning given above. Indeed, we detected 0.7 μm upconversion emission from the $^3F_{2,3}$ levels for 0.8 μm pumping. The 0.7 μm upconversion emission spectrum is identical to the spectrum under direct excitation (Fig. 3.a). The fluorescence decay curve of the $^3F_{2,3}$ levels under 0.8 μm pumping takes on the shape of a double exponential with the first exponential reflecting the $^3F_{2,3}$ levels lifetime for 0.7 μm pumping (Table 3) and the significantly longer second exponential (190 μs for Tm(0.2%):GLS, 77 μs for Tm(1.5%):GLS, and 64 μs for Tm(1.5%),Tb(0.2%):GLS) reflecting the filling of the $^3F_{2,3}$ levels by interactions between Tm^{3+} ions in the metastable $^3H_4$, $^3H_5$, and $^3F_4$ levels for 0.8 μm pumping. Another indication for the existence of the upconversion processes is the shortening of the $^3H_5$ and $^3F_4$ lifetimes for increasing Tm^{3+} concentration (Table 3). A qualitative analysis using rate equations and the measurement of the upconversion parameters will be cumbersome due to the mere number of upconversion and cross-relaxation processes that are involved and determine the decay times of the energy levels.

The 0.7 μm upconversion emission under 0.8 μm pumping has been reported before only once in a GeGaS glass [12]. The authors suggested that the emission may be due to upconversion to the $^1G_4$ level followed by emission on the $^1G_4 \rightarrow {}^3F_4$ transition. The $^1G_4$ level, however, cannot be seen in the absorption spectrum (Fig. 1.a) and is probably quenched by efficient energy transfer to the glass host. Also excited-state absorption measurements show that the $^3F_4 \rightarrow {}^1G_4$ transition is located around 0.65 μm [34]. The 0.7 μm emission is therefore more likely to originate from the $^3F_{2,3}$ levels which have been populated by the upconversion processes described above.

The reported cross-relaxation and upconversion processes in GLS glass will only manifest itself in materials with low phonon energies which increase the lifetimes of the $^3F_{2,3}$ and the $^3H_5$ levels and allow them to interact with other ions. These processes are therefore not expected in fluoride and oxide glasses.

In addition to the 1.22 μm ground state transition from the $^3H_5$ level we also observed a 3.8 μm transition from the $^3H_5$ to the $^3F_4$ level (Fig. 2 and 7).

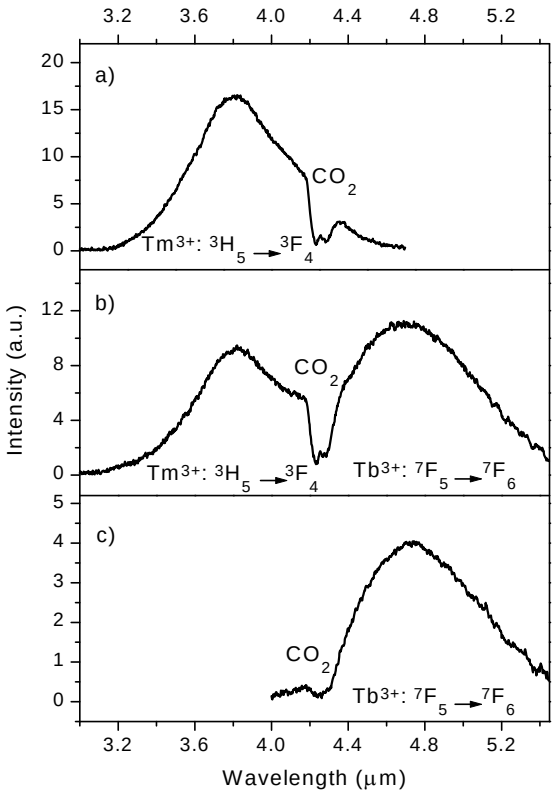

Fig. 7 Uncorrected fluorescence spectra of
a) Tm(1.5%):GLS glass pumped at 0.7 μm
b) Tm(1.5%),Tb(0.2%):GLS glass pumped at 0.7 μm
c) Tm(1.5%),Tb(0.2%):GLS glass pumped at 2 μm

Similar to the 1.22 μm transition the 3.8 μm emission was found to increase for 0.7 μm pumping. The upper level lifetime (730 μs) of this transition is surprisingly long in a low doped GLS glass considering that the $^3H_5$ level is usually quenched in other glass systems. The quantum efficiency of the 3.8 μm transition (3%) is reasonably high for mid-infrared transitions. The fluorescence spectrum of Tm(1.5%)GLS pumped at 0.7 μm in Fig. 7.a has not been corrected for system response in order to show the 4.23 μm absorption band of the atmospheric CO_2. The atmospheric transparency reaches an absolute transmission maximum just below the CO_2 absorption band around 3.9 μm making laser sources in this wavelength range an ideal tool for remote sensing and counter measures.

The Tm(1.5%),Tb(0.2%):GLS sample (Fig. 7.b) pumped at 0.7 μm shows an additional fluorescence at 4.8 μm. This emission band can be attributed to the $^7F_5 \rightarrow {}^7F_6$ transition in Tb^{3+} which is excited by energy transfer from the lowest

excited Tm^{3+} level, $^3F_4$ (Fig. 2). The Tb^{3+} emission is virtually independent of the Tm^{3+} pump wavelength (0.7 μm and 0.8 μm) because the population of the $^3F_4$ Tm^{3+} level does not depend significantly on the pump wavelength.

The same sample emits at 4.8 μm without any additional 3.8 μm emission from Tm^{3+} ions (Fig. 7.c) when the Tb^{3+} ions are pumped directly with a diode pumped Tm:YAG laser at 2 μm, a wavelength where Tm^{3+} absorption is negligible (Fig. 1). The decay time of the 4.8 μm emission is ~ 100 μs which is similar to the 160 μs reported in Tb^{3+} doped telluride glass which has an even lower phonon energy [15]. Comparison to the calculated radiative lifetime shows that the $^7F_5 \rightarrow {}^7F_6$ transition is dominated by non-radiative multiphonon decay which reduces the quantum efficiency of this transition to less than 1% (Table 1). The 4.8 μm emission is quenched below the detection limit in a glass with a higher Tb^{3+} concentration (Tb(1.5%):GLS). A possible explanation for this effect are efficient upconversion processes from the $^7F_5$ level to higher energy levels. Fluorescence from levels higher than the $^7F_5$ level are quenched by non-radiative multiphonon decay. A mid-infrared fibre laser around 4.8 μm based on Tb^{3+} doped GLS glass could find application as a CO gas sensor.

4 Conclusion

In conclusion, we have presented spectroscopic data of Tm^{3+} and Tb^{3+} doped GLS glasses with respect to their suitability for mid-infrared laser devices. A quantitative analysis using Judd-Ofelt calculations, the Füchtbauer-Ladenburg equation, and the modified McCumber theory along with absorption, fluorescence, and lifetime measurements delivered important laser parameters such as the absorption and emission cross sections, laser level lifetimes, and quantum efficiencies. A qualitative discussion of the dependence of fluorescence intensities and lifetimes on the pump wavelength, the Tm^{3+} concentration, and the Tm^{3+}/Tb^{3+} co-doping revealed some interesting interionic processes which can only be observed due to the low phonon energy of the glass host. The observed pump wavelengths dependence shows that a 3.8 μm Tm^{3+} laser can be pumped more efficiently at 0.7 μm than at 0.8 μm, whereas a 4.8 μm Tb^{3+} laser relying on Tm^{3+} to Tb^{3+} energy transfer can be pumped at either wavelength with similar efficiencies. The Tm^{3+}/Tb^{3+} co-doping has two positive effects: (i) the lifetime of the $^3F_4$ Tm^{3+} level, which is the lower level of the 3.8 μm transition, is shortened increasing the inversion on this transition, and (ii) the 4.8 μm Tb^{3+} transition, which can be pumped directly at 2 μm, can be excited at the much more convenient wavelengths of 0.7 μm and 0.8 μm.

GLS glass is a promising host material for mid-infrared fibre lasers because it is one of the few chalcogenide glasses that has been pulled into fibre form successfully [35] and is the only rare-earth doped chalcogenide fibre with demonstrated laser action to date [36].

Acknowledgements

This work was supported by the UK EPSRC/DTI LINK programme (LONGWAVE). Chalcogenide powders were supplied by Merck Ltd. Thanks to R.A. Hayward for providing the 2 μm Tm:YAG laser source and to C.R. Haythornthwaite for his assistance with the CCD spectrometer.

References

1. S.W. Henderson, P.J.M. Suni, C.P. Hale, S.M. Hannon, J.R. Magee, D.L. Bruns, and E.H. Yuen, "Coherent laser radar at 2 μm using solid-state lasers," IEEE Transactions on Geoscience and Remote Sensing **31**, 4-15 (1993)
2. D.C. Hanna, I.R. Perry, and J.R. Lincoln, "A 1-Watt thulium-doped cw fibre laser operating at 2 μm," Opt. Commun. **80**, 52-56 (1990)
3. M.J.F. Digonnet, "Rare-earth doped fiber lasers and amplifiers," Marcel Dekker Inc., New York, Basel, Hong Kong, 1993, pp. 105-120
4. J.Y. Allain, M. Monerie, and H. Poignant, "Tunable cw lasing around 0.82, 1.48, 1.88 and 2.35 μm in thulium-doped fluorozirconate fibre," Electron. Lett. **25**, 1660-1662 (1989)
5. R.M. Percival, D. Szebesta, and S.T. Davey, "Thulium doped terbium sensitised cw fluoride fibre laser operating on the 1.47 μm transition," Electron. Lett. **29**, 1054-1056 (1993)
6. Y Miyajima, T. Komukai, and T. Sugawa, "1-W cw Tm-doped fluoride fibre laser at 1.47 μm," Electron. Lett. **29**, 660-661 (1993)
7. J.N. Carter, R.G. Smart, D.C. Hanna, and A.C. Tropper, "Lasing and amplification in the 0.8 μm region in thulium doped fluorozirconate fibres," Electron. Lett. **26**, 1759-1761 (1990)
8. T. Komukai, T. Yamamoto, T. Sugawa, and Y Miyajima, "Upconversion pumped thulium-doped fluoride fiber amplifier and laser operating at 1.47 μm," IEEE J. Quantum Elect. **31**, 1880-1889 (1995)
9. T. Sakamoto, M. Shimizu, M. Yamada, T. Kanamori, Y. Ohishi, Y. Terunuma, and S. Sudo, "35-dB gain Tm-doped ZBLYAN fiber amplifier operating at 1.65 μm," IEEE Photonic. Tech. L. **8**, 349-351 (1996)
10. F.J. McAleavey and B.D. MacCraith, "Efficient diode pumped Tm^{3+}-doped fluoride fibre laser for hydrocarbon gas sensing," Electron. Lett. **31**, 800-802 (1995)
11. Y.B. Shin, W.Y. Cho, and J. Heo, "Multiphonon and cross relaxation phenomena in Ge-As(or Ga)-S glasses doped with Tm^{3+}," J. Non-Cryst. Solids **208**, 29-35 (1996)
12. Y.S. Kim, W.Y. Cho, Y.B. Shin, and J. Heo, "Emission characteristics of Ge-Ga-S glasses doped with Tm^{3+}/Ho^{3+}," J. Non-Cryst. Solids **203**, 176-181 (1996)
13. J. Heo, W.Y. Cho, and W.J. Chung, "Sensitizing effect of Tm^{3+} on 2.9 μm emission from Dy^{3+}-doped $Ge_{25}Ga_5S_{70}$ glass," J. Non-Cryst. Solids **212**, 151-156 (1997)
14. N. Duhamel-Henry, J.L. Adam, B. Jaquier, and C. Linarès, "Photoluminescence of new fluorophosphate glasses containing a high concentration of terbium (III) ions," Opt. Mater. **5**, 197-207 (1996)
15. L.B. Shaw, D. Schaafsma, J. Moon, B. Harbison, J. Sanghera, I. Aggarwal, "Evaluation of the IR transitions in rare-earth-doped chalcogenide glasses," in Conference on Lasers and Electrooptics, Volume 11 of 1997 OSA Technical Digest Series (Optical Society of America, Washington, DC, 1997), p. 255
16. J. Heo, "Optical characteristics of rare-earth-doped sulphide glasses," J. Mater. Sci. Lett. **14**, 1014-1016 (1995)

17.T. Schweizer, D.W. Hewak, B.N. Samson, and D.N. Payne, "Spectroscopy of potential mid-infrared laser transitions in gallium lanthanum sulphide glass," J. Lumin. **72-74**, 419-421 (1997)
18.L.B. Shaw, B.B. Harbison, B. Cole, J.S. Sanghera, and I.D. Aggarwal, "Spectroscopy of the IR transitions in Pr^{3+} doped heavy metal selenide glasses," Optics Express 1, 87-96 (1997)
19.T. Schweizer, D.W. Hewak, B.N. Samson, and D.N. Payne, "Spectroscopic data of the 1.8-, 2.9-, and 4.3-μm transitions in dysprosium-doped gallium lanthanum sulfide glass," Opt. Lett. **21**, 1594-1596 (1996)
20.S.R. Bowman, L.B. Shaw, J.A. Moon, B.B. Harbison, and J. Ganem, "Spectroscopic studies of potential mid-ir laser materials," in Technical Digest of Advanced Solid-State Lasers, San Francisco, CA, 1996, pp. 277-279
21.K. Wei, D.P. Machewirth, J. Wenzel, E. Snitzer, and G.H. Sigel, Jr., "Spectroscopy of Dy^{3+} in Ge-Ga-S glass and its suitability for 1.3-μm fiber-optical amplifier applications," Opt. Lett. **19**, 904-906 (1994)
22.T. Schweizer, D.J. Brady, and D.W. Hewak, "Fabrication and spectroscopy of erbium doped gallium lanthanum sulphide glass fibres for mid-infrared laser applications," Optics Express **1**, 102-107 (1997)
23.J. Sanz, R. Cases, and R. Alcalá, "Optical properties of Tm^{3+} in fluorozirconate glass," J. Non-Cryst. Solids **93**, 377-386 (1987)
24.K. Hirao, S. Tanabe, S. Kishimoto, K. Tamai, and N. Soga, "UV and blue upconversion in Tm^{3+}-doped fluoroaluminate glass by 0.655 μm excitation," J. Non-Cryst. Solids **135**, 90-93 (1991)
25.C. K. Jørgensen and R. Reisfeld, "Judd-Ofelt parameters and chemical bonding," J. Less-Common Metals **93**, 107-112 (1983)
26.C. K. Jørgensen and B.R. Judd, "Hypersensitive pseudoquadrupole transitions in lanthanides," Mol. Phys. **8**, 281-290 (1964)
27.B.R. Judd, "Optical absorption intensities of rare-earth ions," Phys. Rev. **127**, 750-761 (1962)
28.G.S. Ofelt, "Intensities of crystal spectra of rare-earth ions," J. Chem. Phys. **37**, 511-520 (1962)
29.M.J. Weber, "Probabilities for radiative and nonradiative decay of Er^{3+} in LaF_3," Phys. Rev. **157**, 262-272 (1966)
30.B.F. Aull and H.P. Jensen, "Vibronic interactions in Nd:YAG resulting in nonreciprocity of absorption and stimulated emission cross sections," IEEE J. Quantum Elect. **QE-18**, 925-930 (1982)
31.W.J. Miniscalco and R.S. Quimby, "General procedure for the analysis of Er^{3+} cross sections," Opt. Lett. **16**, 258-260 (1991)
32.X. Zou and T. Izumitani, "Fluorescence mechanism and dynamics of Tm^{3+} singly doped and Yb^{3+}, Tm^{3+} doubly doped glasses," J. Non-Cryst. Solids **162**, 58-67 (1993)
33.F.E. Auzel, "Materials and devices using double-pumped phosphors with energy transfer," PIEEE **61**, 758-786 (1973)
34.T. Schweizer, P.E.-A. Möbert, J.R. Hector, D.W. Hewak, W.S. Brocklesby, D.N. Payne, and G. Huber, "Optical measurement of narrow band rare-earth 4f levels with energies greater than the bandgap of the chalcogenide glass host", Phys.Rev.Lett. **80**, 1537-1540 (1998)
35.D.W. Hewak, R.C. Moore, T. Schweizer, J. Wang, B. Samson, W.S. Brocklesby, D.N. Payne, and E.J. Tarbox, "Gallium lanthanum sulphide optical fibre for active and passive applications," Electron. Lett. **32**, 384-385 (1996)

36.T Schweizer, B.N. Samson, R.C. Moore, D.W. Hewak, and D.N. Payne, “Rare-earth doped chalcogenide glass fibre laser,” Electron. Lett. **33**, 414-416 (1997)

3.11 Ytterbium and co-doping in gallium lanthanum sulphide glass

Ytterbium (Yb^{3+}) is the last optically active ion in the lanthanide series with one electron missing from a filled 4f shell. Yb^{3+} has only two 4f levels, the $^2F_{7/2}$ ground state and the $^2F_{5/2}$ excited state which gives rise to a strong and broad absorption band typically peaking around 0.98 μm. The absorption band overlaps with the emission of high power InGaAs diode lasers making Yb^{3+} ions suitable for two major applications. Firstly, Yb^{3+} doped fibre lasers are attractive for converting low brightness laser diode radiation into high brightness fibre laser radiation with very high efficiencies due to the small quantum defect between pump and laser wavelengths. Up to 35 W of cw singlemode output power at 1.1 μm have been reported from a Yb^{3+} doped silica fibre laser with a slope efficiency of 65% [Mue97]. Secondly, Yb^{3+} has been used successfully as a co-dopant for other rare-earth ions, in particular for Er^{3+} [Chen96,Kri94,Min93a,Rom95]. The co-doping increases the pump absorption and the range of possible pump wavelengths. The energy is subsequently transferred from the Yb^{3+} ions (donor) to the acceptor ion by dipole-dipole interactions. Yb^{3+} co-doping has also been applied to Pr^{3+} and Dy^{3+} in fluoride glasses and efficient energy transfer has been demonstrated [Cha89,Ohi91,Xie95]. Motivated by these results we investigated similar co-doping schemes to enhance the pump absorption properties for the 3.4 μm Pr^{3+} and 4.3 μm Dy^{3+} transitions in GLS glass.

We melted a number of glasses with Yb^{3+}, Pr^{3+}/Yb^{3+}, and Dy^{3+}/Yb^{3+} doping, all of which turned out to have no visible transmission. Fig 3.11.1 shows the transmission spectra of a series of Pr^{3+} doped GLS glasses with different Yb_2S_3 co-doping concentrations. Three interesting features can be distinguished.

i) The "UV absorption edge" of the glass shifts from 0.55 μm to about 0.8 μm with increasing Yb_2S_3 concentration. A possible explanation for this effect is the formation of Yb^{2+} ions with strong dipole-allowed $4f^{14} \rightarrow 4f^{13}5d$ absorption bands in the visible wavelength region [Liz95,Mul94].

ii) The overall transmission in wavelength regions, $\lambda > 1.1$ μm, without contributions from the electronic glass absorption and the ytterbium absorption decreases with increasing doping concentration. This effect can be attributed to the formation of crystals in the glass which are observed under the microscope and act as scattering centres.

iii) The Yb^{3+} absorption band shows a double-peak structure which is not observed in common Yb^{3+} doped glasses [Mix95,Tak96,Zou95]. The double-peak structure suggests the existence of two distinct sites with different local environments (see also Dy^{3+} in section 3.7, page 51). This idea is supported by

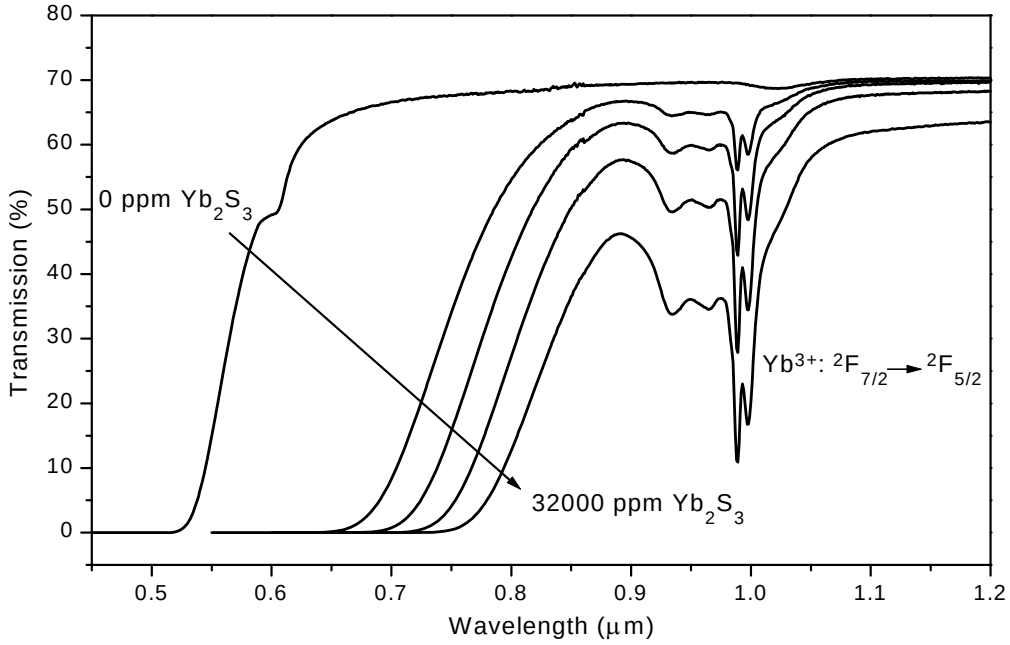

Fig. 3.11.1 Transmission spectra of 6.3 mm thick GLS glasses doped with 2000 ppm Pr_2S_3 and 0, 4000, 8000, 16000, and 32000 ppm Yb_2S_3

two observations:

a) The strength of the 0.988 μm peak increases relative to the strength of the 0.997 μm peak with increasing Yb_2S_3 concentration (not obvious from Fig. 3.11.1). The absorption strengths are lower than expected for a high refractive index host and are not consistent for different concentrations, i.e. absorption cross sections cannot be defined. The last point also supports the idea of Yb^{2+} formation which would decrease the number of Yb^{3+} ions relative to the amount of Yb_2S_3 added to the melt (see point i).

b) The fluorescence spectrum in Fig. 3.11.2.b shows only a single peak at 0.989 μm and its spectral shape cannot be generated from the absorption spectrum in Fig. 3.11.2.a using the McCumber theory (page 22, equation 3.1.13). A second emission peak which would be expected at 0.997 μm does not appear in the fluorescence spectrum. The fact that Yb^{3+} ions in the "long-wavelength-site" apparently contribute to absorption but not to emission whereas ions in the "short-wavelength-site" contribute to both processes needs further investigation.

The Yb^{3+} fluorescence, which was of very low intensity, was measured using the set-up shown in Fig. 7.1.1 which was modified with a 1-μm grating and an InGaAs detector. The $^2F_{5/2}$ level lifetimes were determined by measuring the fluorescence decay through a silicon filter with an InGaAs detector. Yb^{3+} lifetimes in common glasses are typically 1-2 ms [Mix95,Tak96,Zou95] but are

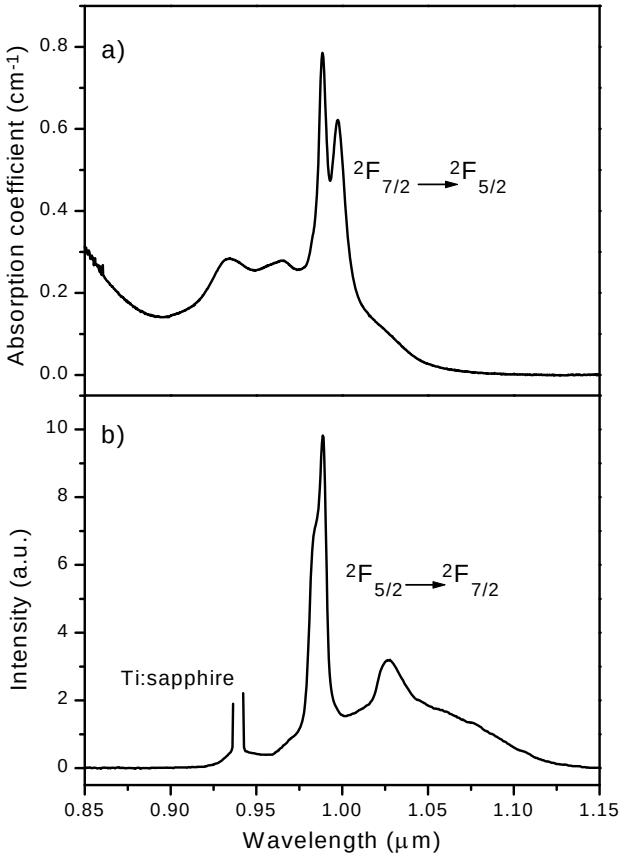

Fig. 3.11.2 Absorption (a) and fluorescence (b) spectra of 0.58 mol% (9240 ppm) Yb_2S_3 doped GLS glass

expected to be much shorter (200-400 μs) in GLS due to its high refractive index. The decay curves for 0.5, 0.58, and 1.5 mol% Yb_2S_3 all showed a double-exponential behaviour with a short first exponential and a longer second exponential of 82+330 μs, 82+327 μs, and 39+133 μs, respectively. The double-exponential decay and the shorter lifetime for the higher concentration (higher migration rates) indicate lifetime quenching by impurities, defects, and crystallisation as reported in other glasses [Mix95,Pas97]. Energy transfer from the Yb^{3+} ions into the visible absorption band (Yb^{2+} or electronic glass absorption) could also contribute to lifetime quenching.

Energy transfer from Yb^{3+} to Pr^{3+} or Dy^{3+} in co-doped GLS samples was not observed. Yb^{3+} is therefore not further considered as a co-dopant in pure GLS glass.

Ytterbium in oxide modified GLS glasses

Doping oxide modified GLS glasses (GLSO) with Yb_2S_3 does not shift the UV absorption edge of the glass and does not induce crystallisation. The absorption and fluorescence spectra both show a single peak and can be related to each

other using the McCumber equation. Fig. 3.11.3 shows the measured absorption cross section and the calculated emission cross section along with a fluorescence spectrum which was measured with an ANDO spectrum analyser. The peak absorption and emission cross sections, 2.88×10^{-20} cm^2 and 3.35×10^{-20} cm^2, are the highest cross sections reported for Yb^{3+} doped glasses to date [Mix95,Tak96,Zou95].

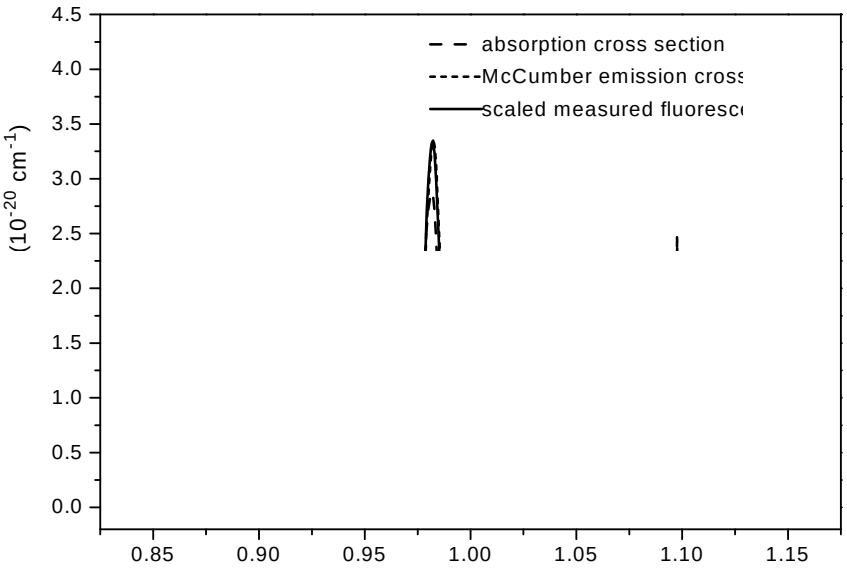

Fig. 3.11.3 Absorption (dashed) and McCumber emission (dotted) cross sections along with scaled measured fluorescence spectrum (solid) of 0.1 mol% Yb_2S_3 doped oxide modified GLS glass (GLSO, $70Ga_2S_3$:$30La_2O_3$)

A second value for the emission cross section was obtained from the Füchtbauer-Ladenburg equation (equation 3.1.12, page 21). The radiative rate, $A=A_{ed}+A_{md}$, which is usually derived from Judd-Ofelt calculations, can in the case of Yb^{3+} simply be calculated from [Zou95]:

$$A = \frac{8\pi c n^2 (2J'+1)}{\lambda_p^4 (2J+1)} \int \sigma_{abs}(\lambda) d\lambda \qquad (3.11.1)$$

where J = 5/2 and J' = 7/2 are the total momentums of the upper and lower levels, λ_p = 0.9815 μm is the absorption peak wavelength, and σ_{abs} is the measured emission cross section. The radiative rate for Yb^{3+} in GLSO (70:30) is 5770 s^{-1} which corresponds to a radiative lifetime of 173 μs. Using this radiative rate an emission cross section of 4.28×10^{-20} cm^2 was derived from the Füchtbauer-Ladenburg equation.

The theoretical radiative lifetime is considerably shorter than the measured lifetime of 245 μs (0.1 mol% Yb_2S_3). Although lifetime lengthening by radiation trapping is known to be a problem in the case of Yb^{3+} [Mix95,Sum94] it cannot explain the large discrepancy. The measured lifetime of a 1.5 mol% Yb_2S_3 doped GLSO glass (60:40) with a fifteen times higher concentration is not significantly longer (250 μs).

Inserting the emission cross section obtained from the McCumber fit into the Füchtbauer-Ladenburg equation yields a radiative rate of 4515 s^{-1} and a radiative lifetime of 221 μs which corresponds much better to the measured lifetime. We therefore conclude that the value of 3.35×10^{-20} cm^2 from the McCumber theory is the more accurate. This is the second largest value for transitions considered in this work with only the 1.08 μm Nd^{3+} transition having a higher cross section.

The crystallisation behaviour of GLSO glasses was studied by Hiromichi Takebe. Glasses were exposed for different time periods to temperatures close

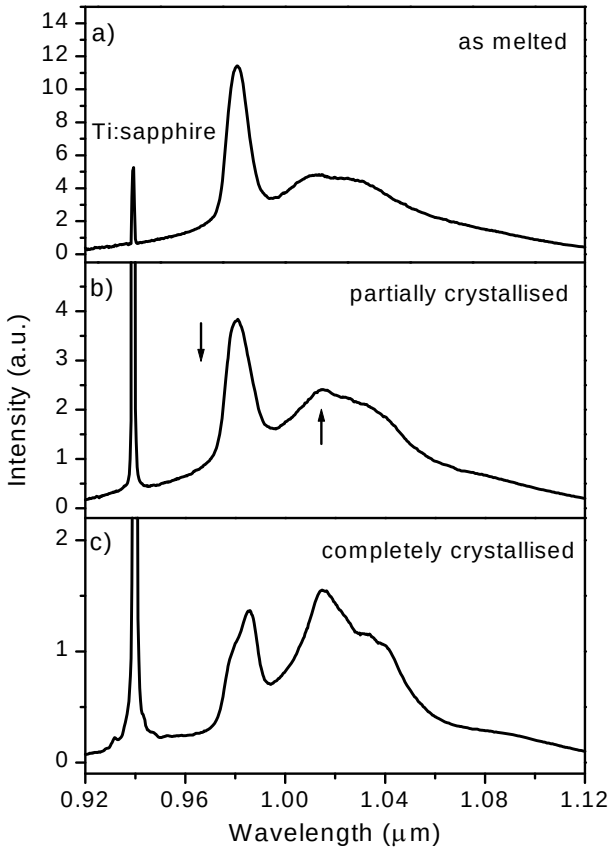

Fig. 3.11.4 Fluorescence spectra of 1.5 mol% Yb_2S_3 doped GLSO glass ($60Ga_2S_3$:$40La_2S_3$) as melted (a), and after 24 hours (b) and 72 hours (c) of heat-treatment at 615°C measured with an ANDO spectrum analyser

to fibre drawing conditions (615°C). One of the samples studies was a 1.5 mol% Yb_2S_3 doped GLSO glass (60:40). The emission spectra of this glass showed some interesting spectral changes with increasing degree of crystallisation. Fig. 3.11.4 shows the Yb^{3+} emission spectra for the untreated sample (a) and the same sample partially crystallised (b) and completely crystallised (c). The intensity of the 0.981 μm peak decreases with increasing crystallisation and shifts to 0.986 μm leaving a short wavelength shoulder at 0.981 μm. In addition a second peak develops at 1.015 μm. These changes indicate a change in the local environment of the Yb^{3+} ions. The spectrum of the completely crystallised sample shows some similarity to the emission spectrum in pure GLS glass (Fig. 3.11.2.b) concerning the shape of the two peaks (not their heights). This suggests that crystallisation and possibly ion clustering within these crystals could be one explanation for the observed Yb^{3+} spectroscopy in pure GLS glass.

Since the spectroscopy of Yb^{3+} in GLSO glass was more promising than in pure GLS we investigated the energy transfer from Yb^{3+} to Pr^{3+} in a GLSO glass doped with 1.5 mol% Yb_2S_3 and 0.1 mol% Pr_2S_3.

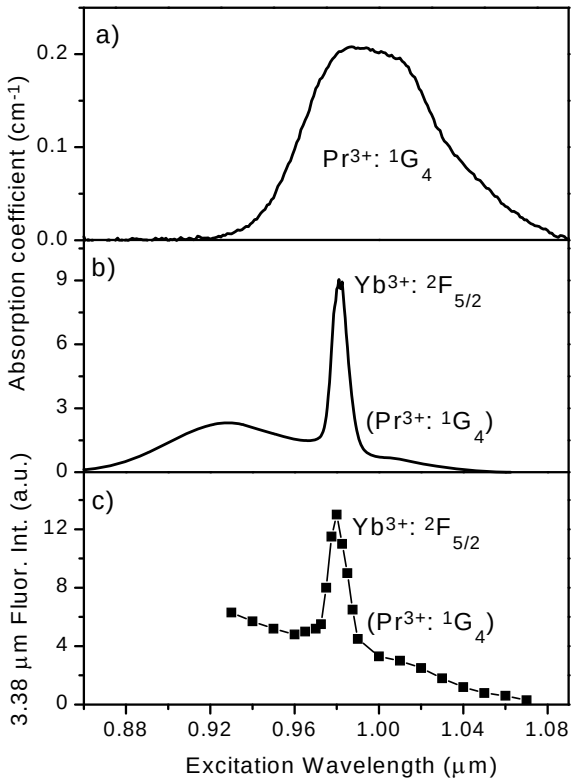

Fig. 3.11.5 a) Absorption spectrum of 1.5 mol% Pr_2S_3 doped oxide modified GLS (GLSO)
b) Absorption spectrum of 0.1 mol% Pr_2S_3 and 1.5 mol% Yb_2S_3 doped GLSO
c) Excitation spectrum of 3.38 μm Pr^{3+} emission from the $^1G_4$ level for same sample as used in b.

Fig. 3.11.5 shows the absorption spectra of the Pr^{3+} only (a) and the Yb^{3+}/Pr^{3+} co-doped sample (b)along with an excitation spectrum of the co-doped glass (c). The Pr^{3+} and Yb^{3+} absorption bands have a good spectral overlap. The excitation spectrum was measured using the fluorescence set-up described in section 7.1 which was modified by inserting a variable attenuator and a tilted glass plate into the Ti:sapphire pump beam. The function of the attenuator is to ensure a constant pump power (270 mW in this case) over the Ti:sapphire tuning range, and the glass plate reflects a few percent of the Ti:sapphire beam into the multimode fibre of an ANDO spectrum analyser for monitoring the excitation wavelength. The intensity of the 3.38 μm Pr^{3+} emission (section 3.4) was monitored while tuning the Ti:sapphire laser (Fig. 3.11.5.c). The excitation spectrum clearly follows the Yb^{3+} absorption indicating energy transfer from the Yb^{3+} $^2F_{5/2}$ level to the Pr^{3+} $^1G_4$ level (Fig. 3.11.6).

In general the Pr^{3+} $^1G_4$ level suffers from lifetime quenching by multiphonon decay in GLSO glasses [Hec98] which leads to lower quantum efficiencies and fluorescence intensities in GLSO glasses compared to GLS glasses. However, the 3.4 μm intensity of the Yb^{3+}/Pr^{3+} co-doped GLSO glass was about twice as high has for a Pr^{3+} only doped GLS glass showing the benefit of the increased pump absorption due to the Yb^{3+} co-doping which is not feasible in GLS glass.

Erbium as a co-dopant in pure GLS glass

Since Yb^{3+} is not a suitable co-doping ion in GLS glass we investigated Er^{3+} which also has an absorption band around 0.98 μm that overlaps with the emission wavelengths of InGaAs laser diodes (section 3.9). Fig. 3.11.6 shows the possible energy transfer routes from Er^{3+} to Pr^{3+} and Dy^{3+}.

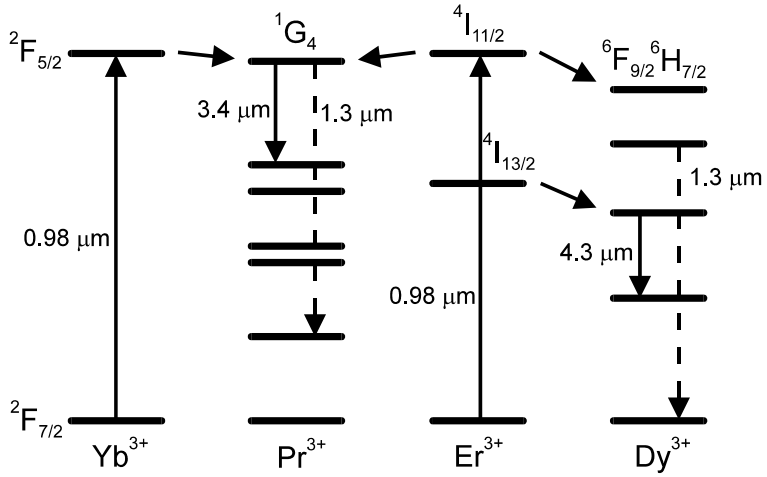

Fig. 3.11.6 Schematic energy level diagram showing energy transfer from Yb^{3+} and Er^{3+} to Pr^{3+} and Dy^{3+}

We melted two GLS glasses (70:30) each doped with 2 mol% Er_2S_3 and either 0.1 mol% Pr_2S_3 or 0.1 mol% Dy_2S_3 and measured the excitation spectra with the set-up described above.

The absorption spectra of the Pr^{3+} only and the Er^{3+}/Pr^{3+} co-doped glasses and the excitation spectrum of the latter are shown in Fig. 3.11.7.

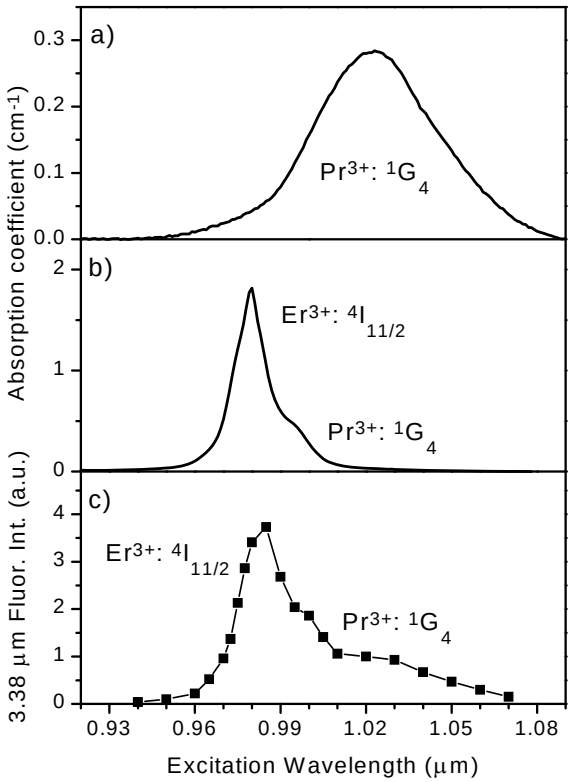

Fig. 3.11.7 a) Absorption spectrum of 1.5 mol% Pr_2S_3 doped GLS
b) Absorption spectrum of 0.1 mol% Pr_2S_3 and 2 mol% Er_2S_3 doped GLS
c) Excitation spectrum of 3.38 μm Pr^{3+} emission from the $^1G_4$ for same sample as used in b.

The overlap of the Pr^{3+} and Er^{3+} absorption band is not as large as for the Pr^{3+}/Yb^{3+} co-doping but the excitation spectrum clearly confirms the $Er^{3+} \rightarrow Pr^{3+}$ energy transfer. The intensity of the 3.4 μm Pr^{3+} emission is increased by more than a factor of three when the Ti:sapphire is tuned from the weak 1.02 μm Pr^{3+} absorption to the strong 0.98 μm Er^{3+} absorption. However, a transfer efficiency of only ~ 4% is estimated from comparing this factor to the relative Er^{3+}/Pr^{3+} absorption strength (Fig. 3.11.7.b). The efficiency could be improved by optimising the relative and absolute doping concentrations.

The results of the Er^{3+}/Dy^{3+} co-doping are summarised in Fig. 3.11.8. Dy^{3+} lacks suitable absorption bands for 0.98 μm pumping, and the Dy^{3+} absorption

bands overlap little with the Er^{3+} $^4I_{11/2}$ level. The overlap is further reduced by the fact that the short wavelength side of the Dy^{3+} absorption bands do not contribute to mid-infrared emission (section 3.7, page 52). The $Er^{3+} \rightarrow Dy^{3+}$ energy transfer therefore relies on the emission or absorption of phonons.

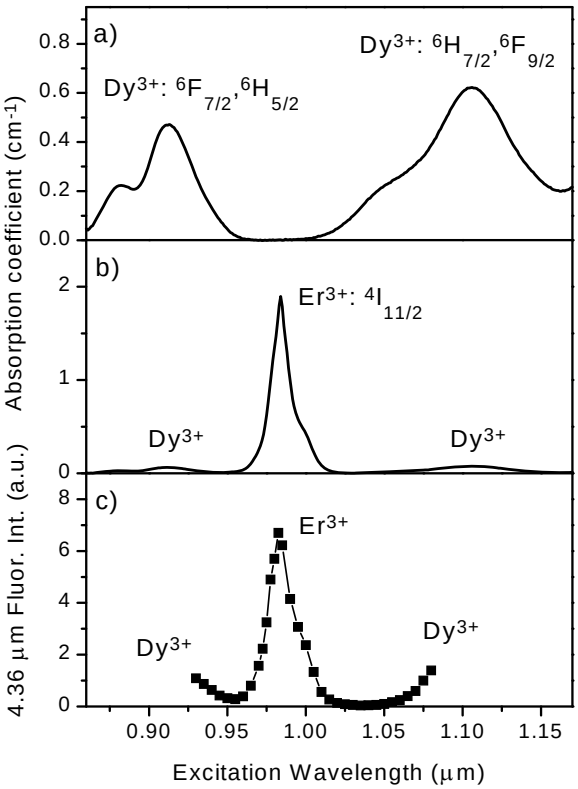

Fig. 3.11.8 a) Absorption spectrum of 0.65 mol% Dy_2S_3 doped GLS
b) Absorption spectrum of 0.1 mol% Dy_2S_3 and 2 mol% Er_2S_3 doped GLS
c) Excitation spectrum of 4.36 μm Dy^{3+} emission for same sample as used in b.

The excitation spectrum of the co-doped sample was measured by monitoring the 4.36 μm emission from Dy^{3+} for a constant pump power of 90 mW over the Ti:sapphire tuning range. As for the Er^{3+}/Pr^{3+} co-doping scheme pumping the Er^{3+} ions increases the Dy^{3+} fluorescence intensity compared to direct Dy^{3+} pumping. The transfer efficiency is estimated to ~10% by comparing the relative heights of the Er^{3+} and Dy^{3+} peaks in the absorption and excitation spectra as before. Again this value could be optimised by varying the doping concentrations.

We conclude that Yb^{3+} is not suitable as a co-dopant in pure GLS glass but may find use in oxide modified GLSO glass as a lasing ion around 1 μm and as a co-dopant to Pr^{3+} for increasing the pump efficiency of the 3.4 μm emission with respect to the incident pump power. Er^{3+} proved to be an interesting

alternative to Yb^{3+} for co-doping Pr^{3+} and Dy^{3+} in pure GLS glass, offering the use of 0.98 μm laser diodes for pumping mid-infrared fluorescence and laser sources. Further excitation and lifetime experiments are necessary for improving the efficiencies of the energy transfer processes and for investigating possible loss mechanisms due to visible emission generated by upconversion processes.

Future work could investigate the benefits of Tm^{3+} co-doping for exciting Dy^{3+} and Er^{3+} ions. It has been shown in other host glasses that Tm^{3+} ions pumped at 0.8 μm populate the two lower Dy^{3+} levels which emit at 3.0 and 4.3 μm and the Er^{3+} $^4F_{9/2}$ level which emits at 3.6 μm in GLS glass (sections 3.7 and 3.9) [Heo97a,Zou95a].

3.12 Conclusion

The spectroscopic results presented in chapter 3 reflect the influence of the glass host on the radiative and non-radiative properties of the RE ions.

The radiative properties have been derived from Judd-Ofelt calculations and are characterised by large radiative rates, i.e. low radiative lifetimes, and large absorption and emission cross sections due to the strongly covalent nature of the glass bonds and the resulting high refractive index. The radiative rates are about five times higher, i.e. the radiative lifetimes are about five times shorter, and the cross sections are two to three times larger than in common silica glasses as it is expected from the local field correction (section 3.1).

The non-radiative multiphonon decay rates for RE levels with small energy gaps to the next lower level, however, are *orders of magnitude* lower than in silica glasses due to the low phonon energy of GLS. The process depends exponentially on the number of phonons necessary to bridge the energy gap, i.e. on the phonon energy of the host and on the size of the energy gap. This exponential dependence was confirmed for GLS glass by calculating the multiphonon decay rates for a number of energy gaps of different RE ions from the calculated radiative rates and the measured lifetimes and plotting these values against the size of the energy gaps (section 3.2). The set of empirical parameters that describes the exponential fit is found to differ considerably from previously published data and predicts lower multiphonon rates for energy gaps in the 3-5 μm region of interest for mid-infrared fibre lasers.

Six out of the ten RE ions studied in this chapter showed fluorescence in the mid-infrared wavelength region (Nd^{3+} is discussed in chapter 5). None of these transitions could be observed in common silica glasses, and a number of them has not been reported in a glass host or any host material before. Some

transitions could be identified for future applications such as the 4.3 μm Dy^{3+} emission for CO_2 sensing, the 3.4 μm Pr^{3+} emission for hydrocarbon sensing, and the 3.9 μm Ho^{3+} and 3.8 μm Tm^{3+} transitions for their high atmospheric transmission. Mid-infrared emission in GLS is limited to just above 5 μm, and lower phonon energy chalcogenide glasses could extend this limit to longer wavelengths.

The dependence of the lifetime of the upper level of the mid-infrared transition on the RE ion concentration determines the maximum doping concentration. Strong lifetime quenching was found for Pr^{3+}, Dy^{3+}, Tm^{3+}, and Tb^{3+} limiting their doping levels to about 1000-3000 ppm. In contrast, Ho^{3+} and Er^{3+} show very little quenching for the energy levels of interest for mid-infrared emission due to the absence of cross-relaxation and upconversion channels and hence offer the possibility of high doping concentrations and short devices.

A number of experiments addressed the choice of the optimum pump wavelength.

Excitation spectra show that Dy^{3+} needs to be pumped at the long wavelength side of the absorption bands, and that Yb^{3+} and Er^{3+} are suitable co-dopants for Pr^{3+} and Dy^{3+} for 0.98 μm pumping. Co-doping Tb^{3+} ions with Tm^{3+} enables 0.8 μm pumping of the 4.8 μm Tb^{3+} fluorescence, and cross-relaxation processes in Tm^{3+} reveal that 0.7 μm is more efficient than 0.8 μm pumping for the 3.8 μm emission.

In general laser transitions in GLS glass should be pumped directly into the upper laser level since the pumping process cannot rely upon fast non-radiative decay from a pump level to the upper laser level in a low-phonon energy glass. This stringent requirement for the pump wavelength can be weakened by using cascade lasing schemes to transfer energy from the pump level to the upper laser level [Kam95,Pol97,Sch95a,Sch97]. Cascade lasing can also be used to depopulate the lower laser level.

The spectroscopic data collected in this chapter are currently being used by GEC for fibre laser modelling and form a firm basis for the development of mid-infrared GLS fibre lasers.

The following chapter 4 describes excited-state absorption measurements in Er^{3+} and Tm^{3+} doped GLS glasses and is presented separately from chapter 3 for its more fundamental bias.

Chapter 4

Excited-state absorption

4.1 Introduction

According to the size of the optical bandgap of ~ 2.6 eV GLS glass can be looked at as an amorphous semiconductor [Mot87]. The “electronic bandgap” may be filled with a continuum of localised states which close the gap between the valence band (VB) and the conduction band (CB) and act as recombination centres for electrons and holes. The electrons in the bandgap will have no mobility so that we can speak about a “mobility gap” and also about an optical bandgap in GLS glass. Most of the deep trap states in amorphous semiconductors are caused by dangling bonds which will be dangling sulphur bonds in the case of GLS. The states in the gap will be equally divided between donor and acceptor-like states leading to an equal number of electrons and holes in the CB and VB and a Fermi level pinned in the middle of the gap. Any additional impurities which may be doped into the glass with the motivation to change its electronic properties will not move the Fermi energy and will not become donors or acceptors but will only change the local coordination to meet the different valence requirements. Doping of amorphous semiconductors, usually in the form of thin films, can be achieved after the dangling bonds have been passivated by hydrogenation.

Rare-earth ions in GLS glass could have energy levels within the bandgap which might lead to optical transitions between the rare-earth ion and the VB or CB of the glass. Such transitions have been reported in rare-earth doped crystals and glasses before (see following paper 6 for references). Fig. 4.1.1.a shows a schematic diagram of the energy bands and the involved transitions in the case of a large gap material. The rare-earth ion is promoted by ground state absorption of a photon (GSA) from the 4f state to the excited 5d state. In a

second step the excited-state absorption (ESA) transfers the electron to the CB of the host. These rare-earth to host transitions are typically observed at ultraviolet wavelengths from high lying 5d levels due to the large bandgaps of common crystals and glasses. The small bandgap of GLS offers the opportunity to study possible ESA transitions from 4f levels to the CB band of the glass at visible or near-infrared wavelengths (Fig. 4.1.1.b). If these transitions existed they would be a serious problem for rare-earth laser operation which could be impeded or completely prevented by ESA at the pump or laser wavelengths. If these transitions cannot be found we can either conclude that the rare-earth energy levels lie deep in the valence band, i.e. the energy necessary for 4f to CB transitions is larger than the bandgap and cannot be measured optically, or that the well shielded 4f levels do not couple to the band states of the glass.

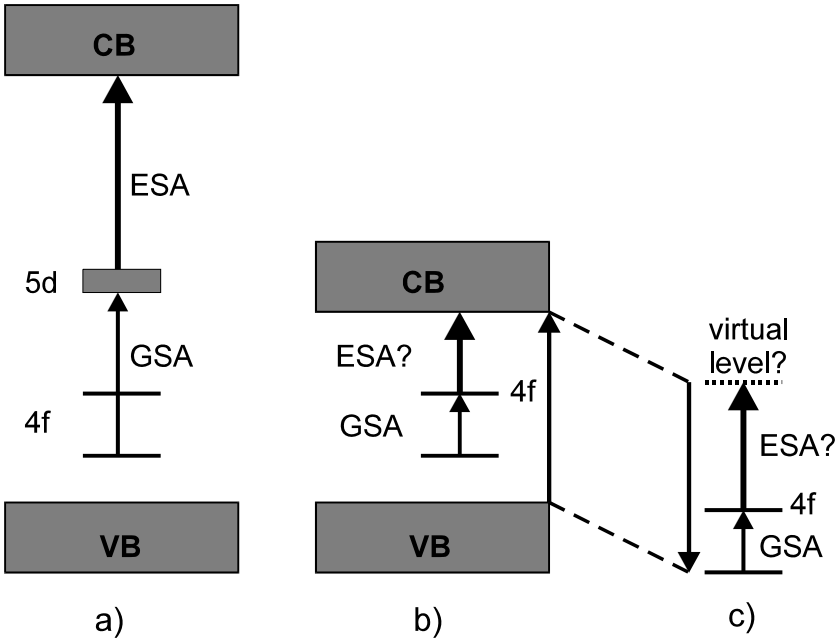

Fig. 4.1.1 Schematic diagram of ESA transitions from excited 5d levels to the CB of a wide gap insulator (a) and potential ESA transitions from excited 4f levels to the CB of a small gap semiconductor via electron transfer (b) and coulombic interactions (c)

Another possible interaction is sketched in Fig. 4.1.1.c. Instead of transferring an electron from the rare-earth ion to the CB the energy may be transferred by coulombic interactions in form of a cross-relaxation from a virtual level when the energy of the excited energy level plus the energy of the incoming photon match the energy gap of the glass. Similar processes have been proposed for energy transfer between rare-earth ions and between rare-earth ions and common semiconductors and work for any arbitrary position of the rare-earth energy levels relative to the CB and VB (see following paper 6 for references).

4.2 Excited-state absorption in erbium and thulium doped GLS glass

The following paper 7 presents ESA measurements on Er^{3+} and Tm^{3+} doped GLS glasses. The measurements were performed at the Institut für Laser-Physik, Universität Hamburg, using the pump-and-probe set-up which is described in appendix 7.2. A detailed description of the set-up, the measurement procedure, and the data analysis was given by Koetke [Koe94].

Optical measurement of narrow band rare-earth 4f levels with energies greater than the bandgap of the host

***T. Schweizer**, P.E.-A. Möbert, J.R. Hector, D.W. Hewak, W.S. Brocklesby, D.N. Payne, and G. Huber*

Abstract

Excited-state absorption spectra of erbium and thulium doped gallium lanthanum sulphide glasses reveal transitions whose final 4f states do not appear in the ground state absorption spectra due to resonance with the fundamental absorption of the glass host. The results give direct evidence for the model of isolated rare earth ions with highly shielded 4f levels showing no noticeable interaction with the host material despite resonance. Only the energy splitting of the 4f levels is relevant for energy transfer processes between rare-earth ions and the host material whereas the absolute energetic position is unimportant.

Excited-state absorption (ESA) describes the absorption from a populated excited electronic state of a system to higher-energy states. In rare earth (RE) doped materials ESA at the emission or pump wavelengths can impede or completely prevent laser action. The final states of an ESA transition from an excited RE level can either be a higher lying RE level of the same configuration or the conduction band of the host material [1-6].

In this work we present ESA measurements on erbium (Er^{3+}) and thulium (Tm^{3+}) doped gallium lanthanum sulphide (GLS) glasses that can be classified as wide-band-gap semiconductors with an energy gap of 2.6 eV which corresponds to a visible transparency down to about 500 nm. The question arises whether ESA transitions from RE 4f levels to the conduction band of the glass or to 4f levels that are “higher” than the conduction band will occur.

ESA transitions from RE impurities to the host material have been observed in a variety of divalent and trivalent RE doped materials [1-6]. The reported ESA transitions into the conduction band originate from the $4f^{n-1}5d$ states of the RE ions and have typical cross sections of 10^{-18} - 10^{-17} cm^2 [2-4]. These values are much larger than the values for the dipole forbidden 4f-4f transitions (10^{-21} - 10^{-20} cm^2) and even for the dipole allowed $4f^n$-$4f^{n-1}5d$ transitions (10^{-18} - 10^{-19} cm^2) [2-4]. ESA transitions have not been measured from highly shielded $4f^n$ levels into the conduction band. Transitions from $4f^n$ levels to the conduction band are expected to be weak compared to those from $4f^{n-1}5d$ levels, due to the much smaller spatial overlap of the $4f^n$ levels with the delocalised Bloch states of the conduction band. In all of the mentioned examples the ground and excited 4f states of the RE ions lie within the wide band gaps of the insulating host

Paper 6: published in Phys. Rev. Lett. **80** (1998) 1537

materials ($E_{gap} \sim 6$ eV for YAG and 12.2 eV for CaF_2) [1-6]. The observed localised to delocalised transitions, i.e. the transfer of an electron from the impurity ion to the host material, while not uncommon in semiconductors, are quite rare in insulators.

In this work we look at chalcogenide glasses which can be classified as semiconductors most of which have the hole type of conductivity [7,8]. Inter-band-gap states formed by extrinsic impurities and intrinsic defects cause the typical weak absorption tail below the Urbach edge [7]. In semiconductors energy transfer between 4f levels of RE ions and the host is a common phenomenon and is the proposed basis for electrically pumped RE lasers [9]. The main processes discussed in the literature are impact excitation (intraband) and Auger recombination (interband) which transfer energy from the semiconducting host material to the RE ions through Coulomb interactions [10,11]. The probability for Auger excitation can be increased by localised electron states in the forbidden gap, such as donors or acceptors, which may be formed by the RE impurity itself [10,12-14]. The inverse processes cause deexcitation of excited RE ions. Only the splitting of the highly localised and shielded 4f levels of the RE ions is of importance for the energy transfer; the absolute energetic position is unimportant. The absolute position of the 4f levels is expected to be much lower than the valence band, in contrast to the RE doped insulators discussed earlier [10,11]. Energy transfer between RE ions and the semiconductor hosts have been observed in Er^{3+} doped silicon, Nd^{3+} and Yb^{3+} doped semiconductors, and also in Nd^{3+} doped β-La_2S_3 crystals which have comparable spectroscopic properties to GLS glass [10,12-16]. A broad-band excitation mechanism including absorption by the glass host and energy transfer to the RE ion has been reported in other Er^{3+} doped chalcogenide glasses [17].

Commonly, lasers are designed so that both pump and signal photons are smaller than half the band gap, in order to avoid ESA interactions with the host material. [1,4]. The question arises whether ESA transitions from RE 4f levels to the conduction band of the semiconducting GLS glass or to impurities in the band gap could occur. As soon as the sum of the energy of an excited 4f level plus the energy of an incoming photon matches the energy of the band gap or an impurity state, energy transfer to the host material might be expected. Such an ESA process could cause a potential loss mechanism for RE lasers in GLS glasses. In order to check these ideas we performed ESA measurements on Er^{3+} and Tm^{3+} doped GLS glasses and used $YLiF_4$ (YLF) crystals with the same dopants as control samples.

Paper 6: published in Phys. Rev. Lett. **80** (1998) 1537

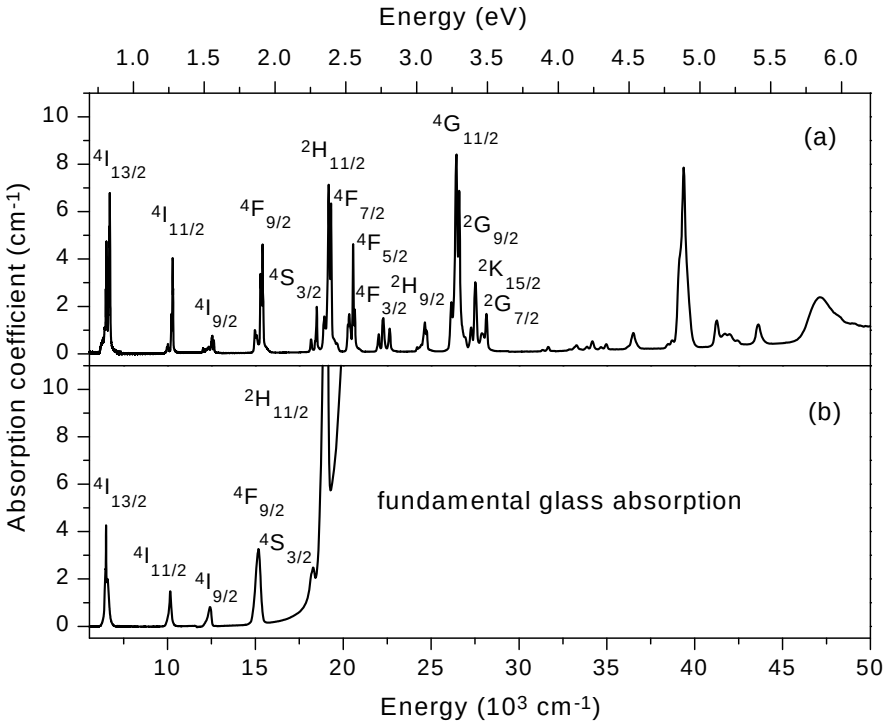

Fig.1 Unpolarised ground state absorption spectra of (a) Er:YLF and (b) Er:GLS show the small bandgap of the glass compared to the crystal. The final energy levels of the ESA transitions between 20,000 and 30,000 cm^{-1} in the Er:YLF spectrum are masked by the fundamental glass absorption in the Er:GLS spectrum.

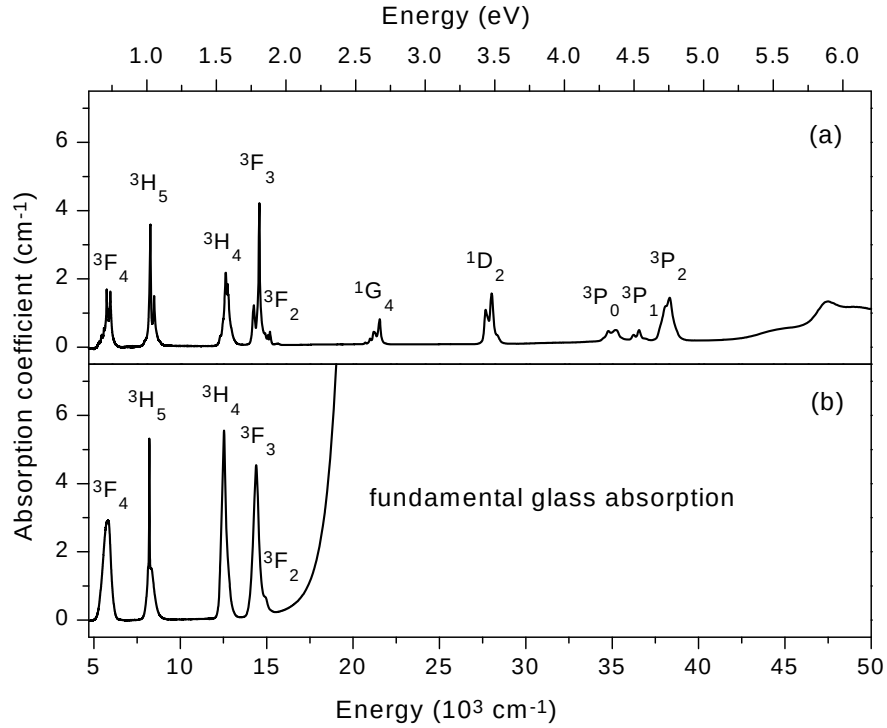

Fig. 2 Unpolarised ground state absorption spectra of (a) Tm:YLF and (b) Tm:GLS show that two of the final energy levels of the ESA transitions lie at energies relative to the ground state of about 22,000 cm^{-1} and 28,000 cm^{-1} which are larger than the energy gap of the glass.

The samples under investigation were an Er:GLS glass (n_{Er} = 2.73×10^{20} ions/cm^{-3}), an Er:YLF crystal (n_{Er} = 6.85×10^{20} ions/cm^{-3}), a Tm:GLS glass (n_{Tm} = 2.63×10^{20} ions/cm^{-3}), and a Tm:YLF crystal (n_{Tm} = 5.48×10^{20} ions/cm^{-3}). The higher RE concentration in the crystals leads to similar absorption coefficients in the crystals and the glasses. This is due to larger cross- sections in the glasses due to higher covalency of the glass bonds (see Fig. 1 and 2) [18,19]. The room temperature absorption spectra (Fig. 1 and 2) show the difference in the size of the bandgap of the glass and the crystal. Both the Er^{3+} and the Tm^{3+} ions in either material have absorption bands around 12500 cm^{-1} (800 nm). These absorption bands were used to excite the ions for the ESA experiments.

The experimental set-up for the ESA measurements and the evaluation and interpretation of the spectra are described in detail in reference [20]. The set-up is based on the pump-and-probe technique using an 810 nm laser diode as the pump source and a white light source as the probe beam. The transmission of the pumped samples compared to the unpumped samples increases in spectral regions with ground state absorption (GSA) due to the reduced population of the ground state ("bleaching", positive signal ΔI). The population of excited states can lead to an increase in intensity of the probe beam in spectral regions with stimulated emission (SE) (positive signal ΔI) and to a decrease in intensity in regions with ESA (negative signal ΔI). The ratio of ΔI to I is proportional to the cross sections:

$$\Delta I / I \propto \sigma_{GSA} + \sum_i (n_i / n_e)(\sigma_{SE,i} - \sigma_{ESA,i})$$

The absorption cross section, σ_{GSA}, is first used to calibrate the $\Delta I/I$ spectra for absolute cross sections and is then subtracted from the $\Delta I/I$ spectra. The remaining spectra give the SE and ESA cross sections weighted with the population of the levels n_i with respect to the total density of excited ions n_e (Fig. 3 and 4). The determination of the absolute cross sections requires the knowledge of the relative population densities.

The Er^{3+} ions are excited into the short-lived $^4I_{9/2}$ level (Fig. 1). Non-radiative and radiative decay populates the metastable $^4I_{11/2}$ and $^4I_{13/2}$ levels. Lifetime measurements show that the $^4I_{13/2}$ level will have the largest relative population density, n_i/n_e, followed by the $^4I_{11/2}$ level [19,21]. The assignment of the possible ESA transitions as derived from the Er:YLF absorption spectrum (Fig. 1) is indicated at the top of Fig. 3. A detailed spectroscopic study of Er^{3+} doped GLS glass is given in Ref. [19].

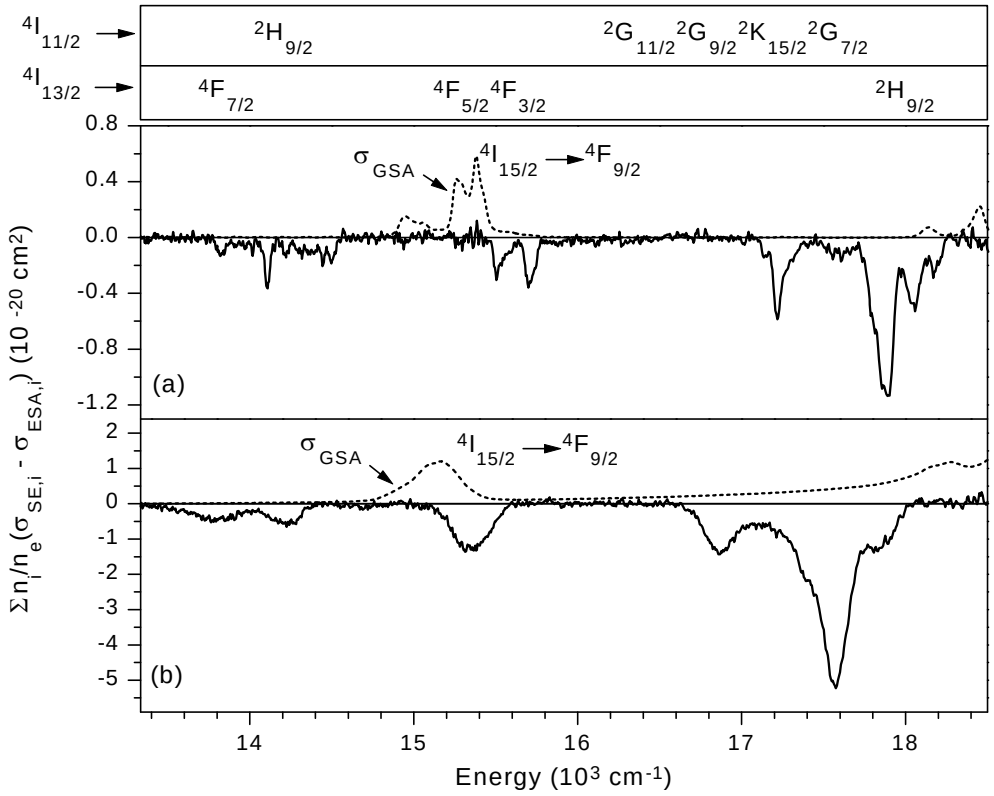

Fig. 3 Unpolarized ESA spectra (solid line) and GSA spectra (dotted line) of Er^{3+} doped YLF (a) and GLS (b) at energies in the region of the glass absorption edge show almost identical features. None of the final ESA levels indicated at the top of the figure can be seen in the GSA spectrum of the glass (Fig. 1).

The Tm^{3+} ions are excited into the $^3H_4$ level. Non-radiative and radiative decay populates the $^3H_5$ and $^3F_4$ levels. As for the Er^{3+} ions, lifetime measurements show that the $^3F_4$ level will have the largest relative population density, n_i / n_e, followed by the $^3H_4$ level [21]. Possible ESA transitions from the short-lived $^3H_5$ level do not fall into the energy regions measured. The assignment of the possible ESA transitions as derived from the Tm:YLF absorption spectrum (Fig. 2) is indicated at the top of Fig. 4. The peaks in the ESA spectra (Fig. 4) at 8200 cm^{-1} are caused by the subtraction of the GSA bleaching spectra. A detailed spectroscopic study of Tm^{3+} doped GLS glass will be published elsewhere.

The ESA spectra of the birefringent YLF crystal and the GLS glass were measured unpolarised and at room temperature. The position and relative strength of the ESA transitions are very similar for each dopant in the two materials. The ESA peaks are slightly broader and smoother and at lower energies in the glass due to the stronger inhomogeneous broadening and the nephelauxetic effect. As for the GSA cross sections the ESA cross sections in the glass are several times stronger than in the crystal due to the higher covalency and higher refractive index (2.52 compared to 1.45 around 640 nm).

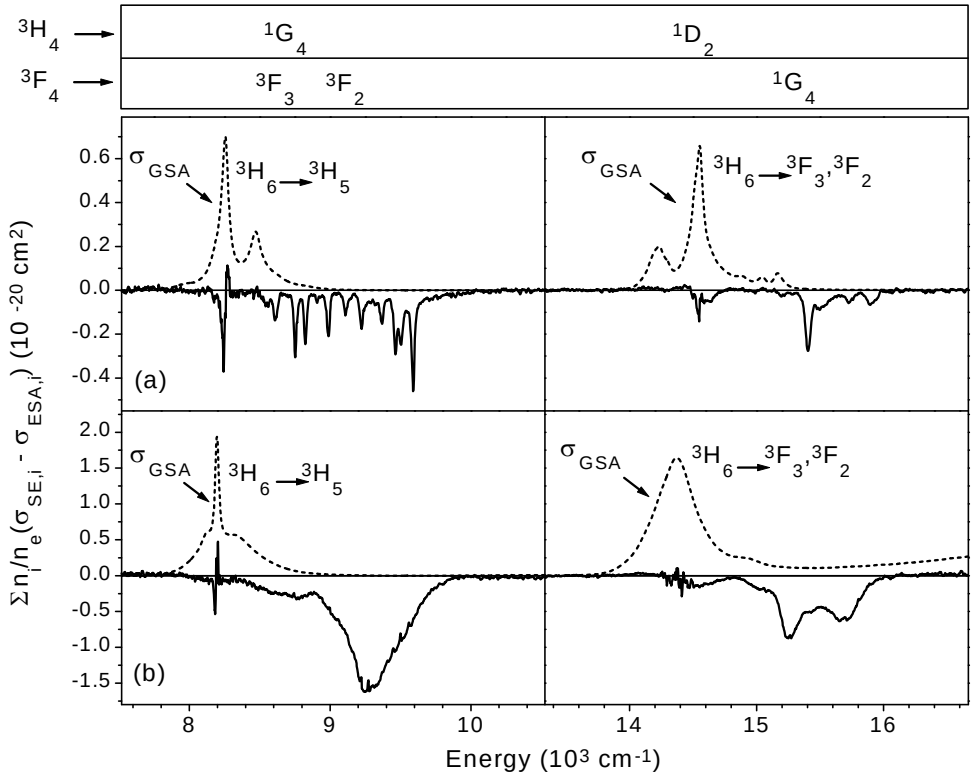

Fig. 4 The unpolarised ESA spectra (solid line) and GSA spectra (dotted line) of Tm^{3+} doped YLF (a) and GLS (b) for two energy regions at either side of the pump energy (~ 12500 cm^{-1}) show ESA and GSA peaks at similar wavelengths for the two materials. Two of the final ESA levels indicated at the top of the figure ($^1G_4$ and $^1D_2$) cannot be seen in the GSA spectrum of the glass (Fig. 2).

As expected there was no measurable stimulated emission (positive signal) in the energy regions measured for both dopants in either material. This was due to the short lifetimes and therefore low relative populations (n_i / n_e) of the energy levels that could show stimulated emission, at energies covered by the measurement ($^4I_{9/2}$, $^4F_{9/2}$, and $^4S_{3/2}$ for Er^{3+} and $^3H_5$, $^3F_3$, and $^3F_2$ for Tm^{3+}). The GSA spectra show the rising glass absorption towards higher energies which renders ESA measurements at higher energies impossible (Fig. 3 and 4). No emission from the final states of the ESA transitions was observed, due to immediate reabsorption by the fundamental glass absorption and likely quenching of these levels due to efficient cross-relaxation between the RE ion and the glass.

The two most striking points about the ESA spectra of both RE ions in the GLS hosts are (i) that all of the possible final states of the ESA transitions shown in figures 3 and 4 (except for the $^3F_4 \rightarrow ^3F_2, ^3F_3$ transition in Tm^{3+}) lie at energies relative to the ground state which are larger than the energy gap of the glass and hence do not appear in the GSA spectra of the glass (Fig. 1 and 2), and (ii) that the oscillator strengths of the ESA peaks, calculated using the integrated

absorption strengths, do not show any increases. This rules out any increase of transition strengths by admixture of resonant states. The integrated absorption strength is a much more sensitive measure of transition strength than studies of the linewidth of the transitions, which in glasses are subject to significant inhomogeneous broadening. These results show that the RE ions in GLS can be treated as isolated ions with strongly shielded 4f levels that have only little overlap with the extended Bloch waves of the glass.

No additional absorption features that could be related to either charge transfer or energy transfer from the RE ion to the host material have been detected within the sensitivity of our experiment. Charge transfer transitions, which have been observed in other RE-doped systems, provide a measure of the "offset" of the RE levels relative to the band gap of the semiconductor, analogous to band offsets in quantum well systems. From previous studies of semiconductor systems, it is generally assumed that the 4f levels lie deep in the valence band [10,11]. This assumption is supported by X-ray and ultra-violet photoelectron spectroscopy (XPS and UPS) of the sesquisulphides γ-RE_2S_3 (RE=Sm,Gd,Dy) and α-Gd_2S_3 which show that the binding energies of the 4f ground levels are larger than the binding energies of the sulphur 3p levels which form the upper part of the valence band of the crystals [22,23]. Thus the absence of charge-transfer transitions within the wavelength range of our experiments is consistent with previous measurements.

Additional absorption features caused by the energy transfer from an excited RE energy level and an incoming photon to the conduction band of the host via a virtual level do not appear in the ESA spectra. This type of transition has been observed between RE ions [24]. Such transitions would probably be broad and would start at energies of 10000 cm^{-1} and 13500 cm^{-1} from the $^4I_{11/2}$ and $^4I_{13/2}$ levels in Er^{3+} doped GLS glass and at energies of 7500 cm^{-1} and 12000 cm^{-1} from the $^3H_4$ and $^3F_4$ levels in Tm^{3+} doped GLS glass.

As in semiconductors, energy transfer between RE ions and the GLS glass host depends only on the energy splitting and not on the absolute energetic position of the 4f levels. ESA measurements can therefore be used to obtain information about energy levels that cannot be otherwise measured. A similar way of gaining information about energy levels which cannot be measured by GSA has been reported in Co doped ZnSe but, to our knowledge, not yet in RE doped systems [25].

An important implication of the ESA experiments is that pumping RE ions with wavelengths close to the fundamental glass absorption is feasible in chalcogenide glass lasers and is only limited by the fundamental glass absorption and the weak absorption tail and not by ESA into the conduction band of the glass.

Chalcogenide starting materials were supplied by Merck Ltd., Poole, UK, and YLF crystals were grown by B.H.T. Chai at CREOL, Orlando, Florida, USA.

References

[1] J.F. Owen, P.B. Dorain, and T. Koabyasi, J. Appl. Phys. **52**, 1216 (1981)
[2] J.K. Lawson and S.A. Payne, Phys. Rev. B **47**, 14003 (1993)
[3] J.K. Lawson annd S.A. Payne, J. Opt. Soc. Am. B **8**, 1404 (1991)
[4] Y.M. Cheung and S.K. Gayen, Phys. Rev. B **49**, 14827 (1994)
[5] D.S. Hamilton et al., Phys. Rev. B **39**, 8807 (1989)
[6] J.J. Ju et al., Mater. Lett. **28**, 149 (1996)
[7] A.B. Seddon, J. Non-Cryst. Solids **184**, 44 (1995)
[8] S.D. Savransky, in Proceedings of X^{TH} International Symposium on Non-Oxide Glasses, June19-22, 1996, Corning NY USA, Paper 43, pp.235-238
[9] L. Suchow and N.R. Stempel, J. Electrochem. Soc. **111**, 191 (1964)
[10] I.N. Yassievich and L.C. Kimerling, Semicond. Sci. Technol. **8**, 718 (1993)
[11] S. Schmitt-Rink, C.M. Varma, and A.F.J. Levi, Phys. Rev. Lett. **66**, 2782 (1991)
[12] F. Priolo et al., J. Appl. Phys. **78**, 3874 (1995)
[13] J. Yu, T. Zhao, and W. Li, J. Lumin. **33**, 427 (1985)
[14] A. Taguchi and K. Takahei, J. Appl. Phys. **79**, 3261 (1996)
[15] V.F. Masterov and L.F. Zakharenov, Sov. Phys. Semicond. **24**, 383 (1990)
[16] M. Leiss, J. Phys. C **15**, 1071 (1982)
[17] S.Q. Gu et al., J. Appl. Phys. **77**, 3365 (1995)
[18] R.Reisfeld and A. Bornstein, Chem. Phys. Lett. **47**, 194 (1977)
[19] C.C. Ye et al., J. Non-Cryst. Solids **208**, 56 (1996)
[20] J. Koetke and G. Huber, Appl. Phys. B **61**, 151 (1995)
[21] C. Li et al., in Proceedings of Advanced Solid-State Lasers **15**, February 1-3, 1993, New Orleans, LA
[22] S. Kaciulis, A. Latisenka, and A. Plesanovas, Surface Science **251/252**, 330 (1991)
[23] M. Leiss, Thesis, Universität Hamburg, Germany, 1981
[24] F.E. Auzel, Proceedings of the IEEE 61, 758 (1973)
[25] A. Ehlert, J. Dreyhsig, H.-E. Gumlich, and J.W. Allen, J. Lumin. **60&61**, 21 (1994)

Paper 6: published in Phys. Rev. Lett. **80** (1998) 1537

4.3 Conclusion

From a practical point of view the most important conclusion which can be drawn from the ESA measurements is that the small energy bandgap of GLS glass does not introduce additional ESA absorption features which could deteriorate or completely prevent laser operation.

From a more physical point of view the experiments represent an interesting example for a measurement which shows clearly and directly that the 4f orbitals of rare-earth ions are well shielded by the outer 5d and 6s orbitals and are not influenced much by the host environment.

Chapter 5

Laser action in bulk glasses and fibres

5.1 Introduction

Although chalcogenide glasses have been proposed as potential rare-earth laser materials for about 20 years laser operation has not been demonstrated prior to this work. The major problems in achieving laser operation are the quality and the physical properties of the bulk and fibre glass samples.

Bulk chalcogenide glasses are far from perfect materials for bulk solid-state lasers due to their poor thermal properties which can either lead to unstable resonators due to strong thermal lensing [Via97] or to the destruction of the samples in the pump beam [Fla83]. We demonstrated the first laser operation in a rare-earth doped chalcogenide glass by choosing a high neodymium (Nd^{3+}) concentration and a thin disk of GLS glass in order to minimise thermal effects.

A method to overcome the thermal problems of the bulk glass configuration is the fabrication of chalcogenide glasses into guiding structures such as fibres and waveguides. As we know from chapter 2 the fabrication of low loss chalcogenide glass optical fibres is a rather difficult task. To date, we have pulled a single Nd^{3+} doped GLS glass fibre which allowed us to demonstrate the first chalcogenide glass fibre laser.

Section 5.2 starts with a review article about the spectroscopy of Nd^{3+} doped chalcogenide glasses and GLS glass in particular (paper 7) and is followed by a review article about lasers in chalcogenide glasses (paper 8). Section 5.2 ends with a brief discussion about the properties of a bulk glass laser with a lower Nd^{3+} concentration, and about the temporal behaviour of the Nd^{3+} fibre laser and the fabrication of the Nd^{3+} doped fibre.

5.2 Spectroscopy and laser properties of neodymium doped glasses

Properties of Glass and Rare-Earth Doped Glasses for Optical Fibres
Part D - Chalcogenide Glasses
D3 Rare-Earth Spectroscopy

D3.2 Spectroscopy of Neodymium-Doped Chalcogenide Glass

T. Schweizer

Introduction

The main reason to study rare-earth doped chalcogenide glasses is their low phonon energy which leads to low non-radiative decay rates of rare-earth energy levels and good infrared transparency. The trivalent neodymium ion (Nd^{3+}) has not been studied widely as a dopant for chalcogenide glasses because the main fluorescent energy level ($^4F_{3/2}$) has a large gap to the next lower lying level and hence does not suffer from competing non-radiative multi-phonon decay. The Nd^{3+} ions have rather been used as a convenient test ion to show the influence of the chalcogenide glass host on the rare-earth dopants and to perform initial laser experiments. About a dozen Nd^{3+} doped chalcogenide glasses have been reported in the literature [1-8], most of which are sulphide glasses of which gallium lanthanum sulphide glass (GLS) is the most extensively studied system [9-13] and the only system with reported laser action in bulk and fibre form [14-16]. For these reasons this review will concentrate on the spectroscopy of Nd^{3+} doped GLS glass and give references to other sulphide glass systems.

Absorption, fluorescence, and lifetime spectroscopy

Fig. 1 depicts the ground state absorption spectrum of a 1.5 mol% Nd^{3+} doped GLS glass. The graph is plotted on a reciprocal wavelength scale in order to show the real energy gaps between the levels. The UV edge of the glass appears at 500 nm, and the multiphonon edge starts at 8 μm.

An interesting feature in the absorption spectrum is the strength of the absorption band at 600 nm ($^2G_{7/2}$, $^4G_{5/2}$ levels) compared to the band at 815 nm ($^2H_{9/2}$, $^4F_{5/2}$ levels). In fluorozirconate glasses these two bands are about equal in strengths [17,18]. The $^4I_{9/2} \rightarrow {}^4G_{5/2}$ transition is one of the so called hypersensitive pseudoquadrupolar transitions which show strongly increased intensities in host media which are highly polarizable (covalent bonding, high refractive index) and provide an inhomogeneous surrounding for the rare-earth dopants [19,20]. The intensity of these transitions increases with increasing Judd-Ofelt parameter Ω_2 [22,23] which has large values in covalent host materials such as chalcogenide glasses [18].

Paper 7: accepted for publication in Volume 20 of EMIS Datareview Series

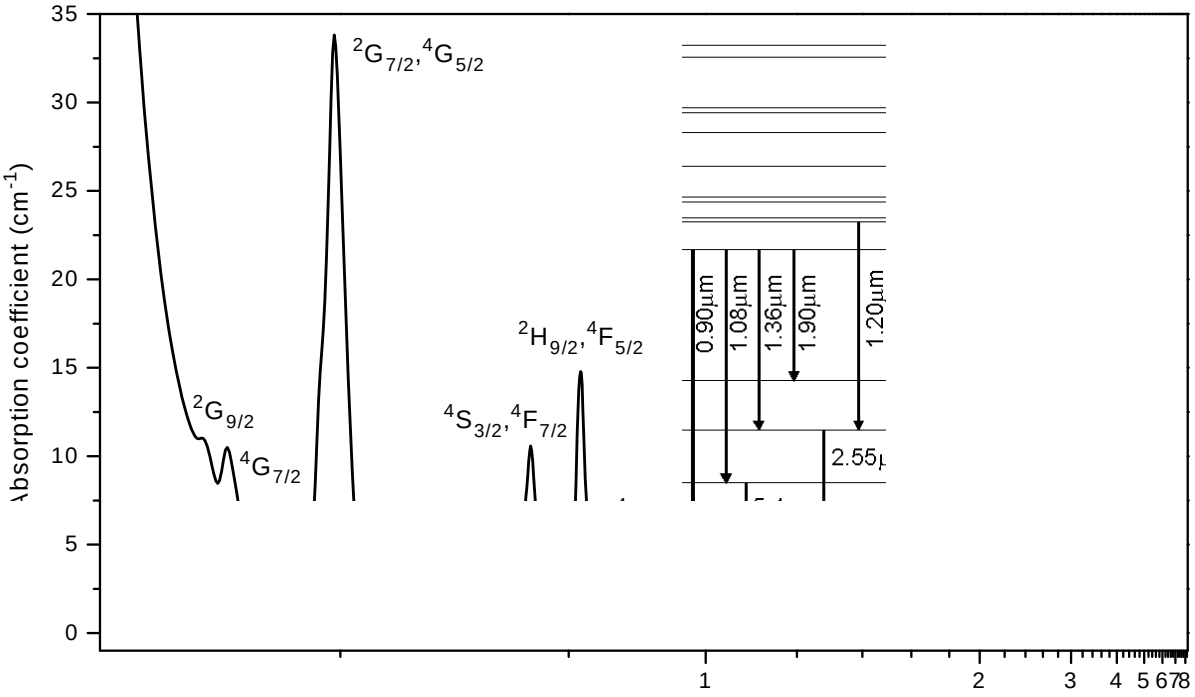

Fig. 1 Ground state absorption spectrum of $70Ga_2S_3$:$28.5La_2S_3$:$1.5Nd_2S_3$ glass and energy level diagram with fluorescent transitions

Table 1 contains spectroscopic data of a number of chalcogenide glasses along with a silicate and a fluorozirconate glass. The list of the Judd-Ofelt intensity parameters shows an increasing parameter Ω_2 going from ionic fluorozirconate glasses to more covalent silicate glasses and on to even more

Table 1 Judd-Ofelt parameters of Nd^{3+} doped glasses, peak emission wavelengths and emission cross sections of the $^4F_{3/2} \rightarrow {}^4I_{11/2}$ transition and calculated radiative lifetimes of the $^4F_{3/2}$ level

Glass	Ω_2 (10^{-20}cm^{-2})	Ω_4 (10^{-20}cm^{-2})	Ω_6 (10^{-20}cm^{-2})	λ_{peak} (nm)	σ_{SE} (λ_{peak}) (10^{-20}cm^2)	τ_{calc} (µs)	Ref.
As_2S_3	-	-	-	1090	-	-	[1]
				1080			[2]
Ga:Na:S	8.2	5.3	3.8	1080	8.0	109	[3]
Ga:Ge:As:S	4.42	9.10	6.79	1078	-	90	[4]
$70Ga_2S_3$:$30La_2S_3$	7.70	7.65	4.86	1078	6.96	61	this work
$3Ga_2S_3$:$1La_2S_3$	6.65	4.39	4.67	1077	7.95	73	[10,11]
$3Al_2S_3$:$1La_2S_3$	9.45	4.84	6.54	1077	8.20	102	[10,11]
Ge:As:Ga:Sb:S	-	-	-	1077	-	-	[5]
25Ge:5Ga:70S	10.6	9.29	7.08	-	-	74	[6]
LG-680 Silicate	3.4	5.0	5.1	1061	2.9	333	[17]
Fluorozirconate	1.7	3.3	3.9	1049	2.7	497	[17]

Paper 7: accepted for publication in Volume 20 of EMIS Datareview Series

covalent chalcogenide glasses. The increase in the line strength of the hypersensitive 600 nm absorption band in chalcogenide glasses is therefore attributed to the more covalent bonding compared to the ionic bonding in fluorozirconate glasses .

The $^4F_{3/2}$ level is the level with the largest energy gap to the next lower lying level ($^4I_{15/2}$) and the only metastable level in the Nd^{3+} system independent of the host material. The four common emission bands from the $^4F_{3/2}$ level are shown in Fig. 2 (see also inset in Fig. 1).

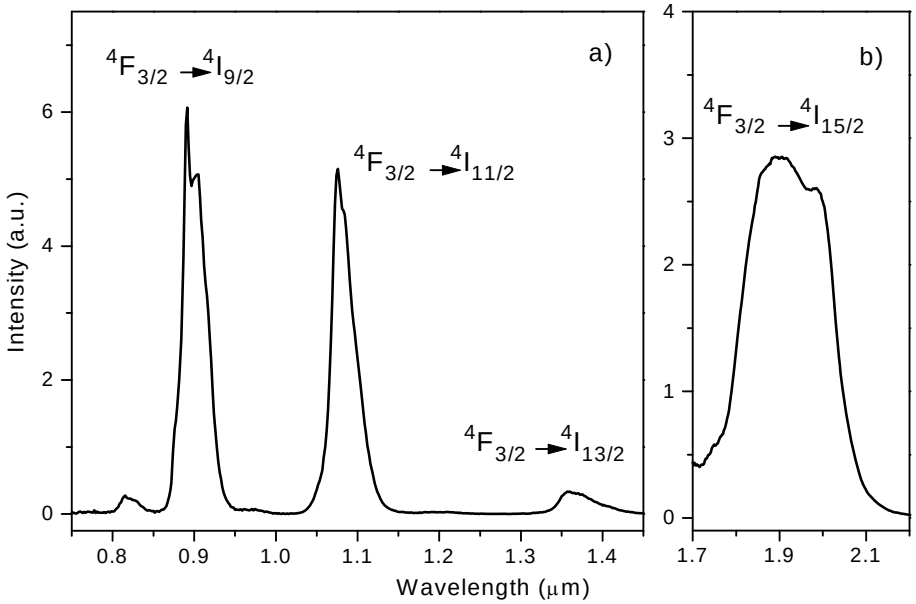

Fig. 2 Emission bands from metastable $^4F_{3/2}$ level of (a) 1 mol% Nd_2S_3 doped GLS glass pumped at 875 nm and measured with an ANDO spectrum analyser and (b) 1.5 mol% Nd_2S_3 doped GLS glass pumped at 815 nm with a Ti:sapphire laser and measured with a 300-mm monochromator and a liquid nitrogen cooled InSb detector (a and b not to scale)

There are two noteworthy points about the fluorescence spectra. Firstly, the peak emission wavelengths are shifted to longer wavelength in chalcogenide glasses compared to silicate and fluorozirconate glasses. The glasses in Table 1 are listed in order of decreasing peak emission wavelength of the $^4F_{3/2} \rightarrow {}^4I_{11/2}$ transition. The shift to longer emission wavelengths in chalcogenide glasses, the so called nephelauxetic effect, has been attributed to the high covalency of the glass bonds [3,18,21]. Secondly, the measured branching ratios of the 900 nm, 1080 nm, and 1360 nm band (50%, 43%, and 7%) which correspond well to the calculated branching ratios (49%, 43%, 7%, and < 1% for the 1.9 μm band) also reflect the covalency of the glass bonds. In more ionic glasses the 1080 nm band has the largest branching ratio with a value of typically > 50% [17,18].

The measured lifetime of the $^4F_{3/2}$ level should correspond, within error, to the radiative lifetime obtained from the Judd-Ofelt calculation (Table 1) as long as

the Nd^{3+} concentration and the excitation power are kept low to avoid ion-ion interactions. Fig. 3 (a) shows the lifetime of the $^4F_{3/2}$ level as a function of the Nd_2S_3 concentration in GLS glass pumped at 890 nm with a Ti:sapphire laser. For low concentrations the measured lifetime is slightly higher than the calculated (Table 1). The lifetime of the $^4F_{3/2}$ level is considerably lower in chalcogenide glasses than in silicate and fluorozirconate glasses, an unfavourable property for laser operation. This is partially counteracted by the larger emission cross sections in chalcogenide glasses (Table 1). The $\sigma\tau$-product which is inversely proportional to the laser threshold, however, is still smaller in chalcogenide glasses because the spontaneous transition probability (inverse of the lifetime) increases more rapidly with increasing refractive index (high in chalcogenide glasses) than the emission cross section [24]. The situation changes for transitions from levels with a small energy gap to the next lower lying level. In this case the lifetimes are considerably longer in chalcogenide glasses due to reduced multiphonon decay rates making chalcogenide glasses the favourable choice as a laser material for this sort of transitions.

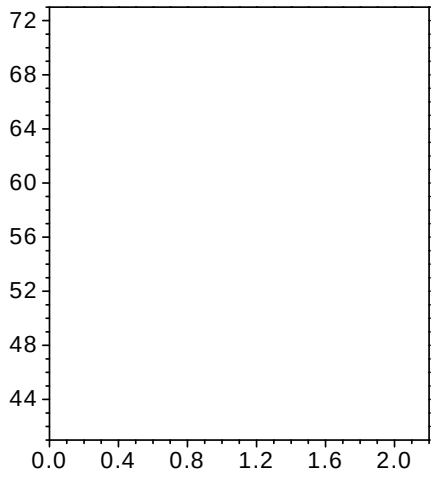

Fig. 3 Lifetime of $^4F_{3/2}$ (a) and $^2G_{9/2}$, $^4G_{7/2}$ (b) levels versus Nd_2S_3 content, x, in $70Ga_2S_3$:$(30\text{-}x)La_2S_3$:xNd_2S_3 glass under 890 nm (a) and 514 nm (b) excitation

The lifetime decreases with increasing Nd^{3+} concentration due to the well known cross-relaxation ($^4F_{3/2}$, $^4I_{9/2}$) $\rightarrow$ ($^4I_{15/2}$, $^4I_{15/2}$). This process was found to be rather strong in chalcogenide glasses with their ground state splitting ($^4I_{9/2}$) of around 500 cm^{-1} exceeding the 450 cm^{-1} value which separates the weak from the strong concentration quenching regime [3,25].

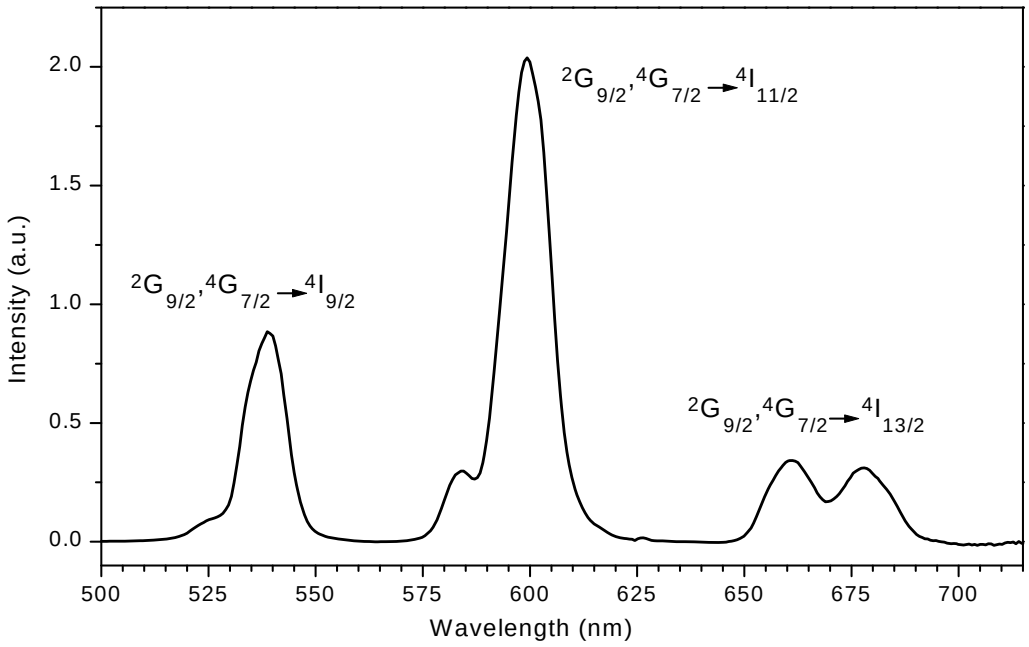

Fig. 4 Visible upconversion emission of 0.05 mol% Nd_2S_3 doped GLS glass fibre pumped at 815 nm with a Ti:sapphire laser and measured with a liquid nitrogen cooled CCD array spectrometer

At higher excitation powers the probability for the interaction between two excited Nd^{3+} ions increases providing an additional decay channel for the $^4F_{3/2}$ level. One ion is promoted down to the ^4I levels and the other is upconverted to higher energy levels leading to visible upconversion emission from the $^2G_{9/2}$, $^4G_{7/2}$ levels (see inset in Fig. 1). Fig. 4 shows the upconversion emission of a 0.05 mol% Nd_2S_3 doped GLS fibre with a 14 μm core and a 230 μm outer diameter pumped at 815 nm by a Ti:sapphire laser. The three emission bands in the green, orange, and red show a double peak structure with varying peak ratios which reflect the branching ratios and the relative population of the thermally coupled $^2G_{9/2}$, $^4G_{7/2}$ levels. The yellow upconversion emission is visible for pump powers as low as 1 mW. The lifetime quenching of the $^2G_{9/2}$, $^4G_{7/2}$ levels (Fig. 3 (b)) is significantly stronger than for the $^4F_{3/2}$ level (Fig. 3 (a)) indicating more efficient cross-relaxation processes. For the lifetime measurements the $^2G_{9/2}$, $^4G_{7/2}$ levels were excited directly with the 514 nm line of an Ar^+ ion laser. The decay time of the $^2G_{9/2}$, $^4G_{7/2}$ levels under 815 nm Ti:sapphire upconversion pumping is 30 μs which is much longer than under direct 514 nm pumping and is about half the value of the $^4F_{3/2}$ level lifetime. This indicates that the upconversion emission is caused by interaction between two excited Nd^{3+} ions in the $^4F_{3/2}$ level and not by excited-state absorption. If the visible upconversion emission were caused by excited-state absorption the lifetime under 815 nm pumping would be similar to the lifetime under 514 nm pumping. The radiative lifetimes of the $^2G_{9/2}$, $^4G_{7/2}$ levels (22 μs and 21 μs) derived from the Judd-Ofelt

Paper 7: accepted for publication in Volume 20 of EMIS Datareview Series

calculations combine to a radiative lifetime of 11 μs for the thermally coupled levels. This is considerably longer than the measured lifetime for low Nd^{3+} concentration (6 μs) indicating that multiphonon decay is an important decay channel for the $^2G_{9/2}$, $^4G_{7/2}$ levels due to the small energy gap of 1900 cm^{-1} (5.2 μm). The lifetime shortening caused by multiphonon decay would, however, be much more severe in silicate and fluorozirconate glasses with higher phonon energies. The upconversion emission is a loss process for laser transitions starting from the $^4F_{3/2}$ level [14-16].

The low phonon energy of chalcogenide glasses also gives rise to new Nd^{3+} emission bands that cannot be observed in other glasses. Fig. 5 shows two fluorescence bands from the $^2H_{9/2}$, $^4F_{5/2}$ levels at 1.2 μm and 1.56 μm (see also Fig. 1) at either side of the 1.36 μm band from the metastable level ($^4F_{3/2}$) under 815 nm Ti:sapphire pumping. The intensities of the 1.2 μm and 1.56 μm bands are of the same order of magnitude as the 1.36 μm band, despite the small energy gap of about 1000 cm^{-1} (10 μm) to the next lower lying level, displaying the low phonon energy of the chalcogenide glass. The radiative transitions from the $^2H_{9/2}$, $^4F_{5/2}$ levels by-pass the $^4F_{3/2}$ level (see Fig. 1) and reduce the pump efficiency for laser transitions starting from the $^4F_{3/2}$ level under 815 nm pumping [14-16].

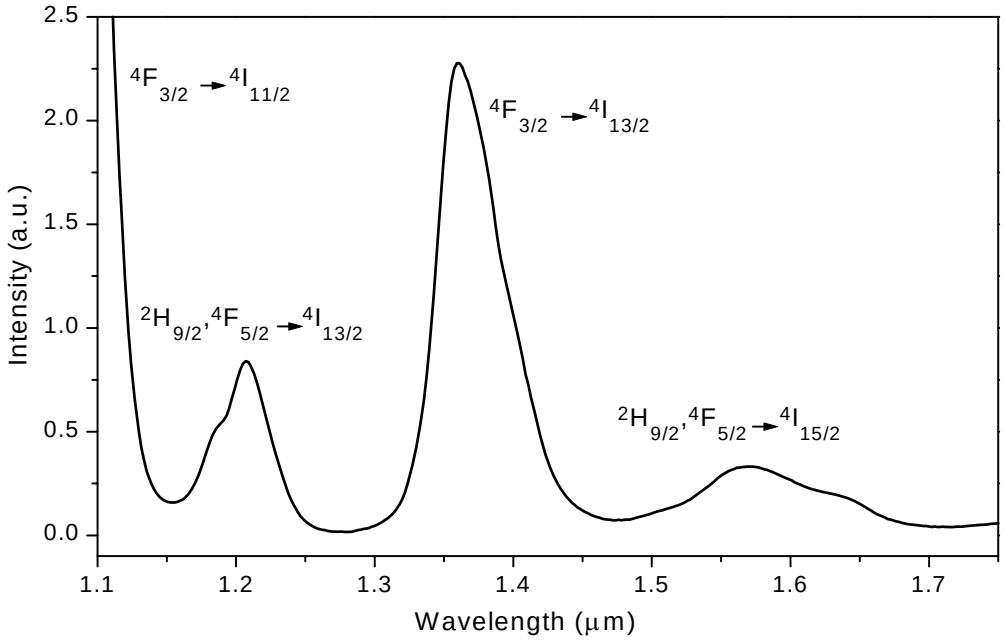

Fig. 5 Emission from $^2H_{9/2}$, $^4F_{5/2}$ levels in 1.5 mol% Nd_2S_3 doped GLS glass pumped at 815 nm with a Ti:sapphire laser and measured with a 300-mm monochromator and a liquid nitrogen cooled InSb detector

The low multiphonon decay rates in chalcogenide glasses also lead to measurable fluorescence from the lower Nd^{3+} energy levels in the mid-infrared

wavelengths region which has not been reported in silicate and fluorozirconate glasses (see Fig. 1). Fig. 6 shows the emission bands from the $^4I_{13/2}$ and $^4I_{11/2}$ levels at 2.55 μm (a) and 5.1 μm (b) for 815 nm pumping. The 5.1 μm ($^4I_{11/2} \rightarrow {}^4I_{9/2}$) band that cannot be measured completely due to limitations of the equipment will only have some minor contribution from the $^4I_{13/2} \rightarrow {}^4I_{11/2}$ transition which is expected to overlap with the $^4I_{11/2} \rightarrow {}^4I_{9/2}$ transition. The $^4I_{13/2} \rightarrow {}^4I_{11/2}$ transition is competing with the stronger $^4I_{13/2} \rightarrow {}^4I_{9/2}$ transition (2.55 μm) and the $^4I_{13/2}$ level is only populated by the 1.36 μm and 1.90 μm transitions whereas the $^4I_{11/2}$ level is populated by the much stronger 1.08 μm transition and has a branching ratio of 100% (see Fig. 1).

The population of the lower energy levels, which is commonly assumed to be negligible in higher phonon energy laser materials, could lead to gain saturation and reabsorption for laser transitions starting from the $^4F_{3/2}$ level [14-16].

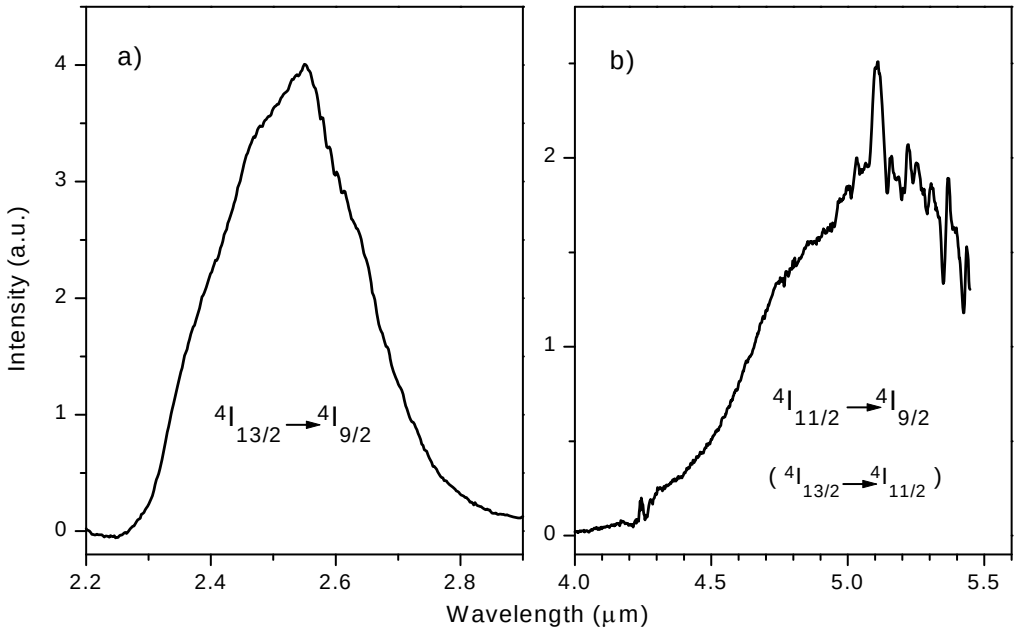

Fig. 6 Emission from the two lowest Nd^{3+} levels, $^4I_{13/2}$ (a) and $^4I_{11/2}$ (b), in 1.5 mol% Nd_2S_3 doped GLS glass pumped at 815 nm with a Ti:sapphire laser and measured with a 300-mm monochromator and a liquid nitrogen cooled InSb detector

The mid-infrared emission shows the potential of chalcogenide glasses as promising materials for mid-infrared lasers. The problem of pumping the lower Nd^{3+} levels directly and efficiently could be avoided by using a cascade lasing scheme including the 1.36 μm or 1.08 μm transitions, respectively. Such a pumping scheme has been realised in a Nd^{3+} doped fluoride crystal with simultaneous laser operation at 1.35 μm and 5.15 μm [26].

Conclusion

The spectroscopic differences in the absorption, fluorescence and lifetime measurements of Nd^{3+} doped chalcogenide glasses compared to silicate and fluorozirconate glasses have been outlined using Nd^{3+} doped gallium lanthanum sulphide glass as an example. The measurements reflect the influence of the covalent glass bonds and the low phonon energy on the spectroscopy of the Nd^{3+} ions and show the potential of chalcogenide glasses as materials for new laser transitions, in particular in the mid-infrared wavelength region.

References

[1] J. Heo [*J. Mater. Sci. Lett.* vol.14 (1995) p.1014]
[2] J.-F. Viens et al. [in *Conference on Lasers and Electrooptics*, vol.11 of 1997 OSA Technical Digest Series (Optical Society of America, Washington, DC, 1997) p.249]
[3] B. Viana, M. Palazzi, O. LeFol [*J. Non-Cryst. Solids (USA)* vol.215 (1997) p.96]
[4] A Belykh et al. [*J. Non-Cryst. Solids (USA)* vol.213&214 (1997) p.238]
[5] A. Mori et al. [*Appl. Phys. Lett. (USA)* vol.70 (1997) p.1230]
[6] K. Abe, H. Takebe, K. Morinaga [*J. Non-Cryst. Solids (USA)* vol.212 (1996) p.143]
[7] J.V. Sathyanarayana, K. Annapurna, S. Buddhudu [*Journal of Alloys and Compounds* vol.224 (1995) p.97]
[8] Y.S. Tver'yanovich, S.V. Degtyarev, S.S. Pivovarov, N.V. Belyakova [*Glass Physics and Chemistry* vol.23 (1997) p.80]
[9] R. Reisfeld, A. Bornstein [*Chem. Phys. Lett.* vol.47 (1977) p.194]
[10] R. Reisfeld [*Ann. Chim. Fr.* vol.7 (1982) p.147]
[11] A. Bornstein, R. Reisfeld [*J. Non-Cryst. Solids (USA)* vol.50 (1982) p.23]
[12] J. Flahaut et al. [*Glass Technology (UK)* vol.24 (1983) p.149]
[13] L. Mattoa Jnr and A.G. Clare [*Physics and Chemistry of Glasses (UK)* vol.34 (1993) p.244]
[14] T. Schweizer, D.W. Hewak, D.N. Payne, T. Jensen, G. Huber [*Electron. Lett. (UK)* vol.32 (1996) p.666]
[15] T. Schweizer, B.N. Samson, R.C. Moore, D.W.Hewak, D.N. Payne [*Electron. Lett. (UK)* vol.33 (1997) p.414]
[16] T. Schweizer [Datareview in this book: *5.2. Fibre Lasers based on Rare-Earth doped Chalcogenide Glass*]
[17] S.E. Stokowski, R.A. Saroyan, M.J. Weber [*Laser Glass, Nd-Doped Laser Glass, Spectroscopic and Physical Properties* vol.1+2 (1981) Lawrence Livermore National Laboratory, University of California, Livermore, California]
[18] M.J.F. Digonnet (Ed.) [*Rare Earth Doped Fiber Lasers and Amplifiers* (Marcel Dekker, Inc., 1993) p.50-72]
[19] C. K. Jørgensen, B.R. Judd [*Mol. Phys.* vol.8 (1964) p.281]
[20] C. K. Jørgensen, R. Reisfeld [*Journal of the Less-Common Metals* vol.93 (1983) p.107]
[21] C. K. Jørgensen [*Orbitals in Atoms and Molecules* (Academic Press, New York, 1962)]
[22] B.R. Judd [*Phys. Rev. (USA)* vol.127 (1962) p.750]
[23] G.S. Ofelt [*J. Chem. Phys. (USA)* vol.37 (1962) p.511]
[24] M.J. Weber, J.D. Myers, D.H. Blackburn [*J. Appl. Phys. (USA)* vol.52 (1981) p.2944]
[25] F. Auzel [*Mater. Res. Bull. (USA)* vol.14 (1979) p.223]
[26] A.A. Kaminskii [*Inorganic Materials* vol.20 (1984) p.782]

Properties of Glass and Rare-Earth Doped Glasses for Optical Fibres
Part D - Chalcogenide Glasses
D5 Selected Applications

D5.2 Fibre Lasers based on Rare-Earth doped Chalcogenide Glass

T. Schweizer

Introduction

The first demonstration of laser action in a rare-earth doped glass fibre by Snitzer [1] triggered off world wide activities to realise fibre lasers at a large variety of emission wavelengths ranging from the ultraviolet [2] to the mid-infrared [3]. Specific applications require different laser wavelengths which in turn require different rare-earth dopants and host materials. Chalcogenide glasses offer some advantages over oxide and fluoride glasses. The small phonon energies of the glass matrix lead to extended infrared transparency and low non-radiative decay rates of rare-earth energy levels; the covalent nature of the glass bonds (high refractive index) increases the radiative decay rates and emission and absorption cross sections (see [4-9] for more details). Based on these favourable properties chalcogenide glasses have been proposed as new laser materials, in particular for new laser transitions from energy levels with a small energy gap to the next lower lying level such as the 1.3 μm transitions in praseodymium [6] and dysprosium [9] and new mid-infrared transitions [10-13]. Most of the research is focused on sulphide glasses which offer transparency at convenient pump wavelengths in the visible and near-infrared wavelength regions compared to the opaque selenide and telluride glasses [4,13]. Most of the rare-earth doped sulphide glass laser work in turn concentrates on trivalent neodymium (Nd^{3+}) as the active ion which is rather used as a convenient test dopant than a dopant with promising new transitions [7,10,14-24]. Out of this group of glasses Nd^{3+} doped gallium lanthanum sulphide (GLS) glasses have been studied in greatest depth and are the only chalcogenide glasses with reported laser action in bulk glass and fibre form [7, 14-18,25,26]. After a brief introduction to other proposed neodymium doped chalcogenide laser glasses this review will therefore focus on neodymium lasers in GLS glass.

Lasers based on neodymium-doped sulphide glasses

A number of Nd^{3+} doped sulphide glasses such as As_2S_3 [10,20], Ga:Ge:As:S [21], $3Al_2S_3$:$1La_2S_3$ [15,16], Ge:As:Ga:Sb:S [19], Ge:Ga:S [22], and Ga:Na:S [24] have been proposed as new laser materials and studied mainly in bulk glass form. Viens et al. [20] reported 1080 nm fluorescence from As_2S_3 waveguides which were thermally evaporated onto oxidised silicon wafers and doped with Nd^{3+} using ion implantation. Internal gain in a Nd^{3+} doped sulphide fibre was reported for the first time by Mori et al. [19]. The fibre with a 1000 ppm Nd^{3+} doped Ge:As:Ga:Sb:S core glass and a Ge:As:S cladding glass was fabricated

Paper 8: accepted for publication in Volume 20 of EMIS Datareview Series

using the rod-in-tube technique, had a core diameter of 5 μm and a cladding diameter of 120 μm, a cut-off wavelength of 2.1 μm, and a transmission loss of 10 dB/m at 1.3 μm. A 5 cm long fibre showed a maximum internal gain of 6.8 dB for a pump power of 180 mW. Net signal gain was not obtained.

Nd^{3+} doped gallium lanthanum sulphide (GLS) glass has been studied extensively [14-18], and a summary of the spectroscopic properties can be found in this book [7]. The first laser operation in a rare-earth doped chalcogenide glass was achieved in this system [25]. A 1.42 mm thick glass disk with the composition $70Ga_2S_3{:}28.5La_2S_3{:}1.5Nd_2S_3$ was placed in a hemispherical laser cavity and pumped with a Ti:sapphire laser at either 815 nm or 890 nm. Figure 1 shows the output power versus the absorbed pump power of the 1080 nm laser transition ($^4F_{3/2} \rightarrow {}^4I_{11/2}$) for 890 nm pumping.

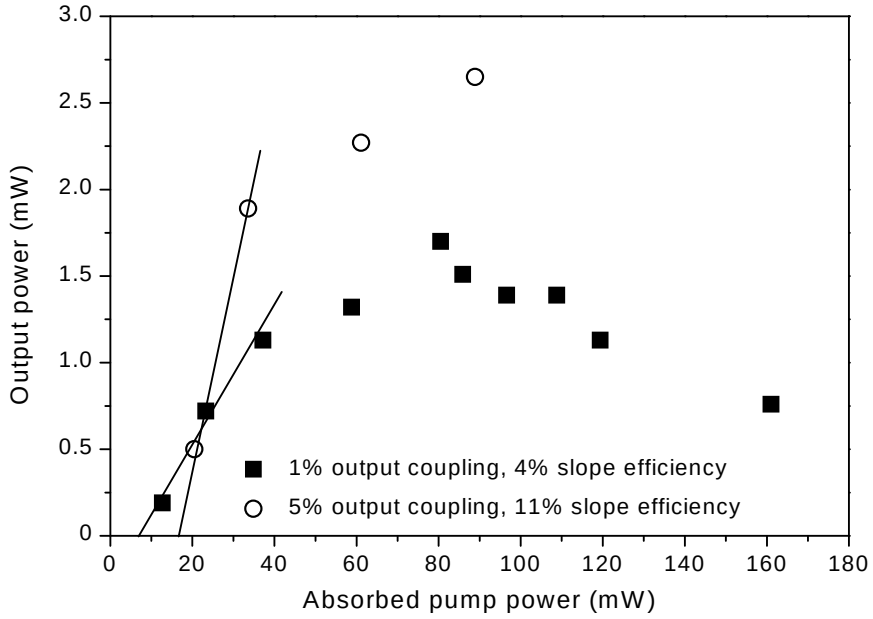

Fig. 1 Output power against absorbed pump power of 1080 nm Nd^{3+} doped GLS glass laser pumped at 890 nm [23]

The laser operated continuous wave at room temperature. The threshold power is reasonably low but the rollover of the output power indicates strong thermal problems in the laser material. Similar thermal problems and measurements of the focal length of the thermal lens have been reported by Viana et al. in Nd^{3+} doped Ga:Na:S glass [24]. The authors concluded that laser action in their system was prevented by thermal lensing and the high threshold power which is caused by the short lifetime of the $^4F_{3/2}$ level and proposed several solutions to this problem such as reduction of the chopped pump duty cycle, convex polishing of the glass end faces and the fabrication of guiding structures such as waveguides and fibres.

Advances in chalcogenide glass fibre fabrication [27] enabled the realisation of a Nd^{3+} doped GLS glass fibre laser [26]. The fibre which was fabricated using

the rod-in-tube method was doped with 0.05 mol% Nd_2S_3 and had a 14 μm core and a 230 μm outer diameter. The fibre laser behaviour of a Ti:sapphire pumped (815 nm) 22 mm long fibre with a high reflecting input mirror and three different output mirrors and wavelengths is shown in figure 2. As expected the output power does not roll over at high pump powers showing the advantage of the fibre geometry.

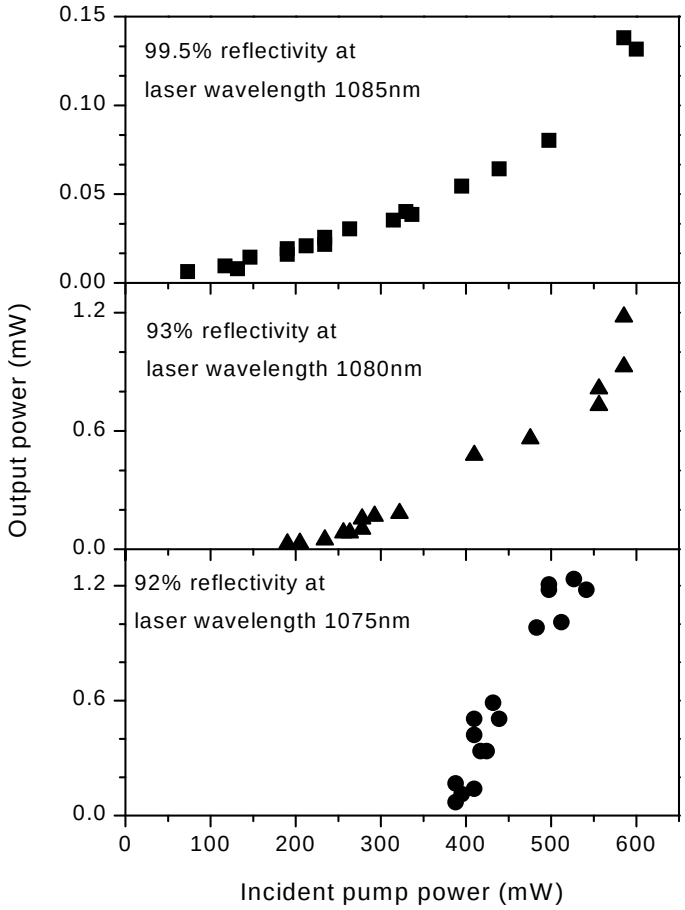

Fig. 2 Output power against incident pump power of Nd^{3+} doped GLS glass fibre laser for different output mirrors and laser wavelengths pumped at 815 nm [24]

The fibre laser was initially reported to be self-pulsing with pulse width of about 0.2 μs and regular pulse spacing between 2 and 3.5 μs [26]. Further experiments showed that the self-pulsing behaviour is not inherent to the fibre itself but depends on the alignment of the resonator mirrors and the focusing objective. Figure 3 shows the two different lasing regimes (continuous wave and self-pulsing) which could be switched on and off by changing the alignment of the output mirror. A graph showing a train of single equidistant pulses can be found in Ref. [26]. We can therefore report true cw laser action at room

Paper 8: accepted for publication in Volume 20 of EMIS Datareview Series

temperature at this point.

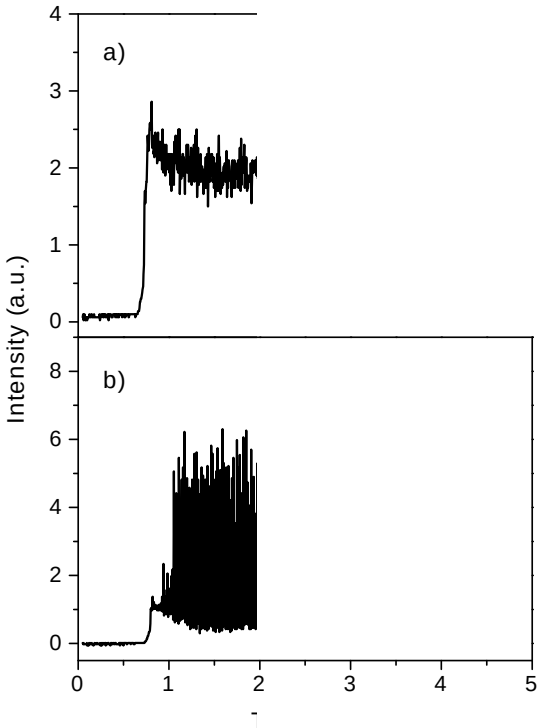

Fig. 3 Continuous wave (a) and self-pulsing (b) laser behaviour of the Nd^{3+} doped GLS glass fibre laser (chopped pump source for clarity)

To our knowledge, there are no other chalcogenide glass fibre lasers reported in the literature although a number of different glasses with different rare-earth dopants have been proposed as new laser materials, in particular for mid-infrared fibre lasers, a wavelength range which is not accessible by common silica fibre lasers.

Conclusion

Fibre lasers based on chalcogenide glasses are still in their infancy but the proof of principle in the form of the demonstration of a Nd^{3+} doped fibre laser, the numerous reports in the literature on new potential laser transitions, and the advances in fibre fabrication show a promising future for new chalcogenide glass fibre lasers.

References

[1] E Snitzer [*Phys. Rev. Lett. (USA)* vol.7 (1961) p.444]
[2] D.S. Funk, J.W. Carlson, J.G. Eden [*Electron. Lett. (UK)* vol.30 (1994) p.1859]
[3] J. Schneider [*Electron. Lett. (UK)* vol.31 (1995) p.1250]
[4] D.J. Brady [Datareview in this book: *1.1. Transmission of Chalcogenide Glass*]
[5] H. Takebe [Datareview in this book: *1.3. Refractive Index and Dispersion of Chalcogenide Glass*]

Paper 8: accepted for publication in Volume 20 of EMIS Datareview Series

[6] J.R. Hector [Datareview in this book: *3.1. Spectroscopy of Praseodymium-Doped Chalcogenide Glass*]
[7] T. Schweizer [Datareview in this book: *3.2. Spectroscopy of Neodymium-Doped Chalcogenide Glass*]
[8] J. Heo [Datareview in this book: *3.3. Spectroscopy of Thulium/Holmium-Doped Chalcogenide Glass*]
[9] B.N. Samson [Datareview in this book: *3.4. Spectroscopy of Dysprosium-Doped Chalcogenide Glass*]
[10] J. Heo [*J. Mater. Sci. Lett.* vol.14 (1995) p.1014]
[11] T. Schweizer, D.W. Hewak, B.N. Samson, D.N. Payne [*Opt. Lett. (USA)* vol.21 (1996) p.1594]
[12] T. Schweizer, D.W. Hewak, B.N. Samson, and D.N. Payne [*J. Lumin.* vol.72-74 (1997) p.419]
[13] L.B. Shaw, B.B. Harbison, B. Cole, J.S. Sanghera, I.D. Aggarwal [*Optics Express (USA)* vol.1 (1997) p.87]
[14] R. Reisfeld, A. Bornstein [*Chem. Phys. Lett.* vol.47 (1977) p.194]
[15] A. Bornstein, R. Reisfeld [*J. Non-Cryst. Solids (USA)* vol.50 (1982) p.23]
[16] R. Reisfeld [*Ann. Chim. Fr.* vol.7 (1982) p.147]
[17] J. Flahaut, M. Guittard, A.M. Loireau-Lozac'h [*Glass Technology (UK)* vol.24 (1983) p.149
[18] L. Mattos Jnr, A.G. Clare [*Physics and Chemistry of Glasses (UK)* vol.34 (1993) p.244]
[19] A. Mori, Y. Ohishi, T. Kanamori, S. Sudo [*Appl. Phys. Lett. (USA)* vol.70(1997) p.1230]
[20] J.-F. Viens et al. [in *Conference on Lasers and Electrooptics*, vol.11 of 1997 OSA Technical Digest Series (Optical Society of America, Washington, DC, 1997) p.249]
[21] A Belykh et al. [*J. Non-Cryst. Solids (USA)* vol.213&214 (1997) p.238]
[22] K. Abe, H. Takebe, K. Morinaga [*J. Non-Cryst. Solids (USA)* vol.212 (1996) p.143]
[23] Y.S. Tver'yanovich, S.V. Degtyarev, S.S. Pivovarov, N.V. Belyakova [*Glass Physics and Chemistry* vol.23 (1997) p.80]
[24] B. Viana, M. Palazzi, O. LeFol [*J. Non-Cryst. Solids (USA)* vol.215 (1997) p.96]
[25] T. Schweizer, D.W. Hewak, D.N. Payne, T. Jensen, G. Huber [*Electron. Lett. (UK)* vol.32 (1996) p.666]
[26] T. Schweizer, B.N. Samson, R.C. Moore, D.W.Hewak, D.N. Payne [*Electron. Lett. (UK)* vol.33 (1997) p.414]
[27] D.W. Hewak [Datareview in this book: *4.3.Drawing of Chalcogenide Glass Optical Fibres, 4.4. Loss of Chalcogenide Glass Optical Fibres*]

Nd^{3+} concentration effect on the bulk laser properties

The bulk-laser experiments were performed by the author in collaboration with T. Jensen and G. Huber at the Institut für Laser-Physik, Universität Hamburg, Germany.

In addition to the reported laser operation of the 1.42 mm thick Nd(1.5%):GLS glass we performed further laser experiments with a glass of lower Nd^{3+} concentration. Laser action could be achieved in 0.6 mol% Nd_2S_3 doped GLS glasses with lengths of 0.73, 1.59, and 4.68 mm. The lower Nd^{3+} concentration reduced the thermal effects in the glass and allowed pumping into the stronger and more convenient 0.815 μm band compared to the 0.89 μm pumping described above. The output powers (~ 1 mW) were slightly lower than the output power measured from the Nd(1.5%):GLS glass (~ 2.5 mW). Laser action did not cease at higher pump powers as it did for the higher concentration but the output power still showed a saturation effect. A further reduction of the thermal effects might be achieved for even lower Nd^{3+} concentrations. This naturally leads to the fabrication of waveguiding structures which offer a long interaction length and good overlap between pump and laser modes. As discussed earlier laser operation could be obtained in a GLS fibre with a thirty times lower Nd^{3+} concentration compared to the glasses used in the initial bulk laser experiments.

Temporal behaviour of the Nd^{3+} fibre laser output

In addition to the 22 mm long fibre laser mentioned above (page 128), laser operation with similar performance was also obtained in 21 and 25 mm long fibres but was not observed in shorter (down to 15 mm) and longer (up to 55 mm) fibres. All of these fibre lasers showed a self-pulsing behaviour. Fig. 5.2.1 shows the spectral and temporal behaviour of the 22 mm long fibre laser. The range of laser wavelengths extended from about 1075-1085 nm, and Fig. 5.2.1.a shows a typical snapshot of lasing at 1080 nm.

As mentioned on page 129 the self-pulsing of the fibre laser (Fig. 5.2.1.b) could be switched on and off by aligning the output mirror, i.e. by changing the loss in the cavity. The reason for this behaviour is not yet understood but it occurs in analogy to self-pulsing in Er^{3+} doped fibre lasers [San93]. In Er^{3+} doped fibre lasers the effect is mainly attributed to ion-ion interactions which modify the rate equations and can lead to Hopf bifurcations, instabilities which can cause self-pulsing of the laser output [Cra91]. The development of these instabilities depends on the ion concentration and the pumping ratio, i.e. how far above threshold the laser is operated. Any changes in the alignment of the output mirror changes the cavity loss and hence the pumping ratio. The self-pulsing observed in our Nd^{3+} doped fibre could therefore be of the same nature as the

self-pulsing reported in Er^{3+} doped fibres but a firm conclusion about the origin of the effect cannot be drawn at this point.

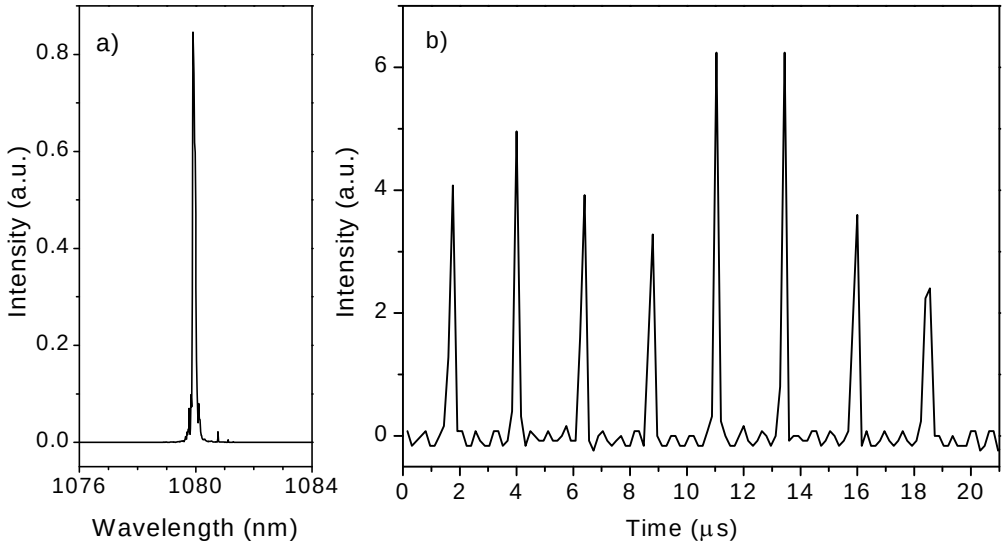

Fig. 5.2.1 a) Spectral and b) temporal behaviour of the fibre laser output. The wavelength spectrum was measured with an ANDO spectrum analyser, and the temporal behaviour was recorded with an InGaAs diode and a TEK2232 digital storage oscilloscope.

A few further details about the GLS glass fibre used for the laser experiments should be mentioned here.

i) The two cladding glass tubes were oxide modified with the composition $72Ga_2S_3{:}28La_2O_3$.

ii) The core glass had a molar ratio of $62Ga_2S_3{:}38La_2S_3$ which matched the viscosity of the cladding glass.

iii) The core glass rod was caned down to 1 mm diameter and inserted into a tube which had been caned to in inner diameter of 1 mm and outer diameter of 3 mm beforehand. This assembly was then inserted into a 3 mm inner diameter tube thus reducing the number of heat cycles for the core glass by one compared to the conventional rod-in-tube method which does not involve the caning of cladding tubes.

The smaller number of heat treatments reduce the tendency for crystallisation and the oxide modified claddings facilitate fibre drawing. These glass compositions and fabrication method should be kept in mind for future fibre drawing trials for fibre lasers.

5.3 Conclusion

The availability of comparable data for other Nd^{3+} doped glass systems makes the spectroscopic study of Nd^{3+} doped GLS glass a rather nice example to show the influence of the chalcogenide glass host on the absorption and emission cross sections, the emission wavelengths, the lifetimes, and the non-radiative properties of the rare-earth ion. A number of new transitions in particular the 2.5 μm and 5.1 μm emission bands are reported for the first time in a Nd^{3+} doped glass host.

Laser operation in RE doped chalcogenide glasses was demonstrated for the first time. Laser action at 1.08 μm was achieved in Nd^{3+} doped bulk glasses and glass fibres. As a result of the bulk laser experiments future laser experiments will concentrate on fibre structures.

To date lasing in GLS fibre has only been achieved on the 1.08 μm Nd^{3+} transition which does not benefit from the low phonon energy of GLS glass. Future laser experiments will look at longer wavelengths transitions of which the 2.7 μm Er^{3+} transitions is the most promising one assuming the OH^- impurities in the glass will be further reduced. Laser experiments will also focus on the transitions which are of interest for the LONGWAVE project such as the 3.4 μm and 4.7 μm Pr^{3+}, the 4.3 μm Dy^{3+}, and the 3.9 μm Ho^{3+} transitions. The caesium modified glasses should also be tested for their use as a fibre laser host whereas the oxide modified are of lesser interest due to their higher phonon energies and therefore lower quantum efficiencies.

Chapter 6

Conclusion

The aim of this project was to investigate the suitability of gallium lanthanum sulphide (GLS) glasses as a host material for rare-earth (RE) doped mid-infrared fibre lasers. The two main questions to be addressed were:

i) Is GLS glass a suitable host for mid-infrared emission from RE ions from a spectroscopic point of view?

ii) Can GLS glass be fabricated into a fibre structure with sufficiently small core diameter and sufficiently low loss levels for fibre laser applications?

The work presented in this thesis concentrated mainly on the first question, i.e. the spectroscopic properties of the RE ions in GLS glass.

GLS glasses were doped with eleven different RE ions and investigated using absorption, fluorescence, and lifetime measurements. The results of these measurements were used to study the radiative and non-radiative properties of the RE ions and to calculate important laser parameters such as the absorption and emission cross sections, branching ratios, and quantum efficiencies.

The non-radiative multiphonon decay rates were determined for a number of energy levels of six different RE ions. The dependence of the multiphonon rate on the size of the energy gap is exponential as predicted by the theory. The rates for gaps in the 3-5 μm region, however, are up to three orders of magnitude lower (for 3 μm) than previously reported by other authors. The radiative quantum efficiencies of transitions around 3 μm are mainly limited by their low branching ratios, whereas the quantum efficiency around 5 μm is reduced to typically 1% by multiphonon rates of up to 10,000 s^{-1}. The multiphonon

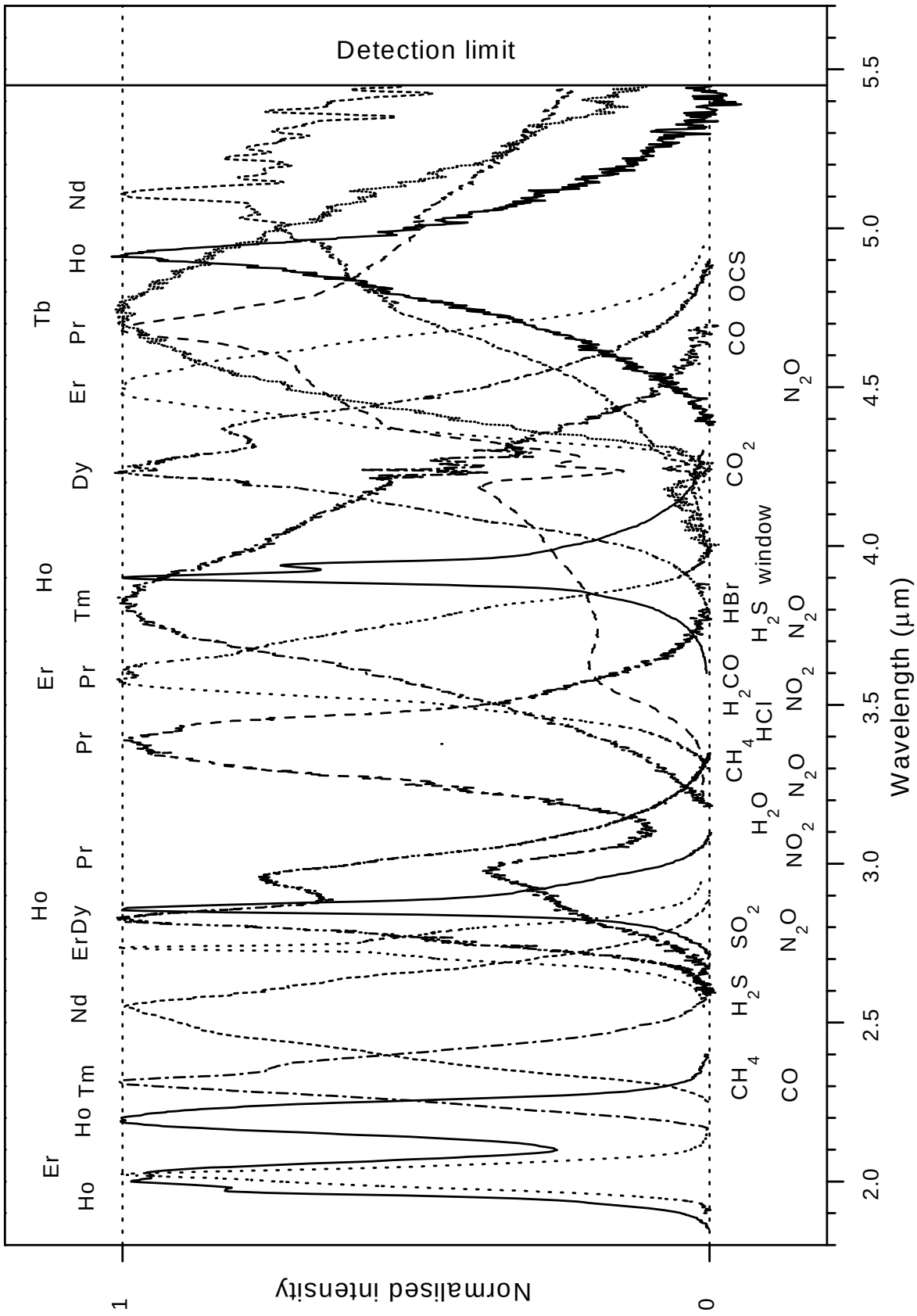

Fig. 6.1 Normalised mid-infrared emission bands of 20 rare-earth transitions in GLS glass and a selection of gas species with absorption bands between 2 -5 μm (2.4 μm Pr^{3+} emission not shown, see Fig. 3.4.4.a)

relaxations limit the use of GLS glass for mid-infrared fibre lasers to transitions with a maximum emission wavelength of approximately 5 μm. Fibre lasers with even longer emission wavelength would require host materials with lower maximum phonon energies such as selenide and telluride glasses.

Fluorescence measurements revealed twenty-one transitions with peak wavelength longer than 2 μm (the practical limit for common silica glasses) from seven different RE ions. Fig. 6.1 shows twenty normalised RE transitions along with a number of gas molecules with absorption bands in the 2-5 μm wavelength range. The mid-infrared region is completely covered by the RE fluorescence bands showing the potential for gas sensing applications. The actual absorption of RE fluorescence by a gas was demonstrated for the cases of CO_2 (4.3 μm Dy^{3+} emission), and CH_4 and C_4H_{10} (3.4 μm Pr^{3+} emission). Two transitions (3.8 μm Tm^{3+} and 3.9 μm Ho^{3+}) coincide with an atmospheric transmission window and have potential as laser sources for applications requiring low atmospheric attenuation.

A number of experiments addressed the choice of pump wavelengths for mid-infrared transitions:

i) Co-doping the active ion (acceptor) with a donor ion increases the number of possible pump wavelengths and the absorption strength by relying on energy transfer from the donor to the acceptor. Energy transfer was demonstrated from Tm^{3+} to Tb^{3+}, from Er^{3+} to Pr^{3+} and Dy^{3+}, and from Yb^{3+} to Pr^{3+} (GLSO only), making 0.8 μm and 0.98 μm diode laser pumping of mid-infrared transitions feasible.

ii) The existence of RE sites with different local environments can impose requirements on the choice of the pump wavelength as demonstrated for the case of Dy^{3+}.

iii) The low phonon energy of GLS which is of advantage with regard to mid-infrared emission imposes restrictions on the number of possible pump wavelength. For high pump efficiencies the upper laser level should be excited resonantly without depending on the weak non-radiative decay from higher pump levels. The range of possible pump wavelengths could be increased by using cascade lasing schemes or cross-relaxation and upconversion processes.

iv) Excited-state absorption (ESA) from RE ions to the conduction band of the glass in the pump wavelength region could have been a potential problem in a small energy gap material like GLS. ESA measurements in Er^{3+} and Tm^{3+}, however, did not reveal any transitions of this type but instead showed transitions to energy levels of the RE which could not be observed in the ground-state absorption spectrum. The measurements reflect the shielded nature of the transitions within the 4f shell of RE ions and rules out additional pump losses due to ESA into the glass host.

First laser operation in a chalcogenide glass host was achieved in Nd^{3+} doped GLS bulk glass and fibres at 1.08 μm. The laser performance was poor compared to common Nd^{3+} lasers and showed the need for improving the glass and fibre qualities. The roll-over of the input-output curves for the bulk glass laser, which reflect the poor thermal properties of the glass host, could be eliminated by using the fibre laser geometry. Hence, GLS is not further pursued as a bulk laser material. Future fibre laser experiments will focus on transitions with longer emission wavelengths such as the 1.5 μm and 2.3 μm Tm^{3+} and the 2.7 μm Er^{3+} transitions and finally reach the 3-5 μm region. The progress in laser development depends critically on the progress in fibre fabrication.

In the course of this work considerable improvement was made regarding the GLS glass fibre fabrication. Core-clad structures fabricated by the rod-in-tube method were demonstrated for the first time. The advances in fibre fabrication formed the basis for the realisation of the first chalcogenide glass fibre laser. However, loss levels are still high compared to fluoride and silica fibres due to impurity absorption, scattering from impurities and from crystals formed during the repeated heat treatments of the core glass, and imperfections of the core-clad interfaces. Further improvement of the fibre is necessary for the development of viable mid-infrared devices. Two routes to higher quality fibres are currently pursued: i) in-house purification and conversion of chloride and fluoride starting materials to sulphide powders and ii) fabrication of preforms with core-clad structures by extruding the core and cladding glasses through a die. Both activities are expected to reduce the fibre loss; the purification by reducing the level of absorption loss from impurities and the number of scattering centres, and the extrusion method by improving the quality of the core-clad interface and by reducing the number of heat treatments. The quality of the fibre could also be increased by replacing part or all of the La_2S_3 with glass modifiers such as La_2O_3, CsCl, Na_2S_3, or any other magic component X which still needs to be identified. In particular gallium sodium sulphide (GNS) looks like an attractive alternative to GLS. The successful improvement of the fibre quality will trigger off activities in a number of research areas such as fibre lasers, passive mid-infrared light transmission, and non-linear optical switching.

With regard to mid-infrared lasers the fabrication of planar waveguides could offer a solution for RE ions with little concentration quenching and strong absorption bands. Planar waveguides of GLS glass which have been fabricated using pulsed-laser deposition could also be achieved by methods such as spin-coating of molten glass, direct bonding, UV writing, and others.

In addition to new fabrication techniques GLS offers a vast amount of

material for further spectroscopic studies. Most RE ions could not be studied in great detail due to the large number of ions covered and the focus on mid-infrared transitions. Points of particular interest for further investigations are co-doping schemes, site-selectivity, doping with transition metals as active ions, the influence of Ce^{3+}, $Sm^{2+/3+}$, and Eu^{2+} on photosensitivity, Pr^{3+} as a saturable absorber at 1.5 μm, and electronic properties with respect to electrically pumped RE lasers.

In conclusion, GLS glass is an interesting RE host material which offers many opportunities for new applications and also for the investigation of more fundamental physical questions concerning the influence of the host material on the RE ions.

7 Appendix

7.1 Experimental set-up for mid-infrared fluorescence measurements

Fig. 7.1.1 shows the set-up which was designed for the measurement of weak mid-infrared fluorescence bands.

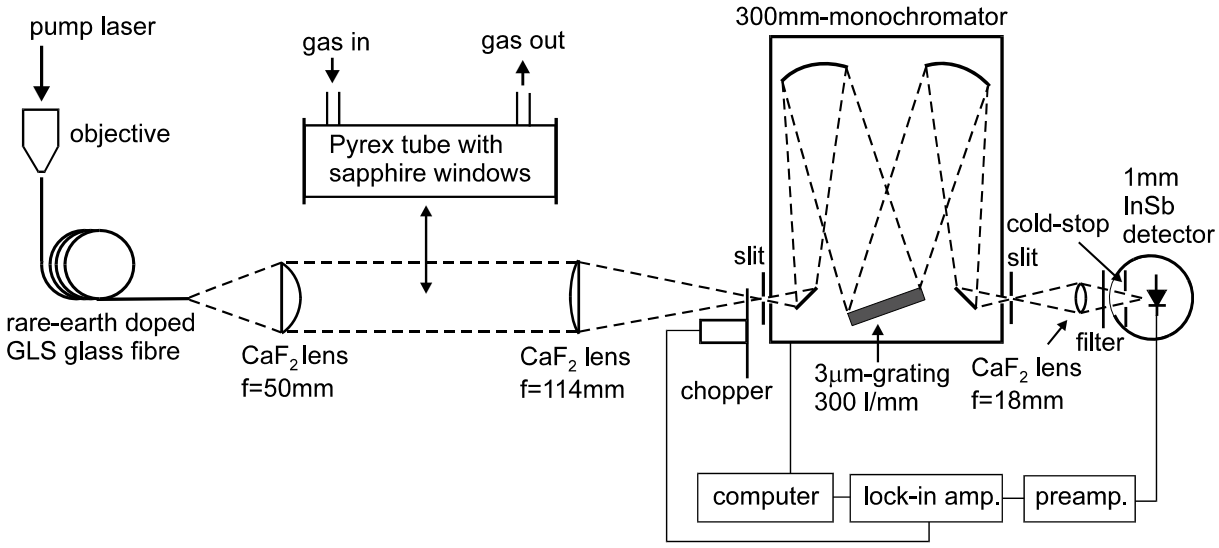

Fig. 7.1.1 Set-up for mid-infrared fluorescence measurements

The pump laser light is either coupled into the rare-earth doped GLS glass fibre with a microscope objective (×10 or ×20) or focused into a bulk glass sample with a silica lens (f = 50 mm). The pump source for most of the experiments is a tuneable Ti:sapphire laser but other pump sources such as a

Nd:YAG laser, a Nd:YLF laser, a dye laser, and a diode pumped Tm:YAG laser have also been used. The mid-infrared fluorescence is collected from the end of the fibre or from the side of the bulk sample and collimated by a CaF_2 lens (plano-convex, f = 50 mm, d = 38 mm). A second CaF_2 lens (plano-convex, f = 114 mm, d = 38 mm) focuses the fluorescence onto the adjustable entrance slit of a monochromator (f = 300 mm) with a grating (300 lines/mm) which is blazed at 3 μm. A third CaF_2 lens (bi-convex, f = 18 mm, d = 13 mm) images the adjustable exit slit of the monochromator through a long wavelengths pass (LWP) filter (1.04, 1.7, 2.54, 3.0, 4.0 μm) and a cold-stop onto the InSb detector area (1 mm^2). The InSb detector and the cold stop are enclosed into a liquid nitrogen dewer with a sapphire window. The signal is first amplified by a preamplifier which is matched to the InSb detector and further amplified by a lock-in amplifier which is synchronised by a chopper which modulates the fluorescence. The lock-in amplifier is read out by a computer.

The system has been designed to maximise the throughput of the fluorescence and minimise the detected stray light which is emitted by all objects (and subjects) in the laboratory at room temperature and increases the signal noise and can even swamp the fluorescence signal completely. The three CaF_2 lenses have been specially fabricated for focal length and diameter to match the F-number of the monochromator and the acceptance angle of the InSb detector. The field of view of the detector is defined by the cold-stop which is an aperture that is mounted inside the dewer to prevent thermal emission from the cold-stop itself. The first two CaF_2 lenses magnify the fibre end or the pump channel in the bulk sample by a factor of 2.3. A typical fibre of 200 μm diameter is magnified to 460 μm which still passes the entrance slit (typical slit width 0.5 to 3 mm) and does not overfill the detector (1 mm^2). Bulk samples are typically 7 mm thick and are excited vertically so that the magnified pump channel (16 mm) is still smaller than the slit height of the monochromator (20 mm). The LWP filter cuts out possible second diffraction orders of shorter wavelengths signals.

In general the fluorescence signal and not the pump laser is chopped to allow for greater chopping frequencies while avoiding any changes in relative fluorescence peak heights due to different energy level lifetimes. Chopping the fluorescence means also chopping the thermal radiation from the sample which is heated by the pump laser absorption. For very weak emission bands, however, the pump laser beam was chopped instead to reduce thermal background noise from the sample. Chopping the pump laser beam means that the absolute heat load of the sample is reduced and that the thermal radiation from the sample is not modulated because the thermal changes cannot follow the chopper speed.

A Pyrex tube with sapphire windows (length = 200 mm, diameter = 38 mm, constructed by Edinburgh Instruments) which can be filled with a gas sample

can be inserted into the collimated fluorescence beam. The system can also be operated with a flowing gas atmosphere.

Fluorescence spectra are corrected for system response by replacing the sample with a blackbody radiation source (Optronic Laboratories Model OL 480) with variable temperature and known emission spectrum (Planck's curve). The measured spectrum of the blackbody source is divided by the theoretical Planck curve at the temperature of the source to obtain the system response curve. The measured fluorescence curve is then divided by this response curve to obtain the corrected fluorescence spectrum which is now corrected for the characteristic absorptions and reflectivities of the optical elements and the atmosphere (e.g. H_2O, CO_2, etc.) in between them.

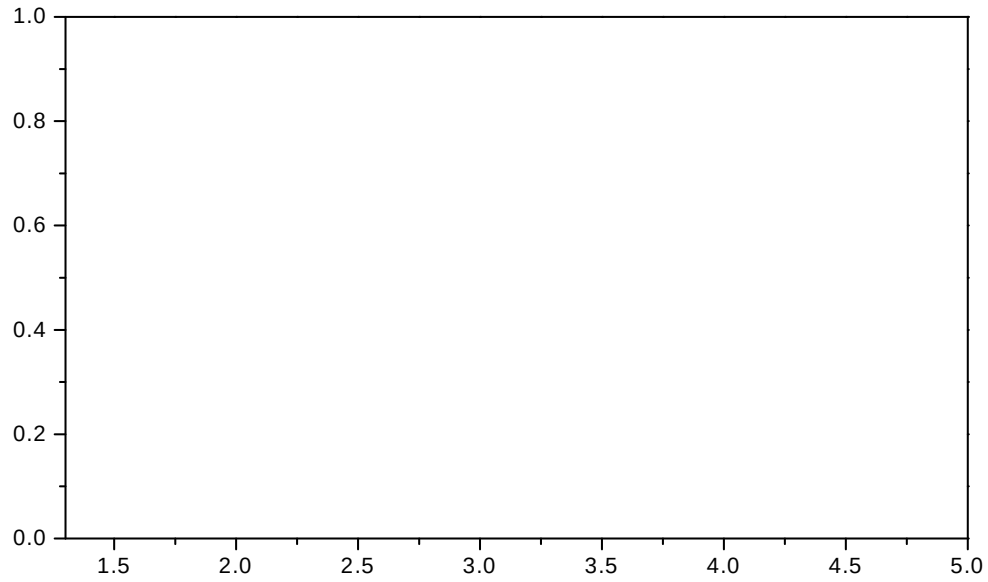

Fig. 7.1.2 System response of fluorescence set-up with silicon filter (1.04 μm LWP)

A response curve of the complete system including lenses, monochromator, 1.04 μm LWP silicon filter, and detector is shown in Fig. 7.1.2. The response is highest for the window between the atmospheric water absorption at 2.7 μm and the carbon dioxide absorption at 4.25 μm and drops off to either side. The sensitivity around 5 μm can be increased by using the 2.54, 3.0, and 4.0 μm LWP filters which have a higher transmission at this wavelength than the silicon filter (T = 60% @ 5 μm). The maximum wavelength of the system is 5.45 μm and is limited by the travel of the monochromator and the decreasing sensitivity of the InSb detector for wavelengths longer 5 μm.

7.2 Experimental set-up for ESA measurements

Fig. 7.2.1 shows the experimental set-up for the ESA measurements.

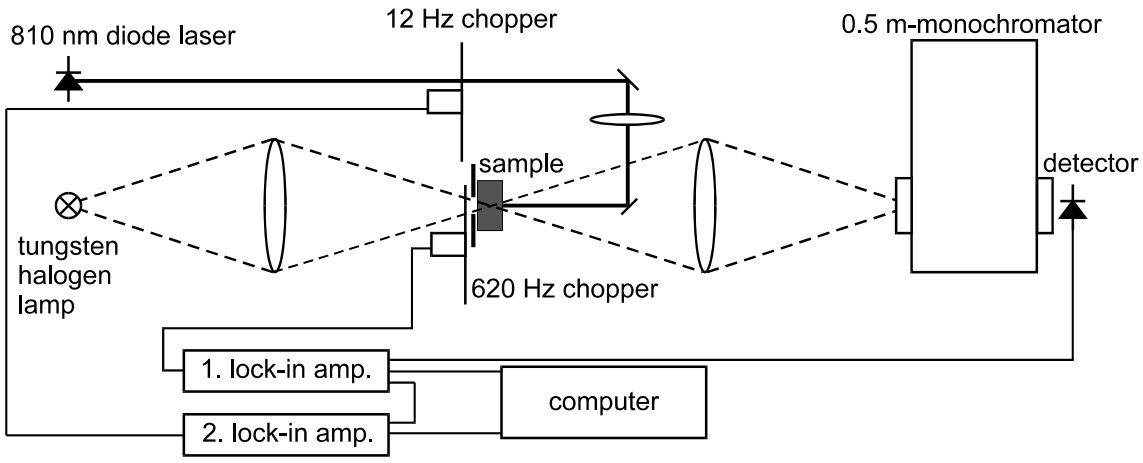

Fig. 7.2.1 ESA set-up

The experimental set-up for the ESA measurements and the evaluation and interpretation of the spectra have been described in detail by Koetke [Koe94]. The set-up is based on the pump-and-probe technique and uses a double-modulation scheme. The beam of the 810 nm pump laser diode was chopped at 12 Hz and focused into the sample through a 500 μm pinhole. The pump power incident on the sample was 80 mW. The probe beam of the tungsten halogen lamp was chopped at 620 Hz, focused into the sample from the opposite direction, and further imaged onto the slit of a 0.5 m monochromator. A silicon detector was used for the spectra from 540 nm to 750 nm and a germanium detector for the spectra from 900 nm to 1330 nm. The first lock-in amplifier synchronised with 620 Hz amplifies the intensity I of the transmitted probe beam, and the second lock-in amplifier synchronised with 12 Hz amplifies the change ΔI between the transmitted intensities in the pumped and unpumped case. See chapter 4 for experimental data and physical discussion.

8 References

[Abd93] I. Abdulhalim et al., "High performance acousto-optic chalcogenide glass based on Ga_2S_3-La_2S_3 systems," J. Non-Cryst. Solids **164-166** (1993) 1251

[Ami96] J. Amin, B. Dussardier, T. Schweizer, and M. Hempstead, "Spectroscopic analysis of Er^{3+} transitions in lithium niobate," J. Lumin. **69** (1996) 17

[Asa97] R. Asal, P.E. Rivers, and H.N. Rutt, "A structural study of gallium lanthanum sulphide glass bulk and thin films by x-ray absorption fine structure spectroscopy," J. Phys.: Condens. Matter **9** (1997) 6217

[Aso96] M. Asobe et al., "Low power all-optical switching in a nonlinear optical loop mirror using chalcogenide glass fibre," Electron. Lett. **32** (1996) 1396

[Aul82] B.F. Aull and H.P. Jenssen, "Vibronic interactions in Nd:YAG resulting in nonreciproc-ity of absorption and emission cross sections," IEEE J. Quantum Elect. **QE-12** (1982) 925

[Auz73] F.E. Auzel, "Materials and devices using double-pumped phosphors with energy transfer," Proc. IEEE **61** (1973) 758

[Bar84] N.P. Barnes and R.E. Allen, "Room temperature Dy:YLF laser operation at 4.34 μm," Technical Digest of Conference on Lasers and Electro-Optics, 19-22 June 1984, Anaheim, California, page 78, paper WA5

[Bar92] S Barnier et al., "Raman and infrared studies of the structure of gallium sulphide based glasses," Materials Science and Engineering **B14** (1992) 413

[Bec92] P.C. Becker et al., "Pr^{3+}:La-Ga-S glass: A promising material for 1.3 μm fibre amplification," Tech. Dig. Topical Meeting Optical amplifiers and their applications, (Optical Society of America, Washington, DC, 1992), Paper PD5, pp. 20-23

[Bow94] S.R. Bowman, J. Ganem, B.J. Feldman, and A.W. Kueny, "Infrared laser chracteristics of praseodymium-doped lanthanum trichloride," IEEE J. Quantum Elect. **30** (1994) 2925

[Bow96] S.R. Bowman et al., "A 7-μm praseodymium based solid-state laser," IEEE J. Quantum Elect. **32** (1996) 646

[Bra97] L.B. Brandon et al., "Evaluation of the IR transitions in rare-earth-doped chalcogenide glasses," 1997 OSA Technical Digest Series, Volume 11, Conference on Lasers and Electro-Optics, 18-23 May, 1997, Baltimore, Maryland, page 255, paper CWF48

[Bra98] D.J. Brady, T. Schweizer, J. Wang, and D.W. Hewak, "Minimum loss predictions and measurements in gallium lanthanum sulphide based glasses and fibre," submitted to J. Non-Cryst. Solids

[Bro96] R.S. Brown, W.S. Brocklesby, D.W. Hewak, and B.N. Samson, "The effect of oxide on the spectroscopic properties of the praseodymium 1.3 μm transition in gallium-lanthanum-sulphide glass," J. Lumin. **66&67** (1996) 278

[Car78] W.T. Carnall, H. Crosswhite, and H.M. Crosswhite, "Energy level structure and transition probabilities of the trivalent lanthanides in LaF_3," Argonne, National Laboratory Report ANL-78-XX-95, 1978

[Cha89] M.A. Chamarro and R. Cases, "Energy transfer study between (Yb, Pr), (Yb, Sm) and (Yb, Dy) in fluorohafnate glasses," J. Non-Cryst. Solids **107** (1989) 178

[Che96] Z.J. Chen, J.D. Minelly, and Y. Gu, "Compact low cost Er^{3+}/Yb^{3+} co-doped fibre amplifiers pumped by 827 nm laser diode," Electron. Lett. **32** (1996) 1812

[Com97] C.M. Combes et al., "Optical and scintillation properties of Ce^{3+} doped $LiYF_4$ and $LiLuF_4$ crystals," J. Lumin. **71** (1997) 65

[Cra91] J.D. Crawford, "Introduction to bifurcation theory," Rev. Mod. Phys. **63** (1991) 991

[Dex53] D.L. Dexter, "A theory of sensitized luminescence in solids," J. Chem. Phys. **21** (1953) 836

[Fab94] A.J. Faber, D.R. Simons, Y. Yan, and H. de Waal, "Photoluminescence quenching by OH in Er- and Pr-doped glasses for 1.5 and 1.3 μm optical amplifiers," in SPIE Proceedings, Vol. **2290**, Fiber optic materials and components, San Diego, California, 1994

[Fai94] J. Faist et al., "Quantum cascade laser," Science **264** (1994) 553

[Fan88] T.Y Fan, G. Huber, R.L. Byer, and P. Mitzscherlich, "Spectroscopy and diode laser-pumped operation of Tm,Ho:YAG," IEEE J. Quantum. Electron. **24** (1988) 924

[Far90] M.C. Farries, P.R. Morkel, and J.E. Townsend, "Spectroscopic and lasing characteristics of samarium doped glass fibre," IEE Proceedings **137** (1990) 318

[Far92] H.M. Farok, G.A. Saunders, W. Poon, and H. Vass, "Low temperature fluorescence, valence state and elastic anomalies of samarium phosphate glasses," J. Non-Cryst. Solids **142** (1992) 175

[Fla83] J. Flahaut, M. Guittard, and A.M. Loireau-Lozac'h, "Rare earth sulphide and oxysulphide glasses," Glass Technology **24** (1983) 149

[För48] T. Förster, "Zwischenmolekulare Energiewanderungen und Fluoreszenz,"Annalen der Physik **2** (1948) 55

[Fre53] R. Frerichs, "New optical glasses with good transparency in the infrared," J. Opt. Soc. Am. **43** (1953) 1153

[Gan94] J. Ganem, S.R. Bowman, and B.J. Feldman, "Excited-state dynamics of Pr^{3+}:$LaCl_3$," J. Lumin. **58** (1994) 298

[Gat97] K. Gatterer, G. Pucker, and H.P. Fritzer, "Structural information in the optical spectra of Eu^{3+} doped glasses from the ternary system Na_2O-B_2O_3-SiO_2," Phys. Chem. Glasses **38** (1997) 293

[Gil95] D.S. Gill et al., "Characterisation of Ga-La-S chalcogenide glass thin-film optical waveguides, fabricated by pulsed laser deposition," J. Non-Cryst. Solids **191** (1993) 321

[Gma97] C. Gmachl, et al. "Distributed feedback quantum cascade lasers," postdeadline paper CPD13 and G. Scarmarcio et al. "High power interminiband superlattice

infrared lasers," paper CthS1 in Technical Digest of CLEO'97, Baltimore, USA

[Gu96] S.Q. Gu, D.A. Turnbull, and S.G. Bishop, "Broad-band excitation of Pr^{3+} luminescence by localized gap state absorption in $Pr:As_{12}Ge_{33}Se_{55}$ glass," IEEE Photon. Technol. Lett. **8** (1996) 260

[Hec97] J.R. Hector et al., "Quantum-efficiency measurements in oxygen-containing gallium lanthanum sulphide glasses and fibres doped with Pr^{3+}," IEEE Photon. Technol. Lett. **9** (1997) 443

[Hec98] J.R. Hector, "Investigation and comparison of modified GLS chalcogenide glasses for active optical fibre devices," PhD Thesis, University of Southampton, 1998

[Heo95] J. Heo, "Optical characteristics of rare-earth-doped sulphide glasses," J. Mater. Sci. Lett. **14** (1995) 1014

[Heo96] J. Heo and Y.B. Shin, "Absorption and mid-infrared emission spectroscopy of Dy^{3+} in Ge-As(or Ga)-S glasses," J. Non-Cryst. Solids **196** (1996) 162

[Heo97] J. Heo, "2.9 μm emission and multiphonon relaxation in $Ge_{25}Ga_5S_{70}$ glass doped with Dy^{3+} and Tm^{3+}," OSA TOPS Vol. **10** Advanced Solid State Lasers 1997, C.R. Pollock and W.R. Bosenberg (eds.), Optical Society of America (1997) 226

[Heo97a] J. Heo, W.Y. Cho, and W.J. Chung, "Sensitizing effect of Tm^{3+} on 2.9 μm emission from Dy^{3+}-doped $Ge_{25}Ga_5S_{70}$ glass," J. Non-Cryst. Solids **212** (1997) 151

[Hew94]D.W. Hewak et al., "Quantum-efficiency of praseodymium doped Ga:La:S glass for 1.3 μm optical fibre amplifiers," IEEE Photon. Technol. Lett. **6** (1994) 609

[Hew94a] D.W. Hewak et al., "Emission at 1.3 μm from dysprosium-doped Ga:La:S glass," Electron. Lett. **30** (1994) 968

[Hig98] H. Higuchi et al., "Optical transitions and frequency upconversion emission of Er^{3+} ions in Ga_2S_3-GeS_2-La_2S_3 glasses," J. Appl. Phys. **83** (1998) 19

[Joh73] L.F. Johnson and H.J. Guggenheim, "Laser emission at 3 μm from Dy^{3+} in BaY_2F_8," Appl. Phys. Lett. **23** (1973) 96

[Jør62] C. Jørgensen, "Orbitals in atoms and molecules," Academic Press, New York, 1962

[Jør64] C.K. Jørgensen and B.R. Judd, "Hypersensitive pseudoquadrupole transitions in lanthanides," Mol. Phys. **8** (1964) 281

[Jør83] C.K. Jørgensen and R. Reisfeld, "Judd-Ofelt parameters and chemical bonding," J. Less-Common Metals **93** (1983) 107

[Ju96] J.J. Ju et al., "Spectroscopic properties of Ce^{3+} ions in barium-sodium borate glass," Mater. Lett. **28** (1996) 149

[Jud62] B.R. Judd, "Optical absorption iontensities of rare-earth ions," Phys. Rev. **127** (1962) 750

[Kad95] K. Kadono et al., "Upconversion luminescence of Ga_2S_3-based sulfide glasses containing Er^{3+} ions," J. Non-Cryst. Solids **184** (1995) 309

[Kam85] A.A. Kaminskii, "Achievements in the field of physics and spectroscopy of activated laser crystals," Phys. Stat. Sol. (a) **87** (1985) 11

[Kam87] A.A. Kaminskii, K. Kurbanov, and T.V. Uvarova, "Stimulated radiation from single crystals of $BaYb_2F_8$-Pr^{3+}," Inorganic Materials **23** (1987) 940

[Kan95] I. Kang et al., "Femtosecond measurement of enhanced optical nonlinearities of sulfide glasses and heavy-metal-doped oxide glasses," J. Opt. Soc. Am. B **12** (1995) 2053

[Kap65] N.S. Kapany and R.J. Simms, "Recent developments in infrared fiber optics," Infrared Phys. **5** (1965) 69

[Koc86] M.E. Koch and W.E. Case, "The photon avalanche laser," in Advances in laser science, W. Stwalley (Ed.), American Institute of Physics, New York, 1986

[Koe94] J. Koetke, "Absorption aus angeregten Zuständen in Ni^{2+}- und Er^{3+}-dotierten Kristallen," Thesis, University of Hamburg, 1994

[Kok96] V.F. Kokorina, "Glasses for infrared optics," CRC Press, 1996

[Kri94] J.T. Kringlebotn et al., "Highly-efficient, low-noise grating-feedback Er^{3+}:Yb^{3+} codoped fibre laser," Electron. Lett. **30** (1994) 972

[Kue89] A.W. Kueny, W.E. Case, and M.E. Koch, "Nonlinear-optical absorption through photon avalanche," J. Opt. Soc. Am. B **6** (1989) 639

[Kum94] P.N. Kumta and S.H. Risbud, "Review: Rare-earth chalcogenides-an emerging class of optical materials," J. Mater. Sci. Lett. **29** (1994) 1135

[Law91] J.K. Lawson and S.A. Payne, "Excited-state absorption spectra and gain measurements of CaF_2:Sm^{2+}," J. Opt. Soc. Am. B **8** (1991) 1404

[Lay77] C.B. Layne, W.H. Lowdermilk, and M.J. Weber, "Multiphonon relaxation of rare-earth ions in oxide glasses," Phys. Rev. B **16** (1977) 10

[Lei81] M. Leiss, "Halbleitende Seltenerdsesquisulfide: Herstellung, optische Verstärkung und Wechselwirkung zwischen Band-, 5d- und 4f-Zuständen," Thesis, University of Hamburg, 1981

[Lia96] S.K. Liaw, A.C.L. Wang, J.W. Liaw, and S. Chi, "A self-frequency-locked multi-wavelength erbium-doped fibre ring laser," Opt. Quant. Electron. **28** (1996) 1407

[Liz95] S. Lizzo, A. Meijerink, G.J. Dirksen, and G. Blasse, "Luminescence of divalent ytterbium in magnesium fluoride crystals," J. Lumin. **63** (1995) 223

[Loz73] A.-M. Lozac'h, M. Guittard, and J. Flahaut, "Sur une nouvelle famille de combinaison soufrees, de type "mellenite"," Mat. Res. Bull. **8** (1973) 75

[Mat93] L. Mattos Jnr. and A.G. Clare, "The crystallisation and optical properties of gallium cerium lanthanum sulphide glass," Physics and Chemistry of Glasses **34** (1993) 244

[Mau96] R. Mauricot, J. Dexpert-Ghys, and M. Evain, "Photoluminescence of the undoped γ-Ln_2S_3 and doped γ-[Na]Ln_2S_3 rare earth sulfides (Ln=La,Ce)," J. Lumin. **69** (1996) 41

[McC64] D.E. McCumber, "Einstein relations connecting broadband emission and absorption spectra," Phys. Rev. **136** (1964) A954

[Min91] W.J. Miniscalco and R.S. Quimby, "General procedure for the analysis of Er^{3+} cross sections," Opt. Lett. **16** (1991) 258

[Min93] W.J. Miniscalco, "Optical and electronic properties of rare earth ions in glass," in "Rare Earth doped Fibre Lasers and Amplifiers," by M.J.F. Digonnet (Ed.), Marcel Dekker Inc., New York, Basel, Hongkong, 1993

[Min93a] J.D. Minelly et al., "Diode-array pumping of Er^{3+}/Yb^{3+} co-doped fibre lasers and amplifiers," IEEE Photon. Technol. Lett. **5** (1993) 301

[Mit98] K. Mitchell, Edinburgh Instruments, private communication, 1998

[Mix95] E. Mix, "Spektroskopie und Lasereigenschaften ytterbiumdotierter Kristalle und Fluorid-Phosphat-Gläser," Diplomarbeit, Universität Hamburg, 1995

[Mot87] N.F. Mott, "Conduction in non-crystalline materials," Oxford Science Publications, Clarendon Press, Oxord, 1987

[Mue97] M. Muendel et al., "35-watt cw singlemode ytterbium fiber laser at 1.1 μm," CLEO '97, Baltimore, Maryland, 18-23 May 1997, postdeadline paper CPD30

[Mul94] M. Muller, J.L. Fabris, A.C. Hernandes, and M.S. Li, "570 nm and 4.8 μm emission in Yb^{2+}/CN^- double doped KCl," J. Lumin. **59** (1994) 289

[Nog94] M. Nogami and Y. Abe, "Sm^{2+}-doped silicate glasses prepared by a sol-gel process," Appl. Phys. Lett. **65** (1994) 1227

[Ofe62] G.S. Ofelt, "Intensities of crystal spectra of rare-earth ions," J. Chem. Phys. **37** (1962) 511

[Oh97] K. Oh, et al., "Photoinduced refractive-index change in Sm^{2+}/Sm^{3+} codoped aluminosilicate fiber by irradiation of an Ar-ion laser," Opt. Lett. **22** (1997) 1192

[Ohi91] Y. Ohishi et al., "Gain characteristics of Pr^{3+}-Yb^{3+} codoped fluoride fiber for 1.3 μm amplification," IEEE Photon. Technol. Lett. **3** (1991) 990

[Ohn92] Y. Ohno, "Valence state and electronic structure of the misfit-layer compound $SmNbS_3$," J. Phys.: Condens. Matter **4** (1992) 7815

[Pas97] R. Paschotta et al., "Lifetime quenching in Yb-doped fibres," Opt. Commun. 136 (1997) 375

[Pat97] A. Patra, D. Kundu, and D. Ganguli, "A study of the structural evolution of the sol-gel derived Sm^{3+}-doped silica glass," Mater. Lett. **32** (1997) 43

[Pea75] R.D. Peacock, "The intensities of lanthanide f ↔ f transitions," in Structure and Bonding **22** (1975) 83, Springer Verlag, Berlin, Heidelberg, New York

[Pea94] A. Pearson, "High-resolution spectroscopy of rare-earth doped novel glasses", chapter 6, PhD Thesis, University of Southampton, 1994

[Pin94] J.F. Pinto et al., "Tunable solid-state laser action in Ce^{3+}:$LiSrAlF_6$," Electron. Lett. **30** (1994) 240

[Poi94] H. Poignant et al., "Efficiency and thermal behaviour of cerium-doped fluorozirconate glass fibre Bragg gratings," Electron. Lett. **30** (1994) 1339

[Pol97] M. Pollnau et al., "Three-transition cascade erbium laser at 1.7, 2.7, and 1.6 μm," Opt. Lett. **22** (1997) 612

[Rei75] R. Reisfeld, "Radiative and non-radiative transitions of rare-earth ions in glasses," in Structure and Bonding **22** (1975) 123, Springer Verlag, Berlin, Heidelberg, New York

[Rei77] R. Reisfeld and A. Bornstein, "Absorption and emission spectra in chalcogenide glass of the composition $0.7Ga_2S_3$:$0.27La_2S_3$:$0.03Nd_2S_3$," Chem. Phys. Lett. **47** (1977) 194

[Rei78] R. Reisfeld and A. Bornstein, "Fluorescence of Er^{3+} doped $La_2S_3 \cdot 3Ga_2S_3$ glasses," J. Non-Cryst. Solids **27** (1978) 143

[Rei80] R. Reisfeld, in "Radiationless Process," By B. Di Bartolo and V. Goldberg (Eds.), Plenum, New York (1980) 489

[Rei82] R. Reisfeld, "Chalcogenide glasses doped by rare earths: structure and optical properties," Ann. Chim. Fr. **7** (1982) 147

[Rei84] R. Reisfeld, "Fluorescence and non-radiative relaxations of rare earths in amorphous media and on high surface area supports: a review," J. Electrochem. Soc. **131** (1984) 1360

[Rei85] R. Reisfeld, "Possible ways of relaxations for excited states of rare earth ions in amorphous media," Journal de Physique **46** (1985) C7-349

[Ris68] L.A. Riseberg and H.W. Moos, "Multiphonon orbit-lattice relaxation of excited states of rare-earth ions in crystals," Phys. Rev. **174** (1968) 429

[Rom95] J.E. Roman et al., "Ion-exchanged Er/Yb waveguide laser at 1.5 μm pumped by laser diode," Electron. Lett. **31** (1995) 1345

[Sam94] B.N. Samson et al., "Dysprosium doped Ga:La:S glass for an efficient optical fibre amplifier operating at 1.3 μm," Electron. Lett. **30** (1994) 1617

[Sam97] B.N. Samson, T. Schweizer, D.W. Hewak, and R.I. Laming, "Properties of dysprosium doped GaLaS fibre amplifiers operating at 1.3μm", Opt. Lett. **22**, 703 (1997)

[Sam98] B.N. Samson, T. Schweizer, D.W. Hewak, and R.I. Laming, "Spectroscopy of dysprosium doped and dysprosium/terbium co-doped GaLaS glass", accepted for publication in J. Lumin.

[San93] F. Sanchez, P. Le Boudec, P.-L. François, and G. Stephan, "Effects of ion pairs on the dynamics of erbium-doped fiber lasers," Phys. Rev. A **48** (1993) 2220

[Sch70] C. Schultz-Sellack, "Diathermansie einer Reihe von Stoffen für Wärme sehr geringer Brechbarkeit," Annalen der Physik und Chemie **139** (1870) 182

[Sch82] E.-G. Scharmer, "Halbleitende Seltenerdsesquisulfide: Elektrische Charakterisierung und ihre Anwendungsmöglichkeiten als schnelle Cer-Phosphore," Thesis, University of Hamburg, 1982

[Sch82a] E.-G. Scharmer, M. Leiss, and G. Huber, "Efficient energy transfer from band excitation to Nd^{3+} in β-La_2S_3:Nd,Ce," J. Phys. C: Solid State Phys. **15** (1982) 1071

[Sch95] J. Schneider, "Fluoride fibre laser operating at 3.9 μm," Electron. Lett. **31** (1995) 1250

[Sch95a] J. Schneider, "Mid-infrared fluoride fibre laser in multiple cascade operation," IEEE Photon. Technol. Lett. **7** (1995) 354

[Sch97] J. Schneider, C. Carbonnier, and U.B. Unrau, "Characterisation of a Ho^{3+}-doped fluoride fiber laser with a 3.9-μm emission wavelength," Appl. Opt. **36** (1997) 8595

[Sha97] L.B. Shaw et al., "Spectroscopy of the IR transitions in Pr^{3+} doped heavy metal selenide glasses," Optics Express **1** (1997) 87

[Shi96] Y.B. Shin, W.Y. Cho, and J. Heo, "Multiphonon and cross relaxation phenomena in Ge-As(or Ga)-S glasses doped with Tm^{3+}," J. Non-Cryst. Solids **208** (1996) 29

[Sim96] B. Simondi-Teisseire et al., "Room temperature cw laser operation at ~1.55 μm (eye-safe range) of Yb:Er and Yb:Er:Ce:$Ca_2Al_2SiO_7$ crystals," IEEE J. Quantum Elect. **32** (1996) 2004

[Sni61] E. Snitzer, "Optical maser action of Nd^{3+} in a barium crown glass," Phys. Rev. Lett. **7** (1961) 444

[Sor61] P.P. Sorokin and M.J. Stevenson, "Solid-state optical maser using divalent samarium in calcium fluoride," IBM J. Research **5** (1961) 56

[Sum94] D.S. Sumida and T.Y. Fan, "Impact of radiation trapping on fluorescence lifetime and emission cross section measurements in solid-state laser media," Opt. Lett. **19** (1994) 1343

[Tak96] H. Takebe, T. Murata, and K. Morinaga, "Compositional dependence of absorption and fluorescence of Yb^{3+} in oxide glasses," J. Am. Ceram. Soc. **79** (1996) 681

[Tan95] S. Tanabe, T. Handa, M. Watanabe, T. Hayashi, and N. Soga, "Optical properties of dysprosium-doped low-phonon-energy glasses for a potential 1.3 μm optical amplifier," J Am. Ceram. Soc. **78** (1995) 2917

[Taw97] H. Tawarayama et al., "Efficient amplification at 1.3 μm in a Pr^{3+}-doped Ga-Na-S fiber," in Postdeadline Papers of Optical amplifiers and their applications, Victoria, BC, Canada, 1997, paper PD1

[Tsu97] T. Tsuneoka, A. Kubo, K. Kojima, and S. Bojja, "Fluorescence and electron spin resonance spectra of Eu^{2+} ions in chloride glass," Phys. Chem. Glasses **38** (1997) 313

[Via97] B. Viana, M. Palazzi, and O. LeFol, "Optical characterization of Nd^{3+} doped sulphide glasses," J. Non-Cryst. Solids **215** (1997) 96

[Wan97] J. Wang et al., "Halide-modified Ga-La sulfide glasses with improved fiber-drawing and optical properties for Pr^{3+}-doped fiber amplifiers at 1.3 μm," Appl. Phys. Lett. **71** (1997) 1753

[Wei94] K. Wei, D.P. Machewirth, J. Wenzel, E. Snitzer, and G.H. Sigel, Jr., "Spectroscopy of Dy^{3+} in Ge-Ga-S glass and its suitability for 1.3-μm fiber-optical amplifier applications," Opt. Lett. **19** (1994) 904

[Wu96] B. Wu and P.L. Chu, "Fast optical switching in Sm^{3+}-doped fibres," IEEE Photon. Technol. Lett. **8** (1996) 230

[Wyb65] B.G. Wybourne, "Spectroscopic Properties of Rare-Earths," Wiley, 1965

[Xie95] P. Xie and T.R. Gosnell, "Efficient sensitisation of praseodymium 1.31 μm fluorescence by optically pumped ytterbium ions in ZBLAN glass," Electron. Lett. 31 (1995) 191

[Ye96] C.C. Ye et al., "Spectral properties of Er^{3+}-doped gallium lanthanum sulphide glass," J. Non-Cryst. Solids **208** (1996) 56

[You93] K.E. Youden et al., "Pulsed laser deposition of Ga-La-S chalcogenide glass thin film optical waveguides," Appl. Phys. Lett. **63** (1993) 1601

[Zou95] X Zou and H. Toratani, "Evaluation of spectroscopic properties of Yb^{3+}-doped glasses," Phys. Rev. B **52** (1995) 15889

[Zou95a] X. Zou, A. Shikida, H. Yanagita, and H. Toratani, "Mechanisms of upconversion fluorescence in Er^{3+}, Tm^{3+} codoped fluorozircoaluminate glasses," J. Non-Cryst. Solids **181** (1995) 100

[Zue76] V.E. Zuev, "Laser-light transmission through the atmosphere," in Laser Monitoring of the Atmosphere by E.D. Hinkley (Ed.), Springer-Verlag Berlin Heidelberg New York, 1976, page 40

9 Acknowledgements

The work presented in this thesis was carried out mainly at the Optoelectronics Research Centre, University of Southampton, and to a minor part at the Institut für Laser-Physik, Universität Hamburg, in the time from fall 1994 to spring 1998.

I would like to express my sincere gratitude to Prof. David N. Payne (Optoelectronics Research Centre, University of Southampton) and Prof. Günter Huber (Institut für Laser-Physik, Universität Hamburg) for making this research project possible. In particular I would like to thank Prof. David N. Payne for inviting me to join the ORC in Southampton, for the many educational fab meetings, and for the generous financial assistance without me submitting my thesis in Southampton. Many thanks to Prof. Günter Huber for his supervision and for accepting my thesis in Hamburg where some of the key experiments (bulk laser, ESA) were performed.

Congratulations to Dr. Dan Hewak who did an excellent job supervising his first PhD student. In particular I appreciated the freedom I had in following my own ideas, his skill in bringing my focus back to the aims of the project, and the additional funding for the third and fourth year. Not to forget the “free” holidays in his cottage looking after the garden (!), the horse, and the cat which I just couldn’t turn down. I also had the “honour” to include Dan’s paper about the first demonstration of GLS glass fibre into the fabrication part of my thesis (paper 1).

A big thank-you also to:

- Dr. Bryce Samson, my great teacher, for escorting me through the last 3 1/2 years from day one on, for handing down all the secrets of applied spectroscopy to his disciple, and for his constant flow of new ideas.
- Roger Moore, the real one, for his practical introduction into glass and fibre fabrication and all the wonderful fibres he pulled.

• Dom Brady for many interesting discussions about questions such as why GLS fibre will never have a loss of 0.5 dB/km, for his patient help with editorial questions, and for the explanation of rather “colloquial” English terms and expressions (“you can kiss my s...”).
• Jason Hector for many successful joint experiments, in particular lifetime measurements.
• Dr. Bill Brocklesby for inspiring spectroscopic discussions, his interest in and support for my experiments, and his teaching about how to write a PRL paper.
• Dr. Evely Martins for some exciting excitation measurements.
• Dr. Hiromichi Takebe for his glass heat treatments.
• All unnamed past and present members of the ORC and the Physics Department who supported me either intentionally or unintentionally through fruitful technical discussions and inspiring private conversations within the ORC and the surrounding pubs.
• All members of the Keeeeeeebab-Club.
• All members of the “Group-F” in Hamburg who allowed their work to be interrupted each time I arrived for my working Christmas holidays, and in particular to Dr. Patrick E.(S.)A. Möbert and Dr. Thomas Bulk-Laser-Jensen for their assistance with two of the key experiments.
• My parents who supported and encouraged me on my seemingly endless journey through the German education system.

The final 1 1/2 years of this project were supported by the UK EPSRC/DTI LINK programme (LONGWAVE). Chalcogenide starting materials were supplied by Merck Ltd., Poole, UK. Glass samples for spectroscopy and laser experiments and glass rods and tubes for fibre drawing were polished by Crystran Ltd., Poole, UK. The Pyrex tube for gas absorption measurements was constructed by Edinburgh Instruments Ltd., Edinburgh, Scotland.